

Study of Spontaneous Polymerisation Inhibition

Thomas Edward Newby

PhD

University of York

Chemistry

May 2014

Abstract

Spontaneous polymerisation is an unwanted reaction, prevented by inhibitor molecules. In order to observe the inhibition of spontaneous polymerisation by different molecules, a small scale dilatometry experiment was developed. This was used to screen structurally related molecules to 2-nitrophenol to determine what structural features give rise to inhibition properties. Compounds with an intramolecular hydrogen bond demonstrated more efficient inhibition of polymerisation.

The product mixture of styrene inhibited by 2-nitrophenol was analysed to determine the reaction pathway. Column chromatography, MS and NMR were used to determine the structure of two intermediates, 2-aminophenol and a compound derived from a Diels Alder styrene initiator and 2-nitrophenol.

The proposed intermediate, 2-nitrosophenol, was synthesised and its stability in styrene was determined. The products of reaction between 2-nitrosophenol and styrene at room temperature were proposed by comparing results with the reaction between styrene and nitrosobenzene. The main product of the inhibition by 2-nitrosophenol, was also determined to be 2-aminophenol, suggesting that 2-aminophenol formed from inhibition by 2-nitrophenol goes via 2-nitrosophenol.

Other intermediates and products identified were also screened in the dilatometry setup. They show inhibition properties at high concentration, but at more realistic concentrations, they did not inhibit styrene polymerisation. An overall mechanism for the inhibition of styrene polymerisation by 2-nitrophenol, was proposed based on the data obtained.

Contents

Abstract.....	2
Contents.....	3
List of figures.....	9
List of schemes.....	15
List of tables.....	18
List of equations.....	20
Acknowledgments.....	21
Authors declaration	23
1. Introduction	24
1.1 Properties of a polymer	24
1.2 Radical polymerisation.....	27
1.2.1 Spontaneous polymerisation	30
1.2.1.1 Bi-radical mechanism.....	30
1.2.1.2 Pericyclic mechanisms	32
1.2.1 Living radical polymerisation	34
1.3 Inhibition of polymerisation.....	36
1.3.1 Direct reaction with initiator radical.....	37
1.3.1.1 Oxygen	37
1.3.1.2 Stable radicals	38
1.3.1.3 Nitroaromatics and nitrophenols.....	39
1.3.1.4 Quinones	41
1.3.1.5 Phenothiazine	42
1.3.2 Reactions of inhibitors with peroxy radicals.....	43
1.3.2.1 Phenolics	43
1.4 Electron paramagnetic resonance	44

1.4.1	Basic principle – Zeeman Splitting	45
1.4.2	Instrumentation and Detection	46
1.4.2.1	Noise reduction and sensitivity.....	47
1.4.3	Analysis and interpretation of spectra.....	47
1.4.3.1	Hyperfine interactions	48
1.4.3.2	Intensity	49
1.4.3.3	Line broadening	49
1.5	Aims of the study	50
2.	Nitrophenols as inhibitors.....	51
2.1	Monitoring polymerisation	51
2.2	Dilatometry	54
2.2.1	Disadvantages of current methods.....	56
2.3	Design of a new and automated dilatometry experiment	57
2.3.1	Rack.....	58
2.3.2	Oil bath and heating.....	60
2.3.3	Sample preparation	61
2.3.4	Camera and lighting	62
2.3.5	Data analysis	62
2.3.6	Standards and calibration of the new setup.....	63
2.3.7	Oxygen diffusion within the samples.....	64
2.4	Case studies for proof of concept	67
2.4.1	Uninhibited styrene	67
2.4.2	Nitroxide inhibited polymerisation (TEMPO).....	68
2.4.3	Oxygen dependent inhibitor (4-methoxyphenol).....	70
2.4.4	Conclusions on the new dilatometry set-up	71
2.5	Dilatometry study of the inhibition properties of ortho-nitrophenols and related compounds	72
2.5.1	DNBP, 2,4-dinitrophenol and 2-nitrophenol.....	72

2.5.2	2-Nitrophenol, 3-nitrophenol and 4-nitrophenol	74
2.5.3	The structural group responsible for inhibition	76
2.5.4	Nitroanilines.....	80
2.5.5	Nitroanisole (removing the hydrogen bond to the nitro group)	82
2.5.6	2-Nitroacetanilide and 2-nitrotrifluoroacetanilide	83
2.6	Conclusions from the dilatometry screening experiment	85
3.	Nitrophenols as inhibitors – Product analysis.....	87
3.1	Introduction	87
3.2	MS analysis of inhibition product mixture	88
3.3	GC and GC / MS analysis of inhibition product mixture	90
3.4	Identification of reactive intermediates by EPR	94
3.5	Isolation and identification of Unknown A and Unknown B.....	96
3.5.1	Acid / Base extraction	97
3.5.2	Methanol precipitation	99
3.5.3	Column chromatography	100
3.5.4	Polymer precipitation by methanol and water	102
3.6	Structure determination of unknown B by NMR.....	104
3.6.1	Degree of unsaturation.....	115
3.7	X-ray crystallography of isolated unknown B	116
3.8	Possible mechanism for the formation of Unknown B.....	119
3.9	Synthesis of the unknown B.....	121
3.9.1	Ketone intermediate (Compound D)	121
3.9.2	Synthesis of deuterated compound D.	127
3.9.3	Synthesis of imine (Compound E)	128
3.9.4	Final cyclisation to compound C	130
4.	Intermediates in the inhibition of spontaneous polymerisation of styrene by nitrophenols.....	134
4.1	Further dilatometry	135

4.1.1	2-Aminophenol	135
4.1.2	Imines as inhibitors	138
4.1.3	Unknown B as an inhibitor	142
4.1.4	2-Nitrosophenol	143
4.2	Further product analysis	145
4.2.1	Nitroso intermediates	145
4.2.1.1	Nitrosobenzene	145
4.2.1.2	2-Nitrosophenol	149
4.2.2	EPR of 2-nitrosophenol in styrene	154
4.3	Conclusions from the additional dilatometry and product analysis.....	156
4.4	The Mechanism of Inhibition	157
4.4.1	Is inhibition stoichiometric or catalytic?	157
4.4.2	Reactions with the initiator radical	159
4.5	Conclusion.....	162
5.	Chloranil Radical Anion	163
5.1	Introduction	163
5.1.1	A new inhibitor.....	163
5.1.2	Aims.....	166
5.2	Chloranil Radical Anion Stability in aqueous solution	167
5.2.1	Products from the decomposition of chloranil radical anion potassium salt. 169	
5.2.2	Chloranil radical anion potassium salt under nitrogen.....	174
5.2.3	Lack of reproducibility.....	175
5.2.4	Conclusions	180
5.3	Comproportionation / disproportionation equilibrium.....	181
5.3.1	Chemical exchange of 2,5 – di-tert-butyl semiquinone in concentrated solutions of 2,5 – di-tert-butyl hydroquinone	183

5.3.2	Equilibrium constants of the comproportionation / disproportionation equilibrium of 2,5 – di-tert-butyl hydroquinone and 2,5 – di-tert-butylquinone in polar media	185
5.3.3	Sensitivity of disproportionation/comproportionation equilibrium to reaction conditions	192
5.3.4	The comproportionation / disproportionation equilibrium in apolar media	195
5.4	Conclusions	202
6.	Final conclusions	204
7.	Experimental	206
7.1	Chemicals and materials	206
7.1.1	Styrene preparation	206
7.2	NMR	206
7.3	EPR	207
7.4	MS	207
7.5	Dilatometry	207
7.6	Oximetry (Oxygen diffusion into chlorobenzene).....	208
7.7	Column Chromatography / Thin Layer Chromatography	208
7.8	X-ray crystallography	208
7.9	Synthesis	209
7.9.1	Chloranil radical anion potassium salt synthesis	209
7.9.2	2-nitrosophenol synthesis.....	210
7.9.3	Unknown B isolation	210
7.9.4	Compound C synthesis – ketone precursor (Compound D).....	211
7.9.5	Synthesis of Compound E	212
7.9.6	Compound E to Compound C reaction	213
7.9.7	N-(1-Phenylethylene)-o-aminophenol – Compound F.....	213
8.	Appendices.....	215
8.1	Glossary.....	233

9. References 234

List of figures

Figure 1. Relationship between chain length of a polymer and its properties; viscosity, tensile and impact strength	26
Figure 2. Relationship between the elastic properties of a polymer and its degree of cross-linkage.....	26
Figure 3. Dimers and trimers found after the self-polymerisation of methyl methacrylate. Two other dimers were observed but could not be characterised due to low quantities	33
Figure 4. The difference in energy levels caused by Zeeman splitting	45
Figure 5. The hyperfine splitting of an unpaired electron interacting with an ¹⁵ N nucleus, in a magnetic field, B.....	48
Figure 6. EPR spectra of TEMPO (Left) and 2,5 – di-tert-butyl semiquinone(Right).....	49
Figure 7. Diagram of a basic dilatometry set-up.....	53
Figure 8. Schematic and digital render of the dilatometry rack. Dimensions, where given, are in millimetres	59
Figure 9. Photo of the dilatometry rack with features labelled.....	59
Figure 10. Temperature equilibration of dilatometry sample. Sample inserted into heated oil bath at time = 20 seconds	61
Figure 11. Dilatometry of toluene, as a demonstration of the equipment stability. Data normalized to the first image taken at t = 0 minutes.	64
Figure 12. The oxygen diffusion into chlorobenzene at 100°C, monitored by EPR	65
Figure 13. A comparison between the oxygen consumption by styrene polymerisation and the oxygen diffusion into chlorobenzene. (At 100°C, monitored by EPR).....	66
Figure 14. Dilatometry of uninhibited styrene at 110°C.....	68
Figure 15. 200ppm TEMPO in styrene polymerisation measured by the dilatometry set-up at 110°C.....	69
Figure 16. Inhibition period against TEMPO concentration.....	69
Figure 17. 3 dilatometry samples of 100ppm MEHQ in styrene polymerisation at 90°C.....	70
Figure 18 Dilatometry trace of uninhibited styrene, 0.1M DNBP, 0.1M 2,4-dinitrophenol, and 0.1M 2-nitrophenol (in styrene) at 110 °C.....	73
Figure 19 Dilatometry traces of styrene, 0.1 M 2-nitrophenol, 0.1 M 3-nitrophenol and 0.1 M 4-nitrophenol (in styrene) at 110 °C.....	75

Figure 20. Contour plot of the isotropic chemical shielding (ppm) through the molecular plane of 2-nitrophenol (a) and 4-nitrophenol (b) calculated at the MP2/6-311++G(d,p) level of theory.....	79
Figure 21. Demonstration of difference in bond order of the nitro group without hydrogen bonding (Left) and with hydrogen bonding (Right)	80
Figure 22. 2-Nitroaniline, 3-nitroaniline and 4-nitroaniline.....	80
Figure 23. Dilatometry of styrene, 0.1 M 2-nitrophenol, 0.1 M 2-nitroaniline and 0.1 M 3-nitroaniline (in styrene) at 110 °C.....	81
Figure 24. 2-Nitroanisole, 3-nitroanisole and 4-nitroanisole.....	82
Figure 25. Dilatometry of styrene, 0.1M 2-, 3- and 4-nitroanisole (in styrene) at 110 °C. ...	82
Figure 26. 2-Nitroacetanilide and 2-nitrotrifluoroacetanilid	83
Figure 27. Dilatometry traces of styrene, 0.1 M 2-nitroacetanilide and 0.1 M 2-nitrotrifluoroacetanilide (in styrene) at 110 °C.....	84
Figure 28. Dilatometry trace for 3 mmol 2-nitrophenol and 2-nitroacetanilide inhibited styrene at 110°C.....	85
Figure 29. ESI MS of the high concentration 2-nitrophenol inhibition mixture.	89
Figure 30. ESI MS of the high concentration 2-nitrophenol inhibition mixture heated for 8 days, until it became too viscous.....	89
Figure 31. Gas chromatogram of 0.01M 2-nitrophenol in styrene heated at 110°C for 24 hours. Sample was split 50:1 at the injection.	91
Figure 32. Gas chromatogram of 0.01M 2-nitrophenol in styrene heated at 110°C for 24 hours. Sample was not split, but detector was deactivated for the first 5 minutes of the chromatogram.	92
Figure 33. 0.1M 2-nitrophenol in styrene at 130°C, average of 40 spectra.	95
Figure 34. ESI MS of the acid extract (Black) and the neutral organic solution (Blue)	98
Figure 35. ^1H NMR of acid extract (Unknown A) in blue and 2-aminophenol in red. (400 MHz, CDCl_3)	99
Figure 36. ^1H NMR of reaction mixture without any separation. (400 MHz, CDCl_3).....	100
Figure 37. MS of fraction containing unknown B ($R_f = 0.33$).	101
Figure 38. ^1H NMR of the first successful isolation of unknown B. (400 MHz, CDCl_3)	102
Figure 39. ^1H NMR of isolated unknown B after water/methanol isolation. (400 MHz, CDCl_3)	103
Figure 40. ^1H NMR of unknown B, low field. (700 MHz, CDCl_3)	105
Figure 41. ^1H NMR of unknown B, high field. (700 MHz, CDCl_3)	105

Figure 42. COSY spectrum of unknown B. (700 MHz, CDCl ₃) The aromatic and non-aromatic protons have been boxed to distinguish the different types of protons.	106
Figure 43. NMR of Unknown B. Close up proton of non-aromatic protons (700 MHz, CDCl ₃)	107
Figure 44. Proposed structure for fragment A.....	107
Figure 45. Fragment A, with coupling constants assigned.....	109
Figure 46. The proposed structure for fragment B.....	109
Figure 47. Close-up of protons C, E and H. (700 MHz, CDCl ₃).....	110
Figure 48. Close-up of protons B, F, G and I. (700 MHz, CDCl ₃).....	111
Figure 49. The proposed structure for fragment C.....	112
Figure 50. The proposed structure for fragment D.....	113
Figure 51. Fragment A, with HMBC couplings shown. Couplings common to protons K, L and M are in red, and those common to protons J, L and M are in blue.	113
Figure 52. The proposed structure and assignment of unknown B.....	115
Figure 53. X-ray crystallography results of a sample of unknown B, crystallised from CDCl ₃	116
Figure 54. Comparison between 2-nitrophenol, unknown B and the spontaneous polymerisation initiator proposed by Mayo ¹⁹	119
Figure 55. NMR of compound D, low field. (400 MHz, CDCl ₃)	124
Figure 56. NMR of compound D, high field. (400 MHz, CDCl ₃)	124
Figure 57. Structure assignment for compound D.....	127
Figure 58. H ¹ NMR of ketone intermediate, synthesised using deuterated benzene. (400 MHz, CDCl ₃).....	128
Figure 59. ESI MS of compound E mixture isolated.	129
Figure 60. H ¹ NMR of compound E mixture, magnified on high field signals. (400 MHz, CDCl ₃)	129
Figure 61. MS spectrum of final synthesis step after 1 hour	131
Figure 62 MS spectrum of final synthesis step after 4 hours.....	131
Figure 63 MS/MS of peak m/z 312 comparisons between inhibited polymerisation mixture (top) and isolated unknown B (bottom)	132
Figure 64. Dilatometry of styrene and styrene inhibited by 0.1 M 2-aminophenol at 110°C	136
Figure 65. Dilatometry traces of styrene, 0.1 M 2-aminophenol in styrene and 0.1 M 2-amino-4-sec-butylphenol in styrene at 110°C	137

Figure 66. Dilatometry of styrene, and styrene inhibited by 3 mM 2-nitrophenol and 3 mM 2-aminophenol at 110°C.	138
Figure 67. Dilatometry traces of styrene, and styrene inhibited by 0.1 M compound B at 110°C.....	140
Figure 68. Dilatometry of uninhibited styrene and styrene inhibited by 0.1M compound F at 110°C.....	141
Figure 69. Dilatometry of styrene and styrene inhibited by 2-nitrophenol , 2-aminophenol, compound E or compound F (3 mM) at 110°C.	142
Figure 70. Dilatometry of styrene inhibited by 0.1 M unknown B at 110°C.....	143
Figure 71. Dilatometry of styrene and styrene inhibited by 0.1 M 2-nitrosophenol at 110°C.	144
Figure 72. Dilatometry trace styrene inhibited with 3 mmol 2-nitrophenol and 3 mmol 2-nitrosophenol at 110°C.	144
Figure 73. Dilatometry traces of styrene and 0.1 M nitrosobenzene prepared fresh and aged for 24 hours at room temperature. Dilatometry performed at 110°C.	147
Figure 74. MS of sample of nitrosobenzene in styrene, analysed immediately.....	148
Figure 75. MS of sample of nitrosobenzene in styrene, analysed after 24 hours at room temperature.....	148
Figure 76. H^1 NMR of the reaction mixture between nitrosobenzene and styrene after solvent removal. (400 MHz, $CDCl_3$).....	149
Figure 77. MS of 0.1M 2-nitrosophenol in styrene after 24 hours.....	150
Figure 78. MS of the products of styrene spontaneous polymerisation inhibited by 0.1 M 2-nitrosophenol.....	152
Figure 79. MS of product mixture of 0.1M 2-nitrosophenol in methyl styrene, heated at 110°C for 5 hours.....	153
Figure 80. EPR of 2-nitrosophenol in styrene, average of spectra taken 35-55 minutes after addition (Black line) and a simulation of the proposed radical formed (Red line).....	155
Figure 81. The amount of radical formed during spontaneous initiation of styrene at 110 °C.....	159
Figure 82. Rate of decomposition of chloranil radical anion potassium salt, as observed from the EPR intensity. The first spectrum was not taken at t = 0 minutes, as the equipment can only be tuned once the sample is prepared and in the equipment.....	168
Figure 83 Negative ion ESI mass spectra of the decay products for chloranil radical anion in water, open to air at room temperature.....	170

Figure 84. Magnification of isotope pattern for peak A in blue, with the calculated isotope pattern in red.....	170
Figure 85 Decay of chloranil radical anion in water under nitrogen environment, as observed from the EPR intensity	174
Figure 86. Comparison of the rates of decay under nitrogen (Blue) and open to air (Red).	175
Figure 87. EPR signal decay for chloranil radical anion in deionised water.....	176
Figure 88. Normalised EPR signal intensities for samples of batch 3 radical anion (100ppm) in water	177
Figure 89. Decay of chloranil radical anion in water under nitrogen environment.....	178
Figure 90. Normalised EPR signal intensities for samples of batch 3 radical anion (100 ppm) in water	178
Figure 91. Comparison of the rates of decay under nitrogen (Blue) and open to air (Red).	179
Figure 92. EPR spectra for the formation of the chloranil radical anion from tetrachloro hydroquinone, sodium hydroxide and chloranil, and combinations thereof.....	182
Figure 93. EPR spectra of di-tert-butyl hydroquinone in ethanol at different concentrations, spectra normalised (1mM - Green, 10mM – Blue and 1M - Red).....	184
Figure 94. The results of three runs for the comproportionation / disproportionation equilibrium at varying molar equivalents of quinone at -30°C.....	188
Figure 95. The results of three runs for the comproportionation / disproportionation equilibrium at varying molar equivalents of quinone at 0°C.....	188
Figure 96. The results of three runs for the comproportionation / disproportionation equilibrium at varying molar equivalents of quinone at 30°C.....	189
Figure 97. The results of three runs for the comproportionation / disproportionation equilibrium at varying molar equivalents of quinone at 60°C.....	189
Figure 98. The effect of excess base on a 1:1 hydroquinone: quinone mixture in ethanol. The concentration on the y-axis is the radical observed.	193
Figure 99. EPR signal of 2,5-diterbutyl semiquinone radical anion in ethanol at room temperature.....	197
Figure 100. EPR signal of 2,5-diterbutyl semiquinone radical anion in THF at room temperature.....	198
Figure 101. EPR signal of the 2,5-diterbutyl semiquinone radical anion in 2% ethanol / toluene at -60°C	199

Figure 102. ^{13}C NMR 700MHz of 312 fraction, low field, in CDCl_3 .	216
Figure 103. ^{13}C NMR 700MHz of 312 fraction, high field, in CDCl_3 .	216
Figure 104. COSY spectra of compound B. (700MHz, CDCl_3)	217
Figure 105. HSQC spectra of compound B. (700MHz, CDCl_3)	218
Figure 106. HMBC spectra of compound B. (700MHz, CDCl_3)	219
Figure 107. MS of compound D synthesised following the procedure by Rendy et al ¹⁰⁰ ...	221
Figure 108. ^{13}C NMR of the compound D . (400MHz, CDCl_3)	222
Figure 109. ^{13}C NMR of the compound D, low field magnification. (400MHz, CDCl_3)	222
Figure 110. COSY spectra of compound D. (400MHz, CDCl_3)	223
Figure 111. HSQC spectra of compound D. (400MHz, CDCl_3)	224
Figure 112. HMBC spectra of compound D. (400MHz, CDCl_3)	225
Figure 113. NMR of compound E mixture. (400MHz, CDCl_3)	226

List of schemes

Scheme 1 Demonstration of tacticity of polymers ³	25
Scheme 2. Initiation and propagation steps in radical polymerisation	27
Scheme 3 Thermal activation of dicumyl peroxide initiator.....	28
Scheme 4. Formation of a propagating radical mid chain in styrene polymerisation	28
Scheme 5. The termination through recombination of radicals.....	29
Scheme 6. Demonstration of disproportionation.....	29
Scheme 7. The initiation of vinyl monomers proposed by Hall ^{11, 12}	31
Scheme 8. The dimer bi-radical proposed by Flory ¹⁰ for the initiator in the thermal polymerisation of methyl methacrylate.	31
Scheme 9. A mechanism dismissed by Flory for the formation of an initiator in the thermal polymerisation of a vinyl compound.	31
Scheme 10. The Mayo mechanism for the self-initiation of styrene ^{18, 19}	32
Scheme 11. The dimerisation of methyl methacrylate following Diels Alder self-addition similar to that described by Mayo ^{18, 19}	33
Scheme 12 The Albisetti mechanism for methacrylate dimerization.....	34
Scheme 13. TEMPO mediated living polymerisation of styrene.....	35
Scheme 14. Formation of peroxy radical, polyperoxide and hydroperoxide. ³⁰	38
Scheme 15. The recombination of a radical initiator and TEMPO.....	39
Scheme 16. The proposed reaction for benzyl radicals with nitrobenzene, proposed by Jackson and Waters ^{45, 46}	40
Scheme 17. A variation of the mechanism in Scheme 16 ⁴⁷⁻⁴⁹	40
Scheme 18. The inhibition mechanism followed by benzoquinones ⁵⁰⁻⁵⁴	41
Scheme 19. Electron donation by PTZ to an initiator radical.....	42
Scheme 20. A possible route the PTZ radical cation can take after the initial inhibition.	42
Scheme 21. The mechanism for radical polymerisation inhibition. Top – Propagation. Middle – Initiator reacting with oxygen. Bottom – Peroxy radical abstracting hydrogen from an inhibitor molecule, ArOH	43
Scheme 22. Schematic of the small scale, automated dilatometry setup, developed to determine the onset of polymerisation after inhibition or retardation.....	58
Scheme 23 A common polymerisation inhibitor (DNBP, left) with analogues investigated; 2,4-dinitrophenol (middle) and 2-nitrophenol (right)	72
Scheme 24. Demonstration of phenolic inhibition mechanism ^{55, 85}	76

Scheme 25. The resonance structures of a phenoxy radical	77
Scheme 26. The resonance structures of 2-nitrophenol after phenolic hydrogen donation.	78
Scheme 27. The proposed mechanism for the formation of a product isolated and characterised by Bushby et al ⁴⁵	88
Scheme 28. Formation of nitroso arene as proposed by Bartlett et al ⁹⁴ , via a nitroxide intermediate.	94
Scheme 29. Formation of nitroso arene proposed by Jackson and Waters ⁴⁶ , via an alkoxynitroxide intermediate.....	95
Scheme 30. Formation of nitroxide from 2-nitrophenol, observed by EPR.....	95
Scheme 31. Proposed formation of Unknown B following previous research by Jackson and Waters ⁴⁶ , and by Bushby et al ⁴⁵	97
Scheme 32. Photolysis of chloroform ⁹⁹	117
Scheme 33. Photooxidation of chloroform ^{97, 98}	117
Scheme 34. Mechanism of oxidation and formation of product observed by X-ray crystallography.....	118
Scheme 35. Possible mechanism for the formation of Unknown B.	120
Scheme 36. Retro-synthetic analysis of compound A.	121
Scheme 37 Synthesis of compound D ¹⁰⁰	122
Scheme 38. Formation of Imine (Compound E) from compound D and 2-aminophenol...	129
Scheme 39. Mechanism of the formation of unknown B from compound E.	130
Scheme 40. Hydrogen abstraction from 2-aminophenol by an initiator radical.	137
Scheme 41. Possible mechanism of an initiator radical adding to the imine, compound E.	139
Scheme 42. Synthesis of compound F	140
Scheme 43. Literature proposed mechanism for reaction of nitrosobenzene and styrene. The m/z values are the [M+H] ⁺ ions observed ¹⁰³	146
Scheme 44. Possible route for the formation of products observed from the reaction between 2-nitrosophenol and styrene	151
Scheme 45. Demonstration of the exchange experiment	153
Scheme 46. Formation of nitroxide from nitron intermediate postulated based on work by Kang et al ¹⁰³	156
Scheme 47. The simplified reactions describing the formation of radical initiators, where M is monomer, D is dimer and R the radical initiator.	158

Scheme 48. The initial reaction between 2-nitrophenol and an initiator radical.....	160
Scheme 49. The formation of Compound B	161
Scheme 50. Formation and degradation of charge transfer complex proposed by Yassin and Rizk.....	164
Scheme 51. The proposed mechanism for the inhibition of polymerisation, at low amine concentrations.....	165
Scheme 52. The initial step in the inhibition of polymerisation at high amine concentrations.....	165
Scheme 53. The second step of the inhibition mechanism.....	165
Scheme 54. Chain transfer from ammonium ion to anion of the complex.....	166
Scheme 55. Synthesis of chloranil radical anion potassium salt.....	168
Scheme 56. Formation of mono-hydroxy substituted chloranil.....	172
Scheme 57. Formation of radical anion dimers at peaks m/z 434.82 and m/z 452.78	172
Scheme 58. Formation of a radical anion trimer at peak m/z 624.76	173
Scheme 59. Comproportionation / disproportionation between chloranil and tetrachloro hydroquinone.....	181
Scheme 60. Chemical exchange of 2,5 – di-tert-butyl semiquinone with 2,5 – di-tert-butyl hydroquinone dianion.....	183
Scheme 61. The comproportionation / disproportionation equilibrium of 2,5 – di-tert-butyl hydroquinone and 2,5 – di-tert-butylquinone.....	186
Scheme 62. A possible mechanism for the formation of mono substituted product observed in the reaction between the quinone and excess base.....	194
Scheme 63. The new comproportionation / disproportionation equilibrium set up in a system of quinone and base	195
Scheme 64. Resonance structures for the radical anion showing the dissociation of the sodium ion and equivalence of the aromatic hydrogens.....	196
Scheme 65. The slow ion exchange of the sodium ion, demonstrating the two different proton environments.....	197

List of tables

Table 1. Inhibition times of potential inhibitors, tested by heating 5 ml sample of the inhibitor in styrene at 130°C. ⁶²	52
Table 2. Table of change in volume after complete polymerisation for a number on monomers ⁷⁵ . Density measured at 25 °C unless denoted by ^a	55
Table 3. Results of GC/MS on styrene inhibited by 2-nitrophenol.	93
Table 4. High field protons of unknown B. From 700 MHz data, performed in CDCl ₃	108
Table 5. Summary of proton signals for Unknown B and their couplings in COSY, HSQC and HMBC NMR experiments. (700 MHz NMR experiments, performed in CDCl ₃ .)	114
Table 6. Summary of proton signals of compound D and their couplings in COSY, HSQC and HMBC NMR experiments. (400 MHz, CDCl ₃).	125
Table 7 Structures of fragments formed in the MS / MS experiment on Unknown B or Compound A	133
Table 8. Possible structures of products from the decomposition of chloranil radical anion potassium salt in water. The MS peaks correspond to [M+H] ⁺ ions of the proposed structures.	171
Table 9. Equilibrium constants, enthalpy and entropy for the comproportionation / disproportionation equilibrium in ethanol	190
Table 10. Structures for possible products for the decomposition of quinone in base	194
Table 11. Equilibrium constants, enthalpy and entropy for the comproportionation / disproportionation equilibrium of 2,5 – di-tert-butyl hydroquinone and 2,5 – di-tert-butylquinone in 2% ethanol / toluene	200
Table 12. CHN results for chloranil radical anion potassium salt	209
Table 13. Summary of carbon signals and their couplings in HSQC and HMBC NMR experiments (700MHz, CDCl ₃).	220
Table 14. Summary of carbon signals of compound D and their couplings in COSY, TOCSY, HSQC and HMBC NMR experiments. (400MHz, CDCl ₃)	226
Table 15. Crystal data and structure refinement for Unknown B.	227
Table 16. Fractional Atomic Coordinates (×10 ⁴) and Equivalent Isotropic Displacement Parameters (Å ² ×10 ³) for vc1301. U _{eq} is defined as 1/3 of the trace of the orthogonalised U _{ij} tensor.	228
Table 17. Anisotropic Displacement Parameters (Å ² ×10 ³) for vc1301. The Anisotropic displacement factor exponent takes the form: -2π ² [h ² a ² U ₁₁ +...+2hka×b×U ₁₂]	229

Table 18. Bond lengths for Unknown B as determined by X-ray crystallography	230
Table 19. Bond Angles for Unknown B as determined by X-ray crystallography	231
Table 20. Hydrogen Atom Coordinates ($\text{\AA}\times 10^4$) and Isotropic Displacement Parameters ($\text{\AA}^2\times 10^3$) for vc1301.....	232

List of equations

Equation 1. Determination of energy levels of an electron in an applied magnetic field. ...	45
Equation 2. Determination of level occupancy using the Maxwell-Boltzmann distribution	46
Equation 3. Formula for the calculation of Double Bond Number, where C is the number of carbons, H the number of hydrogens, X the number of halogens and N the number of nitrogens	116
Equation 4. Rate of formation of initiator radicals, from the reaction between monomer and dimer.....	158
Equation 5. Rate of formation of the styrene dimer.	158
Equation 6. The disproportionation of semiquinone radical to quinone and hydroquinone	166
Equation 7. The rate equation for the equilibrium ([SQ], [Q] and [HQ] are concentrations of semiquinone, quinone and hydroquinone.)	186
Equation 8. The relationship between initial starting concentrations and the concentration of components once equilibrium is established.	186
Equation 9. Combination of Equation 7 and Equation 8.....	187
Equation 10. The rate equation for the equilibrium expanded, then arranged in way that can be solved, and the coefficients a, b and c used to solve the quadratic equation	187
Equation 11. The Eyring equation.....	190
Equation 12. Relationship between pK_a and K_a	190
Equation 13. Determination of the acid dissociation constant, K_a	191
Equation 14. Relationship between starting concentration of the acid ($[HA]_0$) and the concentration of the acid and the conjugate base in the system.	191
Equation 15. Combining Equation 13 and Equation 14	191
Equation 16. Determination of pH.....	191
Equation 17. Method of converting the literature data to a form comparable to the work above.....	192
Equation 18. The relationship between the concentrations of semiquinone, quinone and hydroquinone.....	200
Equation 19. The equilibrium equation simplified to include concentrations of observable species.....	200
Equation 20. The quadratic equation that can be solved, to determine the remaining semiquinone concentration.....	201

Acknowledgments

This thesis would not have been possible without the support, help, advice and distractions from many people. I hope to express my thanks to as many as I can below.

I'd like to thank my parents, Jane and Alastair, and my sister, Lorna, for their never ending support before, during and after my time at university.

I would like to thank Victor for his patience, technical know-how and down to earth support he gave me over the past 4 years. Thanks also to the VC Group over the years; Kazim, Rob S, Chiara, Sindhu, Zhou, Rob T, Dave, Jamie, James and Warsi. I hope I helped you as much you all helped me (probably not though). Thanks also to the people outside of the VC madness; Kate, Chris, Natalie P, Danielle, Rob M, and even to the undergrads who I have demonstrated over the years.

I would like to thank the people at Nufarm Ltd for their support; Peter, Colin, Angela, Andy, Steve and Tony.

A huge thanks and hug has to go to Jennifer, whose help has kept me "sane" through this endeavour. The Gilbert and Sullivan society and Pure Lindy also deserve praise for stopping me from becoming a complete recluse, but especially thanks to Lauren, Chris, Vernia, James G, James K, Morven, Sophie, Natalie S and Ella.

I dedicate this thesis to my grandfathers, Tom and Ted. The astute readers among you may have noticed that I was named after both of them. Ted always asked how my time at university going, but unfortunately passed away before it was complete. My other granddad, Tom, passed away before I was even looking at universities. His nickname for me was "Boots", which I did not connect until recently with the name of another well-known "chemist". I would like to think that, wherever he may be, he is having the last laugh now with a joke 27 years in the making.

That's the sentimental part over. You've read your name (you know who you are) and there is no need to read on any further. It's just chemistry from this point on.

Authors declaration

The following was carried out by Thomas Edward Newby, under the supervision of Dr Victor Chechik. This work has not previously been presented for an award at this, or any other, University. All sources are acknowledged as References.

The NMR analysis of unknown Compound B and ketone compound D was performed with the assistance of Dr Robert J Thatcher.

A number of DFT calculations were performed by Kate Horner.

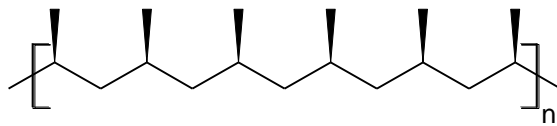
1. Introduction

Polymers are an important material used throughout the world. The production of monomers for plastics is therefore a diverse and grand scale operation. In 2010, approximately 25 million tons of styrene were produced globally.¹ Understanding the production of these polymers, and how they are controlled, is vital to meet the world's demand.

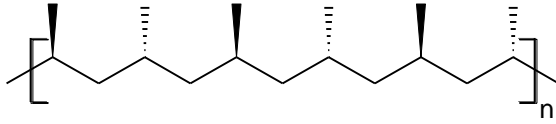
1.1 Properties of a polymer

The properties of the polymer depend upon a number of factors. The most observable property that relates directly to the structure and make-up of the polymer is the Glass Transition Temperature, T_g .² This is given as the temperature when the Gibbs free energy is above the energy needed for the polymer chains to move over each other when a force is applied. Visibly, this results in the plastic going from hard and brittle to malleable and rubber-like. The interactions between the chains affect this value greatly. For example, the addition of hydrogen bonds between chains greatly increase the activation energy needed for the chains to move over one another, and therefore the glass transition temperature increases also.

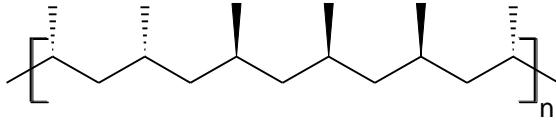
The orientation of the monomer within the chain is also important³. If the tacticity is regular down the chain, then the individual chains can pack closer together forming stronger intermolecular bonds, increasing T_g . If bulky side groups align, then they will keep chains apart forming weaker bonds, lowering T_g . There are three terms associated with tacticity, which are demonstrated in Scheme 1. Isotactic chains have the same chirality for each monomer unit, Syndiotactic alternate the orientations of each monomer unit, and Atactic are randomly orientated. Each form of polymer will have different properties to each other.



Isotactic



Syndiotactic



Atactic

Scheme 1 Demonstration of tacticity of polymers³

The molecular weight of the chains will have an effect on the macroscopic properties of the polymer. Longer chains will result in greater overlap of chains allowing more intermolecular bonds to form. The more intermolecular bonds form between chains, the greater the restriction of movement between the chains. Figure 1 shows the relationship between different properties and the molecular weight of the polymer chains.

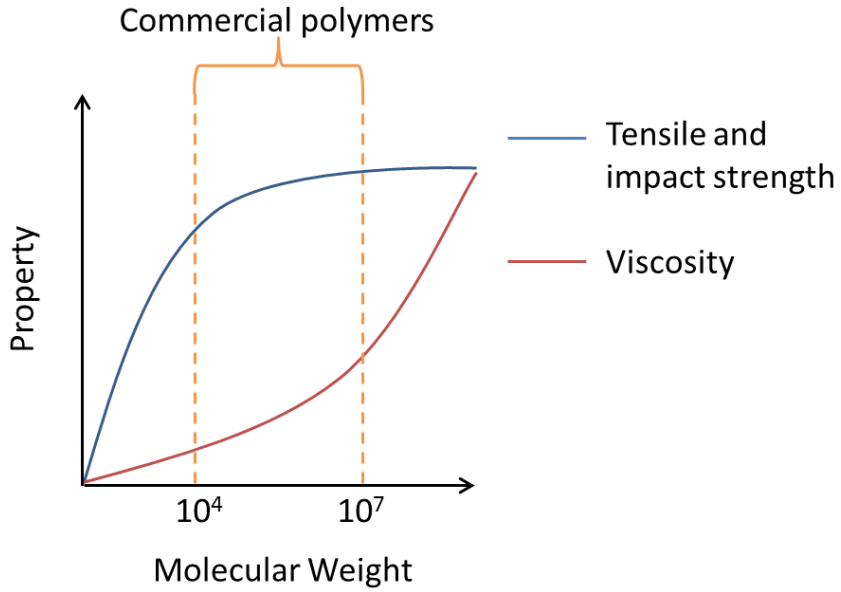


Figure 1. Relationship between chain length of a polymer and its properties; viscosity, tensile and impact strength

Introducing a monomer that can form two bonds with the other monomers is called cross linking. These cross linkages restrict the movement of polymer chains over each other significantly, and form less elastic materials, as shown in Figure 2.

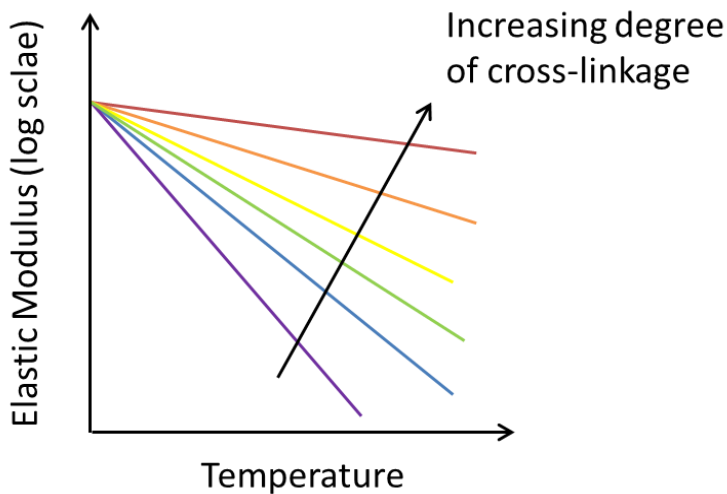


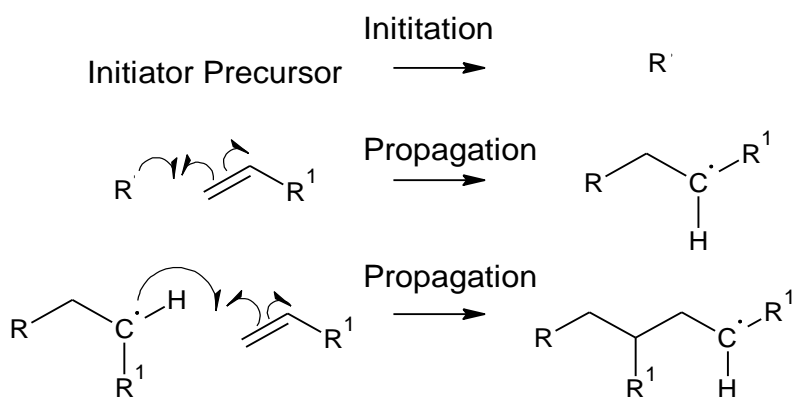
Figure 2. Relationship between the elastic properties of a polymer and its degree of cross-linkage

Controlling the chemical reactions that form the polymer chains is vital to making polymer materials that fit specific physical and mechanical properties.

1.2 Radical polymerisation

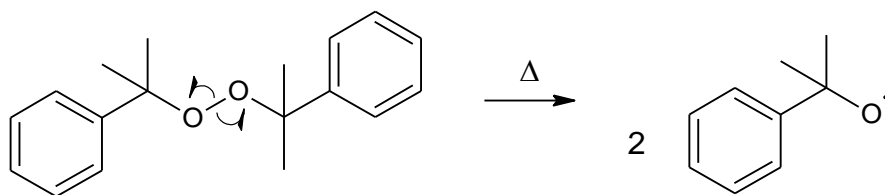
Radical polymerisation describes the mechanism of polymerisation where the propagation species is a radical. Compared to similar cationic and anionic polymerisations, radical polymerisation is less discriminating in the propagating reaction, leading to a greater number of possible propagation and termination routes⁴.

Similarly to other polymerisations, the different reactions fall under the categories, initiation (the start of the process), propagation, (the continuation of the process) and termination (the quenching of the propagation species). A brief demonstration of these reactions is given in Scheme 2, for the radical polymerisation of a vinyl monomer.



Scheme 2. Initiation and propagation steps in radical polymerisation

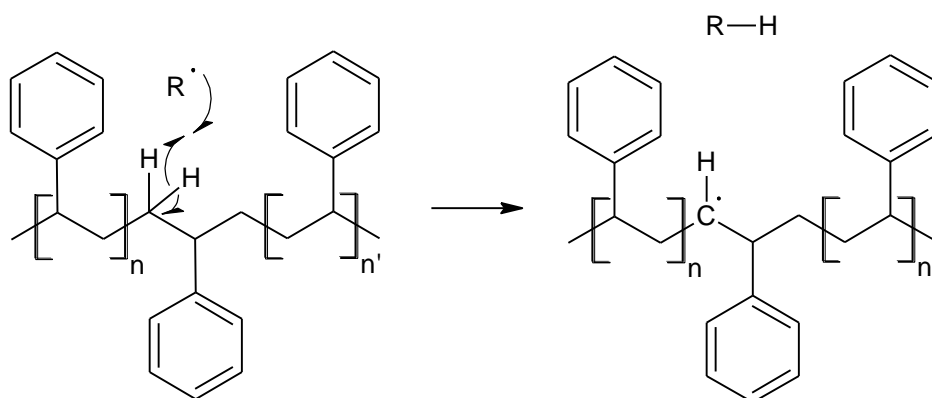
To initiate the radical polymerisation, there are a number of molecules and techniques that can be applied. The use of initiators that activate under different conditions is a common practice. Scheme 3 shows the thermal activation of dicumyl peroxide, demonstrating how one precursor can break down into two radical initiators. Another approach is to break the bond photolytically^{5,6}



Scheme 3 Thermal activation of dicumyl peroxide initiator

The next stage is propagation. This is where an initiator reacts with another monomer, leading to a dimer. The oxygen centred radical initiators have a strong affinity towards the double bonds of the monomers, leading to a rapid and selective reaction. The dimer is also a radical, as shown in the second line of Scheme 2, with no reason to not react with another monomer. Each time the chain grows one unit longer, the terminal unit still contains a radical, with the capability to react further.

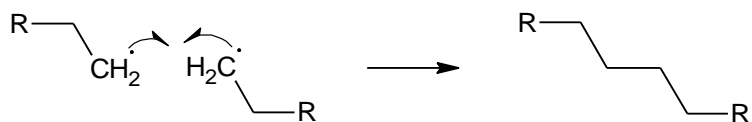
In addition to the propagation, branching may also occur. A branch polymer leads to lower tensile strength and lower melting point. For branching to occur, a hydrogen would need to be abstracted mid chain by another radical initiator, as shown in Scheme 4.



Scheme 4. Formation of a propagating radical mid chain in styrene polymerisation

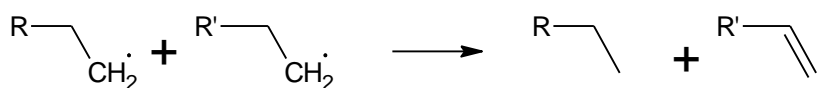
The termination of the propagating polymer chains can occur through different ways. The recombination of two radicals (Scheme 5) is most common and occurs when the

concentration of propagating radicals is high. This removes two propagating species and returns an inactive species.



Scheme 5. The termination through recombination of radicals

Other routes of termination are available. Disproportionation is where two radicals react, forming an alkane and an alkene, as shown in Scheme 6. This is particularly important at high radical concentrations.



Scheme 6. Demonstration of disproportionation

The abstraction of a hydrogen by the propagating species will lead to the chain becoming inactive. Providing the molecule that has lost the hydrogen does not propagate then termination has occurred. The oxidation or reduction of the propagating radical through reaction with metal ions or other redox reagents will also lead to termination. The mechanism and rate of termination are important factors to consider when forming polymers, as these can decide the properties of the plastic. A fast rate of termination will produce a completely different plastic compared to those made with a slow rate of termination.

1.2.1 Spontaneous polymerisation

The use of initiator molecules is not the only way to start polymerisation. All monomers will polymerise in one way or another when stored prior to use or when heated^{7,8}.

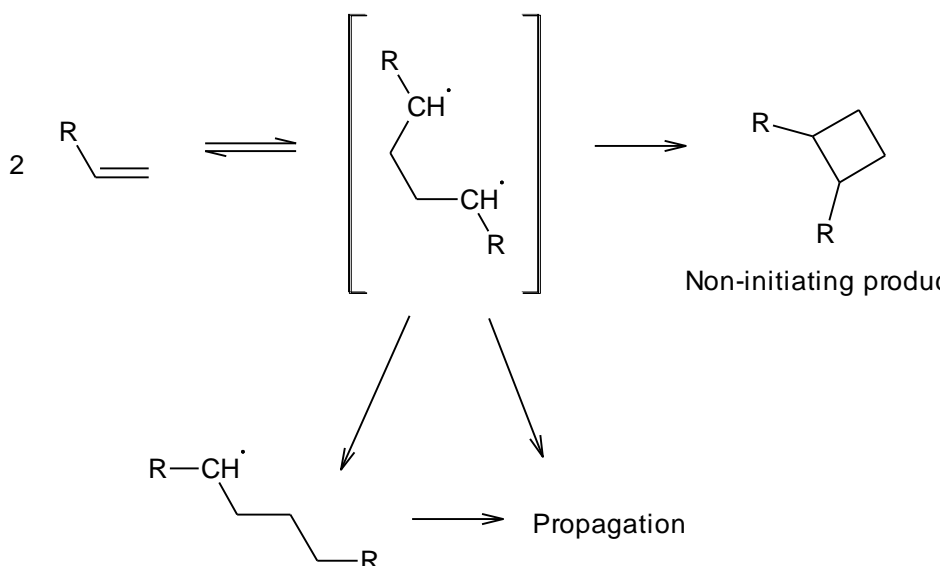
Spontaneous polymerisation produces polymers that have very little practical use, as well as consuming monomer⁹. Another factor to include is the heat of polymerisation, as an unchecked reaction will cause heat to build up in a container, as the polymerisation reaction continues.

The mechanism of this spontaneous reaction varies between different types of monomer. Also, there are cases of what appears to be spontaneous polymerisation, but the observed polymerisation is actually due to other mechanisms. UV radiation can cause the formation of initiators. Most monomers will react with oxygen, some forming hydroperoxides that act as initiators. Monomers can also contain other impurities such as metals which could lead to redox initiation. Combining these factors, apparently spontaneous initiation could occur without the monomer reacting with itself.

However apart from these reactions, there are mechanisms for genuine self-initiation which are discussed in this section.

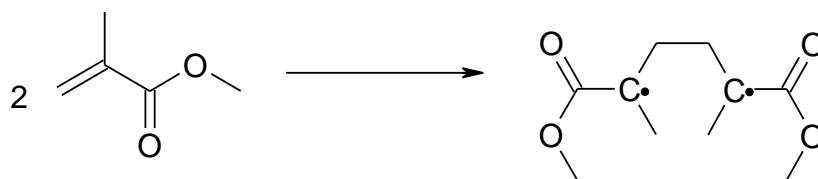
1.2.1.1 Bi-radical mechanism

The first to propose a mechanism for the spontaneous polymerisation of vinyl monomers was Flory back in 1937¹⁰, with more work conducted by Hall et al^{11,12}. This involved the formation a bi-radical. Bi-radicals, by their nature, are extremely reactive and will react by the routes given in Scheme 7; the radicals could recombine to form non-initiating products; a radical could abstract a hydrogen, forming a radical dimer and another radical; or both of the radicals can propagate the polymerisation.

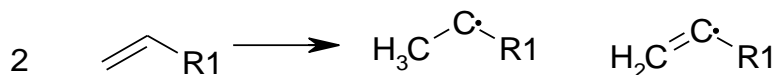


Scheme 7. The initiation of vinyl monomers proposed by Hall^{11,12}

When investigating specifically acrylates and methacrylates, Flory used the experimental activation energies and the known bond dissociation energies to show that the formation of a biradical is a possible route, as shown in Scheme 8, whereas the formation of 2 different radicals as shown in Scheme 9 does not match experimentally found activation energies.



Scheme 8. The dimer bi-radical proposed by Flory¹⁰ for the initiator in the thermal polymerisation of methyl methacrylate.

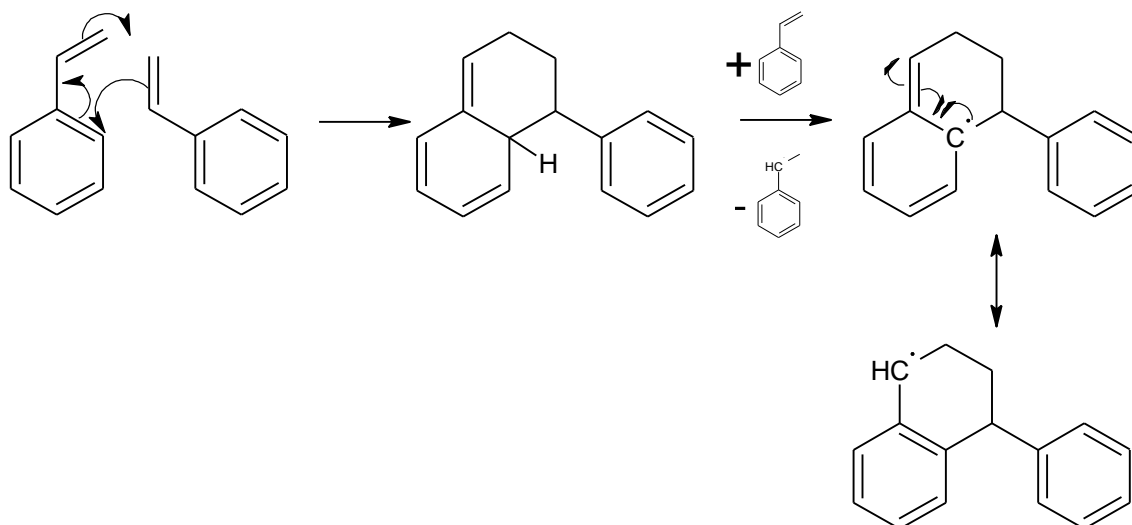


Scheme 9. A mechanism dismissed by Flory for the formation of an initiator in the thermal polymerisation of a vinyl compound.

The biradical mechanism was also suggested for the formation of some of the dimers observed by Lignau et al¹³, as discussed earlier. Figure 3 shows the dimers cCB and tCB, which could form from the biradical.

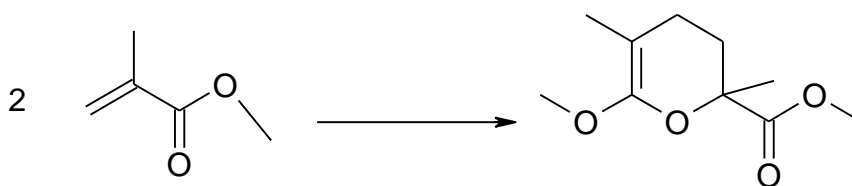
1.2.1.2 Pericyclic mechanisms

In the case of styrene the mechanism of thermal polymerisation has been studied much more^{10, 14-17}. Although the Flory mechanism can take place, Mayo¹⁸⁻²⁰ identified the initiation, given in Scheme 10, that involves the dimerisation of styrene by a Diels Alder mechanism²¹⁻²³. This can then undergo hydrogen abstraction giving a radical initiator. This hydrogen abstraction is relatively favourable due to the aromatic ring reforming due to resonance, shown in Scheme 10.



Scheme 10. The Mayo mechanism for the self-initiation of styrene^{18, 19}

The mechanism that acrylates and methacrylates follow during self-polymerisation is not as well understood²⁴. These, for example, do not follow the same mechanism as proposed by Mayo for styrene. Scheme 11 demonstrates the product formed if they were to follow the Mayo mechanism^{13, 25, 26}.



Scheme 11. The dimerisation of methyl methacrylate following Diels Alder self-addition similar to that described by Mayo^{18, 19}

However, this mechanism has been dismissed very quickly by all authors that have suggested it. There has been much debate as to the mechanism of the initiation²⁷. Lingnau et al¹³ investigated the mechanism by observing the initial products formed. They used gas chromatography to observe a “spectrum” of the dimers and trimers formed. They did not detect the Diels Alder product in their study. Figure 3 shows some of the dimers observed.

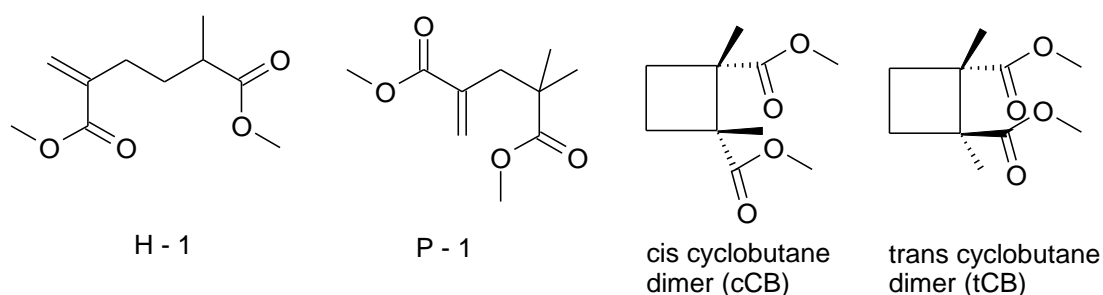
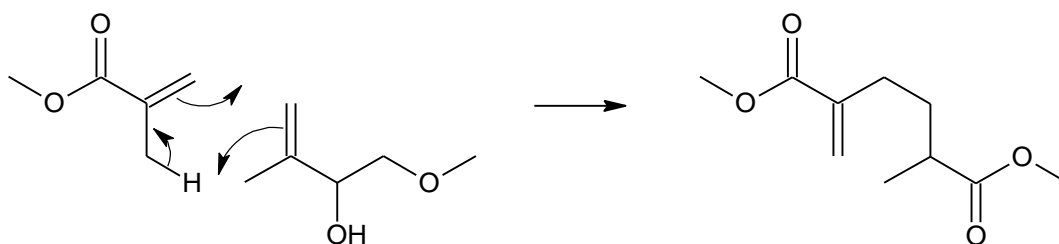


Figure 3. Dimers and trimers found after the self-polymerisation of methyl methacrylate. Two other dimers were observed but could not be characterised due to low quantities

There has been a third mechanism suggested, also by Lingnau et al²⁸. The other dimers in Figure 3, H – 1 and P – 1, are formed through the Albisetti mechanism. The actual mechanism suggested by Albisetti²⁹ is only for the dimerisation, as in Scheme 12, but Lingnau has suggested this dimer has the potential to become a radical initiator, due to an easily abstractable hydrogen on the tertiary carbon. This can be easily removed and propagate the spontaneous polymerisation.



Scheme 12 The Albisetti mechanism for methacrylate dimerization

There is evidence that these “Albisetti dimers” are present in the product mixture. The authors have examined the enthalpies and entropies of thermal initiation. They compared the theoretical values for the formation of a biradical with the formation of the dimers observed. They found that the pathway that fitted the calculated values was through the Albisetti mechanism.

The general consensus for the spontaneous initiation for these monomers, is that the bi-radical is formed by the Flory mechanism (Scheme 8) with the Albisetti dimer forming alongside. The Albisetti dimer could have a hydrogen abstracted leading to the formation of an initiator, but this is still unknown.

Only after the mechanism for the formation of the polymerisation initiator species has been determined can the inhibition and prevention of spontaneous polymerisation be optimised.

1.2.1 Living radical polymerisation

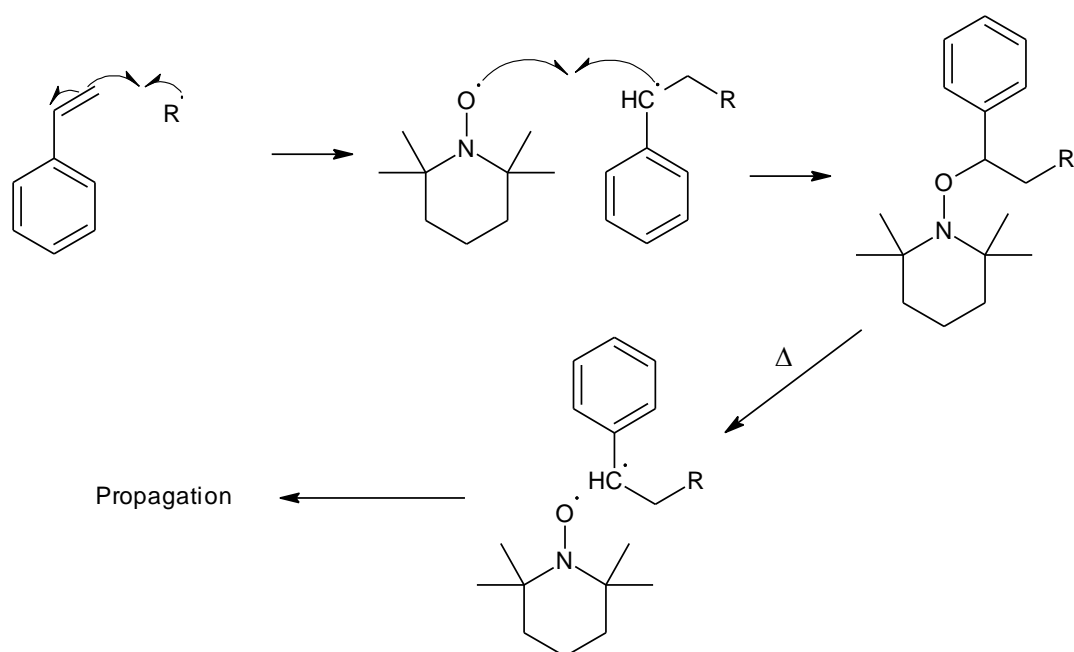
Living polymerisation is a way of controlling the dispersity of molecular weights in a polymer. This mono-dispersity will have an effect on the macroscopic properties of the polymer. This is usually achieved by using polymerisation reactions in which termination does not occur.

Polymerisation with little termination leads to a low poly-dispersity. This means a narrow range of polymer lengths. Controlling the chain lengths will affect the macroscopic properties of the polymer.

Living polymerisations have the ability to continue until all of the monomer is consumed. Then, they have the ability to continue with the addition of more monomer, either the same type or a different monomer. This is one method of producing block co-polymers.

In radical living polymerisation it is difficult to remove the termination pathways, due to the nature of radicals themselves. Therefore, a different approach is used for controlling the polymerisation, such as making the termination step reversible.

To control the radical polymerisation, molecules are used to reversibly cap the end of the living chain. A stable free radical such as TEMPO is a common example, as it acts as an inhibitor, effectively terminating the polymerisation by recombining with the propagating species. The polymer chains now are capped with TEMPO. Applying heat breaks the oxygen-carbon bond formed in the termination step, releasing a propagating species to further react, along with TEMPO. The process is demonstrated in Scheme 13.



Scheme 13. TEMPO mediated living polymerisation of styrene.

1.3 Inhibition of polymerisation

Inhibition is the term used to describe the prevention of spontaneous polymerisation from propagating and consuming the monomer. TEMPO-mediated living polymerisation (Section 1.2.1, page 34) can be viewed as inhibited polymerisation, as the growing chains are capped or terminated by TEMPO. The actual initiation of the monomer cannot be stopped completely, but ways of limiting the initiation are possible. For example, using opaque containers to store UV susceptible monomers will reduce the spontaneous initiation through that mechanism. Another example is to refrigerate the monomer, which will reduce the rate of spontaneous initiation. However, these methods are not practical when the monomer is to be used. You cannot distil a monomer to purify it at cold temperatures, so another method of inhibiting them is needed.

To inhibit the polymerisation, additional compounds can be added to act as inhibitors. These inhibitors must react preferentially with the propagating chain or initiator radical to produce non-initiating products after the reaction. The properties of these inhibitors are chosen for the specific purpose and environment, for example, certain molecules work best at higher temperatures or under specific atmospheres.

True inhibitors react with the initiating radicals very rapidly, which removes them before they can propagate, effectively stopping the polymerisation. These inhibitors are useful during the production of the monomer, as any polymer that forms, even relatively short chain polymers can reduce efficiency or cause damage to the equipment.

Another category of inhibitors are called retarders. These react with initiating radicals more slowly and competing polymerisation is not stopped completely thus leading to a slow build-up of polymer. These are also used in industrial processes where the monomer needs to be heated for a long period of time, for example in a distillation.

As well as in industrial processes, inhibitors are used during the storage of monomers. As well as preventing loss of monomer, they stop runaway polymerisations that cause the build-up of temperature and pressure in the storage vessel. This is a dangerous position that needs avoiding.

In order to choose the correct inhibitor for the practical use in question, the mechanisms of inhibition by different types of inhibitors must be understood. Some types of inhibitors

work under different conditions better than others. Choosing the wrong type can be dangerous as well as wasteful.

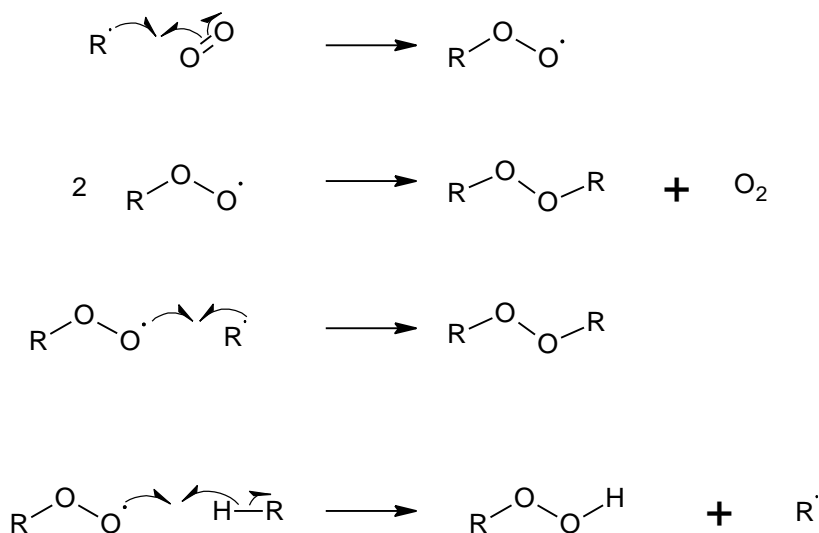
1.3.1 Direct reaction with initiator radical

One mechanism of the inhibitor action is a direct reaction with the initiating or propagating radicals, in order to prevent propagation. There are a number of inhibitors that work in this way, but with differences. Stable free radicals will react with the initiator forming a non-radical species, unable to propagate. Other molecules chosen will react selectively with the initiator and produce non-initiating radicals effectively ending the propagation. These differences in the inhibition mechanisms determine where and when they are used.

1.3.1.1 Oxygen

The way in which oxygen inhibits is through the formation of polyperoxides by directly reacting with the radical initiator, as shown in Scheme 14^{4,30}. The oxygen reacts with the radical initiator and forms the peroxy radical. This is very similar to the auto oxidation of oils and fatty acids, and has been researched regularly. (The references given³¹⁻³⁷ are some examples) This reaction is diffusion controlled and will out-compete the propagation pathway, halting the progress of the polymerisation. Once the oxygen is consumed however, the propagation pathway opens up again, as with all other inhibitors. A practical issue with using oxygen is the addition of inhibitor to the system. Oxygen cannot be loaded into a reactor the same way as a solid inhibitor could.

Once the peroxy radicals form, they react further through similar mechanism to termination reactions, removing them from the polymerisation and inhibition. Examples are given in Scheme 14. The peroxy radicals formed can react further and initiate monomers³⁸, causing polymerisation. Particularly at high temperatures, using just oxygen to inhibit is not an efficient method of inhibition.



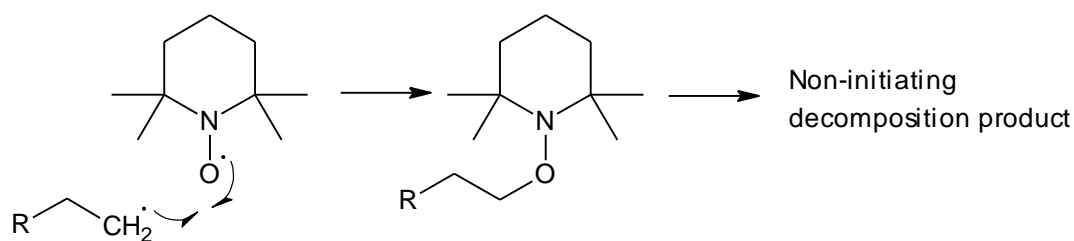
Scheme 14. Formation of peroxy radical, polyperoxide and hydroperoxide.³⁰

1.3.1.2 Stable radicals

The recombination of radicals is an important termination route in any polymerisation. As the concentration of radicals increases, the rate of recombination increases as well. The use of stable free radicals as inhibitors comes from this logic³⁹⁻⁴¹.

A common inhibitor used is 2,2,6,6-tetramethyl-1-piperidinyloxy (TEMPO) and similar derivatives⁴²⁻⁴⁴. By adding these stable radicals to the monomer sample, the polymerisation is inhibited as the propagating radical and a TEMPO radical would recombine, effectively increasing the rate of termination. The rate constant of styrene propagation⁴² is $2.2 \times 10^3 \text{ M}^{-1} \text{ s}^{-1}$, whereas the rate of reaction between TEMPO and a styrene initiator⁴² is $8 \times 10^8 \text{ M}^{-1} \text{ s}^{-1}$. This means TEMPO will out-compete styrene polymerisation propagation even at low concentration.

These inhibitors directly react with the initiator to remove it from the propagation, as in Scheme 15, rather than relying on oxygen to react first.

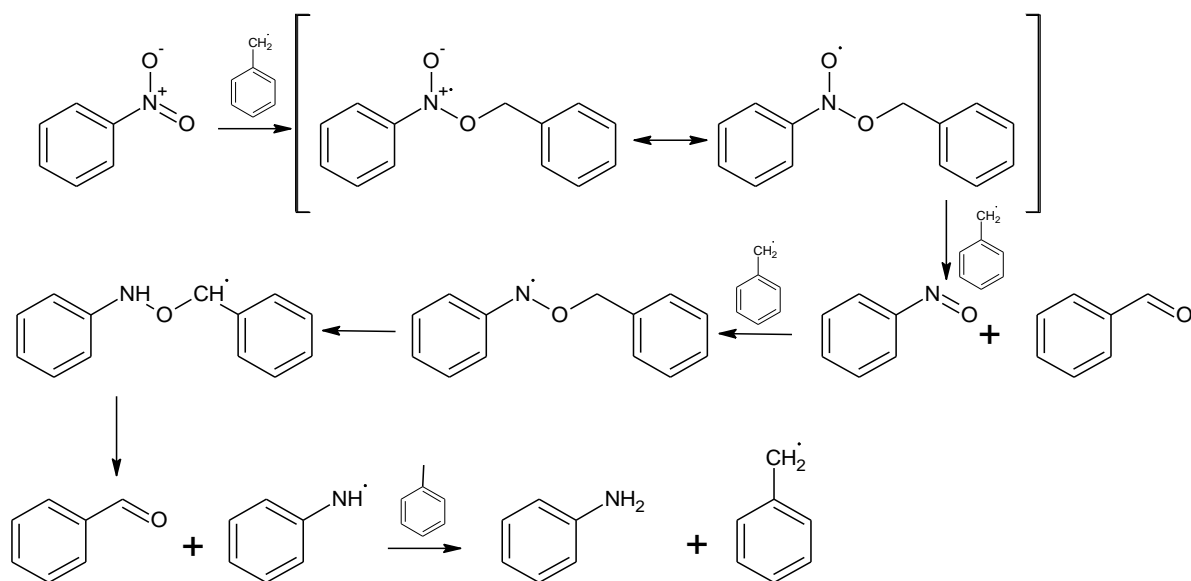


Scheme 15. The recombination of a radical initiator and TEMPO.

1.3.1.3 Nitroaromatics and nitrophenols

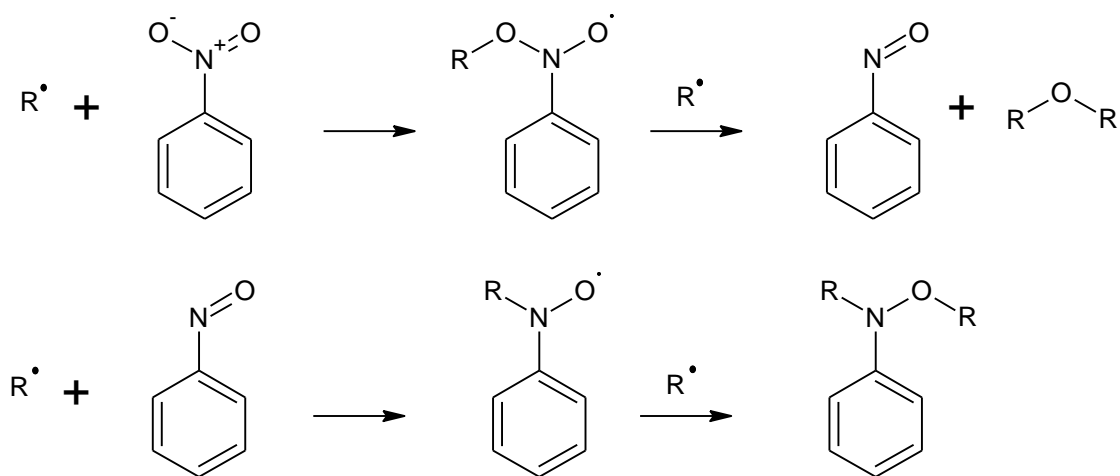
Nitrophenols are also used as polymerisation inhibitors in industry. DNBP (2,4-dinitro-6-sec-butylphenol) is a commonly used styrene inhibitor. The mechanism by which it inhibits is not completely known, but it is believed that there may be a number of pathways, which adds to its efficiency.⁴⁵ The functional groups available lead to two possible mechanisms, via the phenol or the nitro group. Literature has given a number of possible routes for the nitro group pathway.

Jackson and Waters⁴⁶ used benzyl radicals as the styrene initiator analogue. They proposed that the nitro group is reduced via a nitroso group, ending with aniline. The other product is two equivalents of benzaldehyde. This gives 1:2 inhibitor to radical ratio for the reaction and could explain the efficiency of DNBP. Aniline and benzaldehyde were isolated from the reaction mixture and the authors proposed the reaction in Scheme 16.



Scheme 16. The proposed reaction for benzyl radicals with nitrobenzene, proposed by Jackson and Waters^{45,46}

Another mechanism, suggested by Tudos⁴⁷, agreed with Jackson and Waters for the initial stage of the reaction. However, a different pathway for the second reaction was suggested where a nitroso intermediate traps a propagating radical to form a nitroxide. This is shown in Scheme 17. The products of this are an alkoxyamine and an ether. It is unknown if one or both of these proposed mechanisms are true.



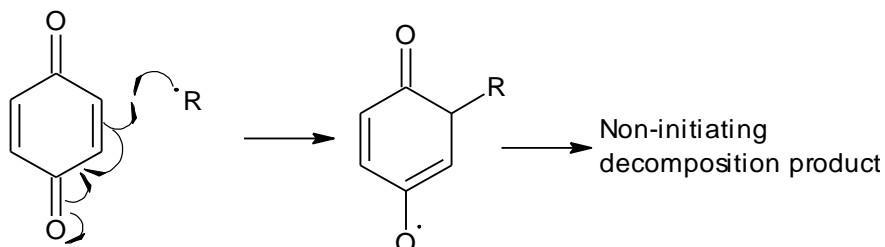
Scheme 17. A variation of the mechanism in Scheme 16⁴⁷⁻⁴⁹

This however only covers the nitro functional group of nitrophenol inhibitors. A phenolic inhibitor mechanism has been presented below (Section 1.3.2.1). DNBP, the industrially used inhibitor is a nitrophenol, is much more efficient than the sum of the equivalent nitro and phenol parts. The mechanism, which would explain synergistic action of nitro and phenol group in the nitrophenol inhibitors, still eludes us at the moment.

1.3.1.4 Quinones

The use of quinones as inhibitors is an example of a non-radical inhibitor that reacts directly with the initiator radical. They work by reacting with the propagating species^{50, 51}, and form a non-initiating radical as a product^{52, 53}.

The added advantage of this is that the non-initiating radical can recombine with another propagating radical to form another non-reactive product. This removes two equivalents of propagating radical per inhibitor, which as stated before is always preferable. Scheme 18 shows the initial reaction between benzoquinone and an initiator.

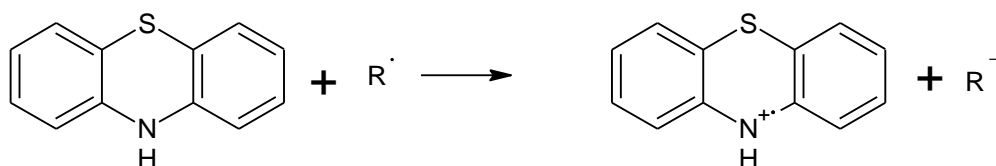


Scheme 18. The inhibition mechanism followed by benzoquinones⁵⁰⁻⁵⁴

Substituted quinones are often the preferred choice in industrial applications for the inhibition of unwanted spontaneous polymerisation.⁵⁴ The substitutions are there to improve stability of the radical adducts, driving the reaction onwards.

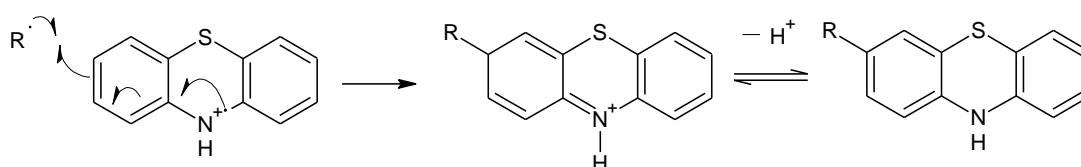
1.3.1.5 Phenothiazine

Phenothiazine (PTZ) and derivatives are known efficient inhibitors⁵⁵. They work via a number of mechanisms. When reacting directly with the initiator radicals, electron transfer occurs, reducing the radical initiator to an anion, as shown in Scheme 19.



Scheme 19. Electron donation by PTZ to an initiator radical

The anion is no longer able to propagate via the radical polymerisation route. The radical cation that is formed can abstract a hydrogen to form a cation that will eventually reform PTZ. Alternatively, another radical initiator can react with the radical cation, as shown in Scheme 20. The loss of a proton reforms a PTZ derivative that can inhibit further.



Scheme 20. A possible route the PTZ radical cation can take after the initial inhibition.

PTZ can also react with a peroxy radical, forming peroxy anion, and the PTZ radical cation. The cation follows the same routes and the peroxy anion will eventually get protonated. This however is not the dominant route of inhibition for PTZ. PTZ is often used due to its ability to work effectively without oxygen.

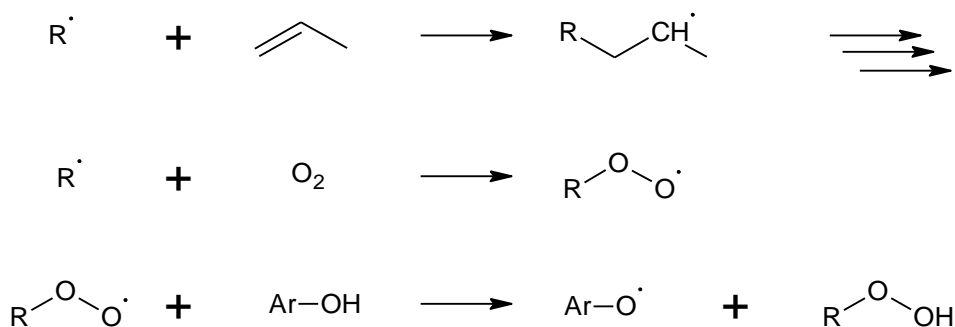
Other inhibitors can react in a similar fashion to PTZ, and react with the peroxy radical formed from an initiator and oxygen.

1.3.2 Reactions of inhibitors with peroxy radicals

To take advantage of the very fast reaction of the propagating radicals with oxygen, some inhibitors are used to work in conjunction with oxygen and remove the peroxy radicals from the system to stop them from initiating the polymerisation.

1.3.2.1 Phenolics

The addition of phenols to the monomer sample inhibits the polymerisation by following Scheme 21 below^{56,57}. The initiator radical that would propagate the polymerisation (Top line) reacts with oxygen (Middle line). The peroxy radical then abstracts a hydrogen atom from the phenol leaving a phenoxyl radical and a peroxide, as in the bottom line. Phenoxyl radicals are not efficient at initiating the polymerisation, due to resonance stabilisation delocalising the lone electron around the molecule. Bickel and Kooyman⁵⁸ compared the rate of a peroxy abstracting a phenolic hydrogen to the rate of abstracting a hydrogen from a polymer chain. Their values for this ratio ranged from 30 to 300 times in favour of the phenolic hydrogen abstraction, depending on the number of substituents on the phenol.



Scheme 21. The mechanism for radical polymerisation inhibition. Top – Propagation. Middle – Initiator reacting with oxygen. Bottom – Peroxy radical abstracting hydrogen from an inhibitor molecule, ArOH

The phenoxy radical that forms can indeed react with another radical initiator, through recombination. This makes the inhibitor more efficient; one molecule of inhibitor removes two initiators.

As demonstrated above, analytical techniques, such as NMR and mass spectrometry, are vital in determining the mechanism of inhibition. This study is to determine possible pathways for old and new inhibitors. A technique that is less common, but could be of great use is Electron Paramagnetic Resonance. This technique can observe radicals directly, so could be used to monitor the rate of reaction with stable free radicals (e.g. TEMPO), or could be used to identify a radical intermediate. Also it can be used to monitor other variables in the reaction system, such as oxygen concentration.

1.4 Electron paramagnetic resonance

As previously stated, analytical techniques such as NMR, MS and GC are used to work backwards to determine the reaction mechanism of inhibitors. However, observing the reactive species may not be possible in radical polymerisation due to their high reactivity. Electron Paramagnetic Resonance may be able to observe stable radical species in situ and shed more light on the intermediates of the inhibition reaction.

Electron Paramagnetic Resonance (EPR, also known as Electron Spin Resonance, ESR) is among the most direct methods of radical characterisation^{59,60}. This method is similar to NMR, with the general difference being that NMR observes the transitions of the nuclear spin, whereas EPR looks at electron spin transitions. EPR spectroscopy therefore can only study systems with unpaired electrons and is particularly useful for characterisation of paramagnetic species.

1.4.1 Basic principle – Zeeman Splitting

An unpaired electron, for example in an organic radical, has a spin angular momentum of $S = \frac{1}{2}$. This means the electron can have a spin quantum number $m_s = +\frac{1}{2}$ or $m_s = -\frac{1}{2}$. When a system with the unpaired electron is exposed to external magnetic field, B , the electron spin can either align with the magnetic field, (parallel, with $m_s = -\frac{1}{2}$) or it can align against the field (antiparallel with $m_s = +\frac{1}{2}$). The energy of these two new levels can be calculated using Equation 1, where g_e is the g-factor of the electron (for a free electron $g_e = 2.0023$) and μ_B is the Bohr magneton. This effect is known as Zeeman interaction.

$$E = m_s g_e \mu_B B$$

Equation 1. Determination of energy levels of an electron in an applied magnetic field.

This splitting can be detected by using electromagnetic radiation to cause the electron to change its alignment with the magnetic field. This is similar to NMR. When the energy of the electromagnetic radiation equals the difference in energy levels, the electron spin changes orientation, and absorption of energy is observed. This is demonstrated in Figure 4.

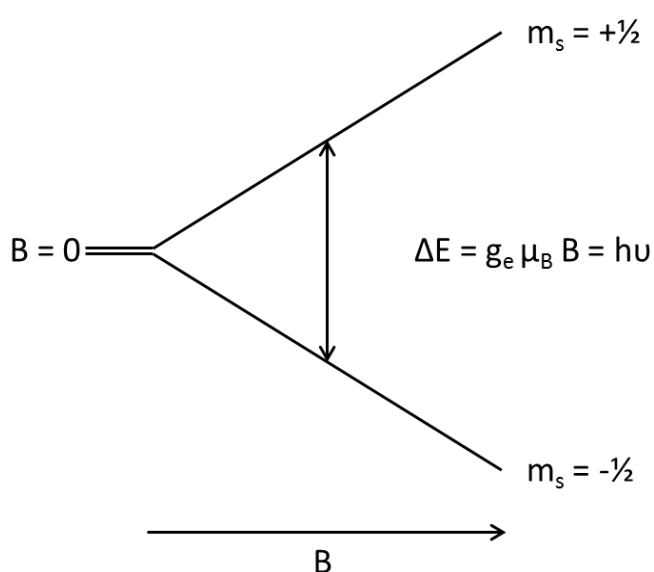


Figure 4. The difference in energy levels caused by Zeeman splitting

The reason that electromagnetic radiation is more likely to be absorbed when the electron moves up in energy, rather than emitted as the electron moves down in energy can be explained using the Maxwell-Boltzmann distribution. This is given in Equation 2, and when using microwave energy (for example $\nu = 9.75\text{GHz}$) the ratio of populations of the upper and lower energy levels is 0.998. The slight excess of electrons in the lower state leads to a net absorption of radiation which is observed in an EPR experiment.

$$\frac{n_{upper}}{n_{lower}} = \exp\left(-\frac{\Delta E}{kT}\right) = \exp\left(-\frac{h\nu}{kT}\right)$$

Equation 2. Determination of level occupancy using the Maxwell-Boltzmann distribution

1.4.2 Instrumentation and Detection

The way the splitting of the energy levels is detected is similar to NMR. A magnetic field is applied to the sample, and electromagnetic radiation is used to give the energy necessary for the transition between the energy levels formed. In continuous wave NMR, a method used in the early days of NMR, the magnetic field applied was kept constant and the radio frequencies were scanned, producing the spectrum, but in EPR the opposite is performed. This is due to the need to use microwave radiation as the energy source. It is far more difficult to produce an accurate range or spectrum of microwave frequencies, than it is to scan the relatively low strength magnetic fields needed for EPR.

For our experiments we are using what is known as an X-Band spectrometer, using $\sim 9\text{ GHz}$ microwave radiation in a magnetic field of $\sim 3500\text{ G}$. This is adequate for the study of organic radicals.

Spectra can also be obtained at different temperatures. The method for controlling temperature is to pass air through the sample cavity to heat the sample while the spectra are taken. If temperatures below room temperature are required, liquid nitrogen is heated slightly to produce cold nitrogen gas to pass through the sample cavity. Care must be taken while doing EPR measurements using this temperature unit. Any movement in

the sample caused by the flow of gas will affect the intensity of the signal observed. Also water condensing in the sample cavity will affect the spectra observed. These can be easily overcome by using a stabilising bracket and passing dry nitrogen through the cavity as well as the heated air or cooled nitrogen.

1.4.2.1 Noise reduction and sensitivity

To improve the sensitivity of the method, a number of techniques are employed. First, the magnetic field is modulated, normally at frequencies around 100 kHz. At the detector, the phase-sensitive detection of the signal oscillations that matches the modulation of the magnetic field results in removing some of the background noise. This is relatively easy to do as the magnetic field is weak compared to NMR.

A final method of improving the signal to noise ratio is to take the average of a number of scans. This will remove more of the background noise. However, this is not applicable to short lived radicals. For example, any decrease in signal from the species being observed in the second scan will decrease the signal of the first scan when averaged. This method is best applied for low concentrations of stable radicals or a steady state concentration of radicals.

From the above, obtaining an informative and complete spectra relies upon a number of parameters. However a large amount of information can be obtained from this technique when decent spectra are obtained.

1.4.3 Analysis and interpretation of spectra

Determining if the sample contains an unpaired electron or not is not the limit of this technique! A lot more information can be obtained from the interpretation of the spectra.

1.4.3.1 Hyperfine interactions

Hyperfine interaction is an interaction between electron spin and a nucleus with a spin angular moment that does not equal zero. For example ^1H , ^{13}C , ^{15}N and ^{31}P all have $I = \frac{1}{2}$, and will cause hyperfine splitting.

The transitions observed by EPR are determined by two selection rules: $\Delta m_s = \pm 1$, which is the change of the electron spin quantum number, and $\Delta m_I = 0$, which is the change in the nuclear spin quantum number. This is demonstrated using TEMPO as an example in Figure 5. There are three different transitions, and as the majority of the electrons start in the $m_s = -\frac{1}{2}$ state, three absorptions are observed.

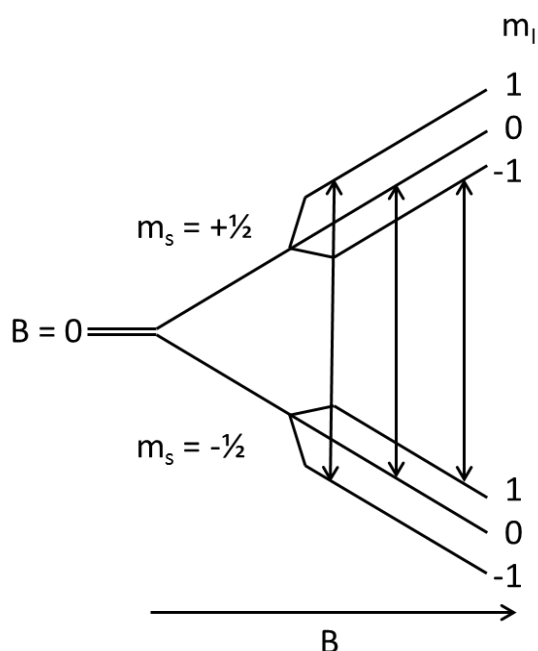


Figure 5. The hyperfine splitting of an unpaired electron interacting with an ^{15}N nucleus, in a magnetic field, B.

Where multiple nuclei (e.g. n is the number of equivalent nuclei) are coupled to the electron, there are $2nI+1$ transitions possible. Figure 6 demonstrates this. The EPR spectrum of semiquinone radical anion shows a 1:2:1 triplet, as the electron is coupled to two equivalent hydrogens ($I=1/2$). In TEMPO only the nitrogen ($I=1$) couples with the electron, resulting in three peaks of the same intensity. These examples demonstrate how the local structure around the unpaired electron can be determined from EPR spectra.



Figure 6. EPR spectra of TEMPO (Left) and 2,5 – di-tert-butyl semiquinone(Right)

1.4.3.2 Intensity

As the selection rules are clearly defined, the absorption is proportional to the concentration of radicals in the sample. EPR spectra are recorded as the first derivative of the absorption spectrum due to the use of field modulation; this also helps improve the resolution of the spectra. The spectra thus must be integrated twice to give a measure of radical concentration that can be compared to standards. By taking a known concentration of a stable radical, e.g. TEMPO, the unknown concentrations of radicals can be calculated by comparing the double integrals.

1.4.3.3 Line broadening

Based on the above theory, the spectra should consist of infinitely narrow lines. This is not the case. The lines will broaden due to a number of different factors, which in turn can reveal more information about the environment around the unpaired electron.

The relaxation of the electron spin affects the line width of the signal. When an electron spin flips, the thermal equilibrium between energy states is disrupted. A faster relaxation rate leads to a broader line shape due to uncertainty in the energy gap between the two spin states according to the Heisenberg uncertainty principle. A lower rate of relaxation leads to a sharper signal.

In a system with multiple unpaired electrons or high radical concentration, spin-spin interactions between the unpaired electrons in the magnetic field increase relaxation rate.

This increases the line broadening. For a system with a high enough radical concentration, the analysis of line broadening can be used to determine radical concentrations.

1.5 Aims of the study

The above literature displays the current understanding and rationale for the inhibition of spontaneous polymerisation. As legislation changes throughout the world, the tools available to inhibit this polymerisation will also change. As stated above, DNBP (Section 1.3.1.3, page 39) is a common industrial polymerisation inhibitor. However, this inhibitor is scheduled to cease production due to the changes in legislation. Therefore a new method of inhibiting spontaneous polymerisation is needed. The overall aim of this research is to develop improved mechanistic understanding of the action of polymerisation inhibitors which will in the long term facilitate development of new inhibitors.

The study breaks down into two areas. The first objective was to investigate the mechanism of polymerisation inhibition by nitrophenols (such as DNBP). This will require the development and use of a method for determining the onset of polymerisation after inhibition, so that structurally related molecules can be screened to observe trends in the inhibition efficiency. Also, the determination of inhibition products would also be an area for investigation in order to provide further details about the inhibition mechanism.

The second area is to evaluate and study the inhibition of spontaneous polymerisation by a potential new inhibitor system. A charge transfer complex between quinones and amines, first reported by Yassin and Rizk⁶¹ has been proposed. Their proposal included identifying the chloranil radical anion part of the complex as the inhibiting species. The stability and properties of the chloranil radical anion, including potential inhibition ability, should serve as the initial investigation.

2. Nitrophenols as inhibitors

2.1 Monitoring polymerisation

To investigate the inhibition of spontaneous polymerisation, a method of monitoring the rate of polymerisation and determining events, such as the onset of polymerisation after inhibition, needs to be determined. The choice of method will be determined by how appropriate it is when applied to spontaneous polymerisation, and practical reasons such as cost. Fortunately, there are many methods to choose from.

The simplest, and least informative is to take an inhibited sample of monomer, heat it and observe when it becomes a solid. Comparing the inhibited samples to uninhibited monomer will make it possible to distinguish between compounds that inhibit and those that do not, but nothing else. The concentration of the inhibitor needs to be relatively high in order to observe inhibition. This means any expensive or difficult to synthesise molecules could not be tested for inhibition properties. This approach is also labour intensive as the samples will need constant monitoring for accurate results.

The results in Table 1 show possible trends in inhibition activity determined by this method. For example, 2-nitrophenol inhibits far more than 3-nitrophenol, 4-nitrophenol and nitrobenzene, with the latter three molecules showing similar activity. The difference in position of the nitro group therefore gives rise to increased inhibition efficiency.

Table 1. Inhibition times of potential inhibitors, tested by heating 5 ml sample of the inhibitor in styrene at 130°C.⁶²

Inhibitor	Concentration / M	Time for Immobile gel formation
Uninhibited	N/A	2h12min
Nitrobenzene	0.01	7h15min
Nitrosobenzene	0.01	4h25min
2-nitrophenol	0.01	25h50min
3-nitrophenol	0.01	7h45min
4-nitrophenol	0.01	7h45min
3-methyl-2-nitroanisole	0.01	2h56min
4-nitroanisole	0.01	7h15min
MEHQ	0.01	5h50min
2-hydroxybenzotrile	0.01	2h56min
Trifluoro-p-cresol	0.01	2h12min
2,4-dinitrophenol	0.01	15h35min
1-chloro-2,4-nitrobenzne	0.01	15h10min
DNBP	0.01	25h40min

The accuracy of the data depends on the frequency of sampling. The data does not distinguish between inhibitors and retarders. However they reveal the trends that can be investigated with better resolution of sampling.

Another method for monitoring polymerisations is to analyse the products of polymerisation. For example, analysing the reaction mixture and using GC to determine the concentration of the remaining monomer can be then used with kinetic equations to determine the rate of polymerisation^{63, 64}.

Hoogenboom et al⁶⁴, as an example, demonstrated the use of GC and GPC as a way to determine the monomer remaining in samples taken from a polymerisation, and designed an automated sampling with on-line analysis. This showed good correlation with other methods of determining the rate of polymerisation. The authors also demonstrated that there were a number of practical aspects of automating the sampling of polymerisation reaction mixture. They described that combining the automated sampler and the GC required more space than expected. Also, there were limits as to how far through the polymerisation they could analyse, as once the sample contains too much polymer the

sample could damage the equipment. They were also limited as to the intervals between samples, but this could be overcome with additional GC's.

The use of IR to monitor the formation of polymer and the consumption of monomer is another way of monitoring polymerisation⁶⁵⁻⁶⁹. This is useful for vinyl monomers, as the change from double bond to single bond is a distinct change in IR or Raman spectroscopy. This can also be an online continuous observation, without having to remove or destroy any of the monomer or solvent^{69,70}. There are however a number of disadvantages to these continuous online methods, such as the scale of the polymerisation needs to be large enough to pump through the equipment.

A much older technique is dilatometry, which follows the reaction through observing the contraction of the solution as it polymerises. This occurs as the density of sample increases due to the increasing ratio of polymer to monomer. This is more pronounced with undiluted monomer samples, which makes observing spontaneous polymerisation a prime candidate. One of the first recorded uses of dilatometry was by Starkweather and Taylor⁷¹ in 1930, who used the set up described in Figure 7 to observe the rate of spontaneous polymerisation of vinyl acetate. Since then it has been a powerful tool in monitoring polymerisation.

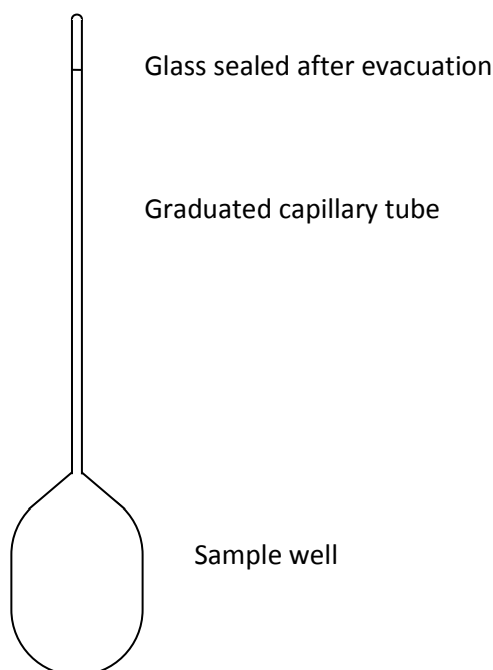


Figure 7. Diagram of a basic dilatometry set-up

Dilatometry can be adapted to run under the complete exclusion of air, as described by authors such as Goldfinger and Lauterbach⁷², and Schulz and Harborth⁷³. These methods involve standard practices in removing oxygen from solutions, and then sealing them into the glass apparatus under vacuum. Although this means that the dilatometry part of the glassware is not recyclable, the apparatus is relatively cheap to make, making this method viable.

As the aim of this project requires a comparative study of the rates of polymerisation in the presence of different inhibitors, dilatometry was chosen as the main method of analysis.

2.2 Dilatometry

As described above, dilatometry is a useful tool for observing the polymerisation of a material. Here, this technique has been utilised to determine the onset of polymerisation after an inhibitor has been consumed. This technique also showed the change in the rate of polymerisation.

The first dilatometry experiments for polymerisation in the literature utilised a capillary tube attached to a large well filled with monomer.⁷¹⁻⁷⁴ The large volume increases the observable change in height of the monomer meniscus. Also, the narrower the capillary leads to a greater the change in meniscus height. As the mass and volume remain the same, and the capillary tube is of uniform dimension, then linear rates of change will be observed as linear rates of change of height.

Using the known densities of polymer and monomer, the change in height for complete polymerisation can be calculated. This has been determined in the literature for a range of monomers at room temperature⁷⁵ and given in Table 2.

Table 2. Table of change in volume after complete polymerisation for a number on monomers⁷⁵. Density measured at 25 °C unless denoted by ^a.

	Density /g ml ⁻¹ @ 25 °C		Volume change / %
	Monomer	Polymer	
Vinyl Chloride	0.919	1.406	34.4
Acrylonitrile	0.800	1.170	31
Vinylidene bromide	2.178	3.053	28.7
Vinylidene chloride ^a	1.213	1.710	28.6
Vinyl bromide	1.512	2.075	27.3
Methacrylonitrile	0.800	1.100	27
Methyl acrylate	0.952	1.223	22.1
Vinyl acetate ^a	0.934	1.191	21.6
Methyl methacrylate	0.940	1.179	20.6
Ethyl methacrylate	0.911	1.110	17.8
Styrene	0.905	1.062	14.5

However at different temperatures the density will change. Patnode and Sceiber⁷⁴ have investigated the change in density over a range of temperature for styrene. There is a linear relationship, where density decreases with increasing temperature, as expected. This information will be needed to determine the change in volume for a dilatometry experiment at higher temperatures.

Measurements are taken over time, which without automation will take up a considerable amount of a person's time. Spontaneous polymerisation is a slow process which means constant monitoring by an operator would be impractical, due to time and a small change in sample height. However there are a number of ways in which the change in height can be magnified and observed easier.

The use of mercury to assist in the observation of the change in volume is one of the oldest modifications to the dilatometry technique. Burnett¹⁷ devised a mushroom type dilatometer that increased the surface area in contact with the mercury, leading to a greater increase in observed change in volume. Other ways in which mercury has been used is to add electronics to the detection of the sample volume. Bernachez et al⁷⁶

constructed a mercury manometer in which the resistance of a wire stretched into the mercury column is varied by changes in the height of the mercury. With a constant current, there is a linear relationship between the signal detected and change in height of the mercury column. The obvious disadvantage of this technique, and the reason it is very rarely used, is due to the toxicity and hazards associated with mercury.

A technique used more recently is based on capacitance. This makes use of changing the distance between two electrodes. As the distance between the electrodes increases, the capacitance changes. Frey et al⁷⁷ describe using mercury within a capillary with a metal outer electrode. As the volume of the sample changes, the volume of mercury within the cylindrical electrode increases, leading to change in capacitance. This change can be monitored, leading to changes in meniscus position beyond 100 nm being observable, providing the meniscus of the mercury is within the electrode.

Another capacitance method has been described by Neumeier et al⁷⁷ which uses a unit built of quartz to minimise the thermal expansion of the device itself. They have observed the changes in volume due to thermal expansion. They have observed sub Angstrom changes in the height measurement and have used the equipment over a temperature range of 5 K to 350 K. The use of capacitance in dilatometry to observe the changes in volume and to automate the process is impressive as to what can be achieved.

2.2.1 Disadvantages of current methods

The traditional setup to monitor polymerisation requires large volumes of inhibited monomer to work effectively. This is not preferable if using dilatometry for proof of concept experiments where a small amount of inhibitor may be available.

A common component of a traditional dilatometry setup involves mercury as a way of observing the volume change. This is toxic and is being phased out of modern laboratories.

Through-put of these techniques is limited. Only one sample at a time can be run in the individual setups. The computer recording the data from the instruments could easily record more than one data stream, but that would require a second piece of equipment to be purchased to make the measurements.

When dilatometers are used for polymerisations specifically, one disadvantage is that the polymerisation cannot be taken to completion. Fully polymerised material is difficult to remove, and will render the equipment completely or partially unusable. This can raise costs of running the equipment, e.g. the need to replace specific sample containers.

2.3 Design of a new and automated dilatometry experiment

Having reviewed the available options, we decided to design our own dilatometry setup.

The main reasons for not using commercially available instruments are:

- Large volume of monomer required for each experiment
- Low throughput
- High cost

Our setup significantly reduced the scale of the experiments and increased the throughput at the expense of accuracy, and was built at very low cost. The lower accuracy of our method is not a problem for screening a large number of inhibitors planned in this work. The setup allows automated monitoring of the polymerisation progress.

To monitor the progress of the polymerisation, the setup developed uses a digital camera to observe the height of the sample. This basic premise is described in Scheme 22, and the more specific details are laid out in the sections thereafter.



Scheme 22. Schematic of the small scale, automated dilatometry setup, developed to determine the onset of polymerisation after inhibition or retardation.

2.3.1 Rack

As mentioned previously, dilatometry relies on the change in height of the meniscus of the sample. As the volumes used are small, the change in height is also very small. Therefore to limit the error in the taking of the measurement, the samples need to remain in the same position. To achieve this, the camera is weighed down and secured, and the samples are held in place by a rack-like holder secured in the oil bath. A schematic of the rack and digital render is given in Figure 8, and a photograph taken from the camera used is given in Figure 9.

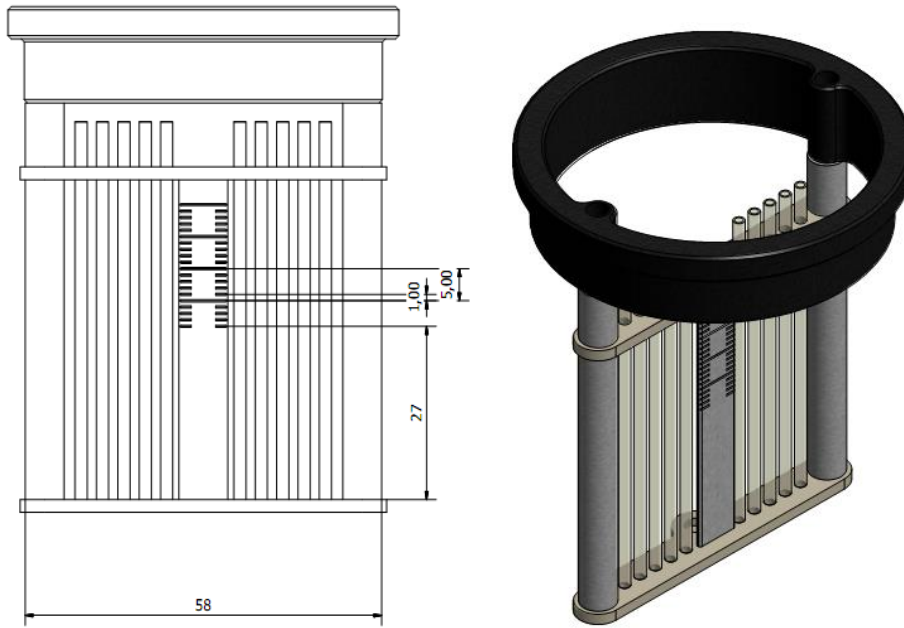


Figure 8. Schematic and digital render of the dilatometry rack. Dimensions, where given, are in millimetres

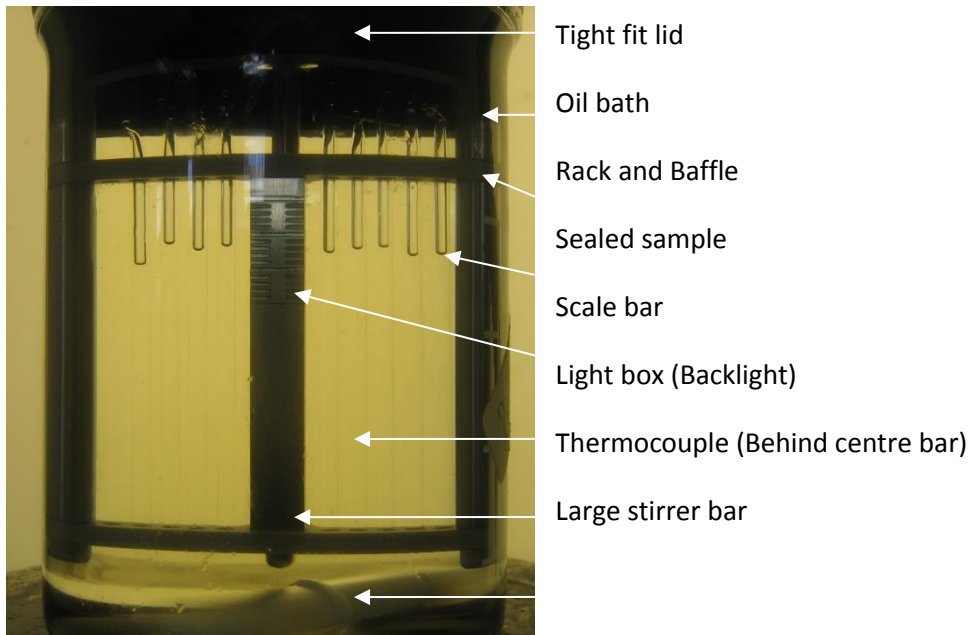


Figure 9. Photo of the dilatometry rack with features labelled

The rack is attached to an open lid, which tightly fits into the bath, reducing movement. The materials used to build the rack are chosen for their lack of thermal expansion. Any

thermal expansion is detectable by the analysis of the images, and can also lead to the samples becoming loose in the holder, and moving around in the loose space.

The rest of the equipment is either weighed down or positioned in a fume hood on rubber feet or other surfaces where nothing is likely to slip or move due to vibrations. Also, as the system is automated, the samples are ran over night or over weekends, as to avoid vibrations and interference from colleagues working around the equipment.

The rack is designed to submerge the samples completely. In initial experiments where samples were partially submerged, monomer condensed at the top of the sealed tube. This gave varying rates of change in height, which was not due to the polymerisation. Therefore, complete submersion is required to maintain accuracy and reproducibility.

2.3.2 Oil bath and heating

The oil bath is heated by a standard stirrer hotplate. A large stirrer bar is used to mix and maintain a constant temperature throughout the oil. However, in the initial development, this was not enough to limit thermal variation in oil. There are ways of improving the heat transfer through the oil bath, such as the use of different agitators (overhead stirrers with different propeller type blades rather than a magnetic stirrer bar) and vessel shapes and sizes^{78, 79}. However, the setup is restricted in what can be used, due to the need for visual measurements. A method of maintaining a constant temperature through a fluid in a stirred vessel is to add barriers that disrupt the flow of the fluid. These are called baffles.

The final holder design acts as a baffle sufficient for the experiment. In this set up the thermal variation in the oil was $\pm 0.2^{\circ}\text{C}$ from the set temperature.

The thermocouple is held behind the scale bar in the rack holder, so that it is in the optimal position and also to maximise the space in the images. Another detail is that the speed of the stirrer bar needs to be optimised so that there is sufficient mixing, but not so much as to cause a vortex to form obscuring the samples and exposing the tops of the samples to the cooler air.

The procedure for starting a dilatometry run for this equipment has been refined to give the reproducible and accurate results. The oil bath is “over-heated” before a run; that is,

for a run at 110°C the oil bath is heated to 113°C. When the rack and samples are added the temperature is reset to 110°C and the camera started. After 2 minutes the temperature of the rack, samples and oil is constant at 110°C. Figure 10 demonstrates the time scale for the equilibration of a samples temperature.

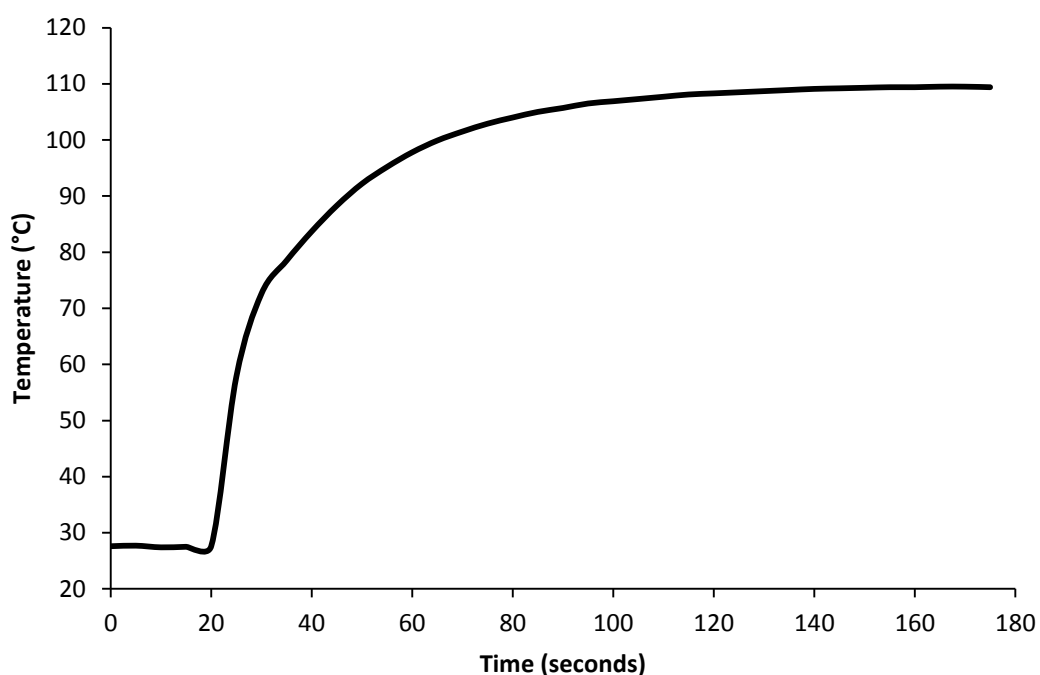


Figure 10. Temperature equilibration of dilatometry sample. Sample inserted into heated oil bath at time = 20 seconds

2.3.3 Sample preparation

The samples used are much smaller than in traditional dilatometry experiments. Here we use capillary tubes, sealed at both ends. The volume used is 0.04 cm^3 , with a head space of 0.03 cm^3 . One end is sealed first with a Bunsen burner, allowed to cool, then the sample added. A fine pulled pipette is used to remove styrene from the walls of the head space with a fine stream of compressed air. Any excess styrene left would decompose upon flame sealing, which results in a variation in rate of polymerisation and no reproducibility. It also allows for easier sealing of the sample.

2.3.4 Camera and lighting

A commercially available 4-megapixel digital camera was used to observe the sample rack. The model has a built in remote shooting function combined with a timer function, used to take an image at regular intervals automatically. The resolution of the camera is high enough to distinguish the small change in height as the polymerisation takes place.

The total change in height can be calculated using the densities of styrene and polystyrene at the temperature the dilatometer is run at. Using information published by Patnode and Scheiber⁷⁴, the densities of styrene and polystyrene at 110 °C are 0.825 g ml⁻¹ and 1.016 g ml⁻¹, respectively. From this the change in volume can be determined as 18.8%. The total height of a sample in an image is on average 950 pixels. Therefore the total change in height in an image for a sample of styrene is 178 pixels. This means 1 % polymerisation is about 1-2 pixels, giving good resolution.

To increase the height of the sample in the image, the camera could be moved closer to the oil bath. Unfortunately the heat from the hot plate would damage the camera, but it was left as close as possible. From the above calculation, the resolution was deemed good enough to distinguish inhibition times and retarded rates.

The camera also has a “macro” function, designed to allow picture of objects close to the camera. Without this, the images are blurred, leading to noise in the analysis.

In order for the meniscus to be easily visible, a light box is used on its side as a back light. This makes the volume of the sample clearly visible for the analysis.

2.3.5 Data analysis

The images are analysed by a purpose written program. The program requires a user to determine where the menisci of the samples are in the images, and where the bottom of the sample is. With this information, the program calculates the relative height of the samples in relation to the first image. This is why it is vital the sample rack is immobile, as

any movement means the positions of the samples in the later images are no longer the same, and the relative height is incorrect.

The original program used at the start of the study would take as long to analyse images as it did to collect them. The program underwent a number of improvements, to make more efficient use of time.

Typically more than one sample of inhibitor being investigated will be run at a time, alongside duplicates of uninhibited monomer. The results for the uninhibited monomer, and the duplication of all samples in a run can be used to eliminate any anomalies, e.g. heating not working correctly or unwanted movement of the camera.

2.3.6 Standards and calibration of the new setup

In order to determine the stability of the equipment and to demonstrate that any change in the values calculated are due to polymerisation, toluene was used as an example of a non-polymerisable sample. Figure 11 demonstrates the variation in the meniscus height measured. Again, all values are relative to the first image. There is very little variation in height.

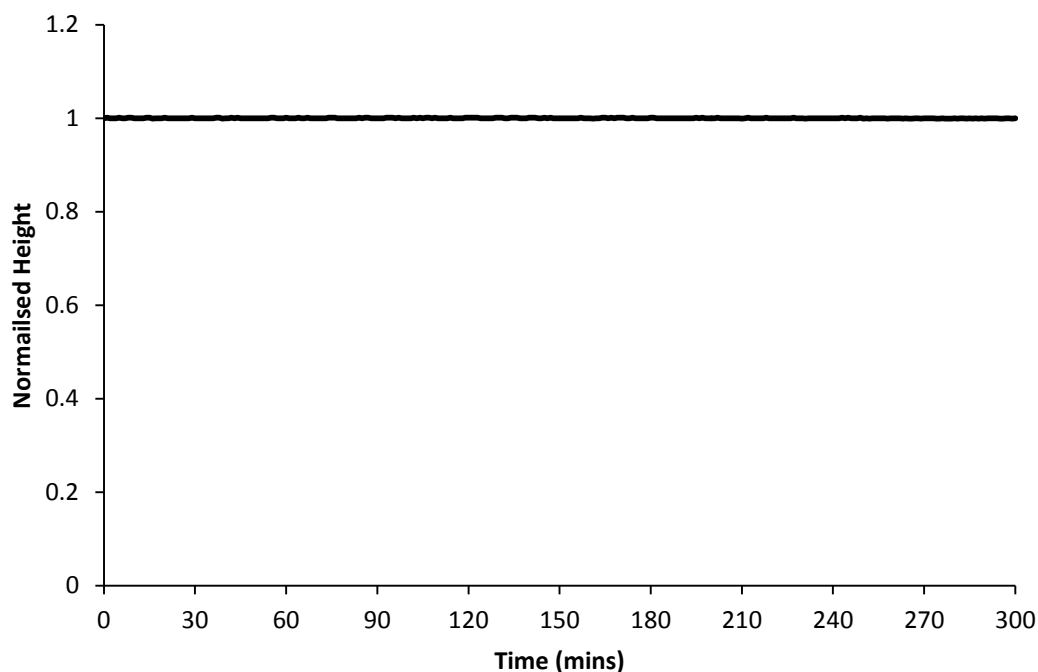


Figure 11. Dilatometry of toluene, as a demonstration of the equipment stability. Data normalized to the first image taken at $t = 0$ minutes.

2.3.7 Oxygen diffusion within the samples

In the early uses of dilatometry to monitor polymerisation⁷¹⁻⁷⁵, the samples were either oxygen free and sealed under vacuum or just sealed under reduced pressure. This new set up is not under reduced pressure, and therefore has oxygen dissolved in the sample. The additional oxygen in the head space may lead to discrepancies in the inhibition and retardation properties of molecules between literature values where available and the new setup described here. Therefore it is important to understand how much oxygen is present in the headspace and what happens to it during the experiment.

To be confident in our analysis of the polymerisation, the diffusion of oxygen from the head space to the solution needs to be understood. If there is high enough concentration of oxygen available for inhibition it may make interpreting data from inhibited samples difficult.

To address this, the diffusion of oxygen in to a solvent was investigated by EPR. TEMPO ((2,2,6,6-tetramethylpiperidin-1-yl)oxidanyl) is a stable nitroxide, and was used to observe

oxygen in the sample. As the oxygen concentration increases, the line width of the TEMPO signal also increases. This is due to spin-spin interactions between the bi-radical molecular oxygen and the TEMPO nitroxide radical⁸⁰⁻⁸³. Chlorobenzene was used as a replacement for styrene as the spontaneous polymerisation initiation mechanism will result in radicals reacting with the oxygen diffused into the solvent, and reacting with the TEMPO. The sample tubes used are the same diameter and contained the same volume of chlorobenzene solution as the dilatometer experiments, so that the results will be comparable. The samples were purged of all oxygen by freeze-pump-thaw method and left frozen with the head space evacuated when transferred to the EPR equipment. The sample is then opened to air as the sample thaws in the preheated EPR cavity. Then the TEMPO EPR signal is monitored, and effect of diffusion calculated by a specific computer package.

Figure 12 shows the rate of oxygen diffusion into the solution. This shows that even at 100°C it is very slow, with complete oxygenation taking far longer than any dilatometry experiments

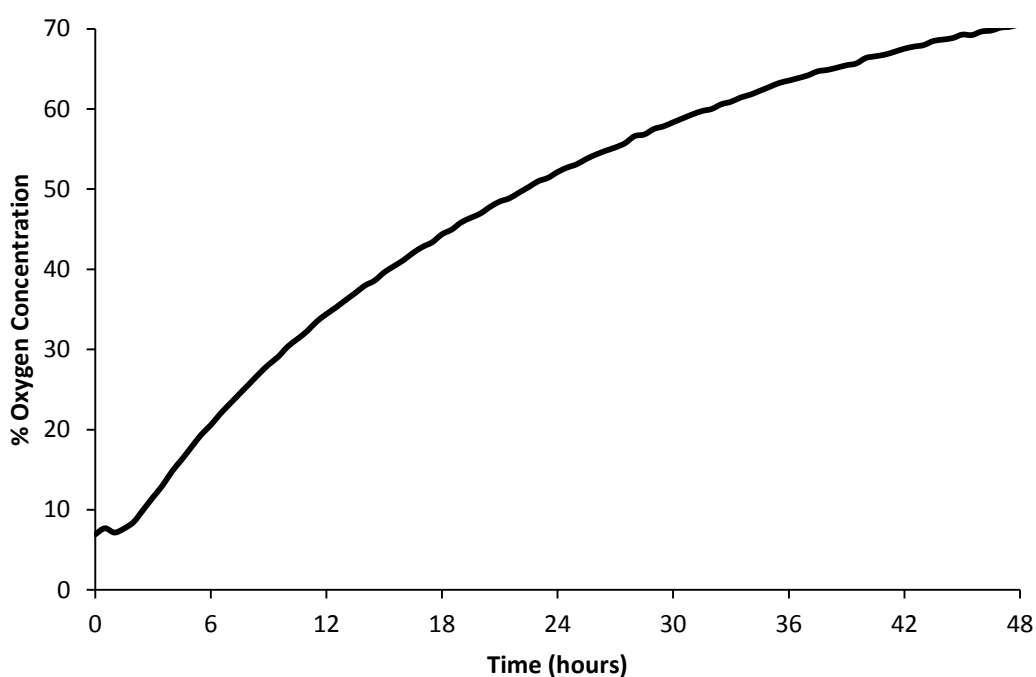


Figure 12. The oxygen diffusion into chlorobenzene at 100°C, monitored by EPR

When the rate of diffusion is compared to the oxygen consumption by styrene spontaneous polymerisation in Figure 13, it is clear that the rate of the oxygen diffusion into the solution is far too slow to impact on the inhibition. The rate of oxygen consumption was observed following the method used by Conte et al⁸⁰, and our data matches theirs well. It can be concluded that as the rate of consumption of oxygen by the styrene spontaneous polymerisation is far quicker than the rate at which the oxygen can diffuse into styrene, the effect of oxygen diffusing from the head space can be ignored.

Therefore only the oxygen already dissolved in the styrene before heating should be considered. However, this oxygen is completely consumed within the few minutes. The possible effect of this amount of oxygen on the results of the dilatometry experiment is investigated later in the chapter (Page 70).

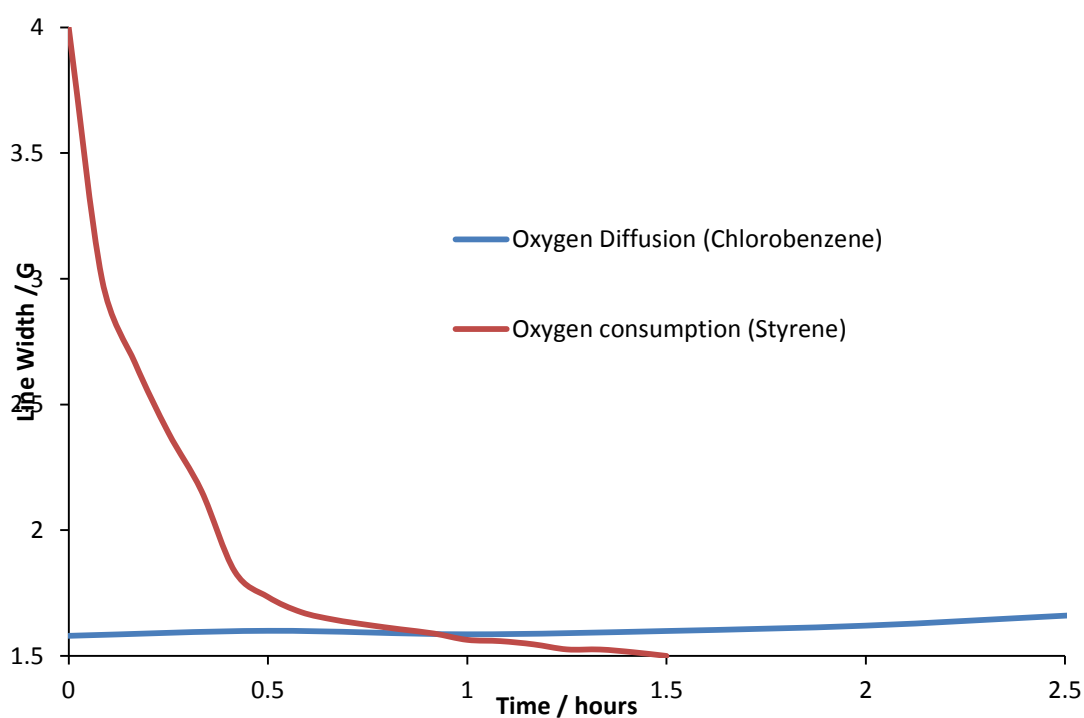


Figure 13. A comparison between the oxygen consumption by styrene polymerisation and the oxygen diffusion into chlorobenzene. (At 100°C, monitored by EPR)

2.4 Case studies for proof of concept

2.4.1 Uninhibited styrene

Styrene has an understood spontaneous polymerisation mechanism¹⁹, and makes a good candidate for testing our dilatometry set up. The change in height due to polymerisation calculated from the data provided by Partnode and Sciber⁷⁴ show that complete polymerisation will reduce the height by 18.8 %. However, this set up reaches completion at a slightly higher meniscus height drop of 20%, suggesting over 100% conversion.

The reason for this apparently anomalous conversion of monomer to polymer is possibly because the shape of the meniscus may change during polymerisation. In larger dilatometry setups, the meniscus will be flat apart from a small area of the surface that will curve up the wall of the glassware. In a smaller sample, the meniscus is mostly curved due to the same effect. If the shape of the curve remained consistent throughout, the change in height after 100% conversion would be identical to literature. However, as the polymerisation progresses, the viscosity of the sample will increase, which will increase the curvature of the meniscus. At this point, a greater volume of the monomer will no longer be accounted for by the camera, and will thus result in an apparent conversion over 100%. We note that this effect is relatively small and is only significant at high degree of polymerisation. As the rates of polymerisation obtained from the dilatometer are self-consistent, a 20% change in height in our setup is used in this thesis as a point for 100% conversion of monomer to polymer (Figure 14).

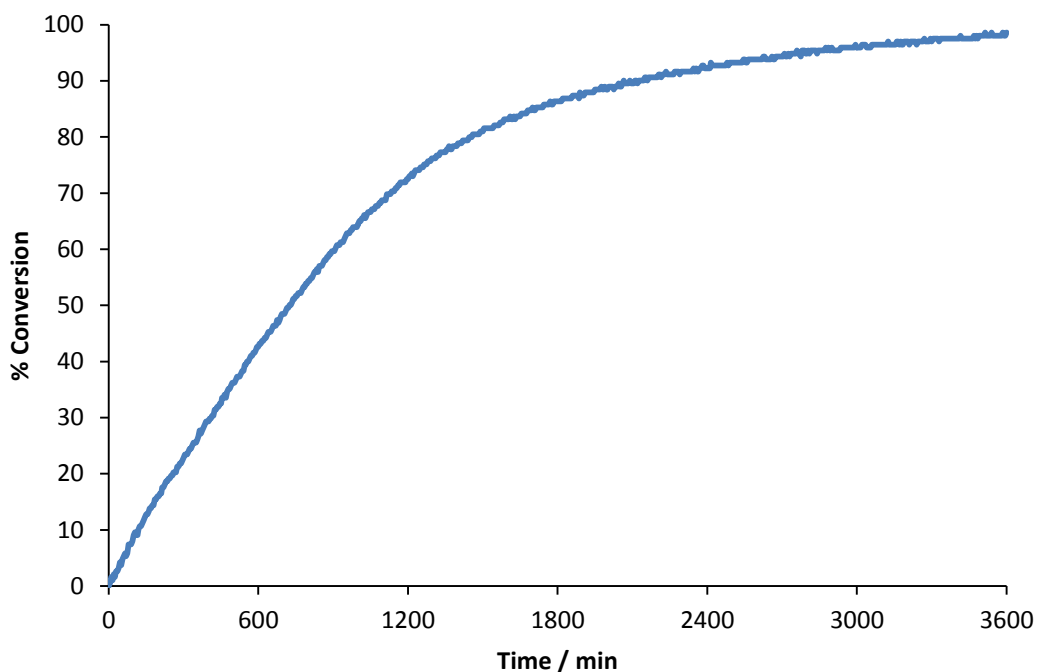


Figure 14. Dilatometry of uninhibited styrene at 110°C

2.4.2 Nitroxide inhibited polymerisation (TEMPO)

TEMPO is a nitroxide radical that has known inhibition properties. It has been chosen as an example of an inhibitor. The dilatometer can accurately determine the onset of polymerisation from the abrupt change in the slope of a dilatometer trace, after TEMPO consumption, as demonstrated in Figure 15. The inhibition period is dependent on concentration, shown in Figure 16. These results demonstrated that TEMPO still acts as an inhibitor without oxygen, as the inhibition period lasts until after the oxygen has been consumed (Figure 13).

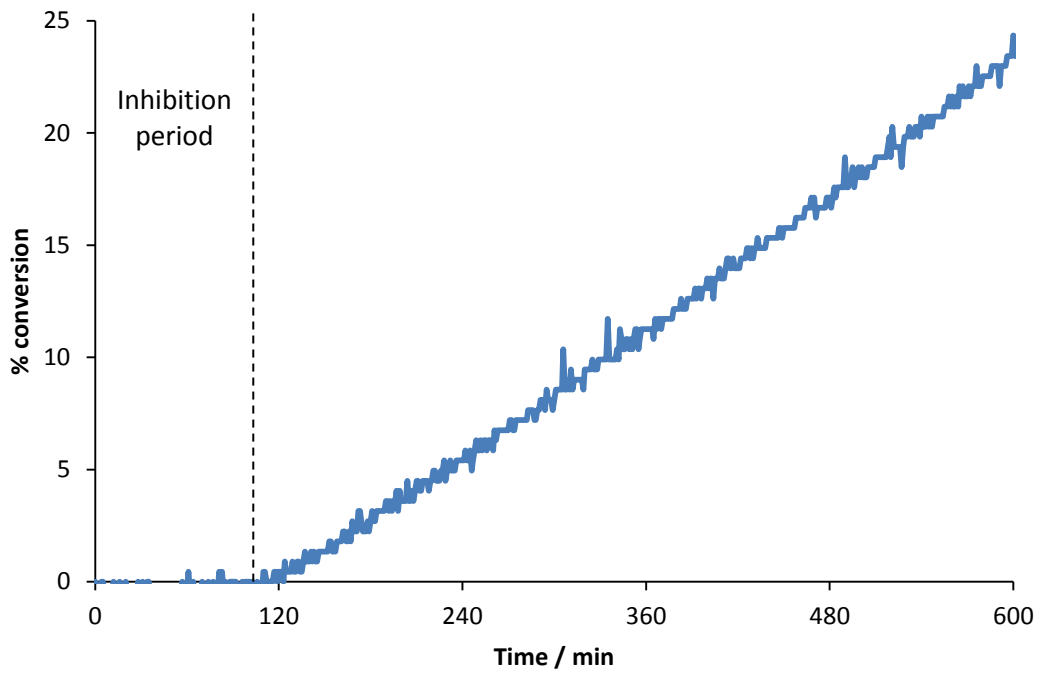


Figure 15. 200ppm TEMPO in styrene polymerisation measured by the dilatometry set-up at 110°C

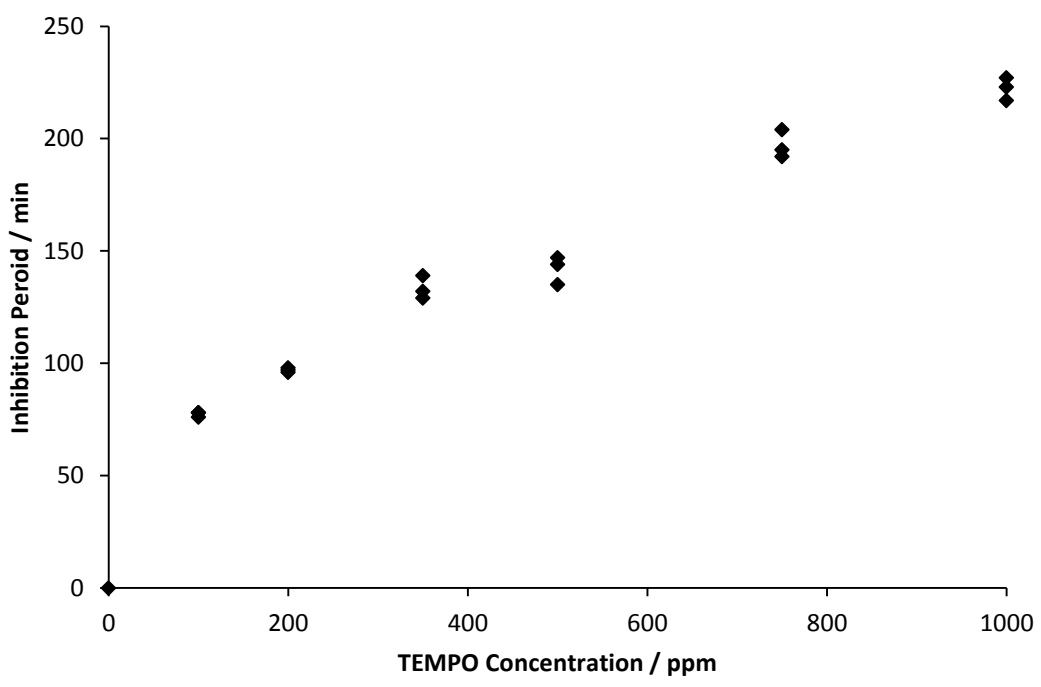


Figure 16. Inhibition period against TEMPO concentration

2.4.3 Oxygen dependent inhibitor (4-methoxyphenol)

4-methoxyphenol (MEHQ) is an oxygen dependent inhibitor (see Page 1.3.2.1 on page 43), commonly used as a storage inhibitor. When MEHQ is run at the standard concentration (0.1 M) and temperature (110 °C) as the other inhibitors investigated there is no inhibition observable.

If MEHQ is ran in the dilatometer at 90 °C, an inhibition period is observed, but only for 15 minutes, shown in Figure 17.. If the concentration is increased, the inhibition period does not change. This demonstrates the dependence on MEHQ on oxygen as no inhibition is observed once oxygen has been consumed in the reaction mixtures. The oxygen present in the styrene is the limiting factor for the inhibition by MEHQ.

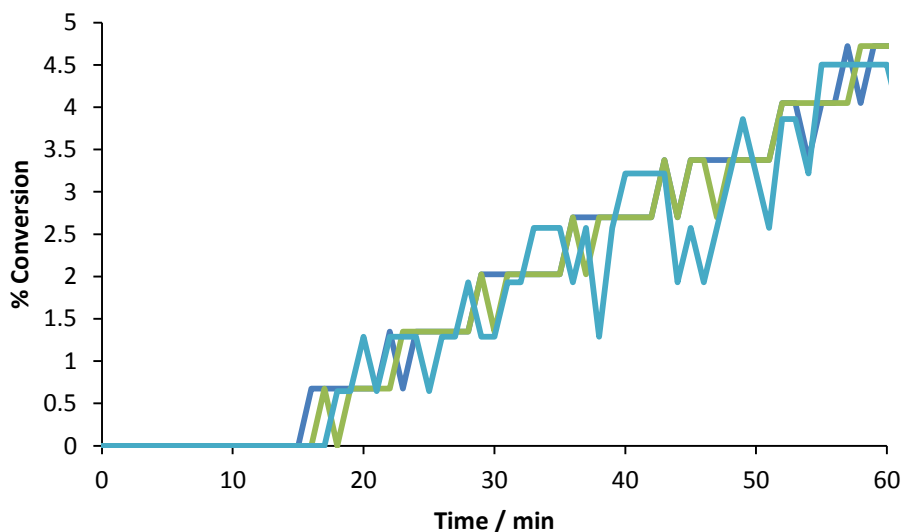


Figure 17. 3 dilatometry samples of 100ppm MEHQ in styrene polymerisation at 90°C

All phenolic inhibitors rely upon oxygen to work. As demonstrated with MEHQ, this dilatometry experiment cannot be easily used to monitor inhibition by oxygen dependent inhibitors, such as phenolic inhibitors.

2.4.4 Conclusions on the new dilatometry set-up

A new dilatometry set has been developed, that uses a small amount (0.03 ml) of inhibited sample. The sample preparation is simple and the data acquisition and analysis are completely automated. Multiple samples can be run simultaneously making this method efficient. As the sample tubes are inexpensive, the polymerisations can be run to completion, without worry of loss of equipment. The method can detect long inhibition periods and can distinguish between inhibitors and retarders.

The rate of oxygen diffusion into chlorobenzene has been observed to be extremely slow at 110 °C. The rate of oxygen consumption by styrene has also been observed by a similar method. As the rate of diffusion is much slower than the rate of consumption, the effect of oxygen diffusing into the solution from the headspace of the dilatometry capillary has been deemed insignificant and can be ignored.

Toluene has been run alongside styrene as an example of a non-polymerisable material, and showed no change in meniscus height when monitored by the dilatometry setup. This demonstrates that the change in height shown by styrene is due to polymerisation.

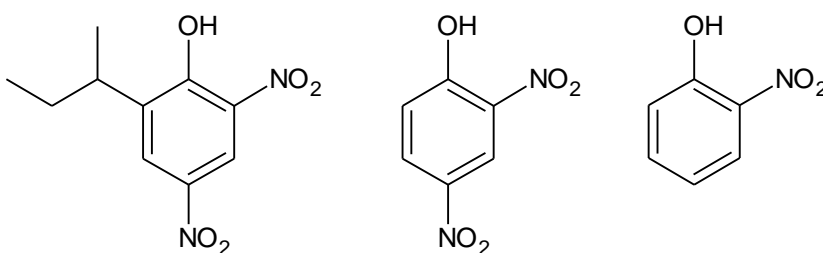
TEMPO has been used as an example of a polymerisation inhibitor. The concentration dependence of the inhibition time has been observed by the dilatometry experiment, and proved the concept of determining the onset of polymerisation after inhibition.

MEHQ was chosen as an example of an oxygen dependent inhibitor. As demonstrated earlier, the oxygen is consumed within the first few minutes. At 110 °C there was no inhibition observable. At 90 °C, there was a short inhibition period of 15 min. At the concentration used, this is a demonstration of the limits of the dilatometry experiment. The method cannot be used to observe oxygen dependent inhibitors. This will be a useful tool for differentiating between inhibitors that need oxygen and those that do not.

2.5 Dilatometry study of the inhibition properties of ortho-nitrophenols and related compounds

2.5.1 DNBP, 2,4-dinitrophenol and 2-nitrophenol

In order to determine why DNBP is an effective inhibitor, the exact functional group where the inhibition takes place needs to be known. By using the dilatometry setup described earlier and taking structurally related molecules, this can be determined. Figure 18 shows the dilatometry trace for DNBP, 2,4-dinitrophenol and 2-nitrophenol, their structures given in Scheme 23. The concentration used was 0.1 M, and is the concentration used throughout the dilatometry screening process.



Scheme 23 A common polymerisation inhibitor (DNBP, left) with analogues investigated; 2,4-dinitrophenol (middle) and 2-nitrophenol (right)

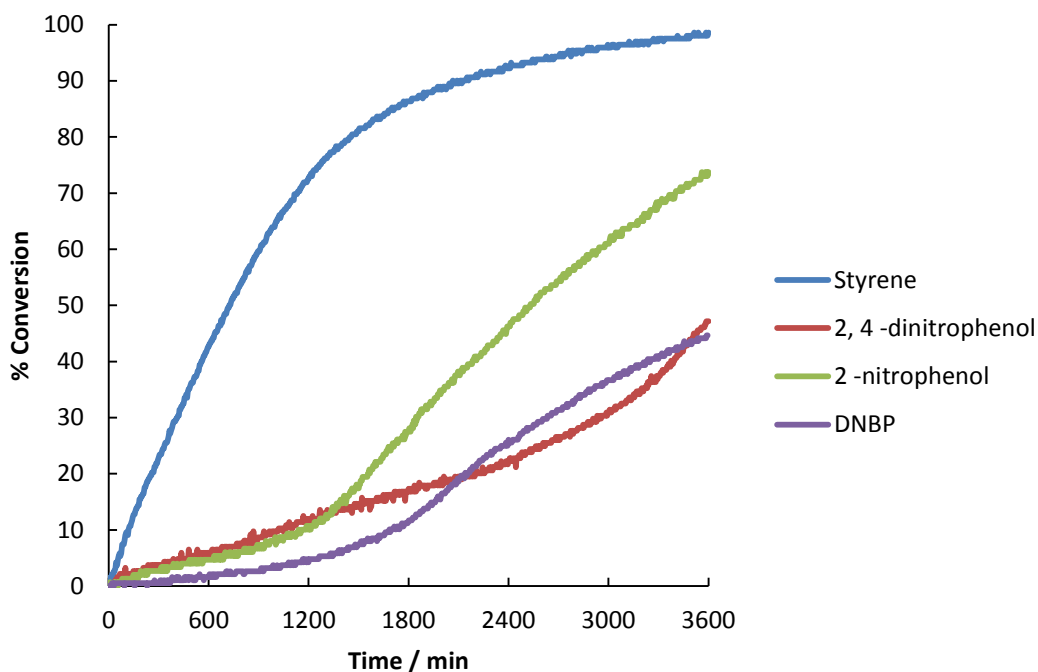


Figure 18 Dilatometry trace of uninhibited styrene, 0.1M DNBP, 0.1M 2,4-dinitrophenol, and 0.1M 2-nitrophenol (in styrene) at 110 °C.

The dilatometry traces show that there is a significant difference in the change in the rate of conversion between the inhibited samples compared to uninhibited styrene. This is due to the polymerisation being retarded due to the presence of the inhibitors. The dilatometry was run until the rate of conversion of the styrene sample slowed down, this change in rate occurs when most of the styrene is polymerised, and the rate of polymerisation is restricted by properties such as low concentration of unpolymerised styrene and viscosity. The inhibited samples are not polymerised (e.g., remain fluid) at this point, which shows that the polymerisation was indeed inhibited.

All the inhibitors used here are nitrophenols and the dilatometry results can determine if the inhibition is taking place at the nitro or the phenol group. As explained in the Introduction section, page 43, and MEHQ inhibitor case study, page 70, phenolic inhibitors require oxygen in order to inhibit the spontaneous polymerisation. The dilatometry has a very limited oxygen supply, as described earlier in section 2.3.7, which is consumed within minutes of the start of the experiment. These compounds appear to inhibit long after this has occurred, and therefore a phenolic mechanism of inhibition is unlikely to be responsible for the inhibition properties of these molecules. This is discussed further in section 2.5.3, on page 76.

DNBP, the industrially used inhibitor, has a number of functional groups in its structure. To aid in the understanding of the inhibition mechanism, 2-nitrophenol, a simpler but related molecule to DNBP will be investigated first. Then if required the effect of the second nitro group and the sec-butyl chain will be investigated.

2.5.2 2-Nitrophenol, 3-nitrophenol and 4-nitrophenol

The first structural detail to investigate is the position of the nitro group relative to the phenol group. By comparing 2, 3 and 4-nitrophenols, and nitrobenzene (i.e. no phenol group), the effect of the orientation of these two groups can be determined. The initial rate of polymerisation in the 3-nitrophenol, 4-nitrophenol and nitrobenzene samples is still less than uninhibited styrene, but nowhere near as slow as for 2-nitrophenol.

As the dilatometry traces for nitrobenzene, 3 and 4-nitrophenol, are nearly identical, it can be inferred there is no interaction between the nitro group and phenol group in these compounds. The inhibition by 2-nitrophenol is much greater, suggesting the interaction between the two groups are need for efficient inhibition.

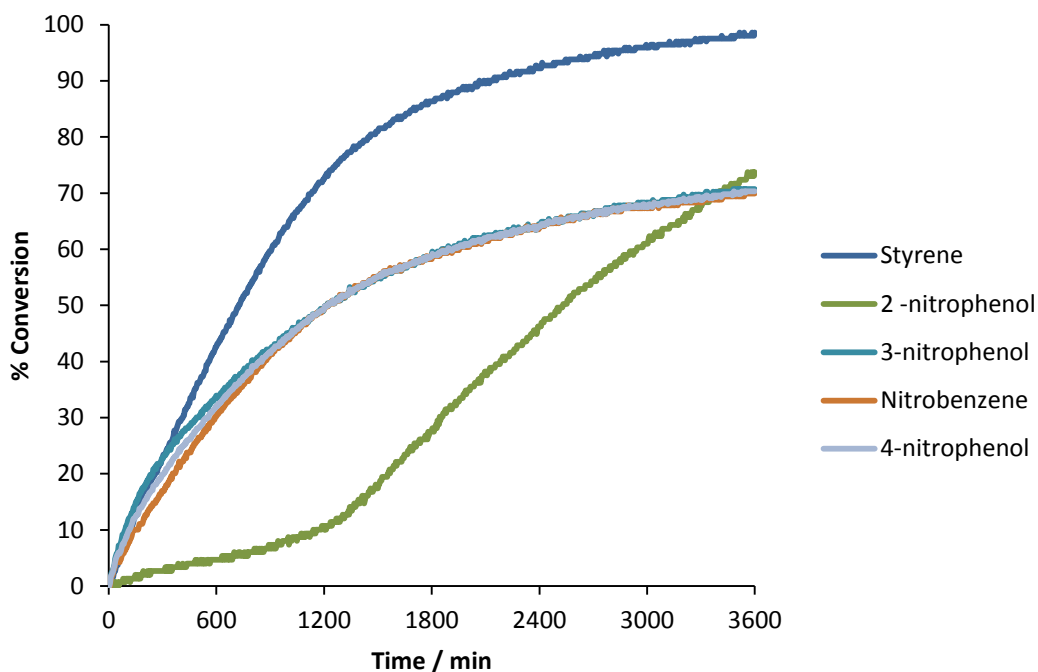


Figure 19 Dilatometry traces of styrene, 0.1 M 2-nitrophenol, 0.1 M 3-nitrophenol and 0.1 M 4-nitrophenol (in styrene) at 110 °C.

Figure 19 has revealed an interesting observation. The dilatometry traces for nitrobenzene, 3- and 4-nitrophenol show that conversion reaches a plateau at ca. 70%. This could be due to these molecules possessing some inhibition activity. East et al⁸⁴ have shown that the density of a polymer is related to the degree of polymerisation. Nitrobenzene, 3-nitrophenol and 4-nitrophenol may be acting as an inefficient inhibitor and limit the chain growth of the polymer. This would result in a less dense polymer, which would be observed by the dilatometer as an incomplete polymerisation.

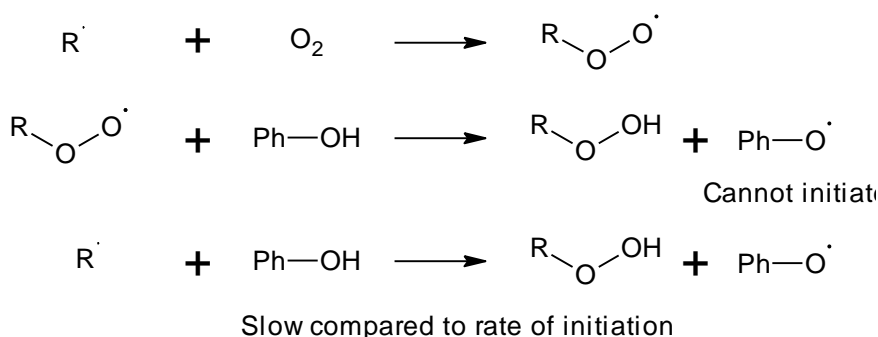
Figure 19 also demonstrates that running the reactions to completion is not necessary to establish inhibition efficiency for these compounds. 2-Nitrophenol is the baseline for the comparisons and has a change in the rate of polymerisation at around 1500 minutes. Any differences in inhibition properties will be observable before then. Therefore, the following dilatometry runs were stopped after 840 minutes to make effective use of time, unless a longer dilatometry run provides more information.

2.5.3 The structural group responsible for inhibition

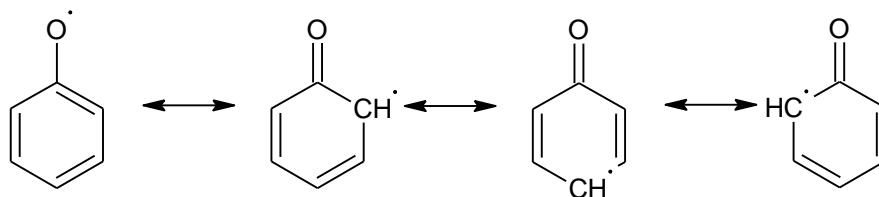
DNBP contains two known inhibitor groups; nitro and phenol. It is not known if the two inhibit separately, through their own separate mechanisms, or through an interaction of the two groups. From the dilatometry experiment, comparing 2, 3 and 4-nitrophenols, there appears to be a structural element to the inhibition efficacy.

Starting with the known mechanisms, phenolic inhibitors work through donating their hydrogen to peroxy radicals, as discussed by Levy et al^{55,85}, and described in the introduction chapter (Section 1.3.2.1. on page 43). Levy et al discussed the properties of 4-methoxyphenol (also called monomethyl ether hydroquinone or MEHQ) which is a common storage inhibitor. They showed that MEHQ is only efficient in the presence of oxygen. Their mechanism suggested that the initial step in the inhibition is due to the initiator radical first reacting with oxygen dissolved in the monomer. Oxygen consumption by monomers has been studied^{37,56,86}, and has been used as a way of monitoring self-polymerisation in stored monomers.

The peroxy radical that forms is then quenched by phenols in the above examples, through the donation of its phenolic hydrogen to form peroxide. The phenoxy radical that is formed is stabilised through resonance, and does not initiate polymerisation. This is depicted in Scheme 24 and Scheme 25. The direct donation of the phenolic hydrogen to carbon-centred radicals (3rd reaction in Scheme 24) is an insufficiently fast reaction to inhibit polymerisation⁸⁷, and hence phenolic inhibitors do not work in the absence of oxygen.



Scheme 24. Demonstration of phenolic inhibition mechanism^{55,85}

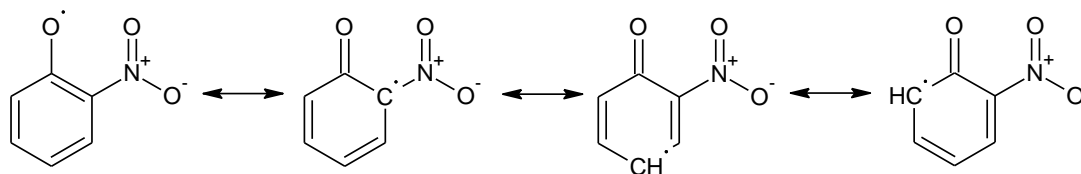


Scheme 25. The resonance structures of a phenoxy radical

The lack of inhibition of styrene polymerisation by phenols in the absence of oxygen is confirmed in this work. In the case of the dilatometry presented above, the experimental setup has a limited supply of oxygen. This was investigated when the dilatometry setup was developed (section 2.3.7 on page 64). MEHQ was shown not to inhibit styrene polymerisation in the absence of oxygen (section 2.4.3 on page 70). The samples of 2-nitrophenol, 2,4-dinitrophenol and DNBP however showed strong inhibition properties in the absence of oxygen, unlike MEHQ. This suggests that the nitrophenols may not inhibit through the same mechanism as MEHQ. To summarise, the very fact that *o*-nitrophenols are efficient polymerisation inhibitors in the absence of oxygen strongly suggests that their inhibition mechanism is not based on the H abstraction from the OH group.

Another strong argument against nitrophenols acting as inhibitors through the OH group is that the dilatometry traces for 3-, 4-nitrophenols and nitrobenzene are all very similar but quite different from that of 2-nitrophenol (section 2.5.2 on page 74). In particular, the fact that nitrobenzene and 3-nitrophenol show nearly identical dilatometry profiles which are very different from that of 2-nitrophenol suggests that inhibition properties of nitrobenzene and 3-nitrophenol are determined by the nitro group. The much higher inhibition efficiency of 2-nitrophenol can be explained by either of the following arguments:

- 2-nitrophenol inhibition properties are due to the OH group which is weaker due to resonance stabilisation of the corresponding phenoxyl radical (Scheme 26), or
- 2-nitrophenol inhibition properties are due to the nitro group but are enhanced by the presence of the OH group in the ortho-position.



Scheme 26. The resonance structures of 2-nitrophenol after phenolic hydrogen donation.

The former argument can be ruled out for two reasons:

- (a) Unlike 2-nitrophenol, 4-nitrophenol shows nearly identical inhibition properties to those of 3-nitrophenol (section 2.5.2 on page 74). Resonance stabilisation of 2- and 4-nitrophenoxyl radicals should be similar; if nitrophenols inhibited by donating a phenolic hydrogen, one would expect very similar inhibition properties for 2- and 4-nitrophenols;
- (b) Bond dissociation enthalpies of the phenolic O-H bond suggest that 2-nitrophenol is a *poorer* hydrogen atom donor than 3- or 4-nitrophenols by up to 50 kJ/mol⁸⁸, and 4-nitrophenol is a poorer hydrogen atom donor than 3-nitrophenol. Hence 2-nitrophenol should be a much worse inhibitor than the 3- and 4-isomers. This apparently counter-intuitive trend can be explained by the fact that organic radicals in general are stabilised by electron-donating substituents⁸⁹, and resonance stabilisation of the phenoxyl radical by (-M) groups such as nitro group is minimal. On the contrary, the OH bond in 2- and 4-nitrophenols is stronger than in 3-nitrophenol as the nitrophenols themselves (e.g., not nitrophenoxyl radicals) are stabilised by resonance (Scheme 26). In addition, a strong hydrogen bond (up to 30-40 kJ/mol) significantly increases the strength of the OH bond in 2-nitrophenol (Figure 21)^{90, 91}

It should be noted that one literature compilation by Borges de Santos et al⁹² suggests an opposite order of bond dissociation enthalpies, in disagreement with the other literature⁸⁷⁻⁸⁹. On inspection however this was traced to the original paper⁹³ which investigated the strength of O-C bonds in substituted anisoles rather than O-H bond in phenols. The authors suggest that the trends in O-C bond strengths in anisoles should match the trends in O-H bond strengths in phenols. While this is likely to be true for 3- and 4-substituted compounds, the trends are very different for 2-substituted compounds which show intramolecular hydrogen bond. We have therefore disregarded the trends for substituted anisoles in the following discussion.

To summarise, bond dissociation energies of the O-H bond predict the following order of inhibition efficiencies if the inhibitors work by donating phenolic hydrogen: 3->4->2-nitrophenol. This is inconsistent with the experimental data.

We conclude therefore that the inhibition properties of 2-nitrophenol are not related to the hydrogen abstraction from the phenolic OH bond. This is further confirmed by the dilatometry results for nitroacetanilides (later in this chapter, section 2.5.6 on page 83). The inhibition properties of 2-nitrophenol are therefore due to the nitro group and are enhanced by the presence of the 2-hydroxy group.

Figure 20 demonstrates the change in electron density of the nitro group between 2-nitrophenol and 4-nitrophenol. There is symmetry in the nitro group when it is para to the phenol group, but when the groups are ortho, there is no symmetry. This asymmetry may lead to a change in the observed bond order, as demonstrated in Figure 21.

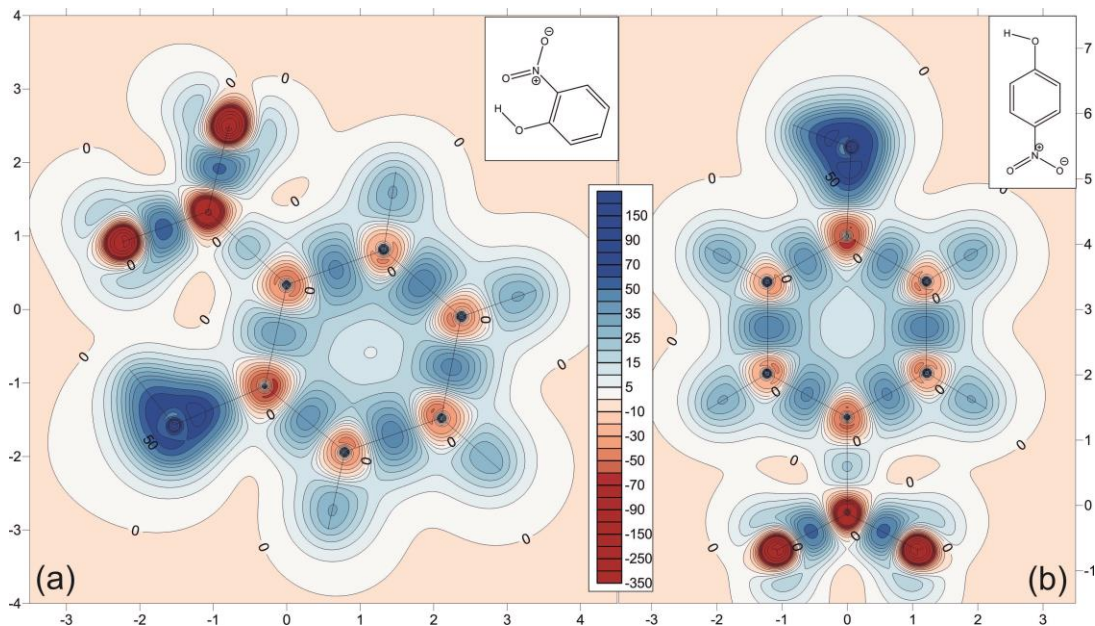


Figure 20. Contour plot of the isotropic chemical shielding (ppm) through the molecular plane of 2-nitrophenol (a) and 4-nitrophenol (b) calculated at the MP2/6-311++G(d,p) level of theory.

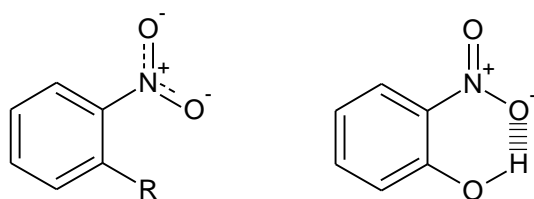


Figure 21. Demonstration of difference in bond order of the nitro group without hydrogen bonding (Left) and with hydrogen bonding (Right)

With hydrogen bonding, the nitro group can be described as asymmetric with one nearly single N-O bond and one nearly double N=O bond. The N=O group with the higher bond order may be more susceptible to attack from the spontaneous polymerisation initiator radical, increasing the rate of attack, and therefore the rate of retardation.

The focus of the investigation should be on altering the strength of the hydrogen bond to the nitro group. If the efficiency changes in relation to the changes in this bond strength, this would be confirmation that nitrophenols inhibit through the nitro mechanisms, enhanced by the hydrogen bonding from the phenol group.

2.5.4 Nitroanilines

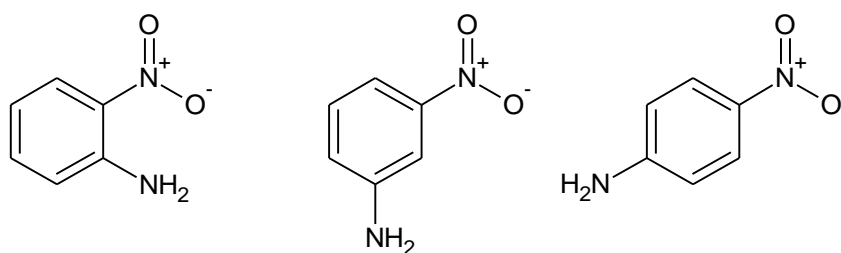


Figure 22. 2-Nitroaniline, 3-nitroaniline and 4-nitroaniline

As stated previously, as nitrophenol inhibitors still work as inhibitors after oxygen is consumed, it is not likely to go via the inhibition mechanism of pure phenolic inhibitors. However, the relative position of the nitro group and the phenol group appears to be an important factor in determining the polymerisation inhibition efficiency of an inhibitor. This could be due to steric or H-bonding effects. Replacing the phenol group with other functional groups may narrow down why the relative position of the nitro group and the phenol affects the inhibition of spontaneous polymerisation.

The dilatometry of 2-nitroaniline (amine group replacing the phenol) is given in Figure 23. 2-Nitroaniline appears to act as a polymerisation inhibitor that is better than nitrobenzene, but not as efficient as 2-nitrophenol. Again, by looking at the same groups, but in a different position, we see a drop in the inhibition efficiency when the two groups are not ortho. 4-Nitroaniline was not analysed, due to poor solubility in styrene. The 3-nitroaniline sample needed to be preheated to dissolve the inhibitor before adding to the glass sample tube.

The interaction with the nitro group that gives rise to the efficiency of 2-nitrophenol appears to also be present in 2-nitroaniline, but not to the same scale. This interaction is not present in meta- or para-substituted molecules. This does not eliminate either steric or H-bonding interactions as the property of a molecule that determines polymerisation inhibition efficiency.

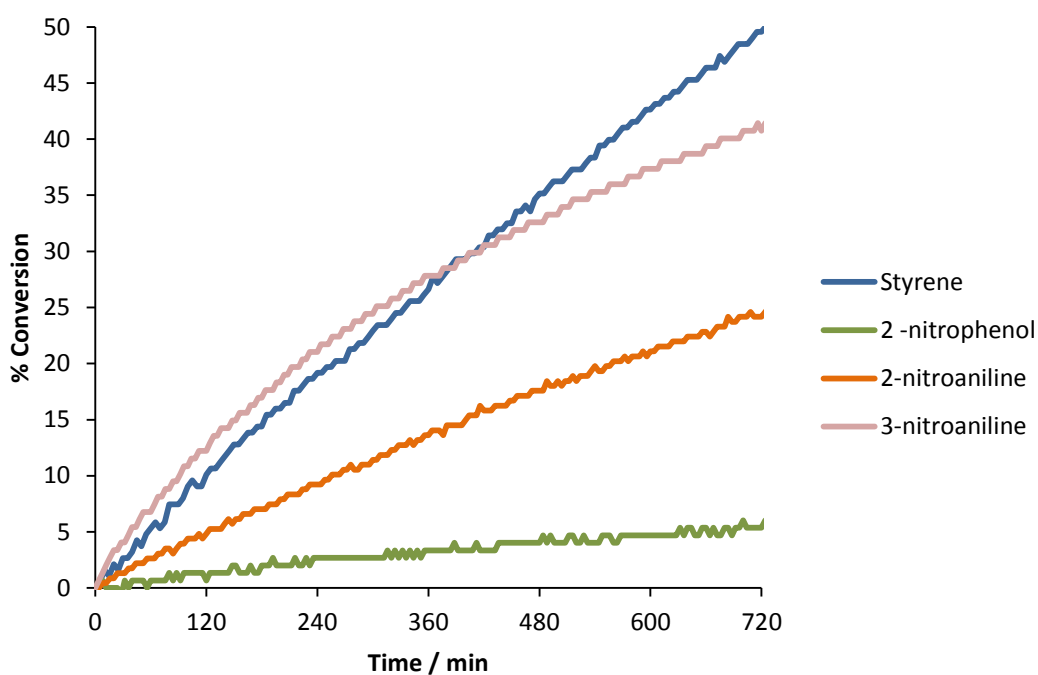


Figure 23 Dilatometry of styrene, 0.1 M 2-nitrophenol, 0.1 M 2-nitroaniline and 0.1 M 3-nitroaniline (in styrene) at 110 °C.

2.5.5 Nitroanisole (removing the hydrogen bond to the nitro group)

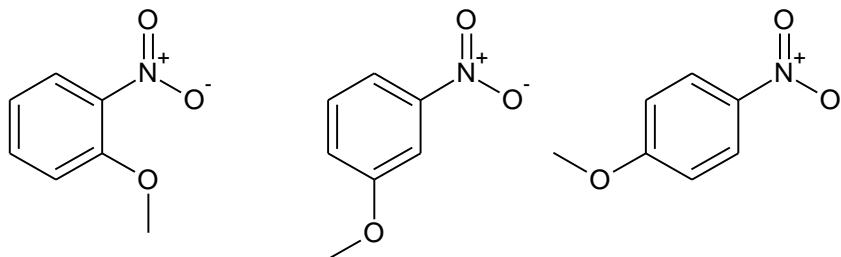


Figure 24. 2-Nitroanisole, 3-nitroanisole and 4-nitroanisole

One possible interaction between the ortho-nitro and phenol groups is hydrogen bonding. 2-Nitroanisole is similar, but lacks the H-bond donor and hence will make it possible to distinguish if the effect of an adjacent group is due to H-bond formation or steric. The results in Figure 25 show that there is little difference in inhibition efficiency between 3 and 4-nitroanisole, with 2-nitroanisole showing slightly more inhibition efficiency. Compared to the inhibition efficiency of nitrobenzene they are all very similar.

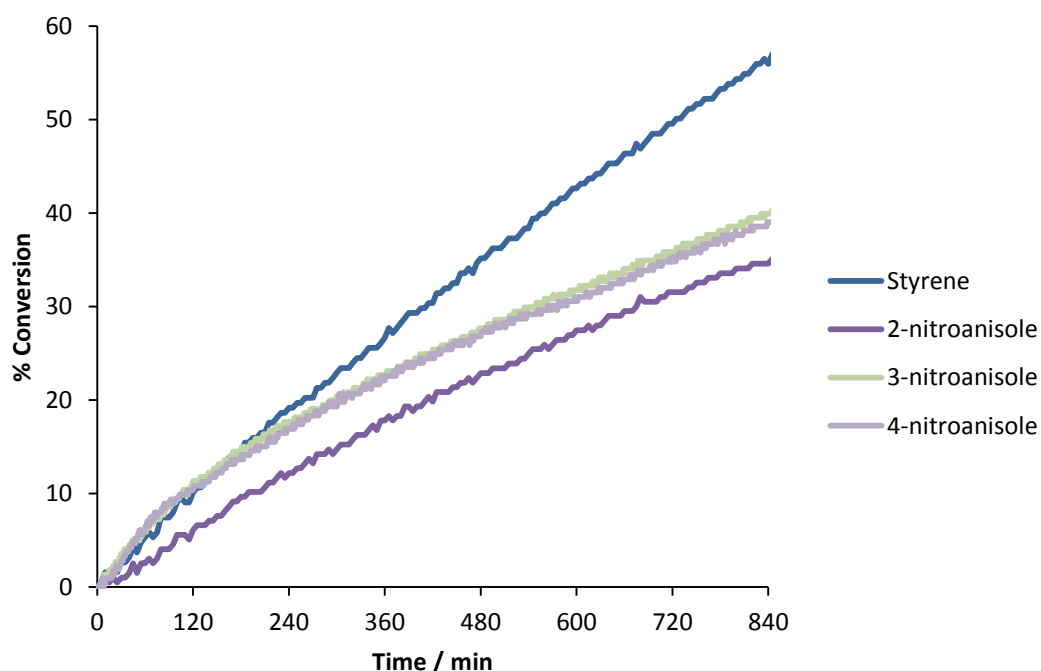


Figure 25. Dilatometry of styrene, 0.1M 2-, 3- and 4-nitroanisole (in styrene) at 110 °C.

2.5.6 2-Nitroacetanilide and 2-nitrotrifluoroacetanilide

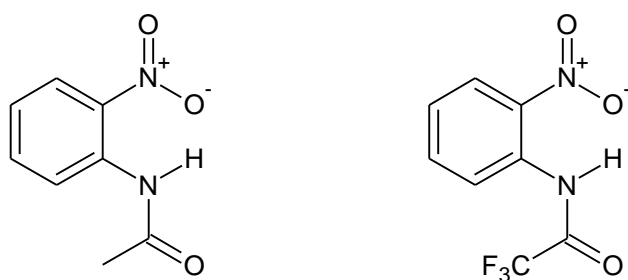


Figure 26. 2-Nitroacetanilide and 2-nitrotrifluoroacetanilid

2-Nitroacetanilide and 2-nitrotrifluoroacetanilide are molecules that may have hydrogen bonding between two functional groups. The trifluoro derivative was used to observe the effects of a more electron withdrawing group.

The increase in inductive effect between 2-nitroacetanilide and 2-nitrotrifluoroacetanilide will also increase the hydrogen bond strength in 2-nitrotrifluoroacetanilide.

The results in Figure 27 show that both acetanilides are indeed efficient inhibitors at 0.1 M. This dilatometry run was extended to the full 3600 minutes, which shows that 2-nitroacetanilide and 2-nitrotrifluoroacetanilide outperform 2-nitrophenol at this concentration. There appears to be little difference between 2-nitroacetanilide and 2-nitrotrifluoroacetanilide, suggesting that the strength of hydrogen bond does not significantly influence the inhibition.

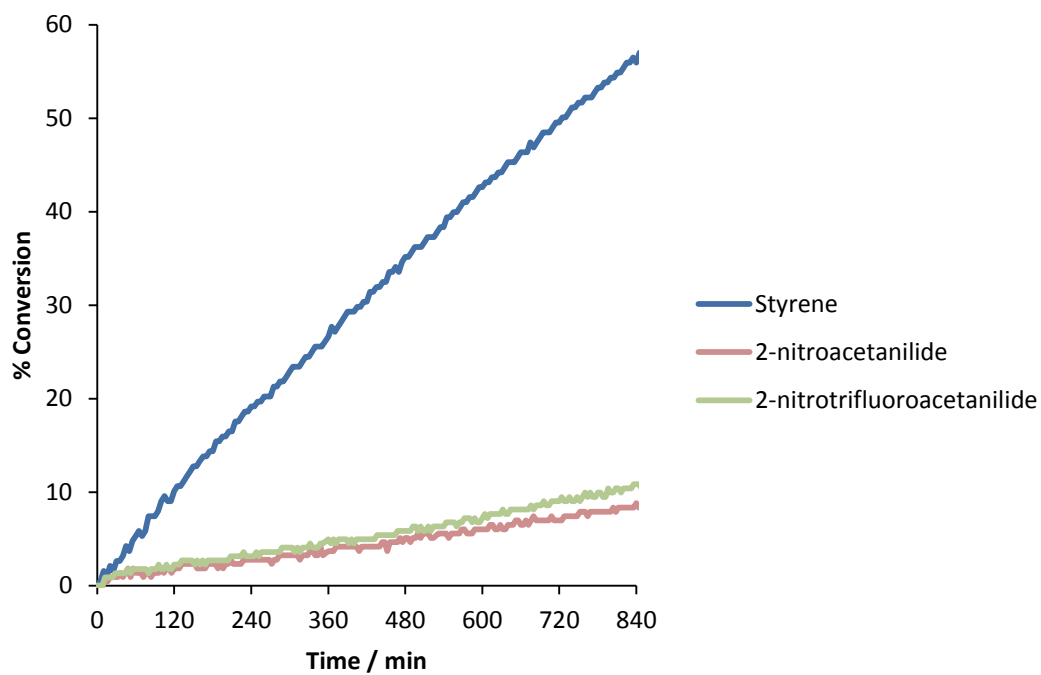


Figure 27. Dilatometry traces of styrene, 0.1 M 2-nitroacetanilide and 0.1 M 2-nitrotrifluoroacetanilide (in styrene) at 110 °C.

Changing the concentration to a more realistic value of 3 mmol, 2-nitroacetanilide still shows a comparable retardation rate to 2-nitrophenol, shown in Figure 28. This is further confirmation the phenolic group is not responsible for the inhibition activity of 2-nitrophenol.

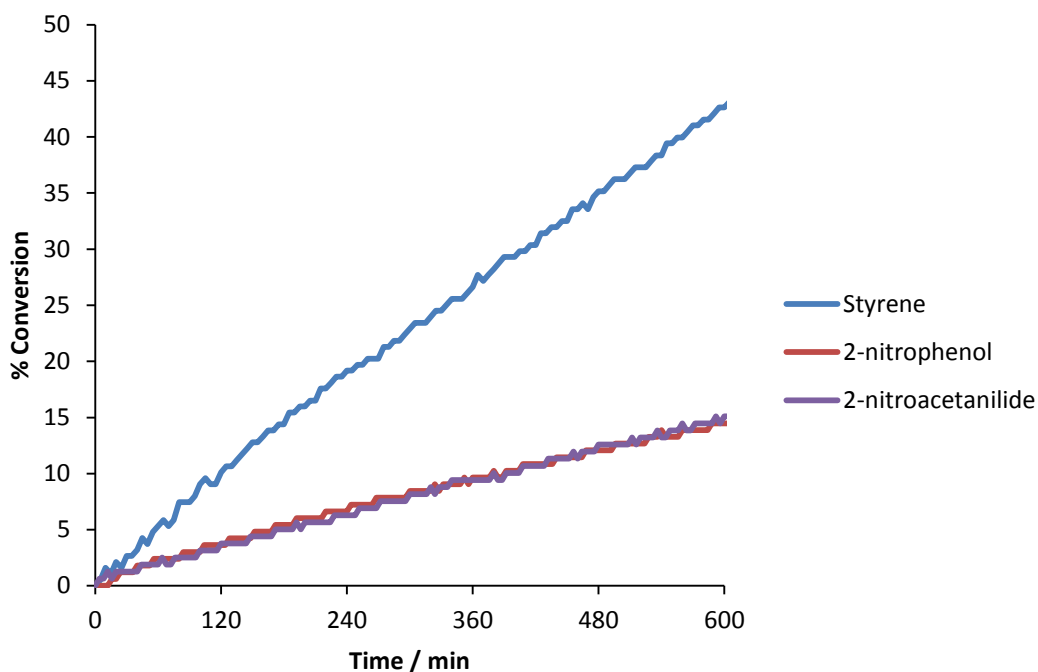


Figure 28. Dilatometry trace for 3 mmol 2-nitrophenol and 2-nitroacetanilide inhibited styrene at 110°C.

2.6 Conclusions from the dilatometry screening experiment

A small scale, automated dilatometry experiment has been designed and developed with the aim of determining the onset of polymerisation after inhibition. The design makes use of a commercial digital camera to observe the change in height caused by the increase in bulk density of the sample as polymerisation occurs. Purpose built equipment has been made to optimise the number of samples that can be run at a time

The effect of oxygen as an inhibitor in these types of samples was studied. The rate of diffusion was determined by monitoring a sample of TEMPO in chlorobenzene by EPR. The diffusion rate at 110 °C is extremely slow. The rate of oxygen consumption by styrene spontaneous polymerisation was also determined in a similar way, and was shown to be quick; complete consumption within a few minutes. By assuming the rate of oxygen diffusion into chlorobenzene is the same as in styrene, it can be concluded that the rate of oxygen diffusion into the styrene will not have an effect on the inhibition period caused by

oxygen. Therefore only the oxygen already dissolved in styrene at the start of the dilatometry experiment should be considered, and the oxygen in the head space ignored.

At a concentration 0.1 M, a number of the different molecules used in the screening showed good inhibition or retardation properties. However, when run at a more realistic concentration (3 mM), nothing could out-perform the industrially used inhibitor DNBP. Even when simplifying the study and using 2-nitrophenol as a baseline comparison, nothing could retard the rate of polymerisation by the same amount. If this method is to be used to evaluate potential inhibitors in the future, the concentration must be taken into account.

The first conclusion from the analysis of different nitrophenol inhibitors by the dilatometer is that they continue to inhibit or retard after the oxygen dissolved in styrene has been consumed. Therefore the inhibitors do not follow the inhibition mechanism that phenolic inhibitors use. This could mean that the nitro group is the functional group responsible for inhibition. Consideration of O-H bond strength and other experimental data support this conclusion.

After screening aromatic nitro compounds a trend in the retardation rate can be seen. The molecules that can hydrogen bond between the nitro group and an adjacent group have increased inhibition efficiency. This is particularly clear when comparing 2-nitrophenol and 3- or 4-nitrophenol. 3- and 4-nitrophenols show the same retardation rate as nitrobenzene showing that the phenol group cannot partake in the polymerisation inhibition. Molecules such as 2-aminophenol and 2-nitroacetanilide, which also have hydrogen bonding to the nitro group from an adjacent group, show an increase in rate of retardation.

To further develop this theory, the product of the inhibition by 2-nitrophenol needs to be analysed. The products may show where the initiator species attacks the inhibitor, possibly confirming the conclusion that the nitro group is the inhibiting group. They may also show to what extent the phenol group is involved in the inhibition mechanism. It may stabilise the intermediates formed, or it may also react with the polymerisation initiators.

3. Nitrophenols as inhibitors – Product analysis

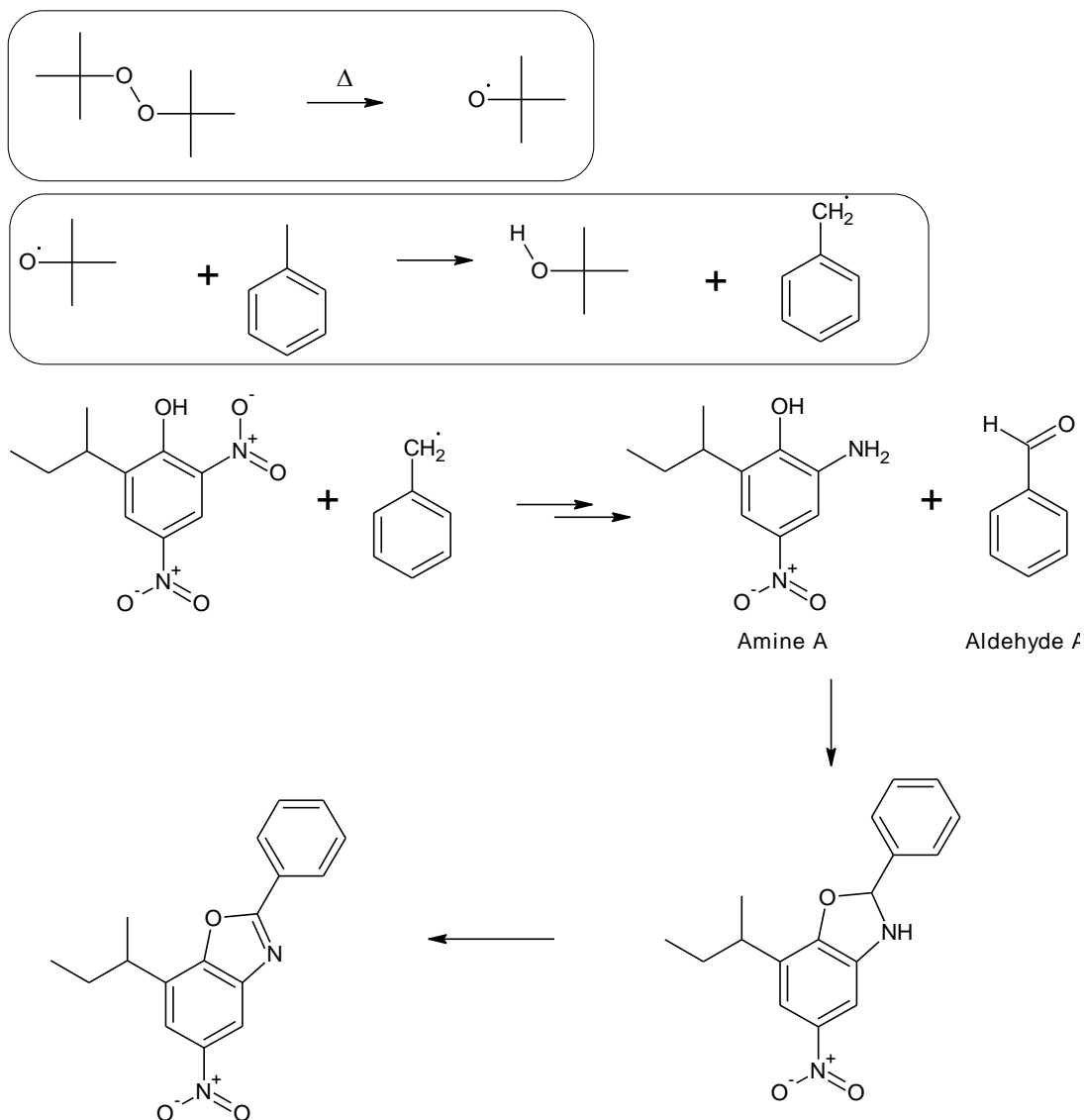
3.1 Introduction

The products of styrene spontaneous polymerisation inhibition by nitrophenols, such as DNBP, are not known. In a similar way to the dilatometry analysis, identifying the products from the inhibition by a simpler related molecule, such as 2-nitrophenol, may allow easier analysis of the inhibition mixture.

The concentrations of inhibitors used in industrial and commercial applications are low, ranging from ~10-750 ppm. This means any intermediates and products will also be in lower concentrations, depending on the mechanism. Therefore in this study, the concentrations of the inhibitors will be increased, as to allow usable and identifiable amounts of intermediates and / or products to be obtained.

In a paper, investigating a similar system to this, Bushby et al⁴⁵ proposed the reaction in Scheme 27. They used tert-butyl peroxide, a radical initiator, to form benzyl radicals from toluene. DNBP reacts with this in the same way as it would with a polymerisation initiator. They isolated the product 7-sec-butyl-5-nitro-2-phenolbenzoxazole from the reaction mixture.

They suggest the reaction follows the mechanism proposed by Jackson and Waters⁴⁶, where the nitro group is reduced to an amine group. From there, the two products from this reduction, (Amine A and aldehyde A in Scheme 27) react to form the dihydrobenzoxazole. This is then oxidised to the benzoxazole isolated. They suggest this route is the simplest of the possible mechanisms, but they do not discuss what the alternatives are. Their separation method may be adapted to isolate the products from a sample of inhibited styrene that has been heated to spontaneously polymerise.



Scheme 27. The proposed mechanism for the formation of a product isolated and characterised by Bushby et al⁴⁵.

3.2 MS analysis of inhibition product mixture

To obtain sufficient amounts of products from the inhibition of styrene spontaneous polymerisation by 2-nitrophenol, a 0.5 M solution of 2-nitrophenol in styrene (50 mL) was heated under reflux for 3 days. The ESI MS in Figure 29 shows the presence of two major peaks at m/z 110 and m/z 312. The identity of these may provide an insight into the mechanism. To ease the description of the identification method they will be referred to as unknown A (m/z 110) and unknown B (m/z 312).

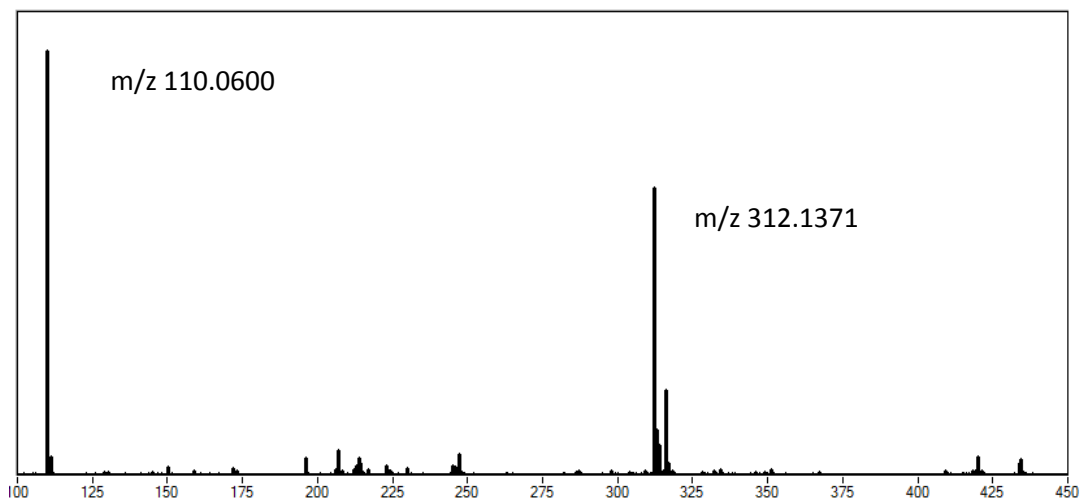


Figure 29. ESI MS of the high concentration 2-nitrophenol inhibition mixture.

In an attempt to increase the yield of these unknown products, a reaction mixture with the same concentration was heated for 8 days, until the viscosity greatly increased (due to styrene polymerisation). The MS results in Figure 30 show that the peak at m/z 312 had decreased. Therefore the 3 day mixture was used for further analysis.

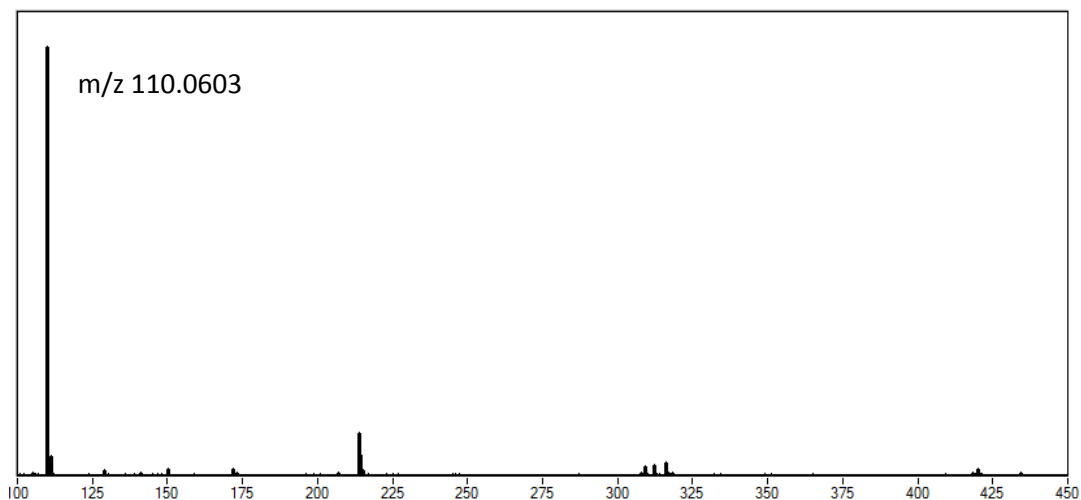


Figure 30. ESI MS of the high concentration 2-nitrophenol inhibition mixture heated for 8 days, until it became too viscous.

3.3 GC and GC / MS analysis of inhibition product mixture

The inhibited polymerisation results in a complex mixture. In order to identify the components, GC-MS was used to analyse the mixture. A few issues were raised with the practicality of analysing the reaction mixture by this method. As there will be the formation of styrene oligomers, as well as an excess of styrene in the sample, there is a possibility that the mixture would damage, or block the instrument. Therefore a sample that was only heated for 24 hours at 110°C was analysed. This should reduce the amount of styrene oligomers in the sample.

To prevent the instrument detector from burning out, the sample had to be split by the injection method. In this method, the sample is diluted as it is injected. Figure 31 shows that the gas chromatogram is dominated by styrene, and only a few oxidation products were observed. These were identified by comparing the MS EI fragmentation patterns to a database of compounds previously examined by this ionisation method. The structures given in Figure 31 are the structures that give the closest match, and can plausibly form in this reaction mixture.

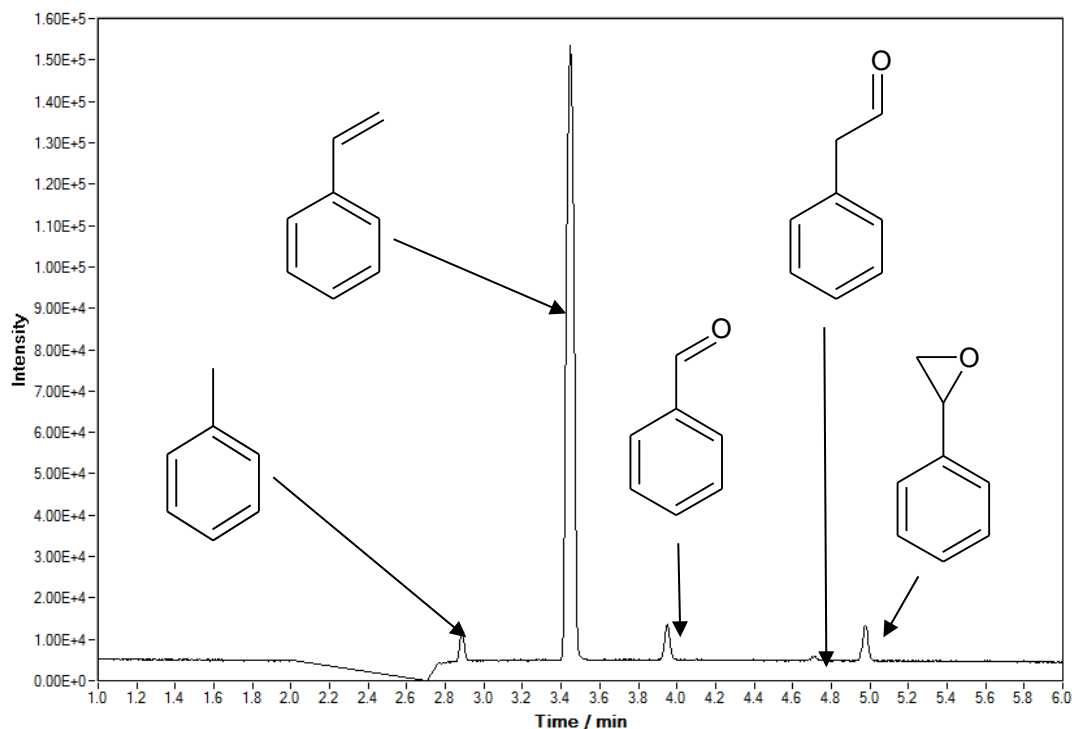


Figure 31. Gas chromatogram of 0.01M 2-nitrophenol in styrene heated at 110°C for 24 hours. Sample was split 50:1 at the injection.

As the sample is dominated by styrene, and the remaining products are not detectable because of the splitting of the injection, a different method was needed. To increase the signal to noise ratio of the other components, the detector was deactivated for the first 5 minutes of the analysis. This allowed a non-split injection to be used, without damaging the equipment. The chromatogram in Figure 32 shows that the inhibition products mixture is complex. The labels on Figure 32 refer to Table 3.

The results in Table 3 were obtained by taking the MS of the GC peaks and again comparing to the database of fragmentation patterns. Not all the GC peaks could be identified, due to the limited information in the database. Manually identifying the structures of the remaining peaks did not yield any further results. The structures given in Table 3 are the closest match to spectra from the database and cannot distinguish between stereoisomers. 2-nitrophenol was also identified, by running a GC of a known concentration of 2-nitrophenol in toluene and comparing to the crude mixture.

The results show the formation of styrene dimers, such as those observed by Mayo in uninhibited styrene polymerisation¹⁹, and other oxidation products. However, there were no observable MS peaks for m/z 110 or m/z 312 in any of the GC peaks.

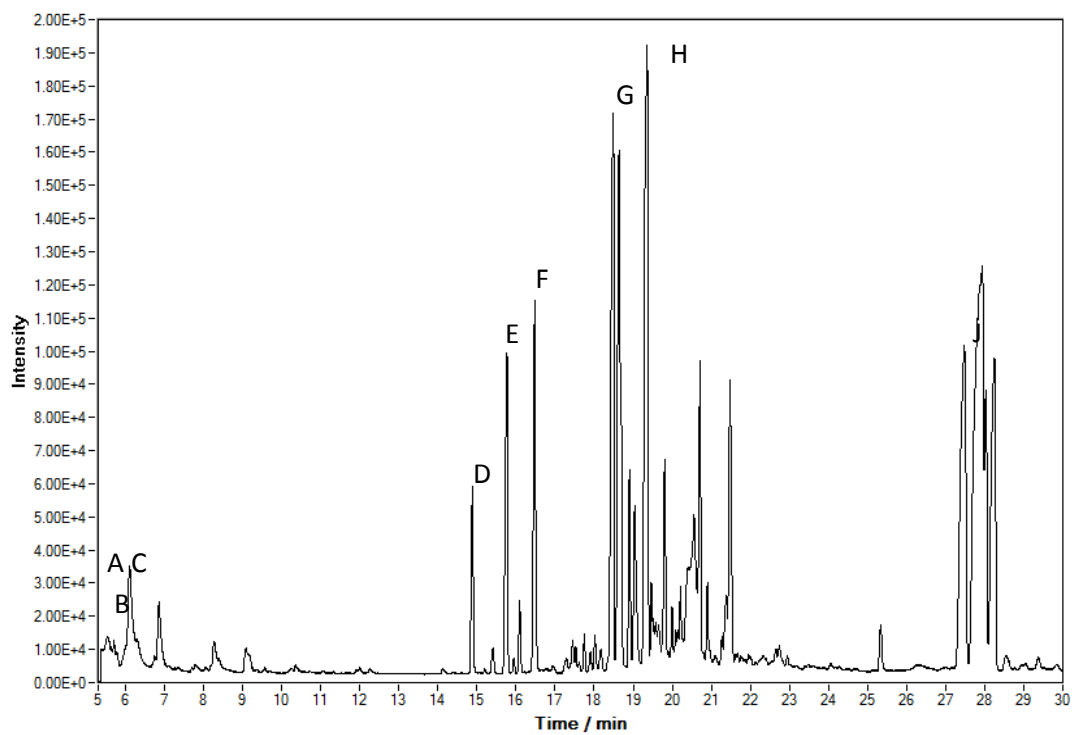
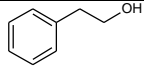
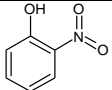
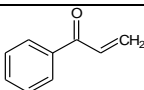
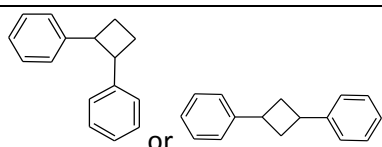
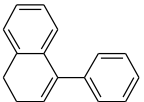
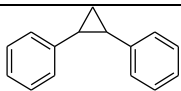
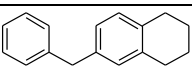
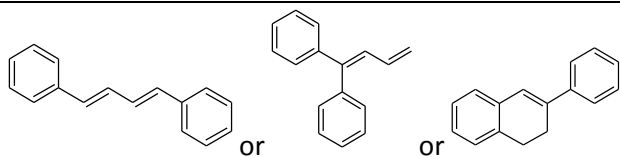


Figure 32. Gas chromatogram of 0.01M 2-nitrophenol in styrene heated at 110°C for 24 hours. Sample was not split, but detector was deactivated for the first 5 minutes of the chromatogram.

Table 3. Results of GC/MS on styrene inhibited by 2-nitrophenol.

GC Peak / min	Label	Possible structure
5.55	A	
5.70	B	 2-nitrophenol – starting inhibitor
6.11	C	
14.88	D	
15.77	E	
16.48	F	
18.49	G	
19.36	H	
27.48	I	

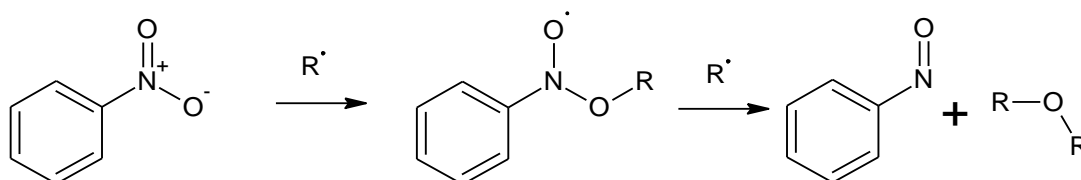
The reaction mixture is dominated by styrene and styrene dimers and short chain oligomers. In order to observe any inhibition products these need to be removed from the reaction mixture. Formation of these oligomers cannot be prevented in the reaction mixture as 2-nitrophenol is a retarder and not a true inhibitor. Bulk separation techniques will be required to isolate these products from the oligomers.

3.4 Identification of reactive intermediates by EPR

Previous studies have shown that propagating radicals will react with nitro groups to form nitroxides as intermediates in the reaction. Bartlett et al⁹⁴ specifically looked at the polymerisation of vinyl acetate inhibited by nitro compounds. EPR spectroscopy should be able to observe any long lived nitroxide radicals formed by the inhibition of spontaneous polymerisation.

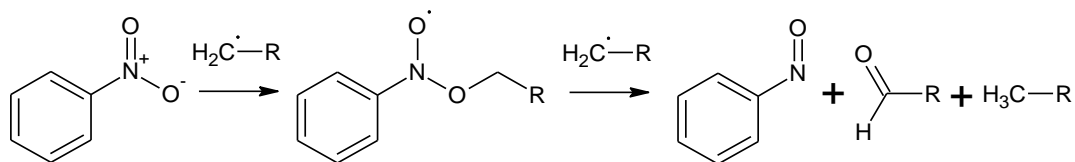
Also, it has been established that TEMPO is an efficient polymerisation inhibitor⁹⁵. If a nitroxide is formed from the reaction between radical initiator and inhibitor, it may be that the nitroxide is the inhibiting species rather than a nitro group itself. Similarly, as observed in the previous chapter, the interaction between the nitroxide and the phenol group may also play a part in the inhibition efficiency of ortho nitrophenols

The reaction in Scheme 28 shows the formation of an alkoxy nitroxide intermediate, followed by fragmentation to give a nitroso compound. Scheme 29 shows an alternative fragmentation of alkoxy nitroxide leading to the formation of nitroso compound, aldehyde and an alkane. Jackson and Waters⁴⁶ proposed this mechanism as they observed the formation of aldehyde in the experiments.

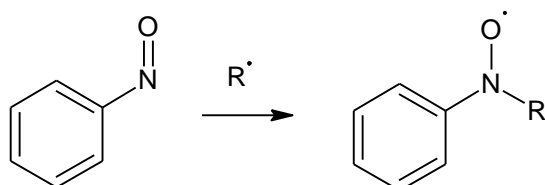


Scheme 28. Formation of nitroso arene as proposed by Bartlett et al⁹⁴, via a nitroxide intermediate.

Motyakin et al⁴⁹ recorded the EPR spectra for the nitroxide formed from nitro and nitroso containing inhibitors. Nitroso compounds can form dialkyl nitroxide radicals when they react with the carbon-centred radicals formed and the authors proposed that the observed radical is the alkyl aryl nitroxide formed from the nitroso compound (See Scheme 30). This also matches the hyperfine splitting from the EPR spectra.



Scheme 29. Formation of nitroso arene proposed by Jackson and Waters⁴⁶, via an alkoxy nitroxide intermediate.



Scheme 30. Formation of nitroxide from 2-nitrophenol, observed by EPR.

Figure 33 shows the EPR signal observed when 0.1 M 2-nitrophenol is heated in styrene at 130 °C. The signal is weak and increasing neither concentration nor temperature can increase the observed signal. Taking the average of the first 40 spectra did increase the signal to noise ratios only slightly, but not enough to measure the hyperfine constants.

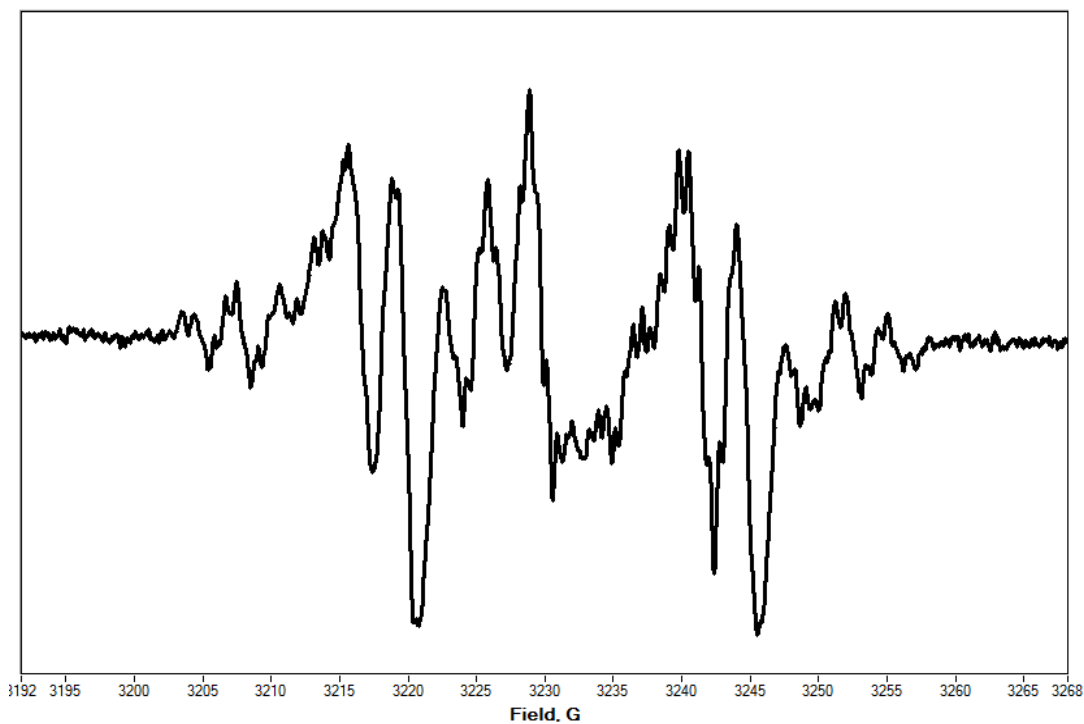
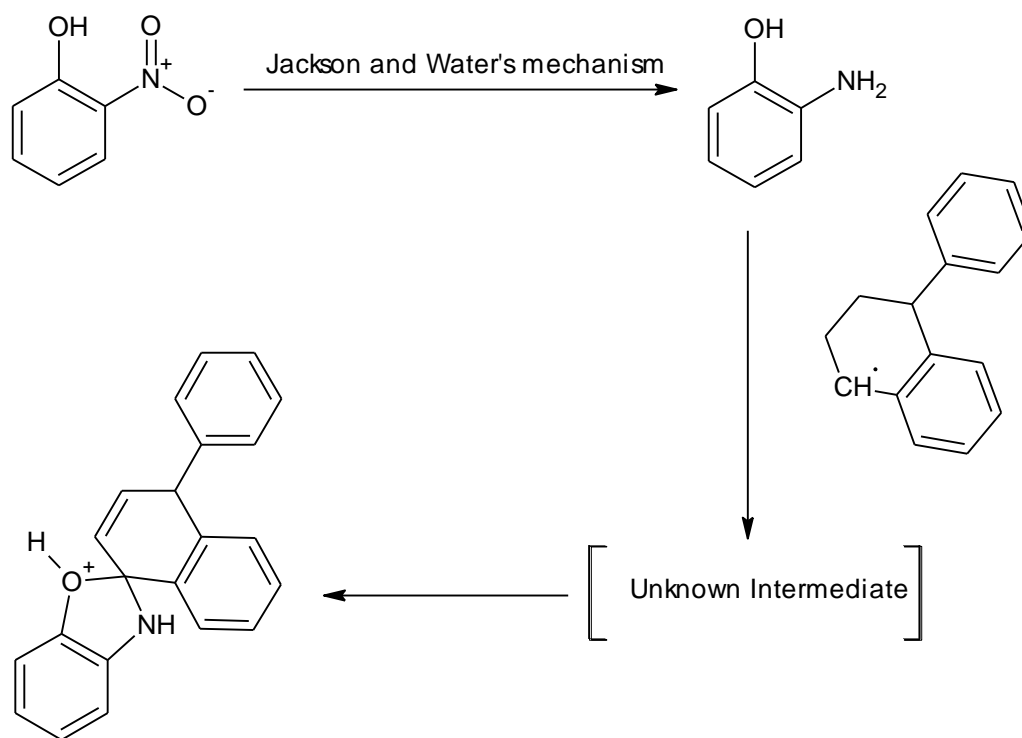


Figure 33. 0.1M 2-nitrophenol in styrene at 130°C, average of 40 spectra.

Motyakin et al⁴⁹ observed similar spectra, but with a much higher intensity when observing the reaction between styrene spontaneous polymerisation initiators and nitrophenol inhibitors. Here, the signal is too weak to extract hyperfine values to compare. It may be that the radical observed by Motyakin et al starts with nitrophenol and proceeds via a nitroso intermediate, however from these results that cannot be confirmed.

3.5 Isolation and identification of Unknown A and Unknown B

By following the procedure set out by Bushby et al,⁴⁵ unknowns A and B may be isolated and identified. By using the mass spectrum shown in Figure 29, the structural formula with the closest mass for unknown B is C₂₂H₁₇NO. By using the mechanism proposed by Bushby (Scheme 27) a similar structure fits the chemical formula. Scheme 31 show a possible mechanism and product that leads to unknown B. The proposed structure for unknown B is similar to the final intermediate proposed by Bushby et al⁴⁵ in Scheme 27. This would require the formation 2-aminophenol by the same mechanism as discussed by Jackson and Waters.⁴⁶



Scheme 31. Proposed formation of Unknown B following previous research by Jackson and Waters⁴⁶, and by Bushby et al⁴⁵.

3.5.1 Acid / Base extraction

To split the polymerisation inhibition mixture into smaller, less complex samples, it was dissolved in diethyl ether (50 mL) and then washed with aqueous acid (5 M HCl) and base (5 M NaOH) to isolate compounds with different acidic or basic groups. Normally the aqueous acidic or basic washes are neutralised and extracted with an organic or halogenated solvent. This however yielded nothing observable by NMR or MS.

Figure 34 shows the ESI of the acid extract and the remaining neutral organic layer. This shows that unknown A has been removed from the product mixture, leaving unknown B in the neutral organic solution. The neutral organic fraction yield after removal of solvent was 1.88 g from an input of 5 g crude; this suggests that a significant amount of material was extracted during washes.

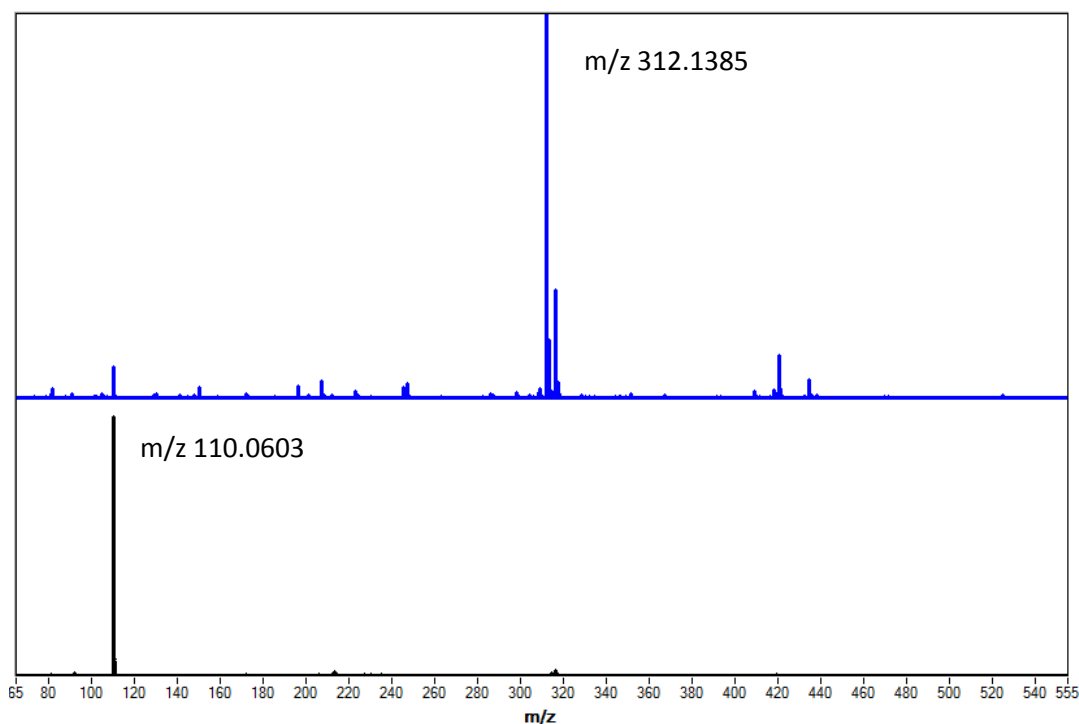


Figure 34. ESI MS of the acid extract (Black) and the neutral organic solution (Blue)

As nothing is isolated when neutralising the acid wash, analysis without neutralising may lead to m/z 110 being identified. By removing the water from the extract by a rotary evaporator and re-dissolving in deuterium oxide, the blue NMR spectrum in Figure 35 was obtained. From this and the MS data in Figure 29 on page 89, it can be confirmed that unknown A is 2-aminophenol. The yield obtained was $\sim 50\%$ of the input 2-nitrophenol.

To strengthen this assignment, a sample of stock 2-aminophenol was dissolved in acid (5 M HCl), solvent removed, and the residue re-dissolved in deuterium oxide, to recreate the conditions of the extracted sample. In Figure 35, the NMR of isolated unknown A (in blue) is compared the NMR of stock 2-aminophenol (in red). They are identical and the identification of unknown A is thus confirmed.

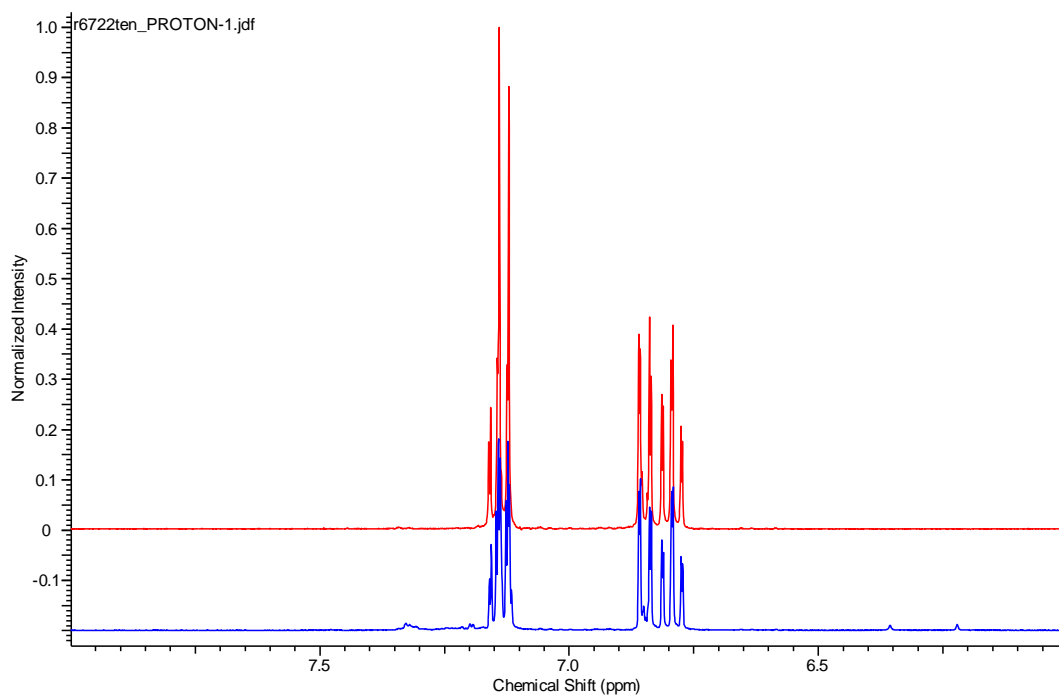


Figure 35. ^1H NMR of acid extract (Unknown A) in blue and 2-aminophenol in red. (400 MHz, CDCl_3)

3.5.2 Methanol precipitation

The styrene dimers and short chain oligomers formed in the reaction mixture mask the inhibition products, as seen previously (Section 3.3 on page 90) and need to be removed. Figure 36 shows the NMR spectrum of the spontaneous polymerisation inhibited by 2-nitrophenol reaction mixture, without any separation procedures applied. The spectrum is dominated by styrene but the shoulder on the aromatic peaks leads to inaccurate integration of the signals. If the oligomers are not removed from the inhibition products during the isolation, identification of the products will be difficult, as the products are expected to be aromatic.

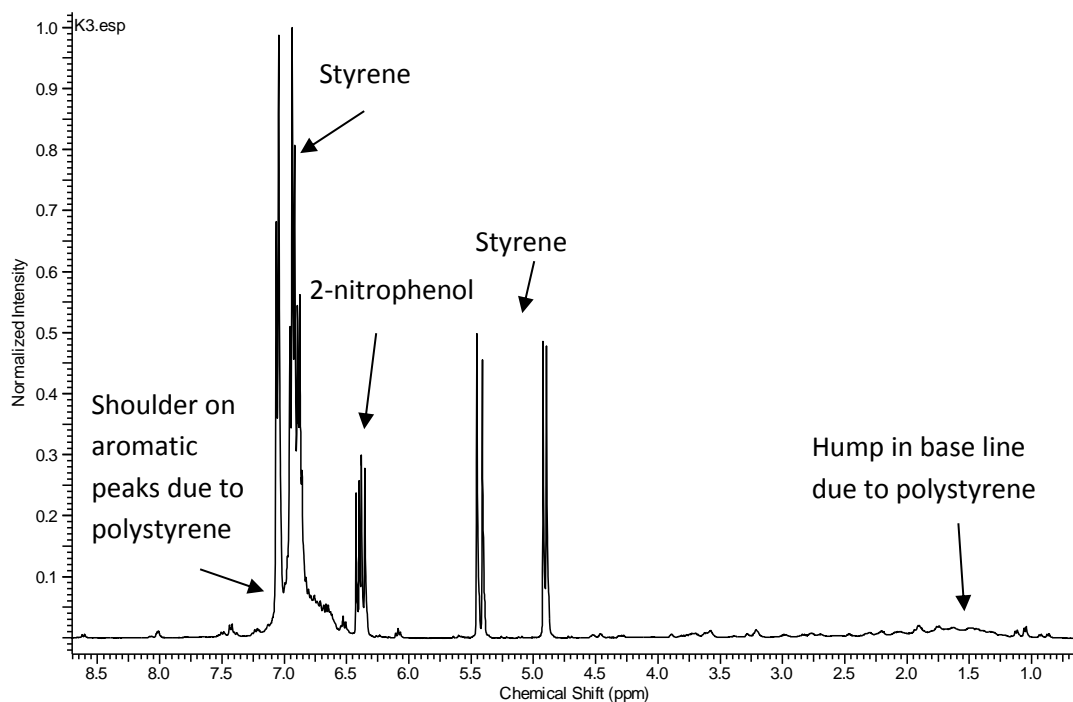


Figure 36. ^1H NMR of reaction mixture without any separation. (400 MHz, CDCl_3)

The longer polystyrene chains were therefore precipitated out by methanol. A slurry was obtained by adding the neutral fraction from the acid / base extraction to methanol. This was then cooled in a freezer for at least 2 hours then filtered through celite.

The precipitate obtained was not white as is expected for pure polystyrene, but was dark brown. This suggests there will be other inhibition products in the precipitate. Additional washes do not improve the yield of the methanol wash residue.

The methanol was removed by rotary evaporation. This also removes any excess styrene and other volatile compounds from the mixture.

3.5.3 Column chromatography

The next stage of separation was by column chromatography, monitored by TLC. The isolation of unknown B took longer than anticipated due to a number of factors that increased the difficulty of the isolation, such as its decomposition observed once isolated. The dominance and persistence of the polystyrene oligomers made identification of the compound after isolation difficult. The chromatography was performed as reported by Still et al⁹⁶, with further alterations, as described later. Through the use of different solvent

systems the separation of unknown B was obtained. The optimised procedure used two successive separations in different solvent systems: diethyl ether and 1:1 DCM : hexane. This was after many attempts, due to the poor stability of unknown B in neat form and due to the issues caused by polystyrene any other styrene oligomers remaining. The procedure given below is the final and most successful procedure developed.

A TLC using diethyl ether shows two main components, with R_f values of ~ 0.5 and ~ 0 . The spots at $R_f 0.5$ contained unknown B, as observed by MS. When evaluating the different systems, it was noticed that performing this separation first, allows the following samples to be separated easier, i.e. there is less streaking of the fractions visible on TLC plates.

The solvent system for the next separation was 1:1 DCM : hexane. Although similar separation can be achieved by other solvent systems, the reaction mixture is most soluble in this solvent system. This facilitates separation of larger samples.

Figure 37 is the MS of a fraction obtained from the mixture ($R_f = 0.33$ in 1:1 DCM: hexane, 72 mg collected). A strong peak with m/z 312 dominates the spectrum. The NMR of the fraction (Figure 38) shows that the sample is not pure, and the broad peaks from the impurities suggest that there are still short chain polystyrene oligomers present. These oligomers are soluble in methanol and are not volatile enough to be removed by vacuum distillation.

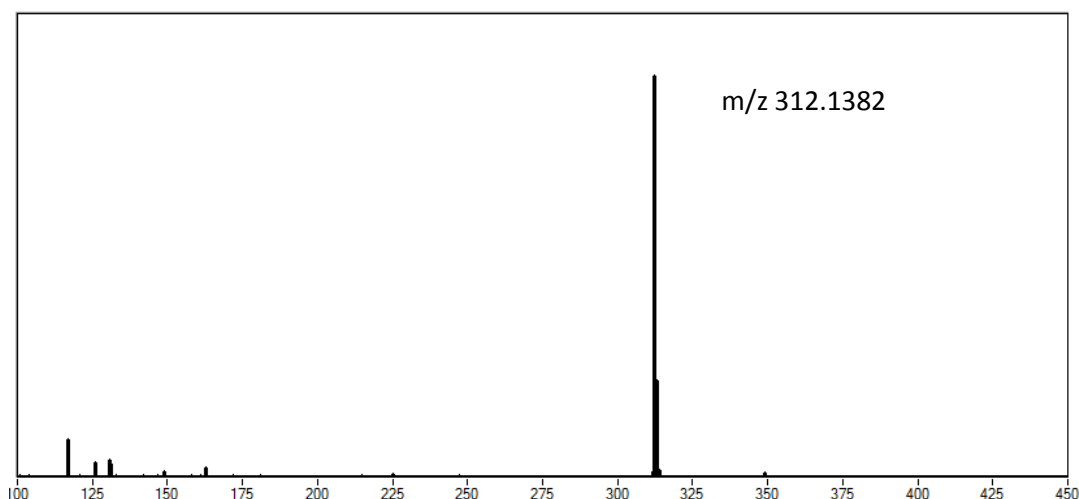


Figure 37. MS of fraction containing unknown B ($R_f = 0.33$).

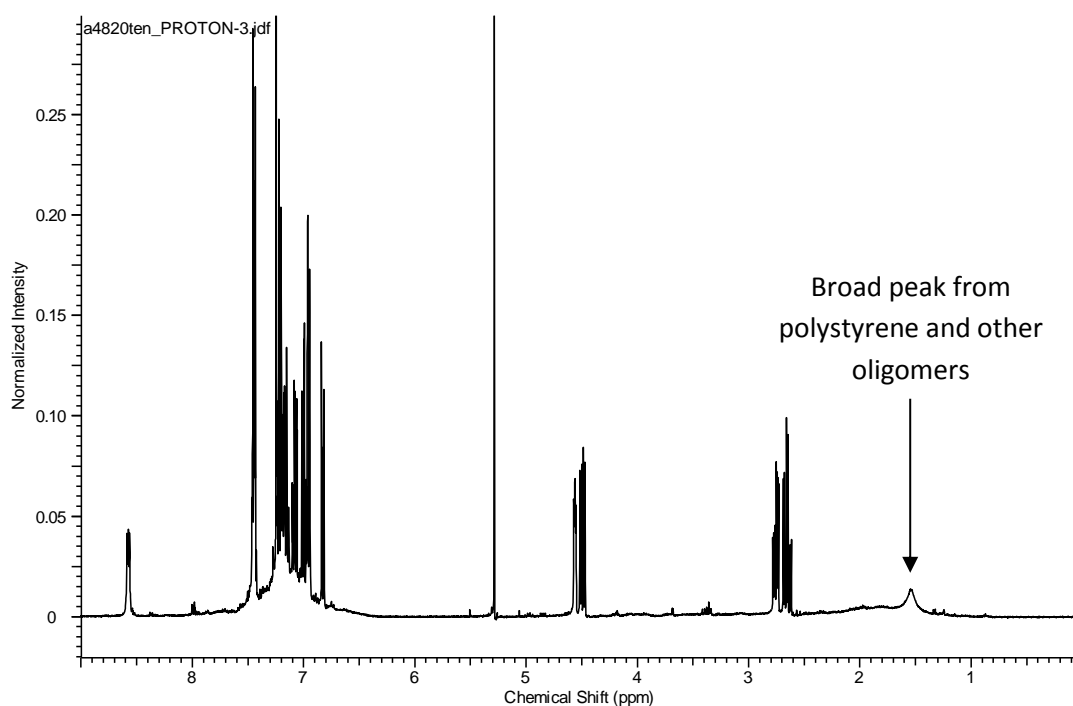


Figure 38. ^1H NMR of the first successful isolation of unknown B. (400 MHz, CDCl_3)

3.5.4 Polymer precipitation by methanol and water

To increase the amount of polystyrene and short chain oligomers removed during the precipitation step, the composition of the wash was varied. By diluting the methanol with water, the amount of precipitate formed increased. Using water alone results in two liquid phases forming with no compounds dissolving in the aqueous phase. Using 1:1 methanol : water gave the most material isolated from the wash without two liquid phases separating. The yield of the residue (250 mg) is considerably less than what was obtained from just methanol (0.9 g).

Purifying the mixture obtained from the 1:1 methanol : water precipitation with the same column chromatography conditions as previously, yielded only 33mg of unknown B. The NMR of the fraction (Figure 39) shows that the baseline is less deformed by polystyrene than previous NMR spectra, however the sample is still not pure. Also the yield was lower than previously, and before the sample could be submitted for further analysis, it had

degraded. The degradation is investigated later in the analysis. A compromise between purity and yield had to be made.

In order to improve yield of the chromatography, a larger (100 mm diameter) column was used to chromatograph 0.9 g of input material obtained from a methanol precipitation. This did improve the separation, which led to an increased yield of unknown B being isolated (190 mg). However the isolated sample of unknown B obtained did not show improvement on the amount of styrene oligomers in the sample. This is the compromise that had to be made, as the increase in yield meant that further analysis could be performed.

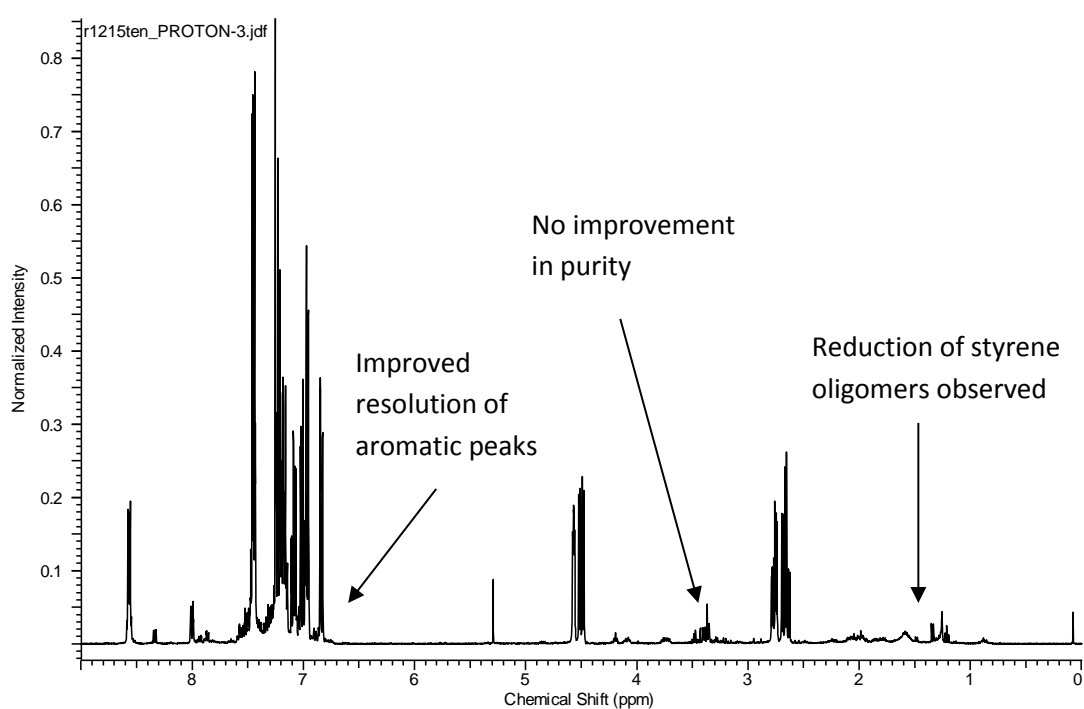


Figure 39. ^1H NMR of isolated unknown B after water/methanol isolation. (400 MHz, CDCl_3)

It should be noted that unknown B was prone to degradation upon storage. This is surprising as unknown B forms in inhibited styrene at reflux for long periods of time. It is possible that unknown B is easily oxidised by oxygen in the air, and as oxygen is consumed by inhibiting the polymerisation initiators formed in the refluxed styrene, the solution is deoxygenated enough for unknown B to survive.

As the yields of the earlier columns were low for the input material, (10-15 mg out of 5 g input initially) it would require the whole procedure repeating to obtain a quantity of

unknown B to analyse before oxidation. A lot of time, energy and resources were thus spent on this section of the study.

3.6 Structure determination of unknown B by NMR

The fraction containing unknown B was analysed by ^1H NMR spectroscopy. The 400 MHz spectrometer available does not provide sufficient resolution to distinguish all the proton signals (see Figure 38 and Figure 39). Therefore, a 700 MHz spectrometer was used for analysis and structure determination.

There are 9 unique proton signals, labelled in Figure 40 and Figure 41 from low to high field. The integration of the peaks will be somewhat inaccurate due to the remaining polystyrene in the sample, missed by the methanol precipitation step of the isolation. However the total integration from the protons signals can be estimated at 17 in total.

The ^{13}C NMR signals are labelled with a similar system in Figure 108, page 222 in the appendix. This system is used in Table 5 and Table 6 below, and in Table 13 and Table 14 in the appendix, show all the couplings determined from the homonuclear correlation spectroscopy, heteronuclear single-quantum correlation spectroscopy and heteronuclear multiple-bond correlation spectroscopy (COSY, HSQC and HMBC respectively) 2D NMR experiments. The 2D spectra are given in the Appendix, starting page 216.

There are 20 carbon signals in the ^{13}C spectra. By combining this data with the MS information, the chemical formula could be $\text{C}_{22}\text{H}_{17}\text{NO}$. This would mean there are 2 carbon environments that represent 2 carbons each.

Carbons 14 and 15 are so close in the spectrum, any couplings in the HMBC spectra cannot be separated between the two. Proton B appears to represent 3 protons, but this may not mean 3 of the same chemical environment. The splitting pattern and the number of couplings in the 2D data suggest it is multiple chemical environments that have the same chemical shift. This will make a complete assignment difficult.

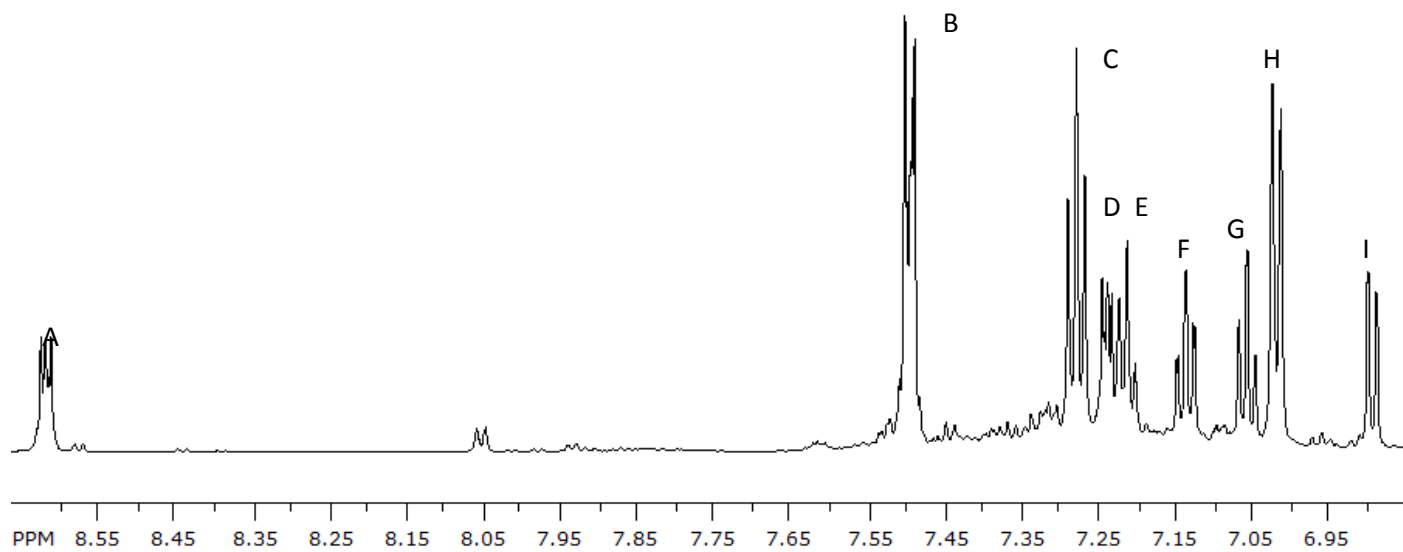
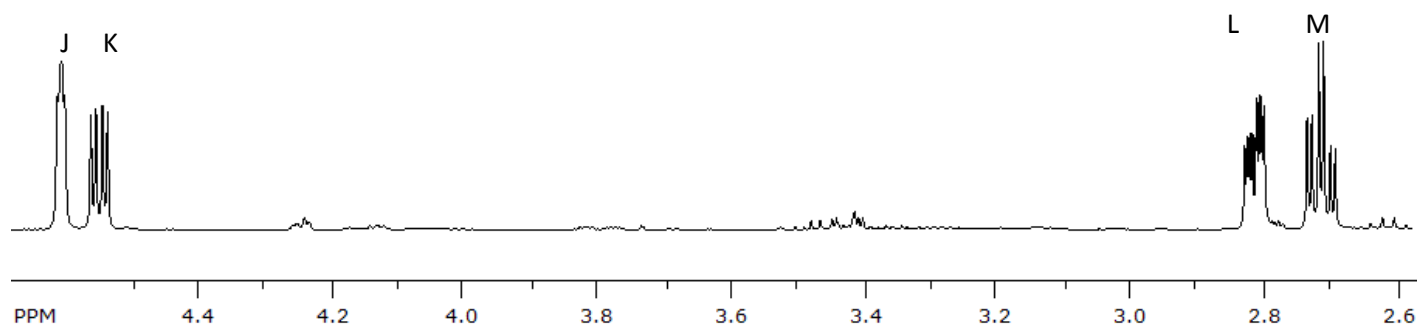


Figure 40. ¹H NMR of unknown B, low field. (700 MHz, CDCl₃)



105 Figure 41. ¹H NMR of unknown B, high field. (700 MHz, CDCl₃)

The first step is to divide the protons signals into those that couple together. The COSY couplings will show the protons that are close together, possibly adjacent on the aromatic rings of the structure. The aromatic protons are A through I. These aromatic signals only show COSY couplings to other aromatic protons, and similarly the non-aromatic protons only couple with themselves. This is shown in Figure 42, which clearly shows there is no coupling between the aromatic protons and non-aromatic protons. The non-aromatic protons, J – M, will be referred to as fragment A.

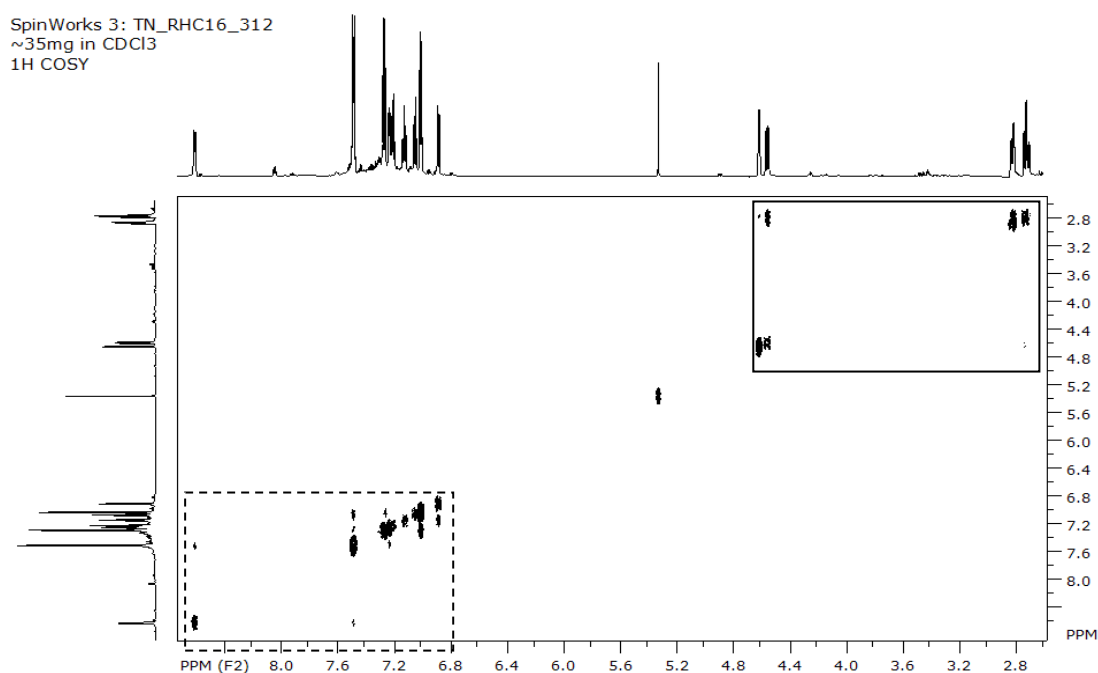


Figure 42. COSY spectrum of unknown B. (700 MHz, CDCl₃) The aromatic and non-aromatic protons have been boxed to distinguish the different types of protons.

From the COSY spectrum, three more fragments can be suggested, containing just aromatic protons. They involve couplings between protons C, E and H (Fragment B); protons B, F, G and I (Fragment C) and between protons A, B and D (Fragment D). The HSQC also suggests there are 6 quaternary carbons (Carbons 15 – 20), due to no cross couplings in the spectrum.

The first peaks to assign are the high field protons J-M. The different characteristics of these protons are given in Table 5, and a close-up of the peaks is given in Figure 43.

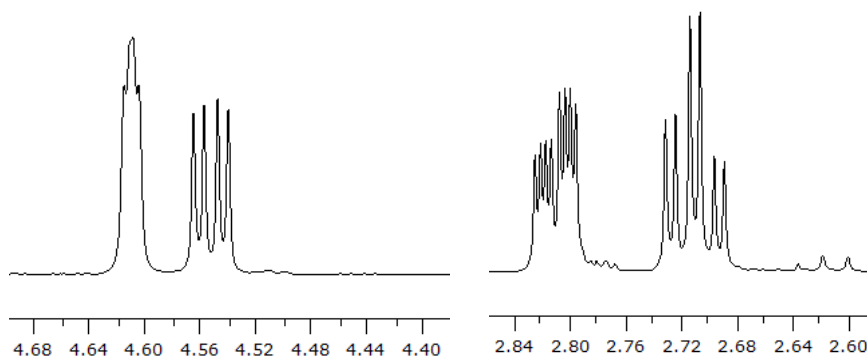


Figure 43. NMR of Unknown B. Close up proton of non-aromatic protons (700 MHz, CDCl₃)

There are four distinct peaks, each integrating to one proton each. The HSQC spectrum shows that despite their chemical shift suggesting an alkene, protons H_L and H_M are bonded to the same carbon C₁. They have a diastereotopic relationship resulting in two peaks. This also suggests that C₁ is a part of a conformationally restricted structure. The chemical shift suggests that there is a heteroatom in close proximity to these protons, as C₁ cannot be part of a double bond. The COSY spectrum shows that H_L and H_M interact with H_K and H_J respectively, and combined with the HSQC data suggests that C₁ is bound to C₂ and C₃. Therefore the fragment in Figure 44 has been proposed for these three carbons and four protons, labelled as fragment A.

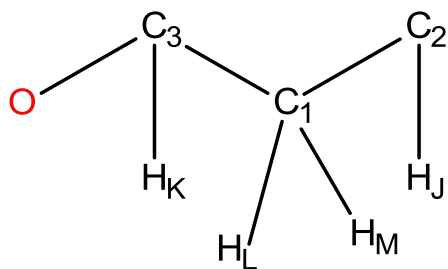


Figure 44. Proposed structure for fragment A

Table 4. High field protons of unknown B. From 700 MHz data, performed in CDCl₃.

Proton	δ (ppm)	Splitting pattern	Integration	J(Hz)	COSY	HSQC	HMBC
J	4.59	dd	1	4, 3	M	2	18, 17, 14/15, 3(w), 1, 13, 10
K	4.54	dd	1	12, 5	L	3	16, 19, 20, 1
L	2.79	ddd	1	12, 5, 3	K, M	1	17, 18, 20, 2(w)
M	2.69	td	1	12, 5	J, K, L	1	17, 18, 20, 2, 3

Analysis of the splitting patterns and coupling constants supports the proposed structure. Proton L appears as a double double doublet, indicative of being coupled to 3 protons. Proton M appears as a triplet of doublets, however 2 of the couplings, (12 Hz) are the same, making two “doublets” appear as a triplet. Protons J and K are double doublets and are coupled to protons L and M. The couplings and the protons that they are between are shown in Figure 45.

The size of the couplings suggests more about the structure of carbons 1-3 and protons J-M. The couplings between L and M (12 Hz) suggest they are indeed bound to the same carbon. The coupling between M and K (the second 12 Hz coupling) suggests a trans arrangement. The low 3 Hz coupling between M and J suggests a dihedral angle of around 90 °.

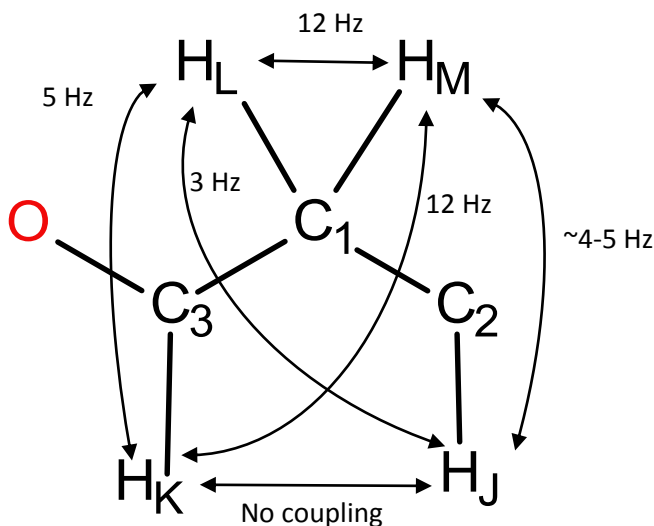


Figure 45. Fragment A, with coupling constants assigned.

Focusing on the next fragment, protons C, E and H highlighted in Figure 47, the integration of the peaks suggests that there are five protons in 3 chemical environments. The integrations of protons C and H equal 2 protons each. The splitting patterns of protons E and H (each a triplet) shows that they are each next to two protons. The splitting of proton H (a doublet) shows that it is next to one proton. Fragment B proposed in Figure 46 shows the symmetrical aromatic system for these three peaks.

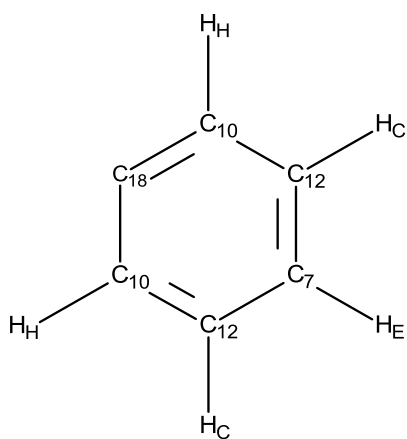


Figure 46. The proposed structure for fragment B.

In the proposed fragment, proton C is split by two protons in two different chemical environments, which would normally be seen as a double doublet. However a triplet is

observed, which suggests that the coupling constants between protons C and E, and protons C and H are the same.

HMBC data shows coupling between proton C and carbon 10 suggesting they are adjacent. The couplings between proton H and carbon 7, and proton E and carbon 10 suggest that they are all in the same aromatic ring, based on the HSQC data establishing which proton is bound to which carbon. This same data shows that carbon 18 is the quaternary carbon that couples the strongest with these protons, and finishes this aromatic ring.

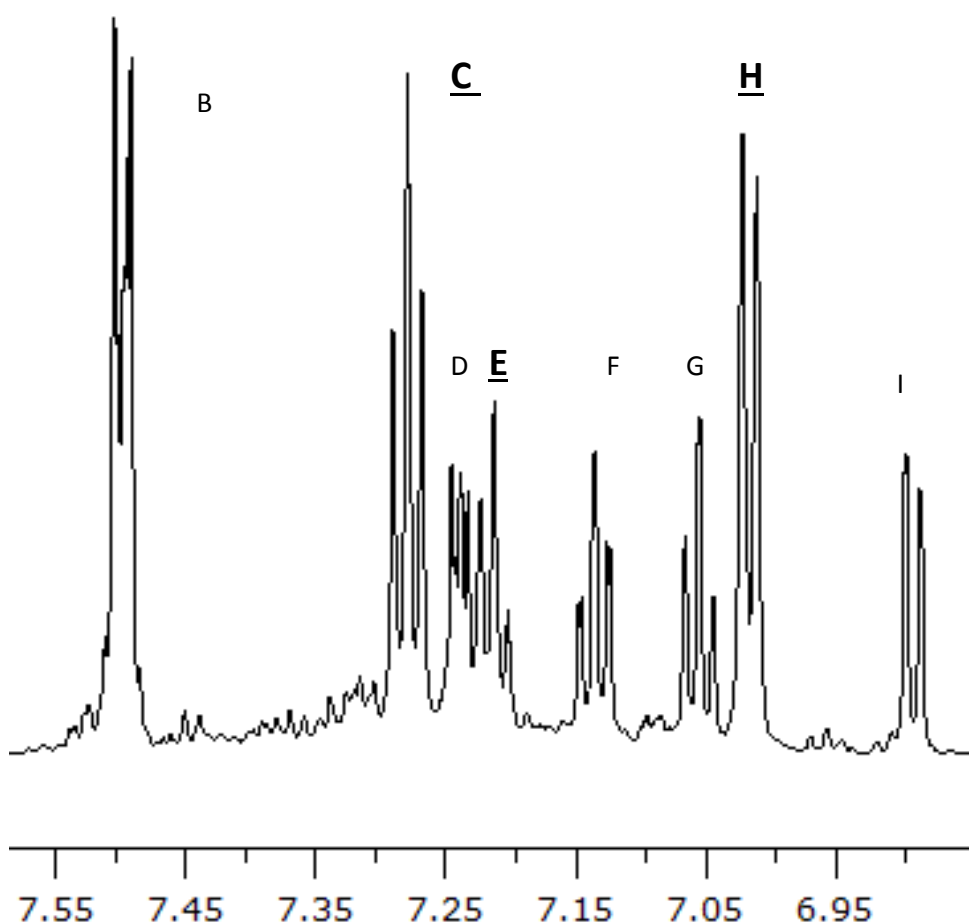


Figure 47. Close-up of protons C, E and H. (700 MHz, CDCl₃)

The next fragment, fragment C in Figure 49, consists of four protons; B (one proton), F, G and I. This is taken from the couplings from the COSY spectrum. The HSQC can show which carbons 3 of the protons are bound to; H_F to C₁₁, H_G to C₅ and H_I to C₄. Proton B is more difficult due to the 3 signals overlapping, but the COSY shows clear coupling to one of the “B” signals to this group of protons. Proton peak B shows HSQC couplings to carbons 8, 9

and 14. To determine which of these carbons belong to fragment C, the HMBC couplings to protons F and G are used. The HMBC only shows coupling to protons F and G and carbon 8, with no couplings to carbons 9 and 14. This means carbon 8 is somewhere near to protons F and G, within fragment C. This suggests that the proton B signal from fragment C is bound to carbon 8.

The order in which the protons are placed around the aromatic fragment can be determined firstly by the splitting in the proton spectrum and then by the HMBC couplings. Protons F and G are triplet of doublets, suggesting they are adjacent to two protons each. Whereas proton I is a double doublet, suggesting it is adjacent to only one proton. As there are HMBC couplings of the "inner" protons F and G to proton B, the fragment in Figure 49 is proposed.

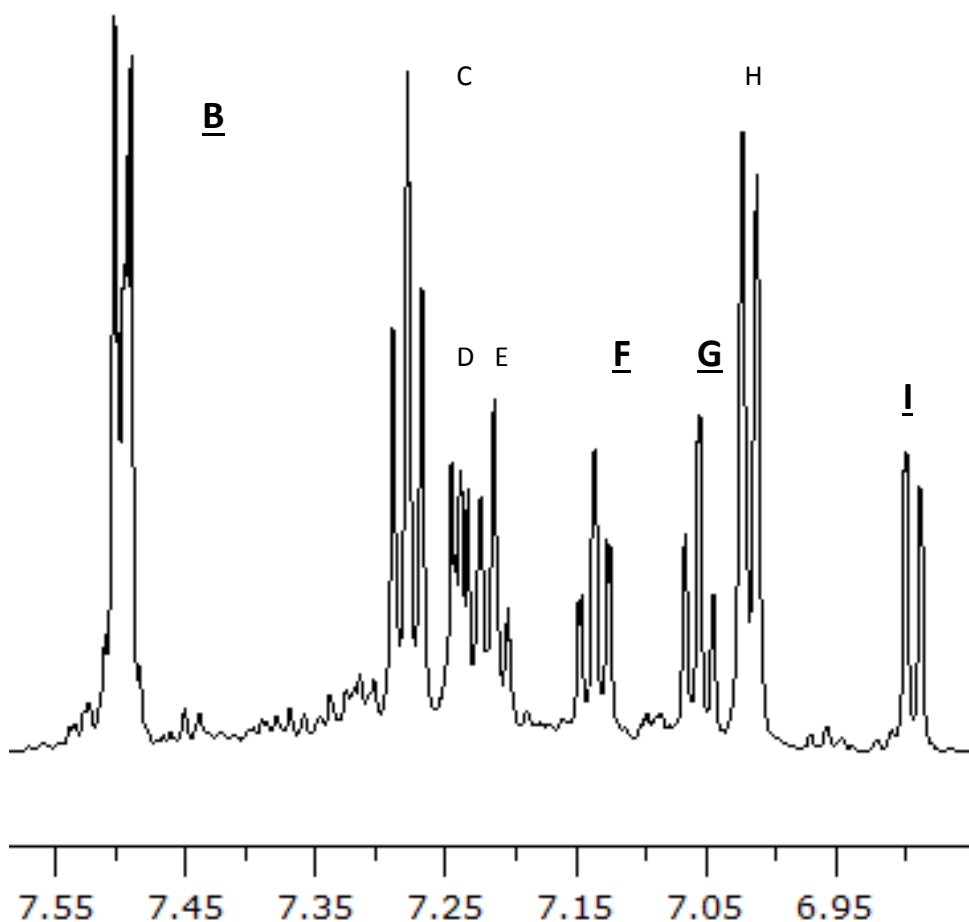


Figure 48. Close-up of protons B, F, G and I. (700 MHz, CDCl₃)

The final two carbons are assigned based on the HMBC coupling. All the protons have strong coupling to carbons 16 and 19. Their arrangement is assigned based on their chemical shifts. The chemical shift of proton B and carbon 19 is high, possibly due to a nearby heteroatom, putting them adjacent to each other. Carbon 16 is also a quaternary carbon and fits in with the rest of the fragment.

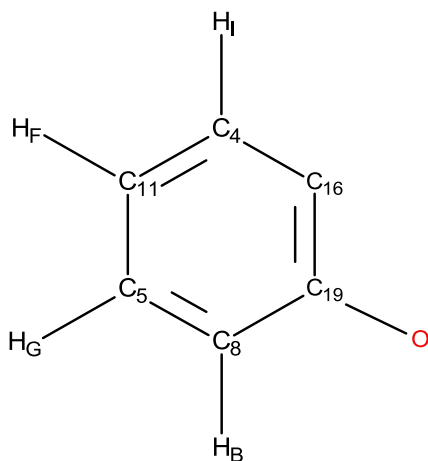


Figure 49. The proposed structure for fragment C.

The remaining aromatic protons are more difficult to assign than the others, due to the overlap of the three proton B peaks. However, the fragment in Figure 50 shows the proposed position for these last 4 protons. As the splitting of the proton peaks cannot be resolved, the assignment comes from the chemical shift of the protons and the carbons bound to them. Proton A has the highest shift and this suggests it is next to a shielding functional group, and the effect is reduced as you move around the ring, to proton D. The assignment is also consistent with the COSY and HMBC couplings.

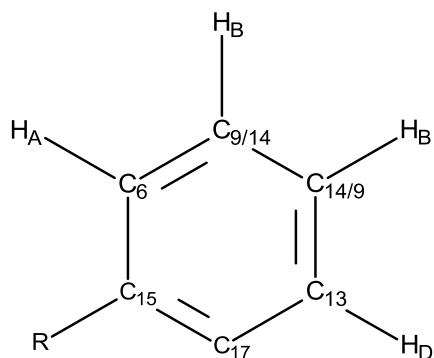


Figure 50. The proposed structure for fragment D.

The final unassigned carbon is carbon 20, and its chemical shift is consistent with an imine. This could be the functional group that causes the chemical shift of proton A.

To combine these fragments into one structure, the long range couplings of fragment A were used. Any HMBC couplings that are common to protons K, L and M can be said to come from a fragment next to carbon 3 / proton K. Similarly, if the couplings are common between protons J, L and M, then they are from a fragment next to carbon 2 / proton J. If couplings to protons K or J are not found with L or M, then the fragments responsible for those couplings are further away from fragment A.

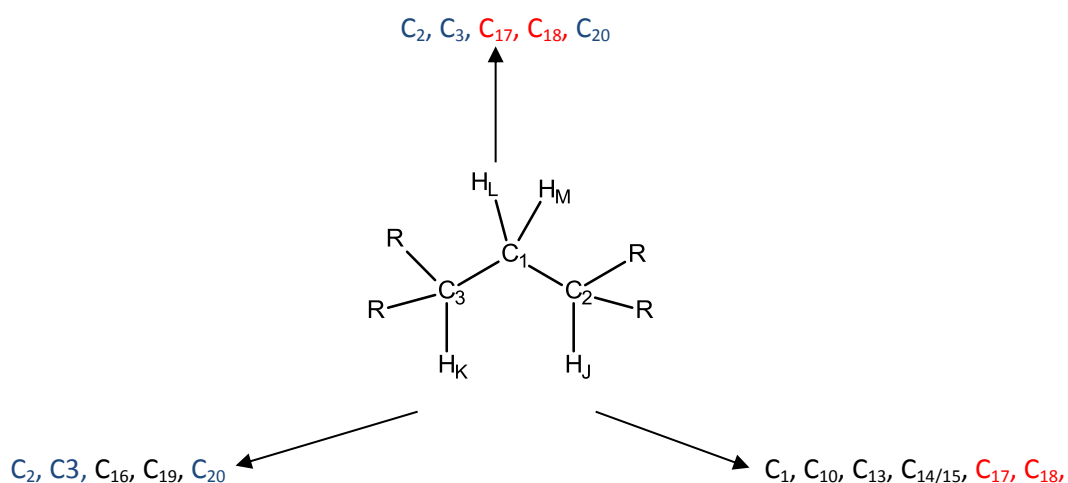


Figure 51. Fragment A, with HMBC couplings shown. Couplings common to protons K, L and M are in red, and those common to protons J, L and M are in blue.

Table 5. Summary of proton signals for Unknown B and their couplings in COSY, HSQC and HMBC NMR experiments. (700 MHz NMR experiments, performed in CDCl₃.)

Proton	δ (ppm)	Splitting pattern	Integration	J(Hz)	COSY	HSQC	HMBC
A	8.59 - 8.62	m	1		B, D	6	14/15, 17, 20, 13(w)
B	7.47 - 7.49	m	~3		D, G, F(w)	8, 9, 14	20(w), 19, 17, 16(w), 6, 14/15, 13, 11
C	7.26	t	2	8	E, H	12	18, 12, 10
D	7.21 - 7.23	m	1		A	13	17(w), 20(w), 9, 2, 14/15
E	7.19	t	1	7	C, H(w)	7	10, 18(w)
F	7.12	td	1	8, 1	B(w), G, I	11	4(w), 16(w), 19, 8
G	7.04	td	1	8, 1	B, F, I(w)	5	4, 8(w), 16, 19
H	7.00	d	2	8	C, E(w)	10	7, 10, 2
I	6.87	dd	1	8, 1	F, G(w)	4	5, 16, 19

Note: The meaning of (w) is that a weak coupling was observed between these signals in that spectrum.

Based on these observations, the structure in Figure 52 is proposed. The fragments are labelled in the figure.

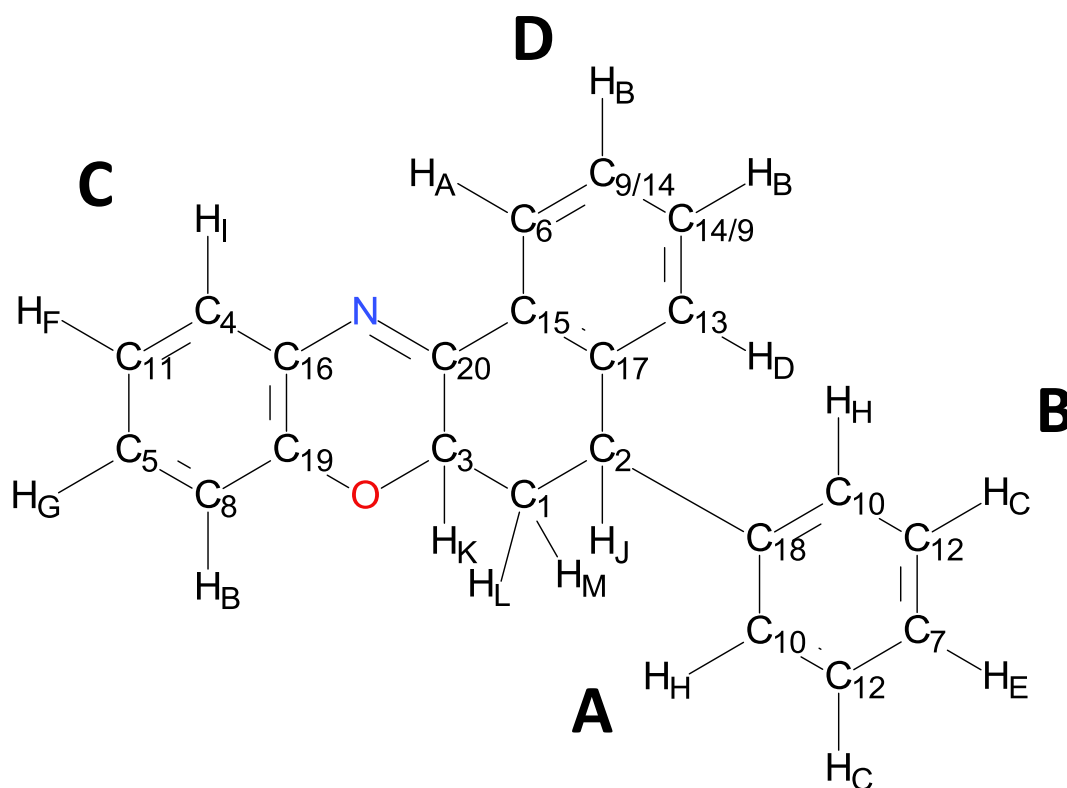


Figure 52. The proposed structure and assignment of unknown B.

3.6.1 Degree of unsaturation

The degree of unsaturation can be determined using Equation 3. In a structure, each double bond and ring adds one to the Double Bond Number (DBN). For the proposed formula for unknown B, the DBN is 14.

The structure proposed in Scheme 31 (Page 97) does not match this degree of unsaturation, as it has 15 counts of rings or double bonds. In Figure 52 the number of double bonds and rings in the proposed structure matches the DBN calculated from the chemical formula. This is more evidence that the proposed structure in Figure 52 is correct.

Equation 3. Formula for the calculation of Double Bond Number, where C is the number of carbons, H the number of hydrogens, X the number of halogens and N the number of nitrogens

$$DBN = C - \frac{H}{2} - \frac{X}{2} - \frac{N}{2} + 1$$

3.7 X-ray crystallography of isolated unknown B

An NMR sample of unknown B was left to crystallise as the deuterated chloroform evaporated slowly. The crystals that formed were submitted to an X-ray diffraction analysis. The obtained structure is given in Figure 53. This is not what has been proposed from the NMR data obtained, but does show some similarities.

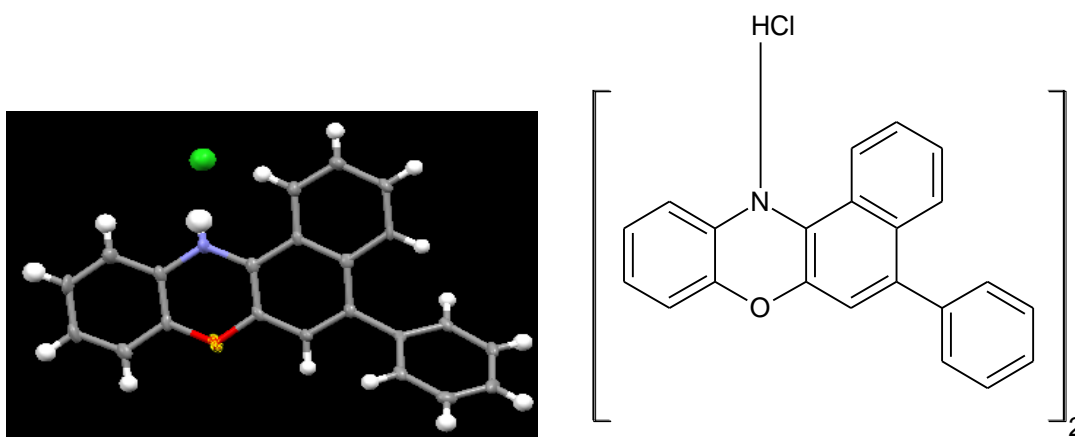


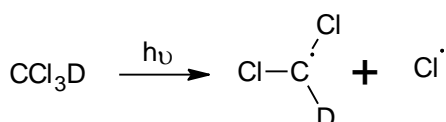
Figure 53. X-ray crystallography results of a sample of unknown B, crystallised from CDCl_3 .

There are a number of possible explanations for this observation. Unknown B could be unstable under these conditions, where it could oxidise when exposed to oxygen from the air, exposure to light, or react with the deuterated chloroform that was left in.

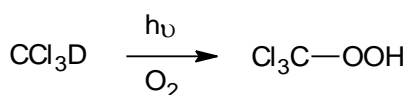
Another theory explaining the presence of the chlorine atom observed is that Unknown B is a salt formed during the acid wash treatment, towards the start of the extraction process. This is unlikely, due to the column chromatography purification used after the acid wash.

Any salts formed would be removed during column purification when using the solvent system used to isolate Unknown B.

Another explanation is that the chloroform reacts with unknown B, causing the formation of the observed structure. Chloroform is known to decompose under light⁹⁷⁻⁹⁹. It also autoxidises when open to air with light exposure. These two possible routes for chloroform to decompose are shown in Scheme 32 and Scheme 33. This leads to intermediates that could react with unknown B.



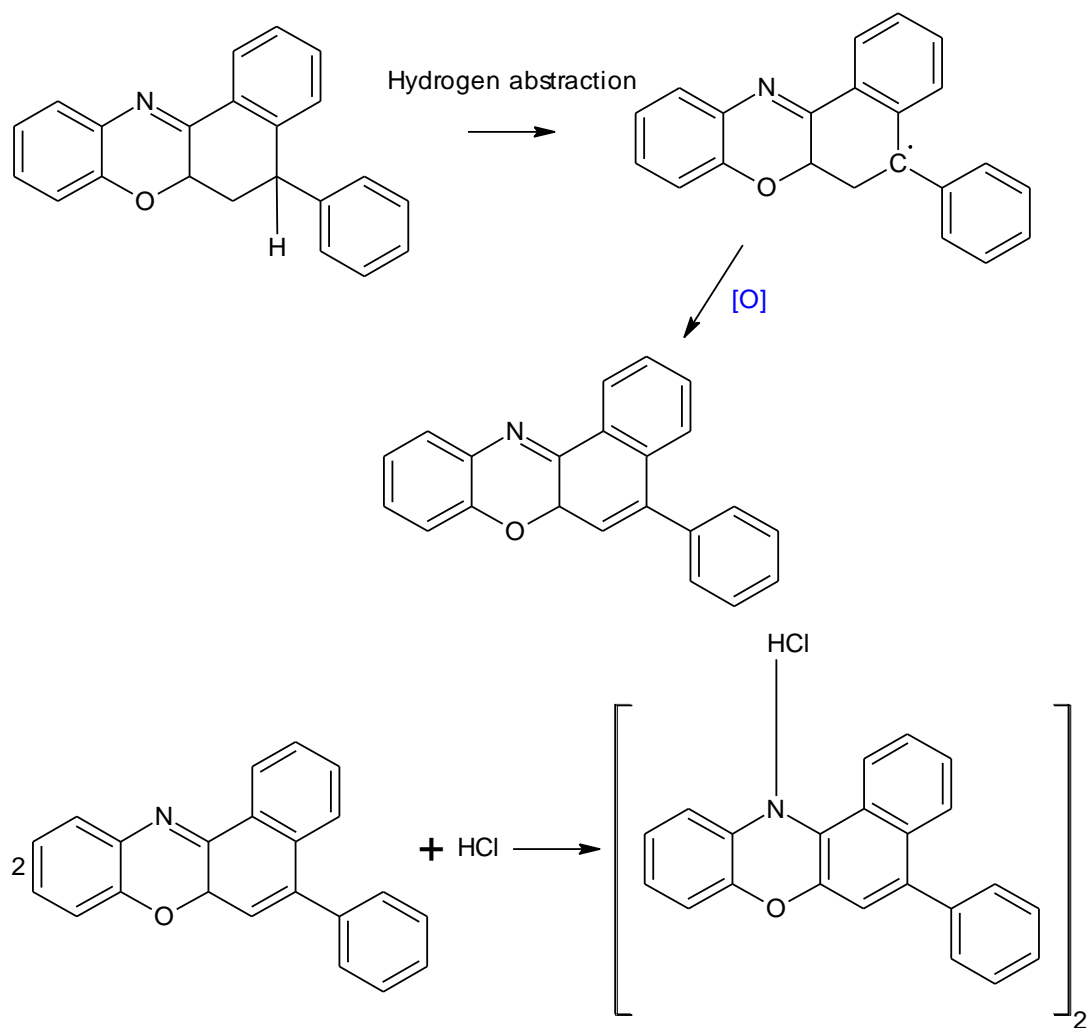
Scheme 32. Photolysis of chloroform⁹⁹.



Scheme 33. Photooxidation of chloroform^{97, 98}.

These decomposition products may react with unknown B by hydrogen abstraction. The resulting radical will be resonance stabilised. This can then be further oxidised to the structure observed, as described in Scheme 34. The chlorine atom observed in the crystal structure would have to come from the decomposition of chloroform

The crystal lattice contains a number of interesting features. First is the inclusion of chlorine, which is from the photolysis of chloroform. The second is the flat fused ring system. In the analysis of the NMR spectra of unknown B, it was determined that the protons were locked conformationally, as shown by the couplings of the non-aromatic protons. The X-ray structure determined has a similar flat fused ring system to what would be expected for unknown B.



Scheme 34. Mechanism of oxidation and formation of product observed by X-ray crystallography.

3.8 Possible mechanism for the formation of Unknown B

In order to determine why 2-nitrophenols and derivatives are effective inhibitors, the mechanism of reactions occurring in the inhibition mixture needs to be understood. If unknown B is a product of the inhibition, then working backwards from the structure determined by NMR may offer an insight into the inhibition mechanism. There is no real evidence that unknown B is a direct product of inhibition so far.

By breaking down the structure of unknown B, two similar and related molecules can be seen. Demonstrated in Figure 54, the yellow section represents 2-nitrophenol, the inhibitor in the polymerisation mixture. This suggests that unknown B is involved in the inhibition of the polymerisation, as it contains the inhibitor.

The second part shows similarities to the initiator proposed by Mayo¹⁹. This is shown in red in Figure 54. This is more evidence that unknown B is a product of the inhibition of styrene polymerisation by 2-nitrophenol.

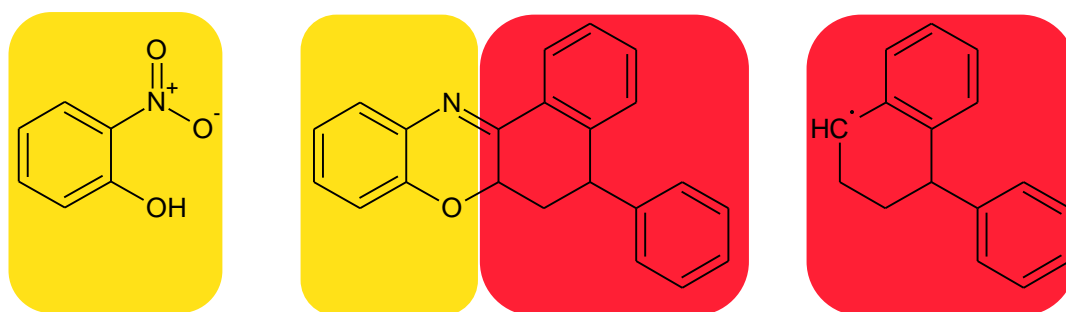
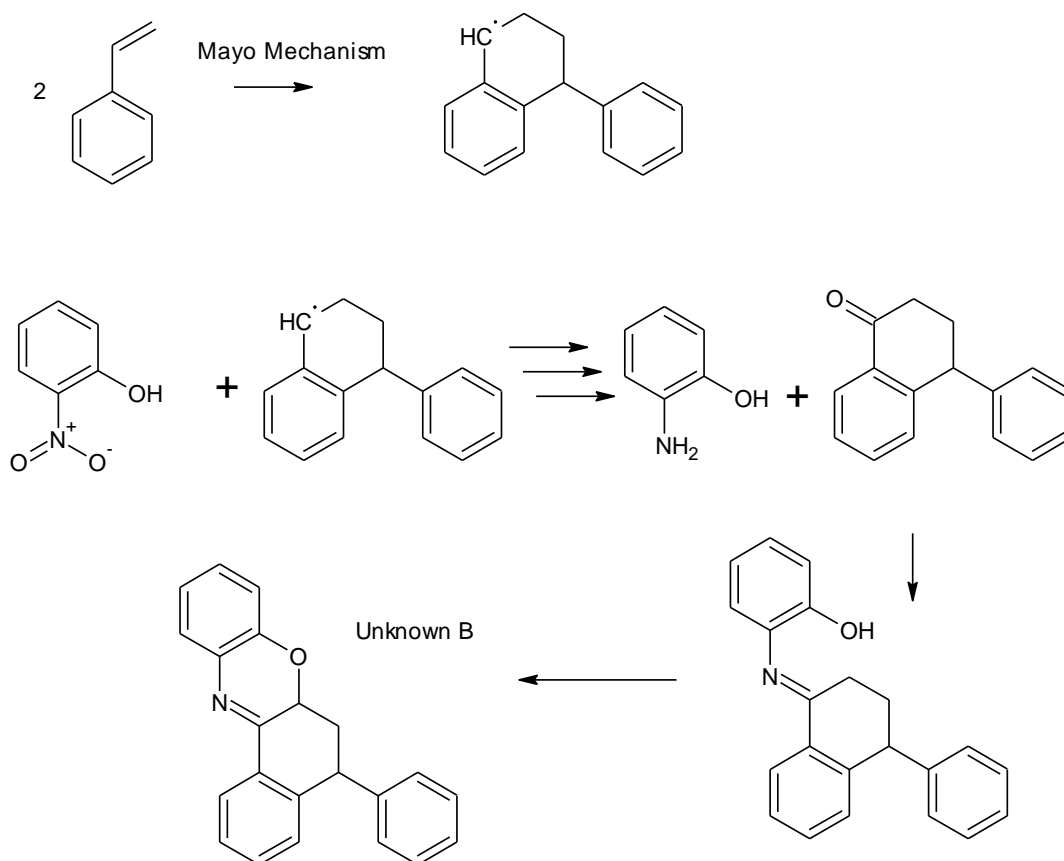


Figure 54. Comparison between 2-nitrophenol, unknown B and the spontaneous polymerisation initiator proposed by Mayo¹⁹.

Comparing this proposed structure to the mechanism proposed by Bushby et al⁴⁵ has led to the suggested mechanism for the formation of unknown B outlined in Scheme 35. First the styrene undergoes the Diels-Alder reaction, leading to the formation of the initiator radical after H atom abstraction. The nitro group of the inhibitor is reduced following the

Jackson and Waters⁴⁶ mechanism, to give 2-aminophenol. This part of the mechanism also explains the formation unknown A (2-aminophenol).

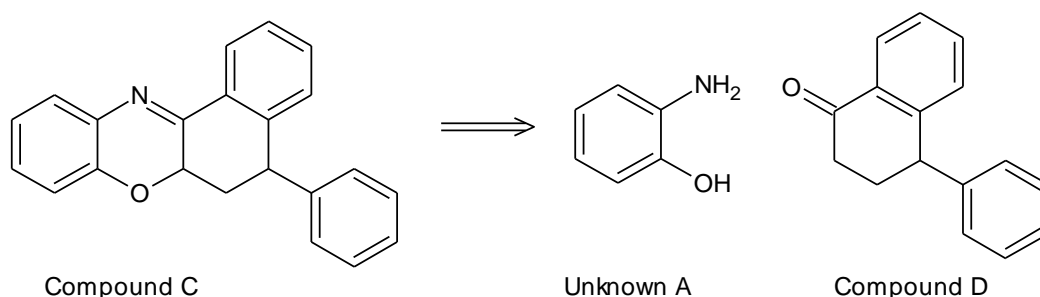
The next step is the formation of a Schiff base between 2-aminophenol and the ketone formed by the reduction of 2-nitrophenol. This imine should then cyclise to give unknown B.



Scheme 35. Possible mechanism for the formation of Unknown B.

3.9 Synthesis of the unknown B

The structure of unknown B product has been assigned with some confidence, but the mechanism by which it is formed is still unknown. By synthesising it independently, the way in which it is formed in the inhibition mechanism may also be explained. Scheme 36 shows the retro-synthetic analysis on the proposed structure for unknown B and the 2 possible starting materials needed. The synthesised compound will be referred to as compound C to distinguish itself from the isolated unknown B. Interestingly, this appears to follow the proposed mechanism in Scheme 35. Also one of the starting materials is 2-aminophenol, the product isolated from the acid wash during the isolation of the product (Unknown A). Once compound A is synthesised, comparing its physical properties and spectra information should confirm the assignment from the NMR data obtained.



Scheme 36. Retro-synthetic analysis of compound A.

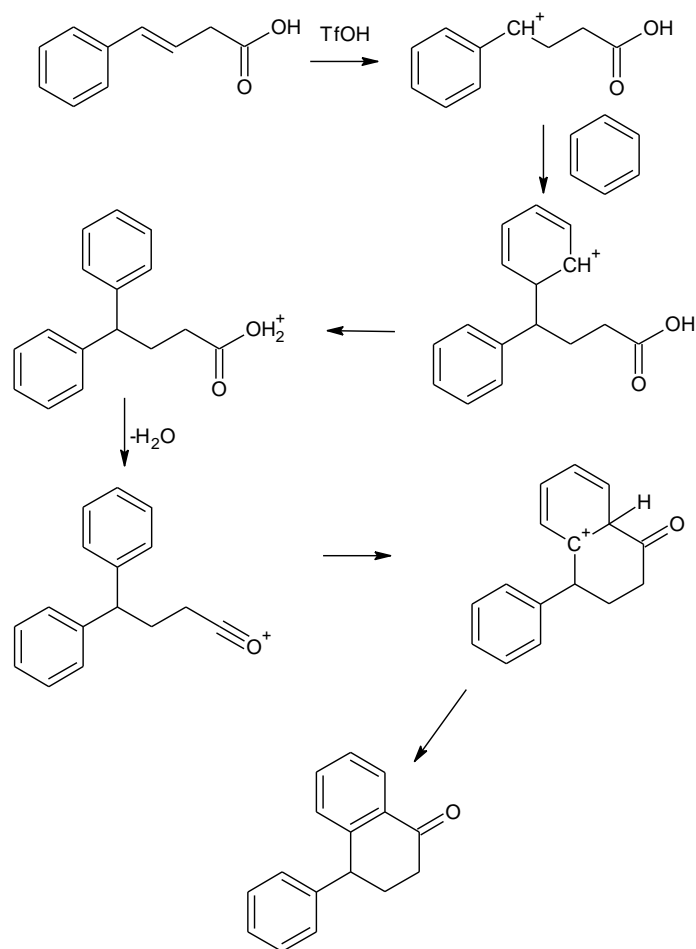
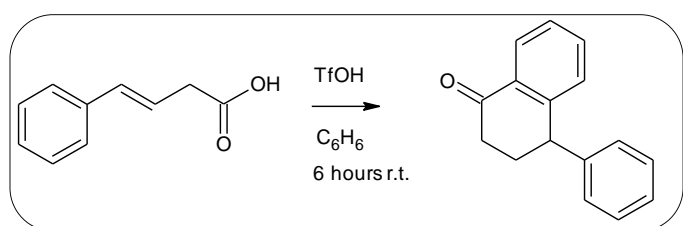
2-Aminophenol is commercially available, however the ketone is not. Therefore it was synthesised.

3.9.1 Ketone intermediate (Compound D)

The ketone was obtained following a procedure reported by Rendy et al¹⁰⁰ and depicted in Scheme 37. This will be referred to as compound D for clarity. The reaction follows a similar route to a Haworth mechanism.¹⁰¹ The starting material is protonated by the triflic acid, which is followed by a Friedel-Crafts reaction. The protonated carboxylic acid formed

eliminates water to form an acylium ion, which then undergoes an intramolecular Friedel-Crafts reaction. A final deprotonation reforms the aromatic ring, giving the target product.

The reaction mixture was run through a column (1:3 ethyl acetate : petroleum ether, $R_f = 0.35$) to give the target compound in isolated yield of 98 mg, (35%), following the procedure as given. By increasing the amount of starting material to 1 g, a yield of 1.01 g, (73%) was obtained. This increase in scale resulted in an increase in yield allowing more analysis to be performed. This change was worthwhile as it saved time and resources.



Scheme 37 Synthesis of compound D¹⁰⁰

Unknown B was characterised by MS and NMR. The ESI MS gave a peak at m/z 222, corresponding to $[M + H]^+$. The proton NMR is given in Figure 55 and Figure 56. The NMR spectra are labelled in the same way as previously, and these notations used in Table 6.

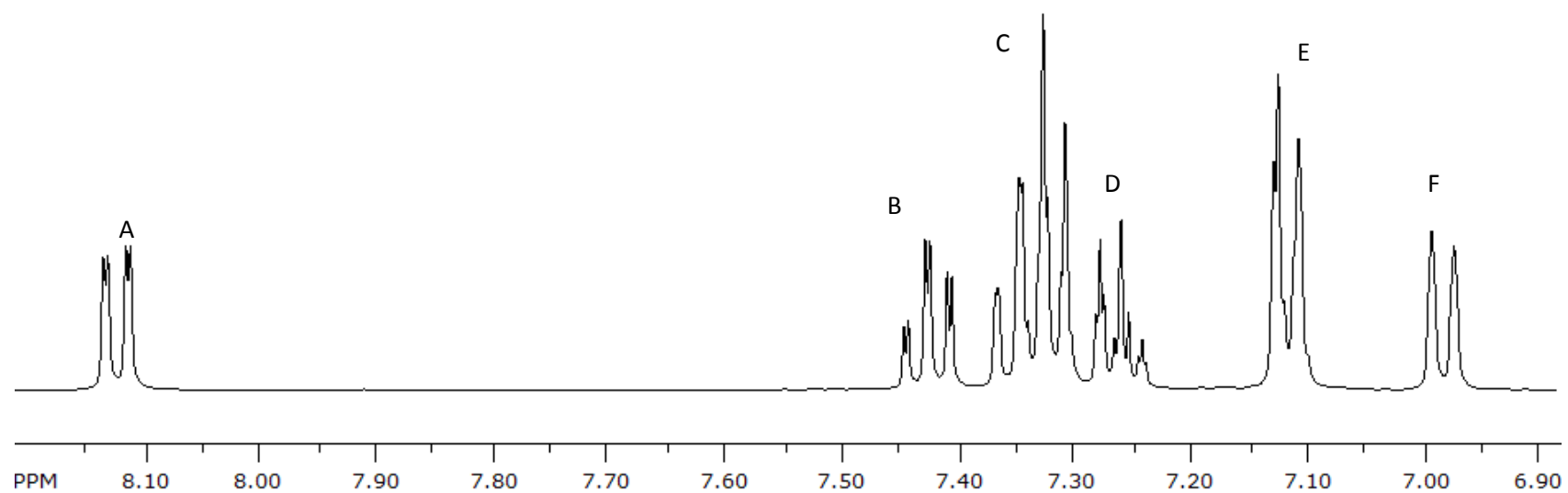


Figure 55. NMR of compound D, low field. (400 MHz, CDCl₃)

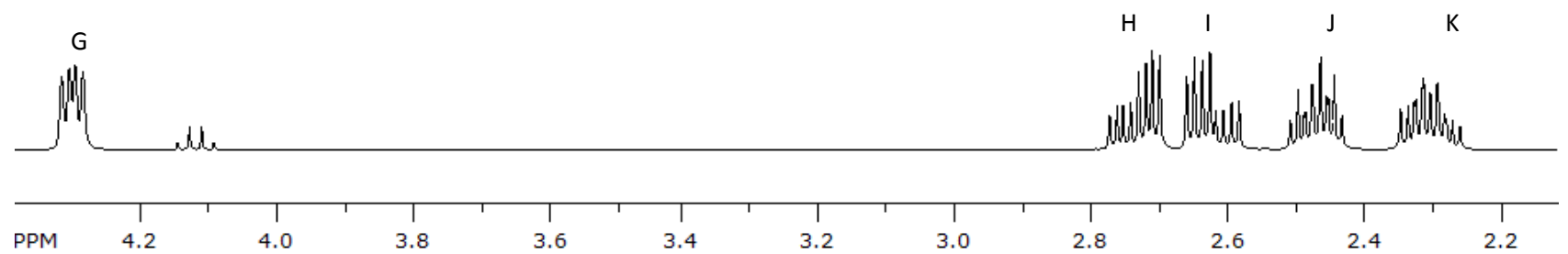


Figure 56. NMR of compound D, high field. (400 MHz, CDCl₃)

Table 6. Summary of proton signals of compound D and their couplings in COSY, HSQC and HMBC NMR experiments. (400 MHz, CDCl₃)

Proton	Chemical shift (ppm)	Integration	Splitting Pattern	COSY	HSQC	HMBC
A	8.06	1	dd	C	5/6	11, 13, 14
B	7.36	1	td	F	11	5/6, 13
C	7.30-7.24	3	m	A	7/8, 5/6	7/8, 10, 12
D	7.21-7.17	1	m		4	7/8
E	7.06-7.03	2	m	C, D	7/8	3, 4(w), 5/6, 7/8
F	6.92	1	dd	B	9	3, 5/6, 10, 14(w)
G	4.24	1	dd	K (w)	3	1, 2(w), 7/8, 12, 13
H	2.67	1	ddd	I	2	1, 3, 14
I	2.55	1	ddd	H	2	1, 3
J	2.44-2.36	1	m	K, G	1	2, 3, 12, 13, 14
K	2.28-2.19	1	m	J, G	1	2, 3, 12, 13, 14

Note: The meaning of (w) is that a weak coupling was observed between these signals in that spectrum.

Starting with the high field protons, we see there are 5 protons bound to 3 carbons. They show COSY couplings to their adjacent protons and can be arranged as depicted in Figure 57.

The two aromatic rings can also be separated following the COSY couplings; protons C, D and E, and protons A, B, C and D. Proton C is 3 protons in two different chemical environments. The proton C signal for the C, D and E group is from 2 protons in the single chemical environment, suggesting a symmetrical structure. Also, proton E integrates to 2, and therefore the symmetrical aromatic ring can be suggested.

Protons A, B and F, along with the remaining C proton can be arranged into the remainder of the structure given in Figure 57, following the splitting of peaks. The doublet of doublets are the external protons and the triplet of doublets are the internal protons, arranged following the COSY couplings. Proton A is positioned in the structure due to the high chemical shift which is explained by the proximity to the ketone oxygen atom. The rest of the fragment then falls into place, confirming the structure of the product for this step in the synthesis.

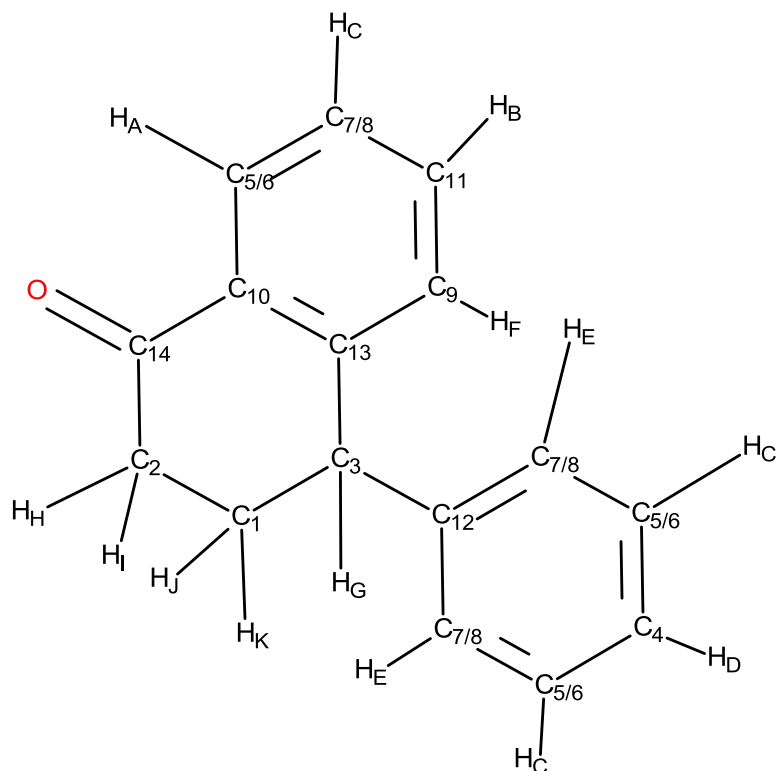


Figure 57. Structure assignment for compound D

3.9.2 Synthesis of deuterated compound D.

The mechanism for the synthesis of compound D has not been confirmed. By using deuterated benzene as a starting reagent, we will be able to show if there are multiple reaction pathways to follow.

In the NMR shown in Figure 58, the integration of all the aromatic peaks are half of what there were in the previous experiment, compared to the non aromatic peaks. This is because the acylium intermediate formed is symmetrical and either isomer can be formed. This is confirmation of the mechanism given in Scheme 37 on page 122.

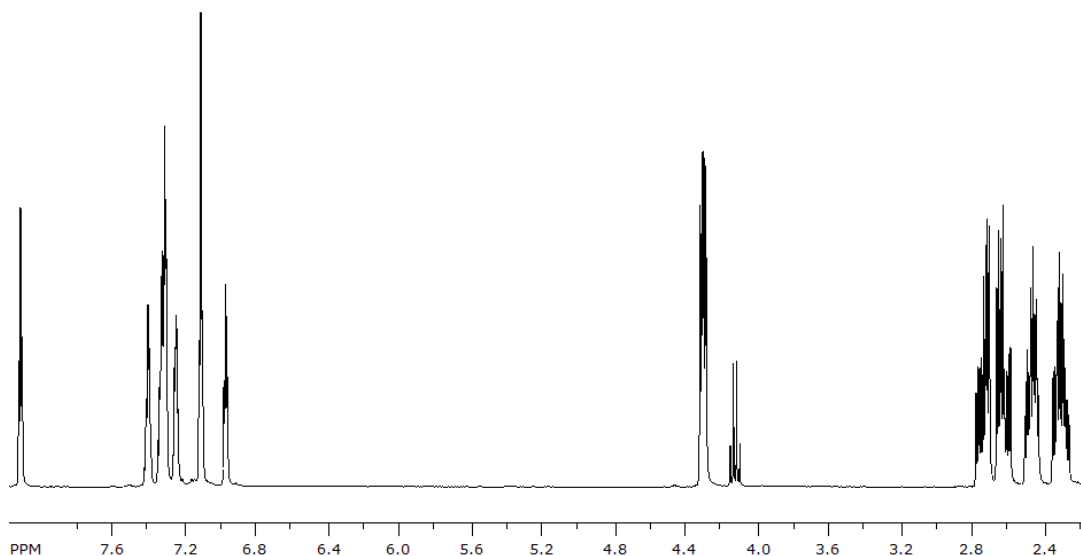
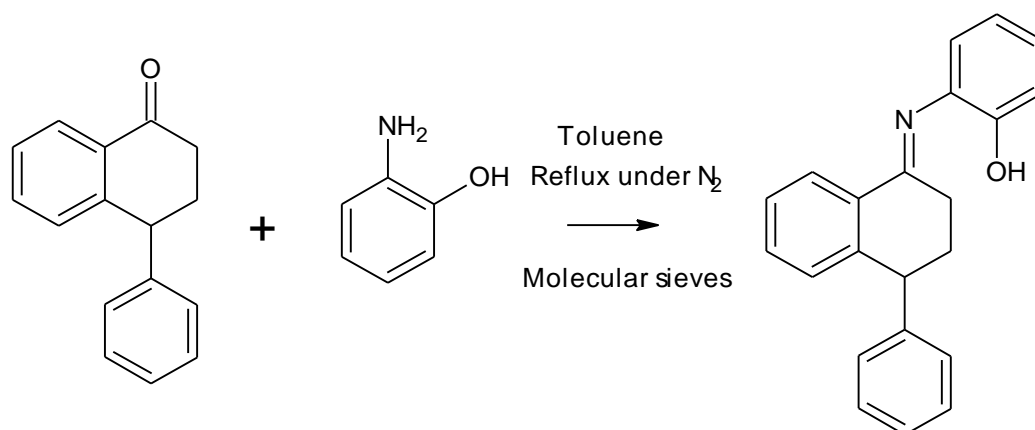


Figure 58. ^1H NMR of ketone intermediate, synthesised using deuterated benzene. (400 MHz, CDCl_3)

3.9.3 Synthesis of imine (Compound E)

The next step of the synthesis is to connect compound D and 2-aminophenol by forming an imine (Compound E). The reaction is given in Scheme 38, following the procedure given by Tauer et al¹⁰². The imine is moisture sensitive, as imines are, meaning the synthesis and isolation must be done under inert atmosphere.

Even when leaving the reaction for long times (24 hours +), the reaction does not produce pure imine. The NMR spectrum in Figure 60 shows that there is still starting material present, and by comparing the integration between ketone and imine peaks, the yield is 1:1, imine : ketone. This also suggests that there is one equivalent of aminophenol remaining in the mixture. This is confirmed by the MS spectra in Figure 59. The peak at m/z 110 represents the remaining aminophenol, and the peaks at 222 and 245 m/z are the $[\text{M}+\text{H}]^+$ and $[\text{M}+\text{Na}]^+$ peaks of the ketone.



Scheme 38. Formation of Imine (Compound E) from compound D and 2-aminophenol

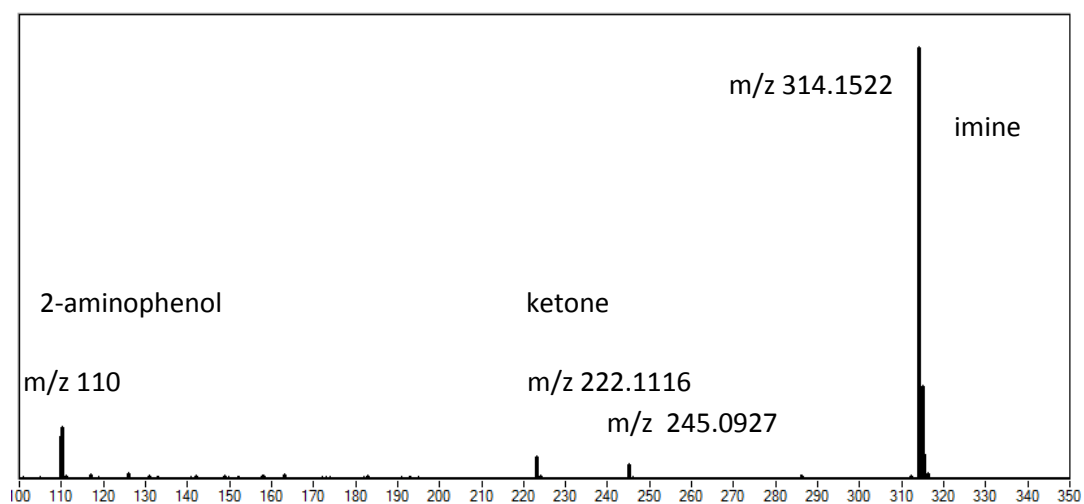


Figure 59. ESI MS of compound E mixture isolated.

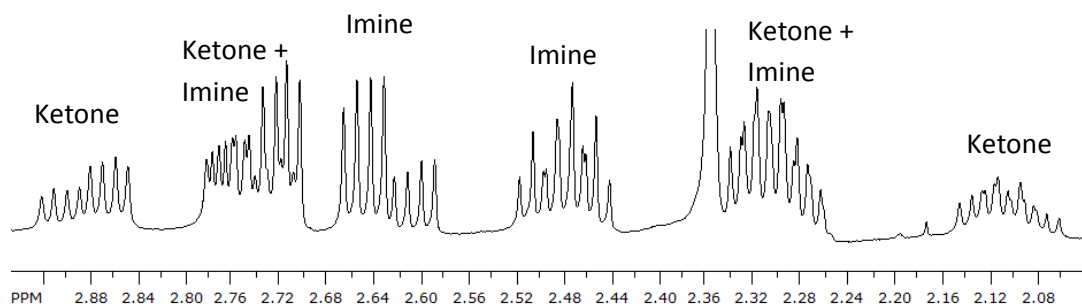
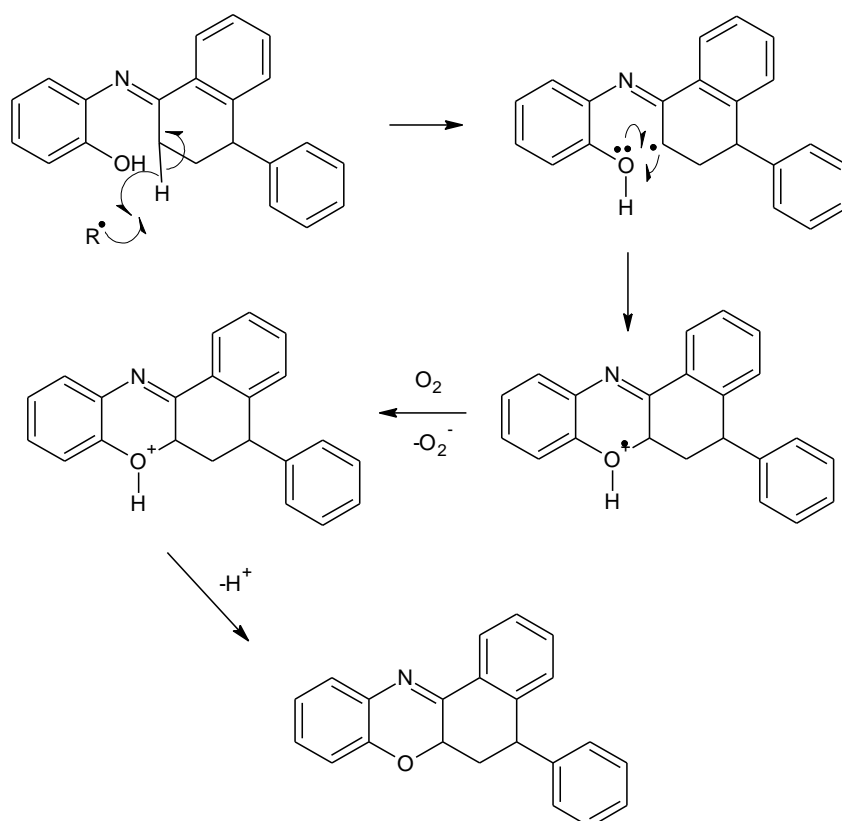


Figure 60. ¹H NMR of compound E mixture, magnified on high field signals. (400 MHz, CDCl₃)

When attempting to separate the mixture by column chromatography, compound E underwent hydrolysis, and only compound D and 2-aminophenol were isolated. However, the crude reaction mixture was used in the final step of the synthesis.

3.9.4 Final cyclisation to compound C

The crude reaction mixture of compound E was dissolved in 1:1 toluene : styrene (0.1 M, prepared assuming 100 % pure imine sample, 5 mL) and heated to 110°C. The aim was to use the spontaneous polymerisation of styrene to generate free radicals that would react with the imine and close the final ring. Scheme 39 demonstrates one possible route for the formation of compound C from compound E. Diluting the styrene in toluene was to prevent the solution polymerising to a solid block, which would make analysis extremely difficult.



Scheme 39. Mechanism of the formation of unknown B from compound E.

The reaction was monitored by MS. It has been shown previously (MS analysis of inhibition product mixture, page 88) that the unknown B is eventually consumed by the spontaneous polymerisation, suggesting itself as a possible inhibitor. Therefore the sample needed to be monitored so that the compound A was not consumed. Figure 61 shows the MS of the reaction after 1 hour, where the peak at m/z 312 is increasing. Figure 62 shows the progress after 4 hours. At this point there is very little imine remaining, and increase in intensity of the peak at m/z 312 is clear.

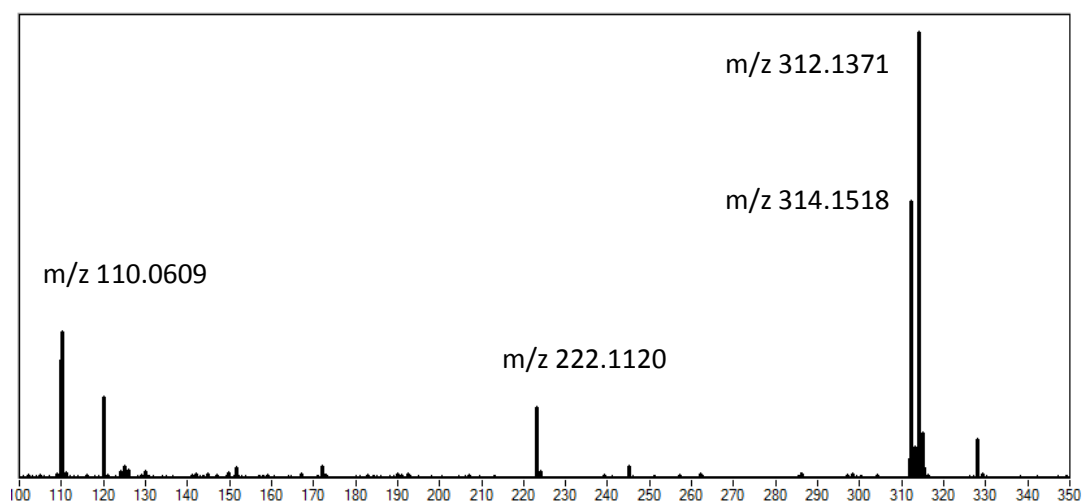


Figure 61. MS spectrum of final synthesis step after 1 hour

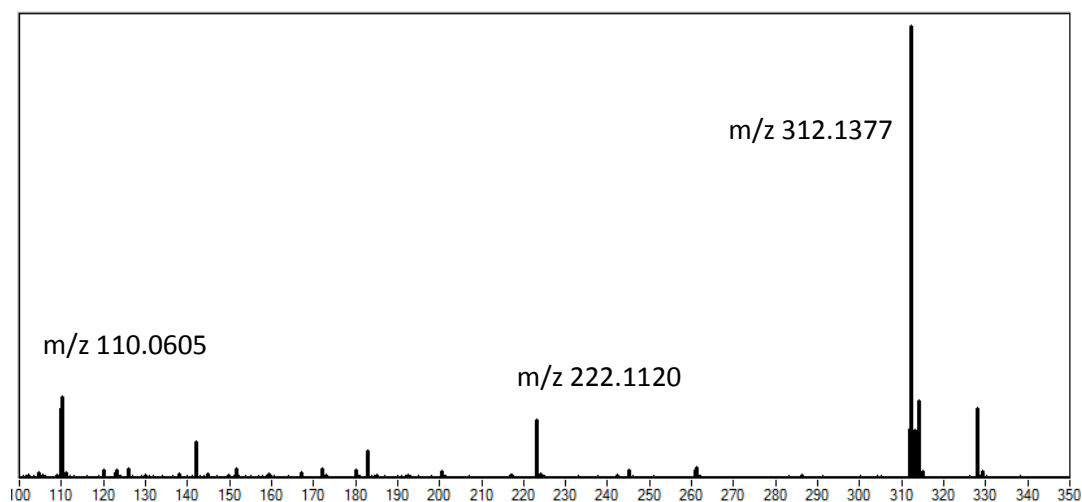


Figure 62 MS spectrum of final synthesis step after 4 hours

Isolation of the product observed in the MS at m/z 312 is not necessary as the characterisation of unknown B is almost complete. The aim was to determine if unknown B could be formed via an imine intermediate. To determine the identity of compound A, the fragmentation pattern of an MS/MS experiment of the compound A was compared to the same results from a sample of Unknown B, focussing on the peak at m/z 312. As Figure 63 shows, the fragmentation patterns are identical.

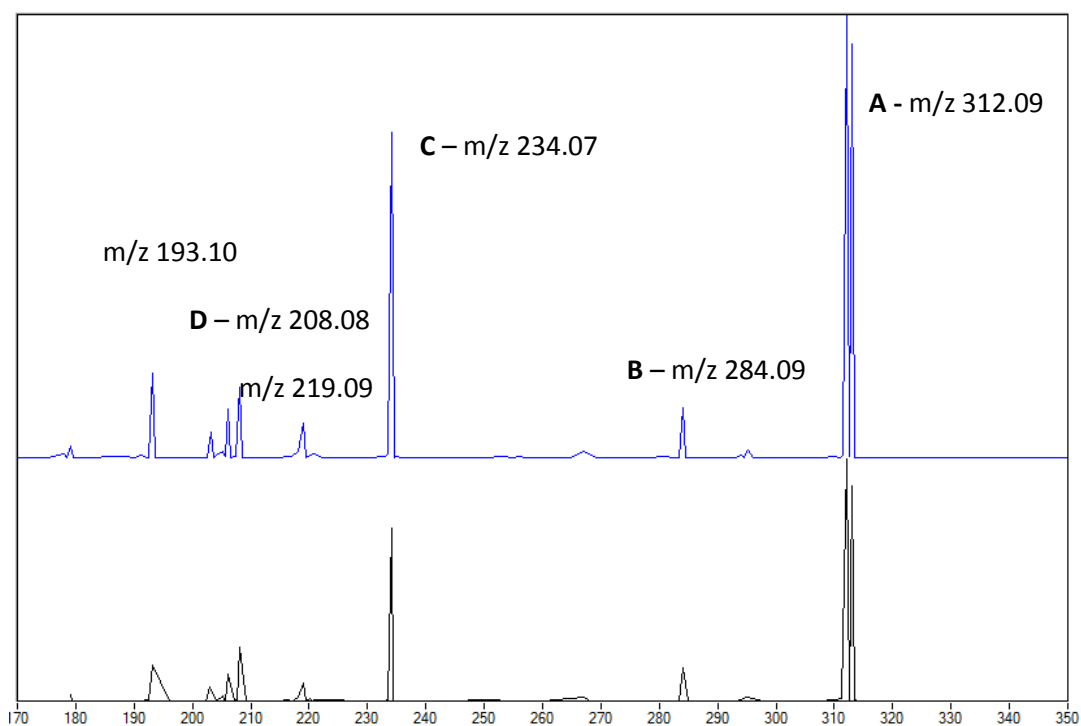
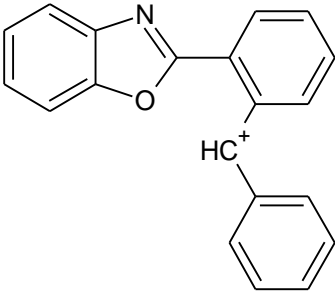
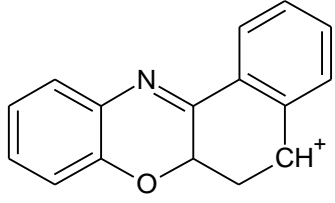
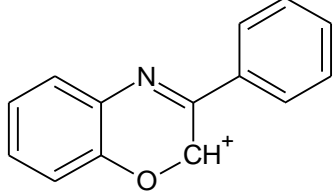


Figure 63 MS/MS of peak m/z 312 comparisons between inhibited polymerisation mixture (top) and isolated unknown B (bottom)

Table 7 Structures of fragments formed in the MS / MS experiment on Unknown B or Compound A

	m/z	Structure	Loss
A	312.09	$[M + H]^+$	None
B	284.09		C_2H_4
C	234.07		C_6H_5
D	208.08		C_8H_7

The possible structures of the observed fragments given in Table 7 can be used as evidence for the structure of unknown B. The fragments observed show structural similarities with the proposed structure, partially Fragment C at 234 m/z, which shows the loss of the external aromatic ring, fragment C in the NMR analysis.

The data and evidence review through the final part of this chapter shows good support for the proposed structure of compound B.

4. Intermediates in the inhibition of spontaneous polymerisation of styrene by nitrophenols

A number of intermediates and products have been identified in the spontaneous polymerisation of styrene inhibited by 2-nitrophenol. The role of these intermediates and products in the inhibition process is not clear. There are a number of different routes they could take.

The intermediates observed may be the only inhibiting species in the mechanism, and need to form first in order for the inhibitor to work. This would mean that factors, such as stability of these intermediates, and the rate of their formation, would determine the inhibition efficiency. If the intermediate is stable and formed quickly, then these intermediate species would be readily available to react with the slow flux of initiators formed spontaneously from styrene.

An alternative hypothesis is that these products are additional inhibitors formed from the starting inhibitor, which would further inhibit the polymerisation. From the product analysis we see that 2-aminophenol is formed from 2-nitrophenol during the inhibition of polymerisation. It could be possible that these inhibit further. This is covered later in the chapter.

Other possibilities are that these products no longer take part in inhibition or the products and intermediates break down or further react via a non-inhibiting mechanism. This effectively ends the inhibition mechanism.

An unlikely route is that these products initiate polymerisation, or form initiators in the reaction mixture, effectively increasing the rate of polymerisation. This would be counter-intuitive, as the aim of inhibitors is to stop the polymerisation, and any compound that could give rise to an initiator would be avoided.

The aim of this chapter is to investigate the stability, reactivity and inhibition properties of the intermediates proposed or observed in the last two chapters. The methods used will involve the use of product analysis and dilatometry, similar to the previous study. The

products to be study are 2-aminophenol, 2-nitrosophenol, compound B observed in the product mixture and derivatives of imines that were used in the synthesis of Compound B. These potential intermediates may give clues as to the overall mechanism of inhibition followed by 2-nitrophenol, but may also reveal related compounds that can act as inhibitors.

4.1 Further dilatometry

4.1.1 2-Aminophenol

The product analysis of the spontaneous polymerisation of styrene inhibited by 2-nitrophenol showed that 2-aminophenol is formed as the main product at the end of reaction. The dilatometry analysis of structurally related molecules to 2-nitrophenol demonstrated that hydrogen bonding between the nitro group and another adjacent functional group increased the inhibition efficiency of the molecule. Aminophenols contain relatively labile hydrogen in the N-H group that could be easily donated to initiator species. Also, the same asymmetry in the amine group caused by the hydrogen bonding from the phenol may improve the inhibition properties, in a similar way this occurs in ortho nitrophenols.

The inhibition of styrene polymerisation by 2-aminophenol, which was identified as unknown A in the product analysis, at 0.1 M concentration, was investigated using dilatometry. Figure 64 shows that at this concentration it acts as a very good retarder, lasting longer than other nitrophenol inhibitors.

This concentration is difficult to use practically, as 2-aminophenol has a low solubility in styrene. However, it is quite soluble at high temperature. Heating the sample before inserting into a sample tube allows the analysis to be performed, and should not affect the results observed.

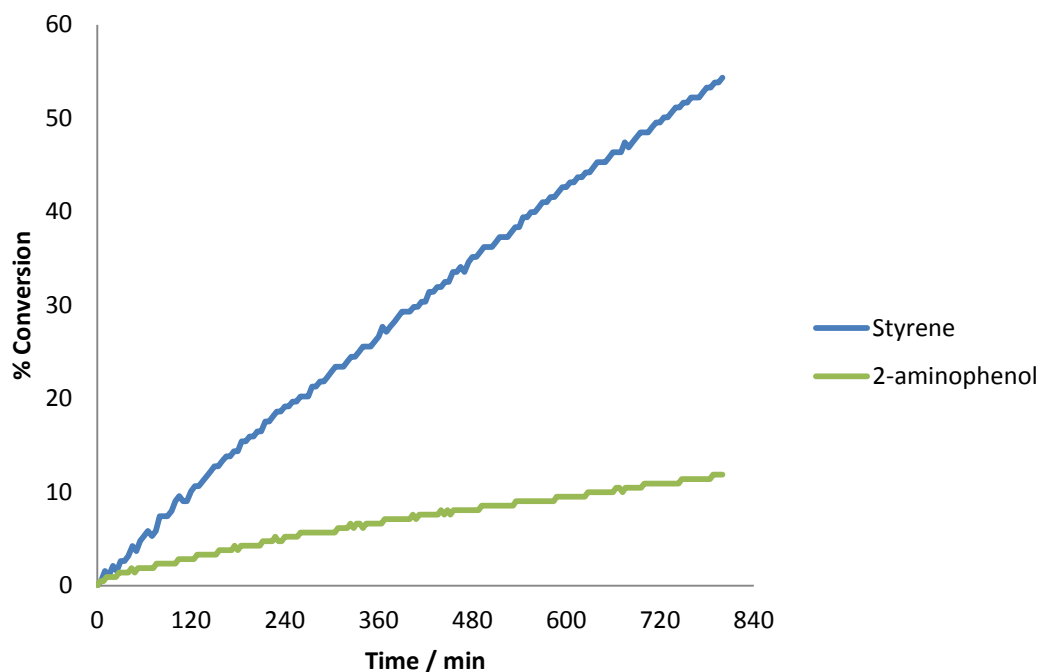


Figure 64. Dilatometry of styrene and styrene inhibited by 0.1 M 2-aminophenol at 110°C

Addition of an aliphatic group to 2-aminophenol should increase the solubility in styrene, allowing better observation of its inhibition properties. To do this, 2-amino-4-sec-butylphenol was used. 2-amino-4-sec-butylphenol also needed heating to dissolve at 0.1 M concentration, but the initial amount dissolved in styrene at room temperature, was far greater than for 2-aminophenol.

A comparison between these two amine inhibitors is given in Figure 65. The sec-butyl derivative shows a small increase in inhibition. These dilatometry experiments confirm that at this concentration, an ortho-aminophenol structural moiety acts as a good retarder.

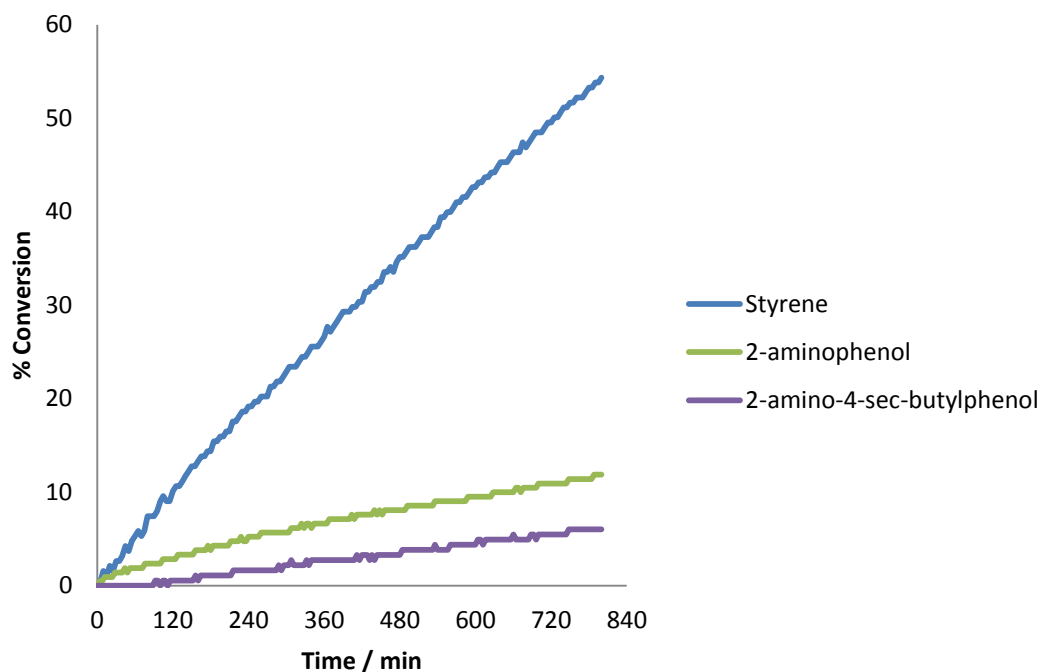
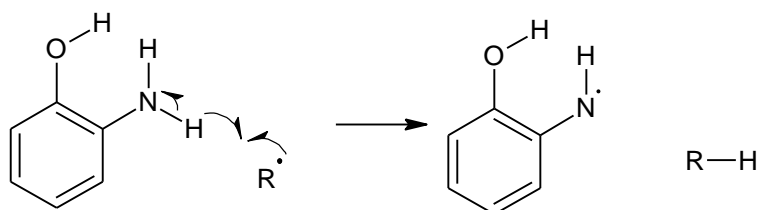


Figure 65. Dilatometry traces of styrene, 0.1 M 2-aminophenol in styrene and 0.1 M 2-amino-4-sec-butylphenol in styrene at 110°C

At 0.1 M concentration 2-aminophenol appears to outperform retarders such as 2-nitrophenol and DNBP in terms length of retardation period, even though the reduction in the rate of polymerisation is not as much as for the standard retarders. The retardation of polymerisation by 2-aminophenol possibly occurs through hydrogen abstraction from the nitrogen-hydrogen bond.



Scheme 40. Hydrogen abstraction from 2-aminophenol by an initiator radical.

At realistic concentrations, however, the dilatometry does not support 2-aminophenol as a useful inhibitor. Figure 66 shows that at 3 mM, 2-aminophenol produces an inhibition period of about 100 minutes, followed by polymerisation at a similar rate to uninhibited styrene.

Therefore it can be concluded that 2-aminophenol has limited inhibition properties. This also suggests that 2-aminophenol is not the main inhibition species when 2-nitrophenol is used as an inhibitor.

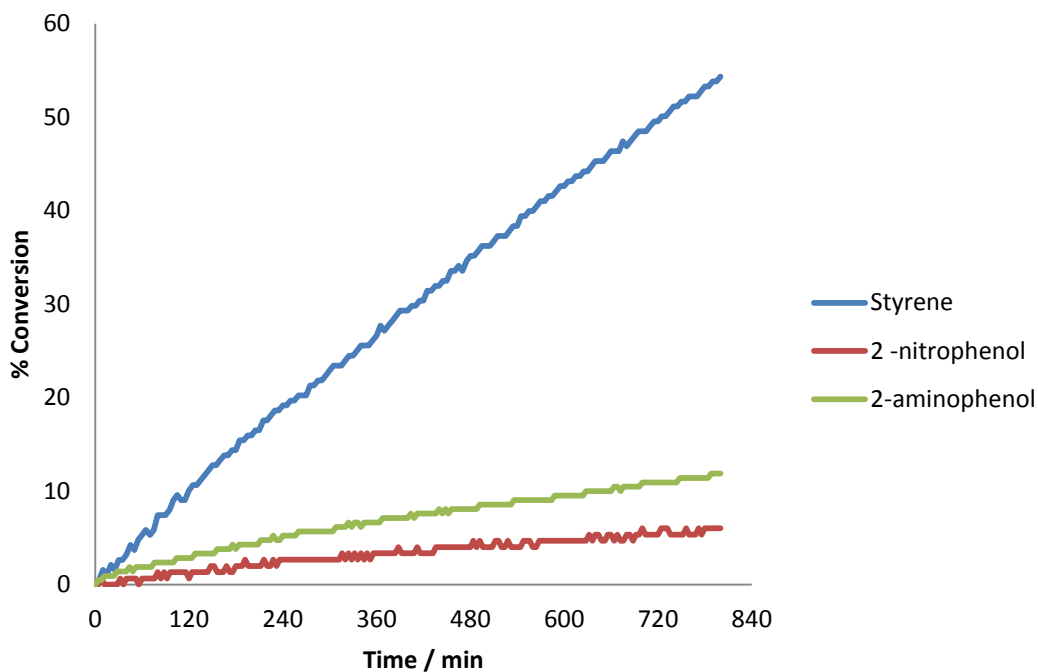
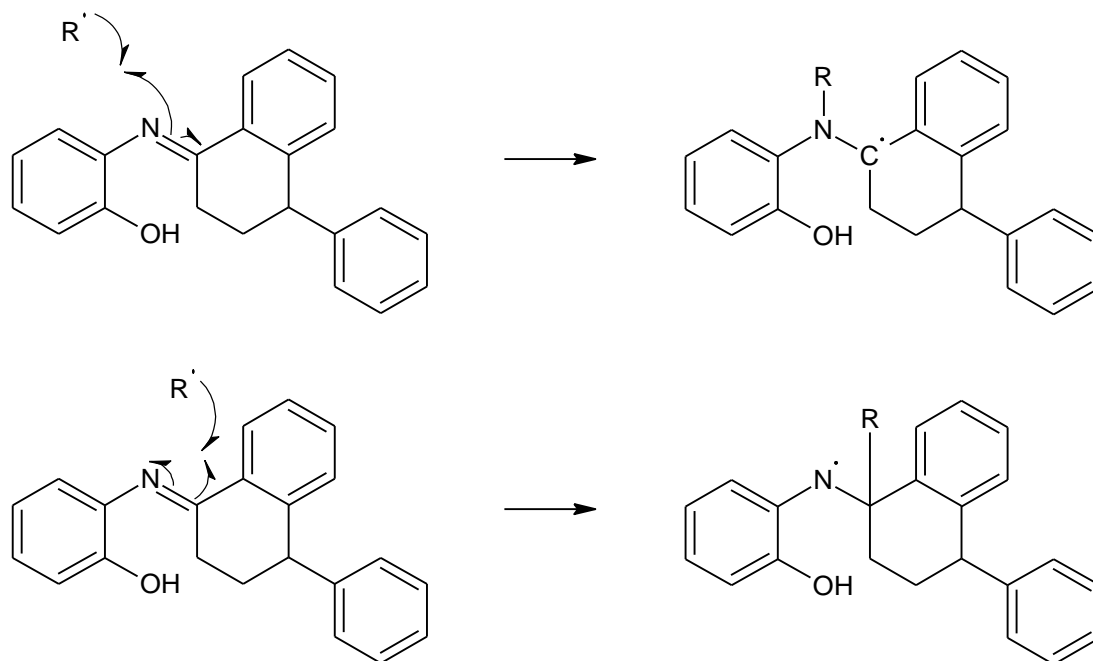


Figure 66. Dilatometry of styrene, and styrene inhibited by 3 mM 2-nitrophenol and 3 mM 2-aminophenol at 110°C.

4.1.2 Imines as inhibitors

If 2-aminophenol, formed from the inhibition of styrene spontaneous polymerisation by 2-nitrophenol, shows some inhibition properties in the dilatometry experiment, then perhaps other intermediates or products observed previously also show inhibition properties. In the previous chapter, Section 3.5 page 96, it has been shown that the product unknown B could be made via an imine intermediate formed from 2-aminophenol and the Diels-Alder adduct from spontaneous styrene initiation. Analysing Compound E, the imine intermediate, by dilatometry may yield more information about the mechanism of inhibition by nitrophenols. The imine E contains a phenolic group and therefore could act as an inhibitor in the same way a phenolic inhibitor does, through hydrogen donation to a peroxy radical. Also, the initiator could add to the double bond, as demonstrated in

Scheme 41. However, this mechanism does not offer information on the formation of compound B, but it has been shown to be a product when the imine is added to a sample of heated styrene.



Scheme 41. Possible mechanism of an initiator radical adding to the imine, compound E.

Figure 67 shows that the imine inhibits on a similar scale to 2-nitrophenol at 0.1 M concentration. The imine formed may be the inhibiting species in the inhibition by 2-nitrophenol, or more likely, it adds to the nitrophenol efficiency, in the same way as 2-aminophenol does.

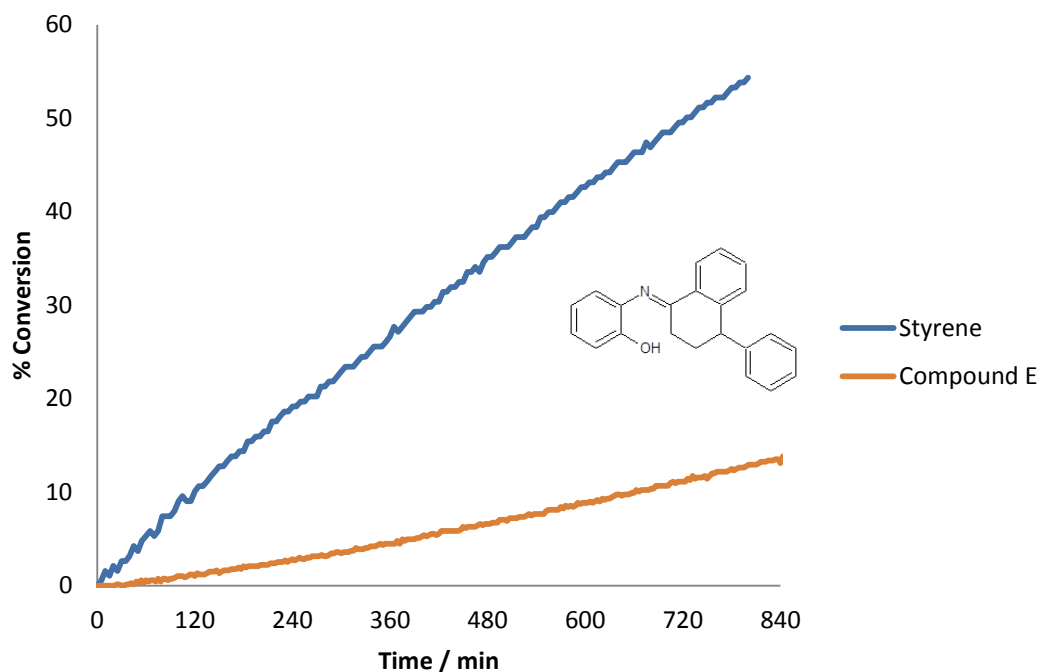
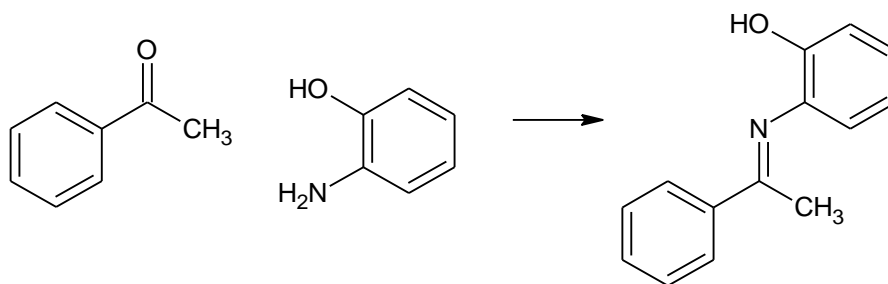


Figure 67. Dilatometry traces of styrene, and styrene inhibited by 0.1 M compound B at 110°C

Compound E's effective inhibition could be due to a number of mechanisms. The imine group may be where the inhibition occurs, and to investigate this, compound F was synthesised from aminophenol and acetophenone, shown in Scheme 42. This compound was chosen to confirm if the inhibition is due to the imine functional group.



Scheme 42. Synthesis of compound F

Figure 68 shows that Compound F is also a good inhibitor, with a similar trend to compound E.

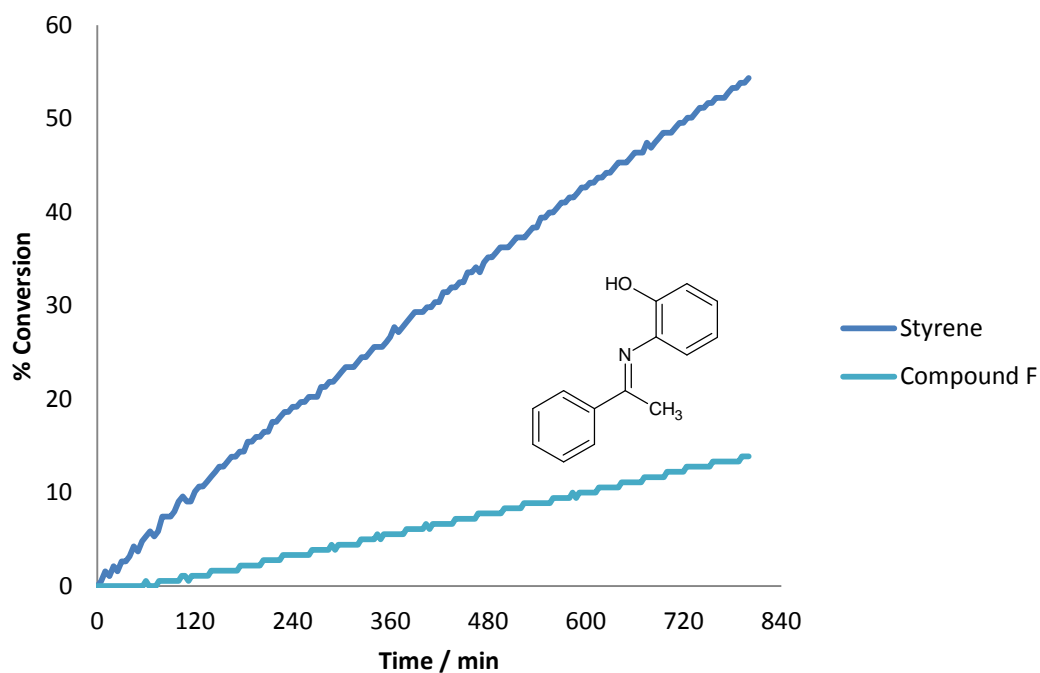


Figure 68. Dilatometry of uninhibited styrene and styrene inhibited by 0.1M compound F at 110°C.

However, as discussed previously, 0.1 M would not be used in real situation. Also the imine intermediate would not be found at this concentration either. Therefore a 3 mM solution was used as a more practical concentration. Figure 69 shows a comparison of the imine inhibitors. The imine shows a dilatometry trace with a 100 minute inhibition period followed by polymerisation. This is the same as for 2-aminophenol and suggests that the inhibiting species here is actually 2-aminophenol. This would require the imine to break down into 2-aminophenol and the corresponding ketone, allowing 2-aminophenol to inhibit the polymerisation. For this to happen, water must also be present in the styrene sample to allow the imine to decompose this way. This is not unreasonable at 3 mM, but at 0.1 M, there simply is not enough water to decompose all the imine present. There may be a mixture of different mechanisms that occur at higher concentrations.

Whichever mechanism the imine proceeds via, the fact that there is little inhibition when 3 mM are used excludes the imine and 2-aminophenol as the main inhibiting species when 2-nitrophenol inhibits.

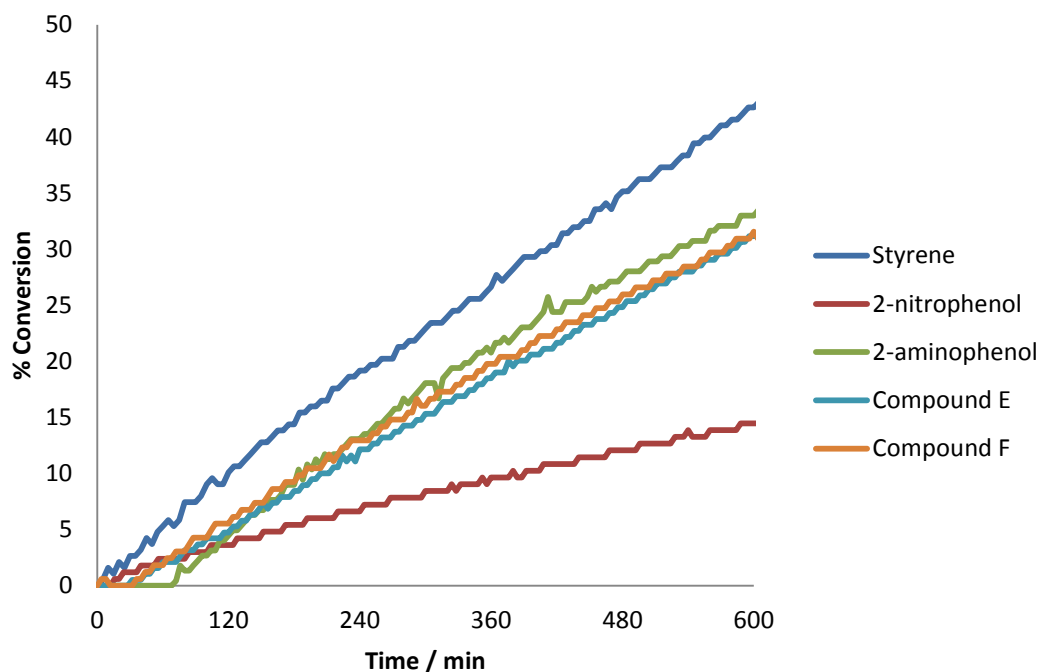


Figure 69. Dilatometry of styrene and styrene inhibited by 2-nitrophenol , 2-aminophenol, compound E or compound F (3 mM) at 110°C.

4.1.3 Unknown B as an inhibitor

A hypothesis developed from the product analysis is that when a nitrophenol inhibitor reacts with an initiator species, the products of the initial inhibition can also inhibit the polymerisation. This is true for 2-aminophenol and compound E, but these two products only show a small amount of retardation at the low, realistic concentration of 3 mM. It is unknown where down the series of reactions this property stops. Therefore the isolated sample of unknown B from the previous chapter was run in the dilatometer at 0.1 M.

Figure 70, shows that it is not an efficient inhibitor, and as it is found in very low concentrations in the reaction mixture it would not contribute to the overall inhibition.

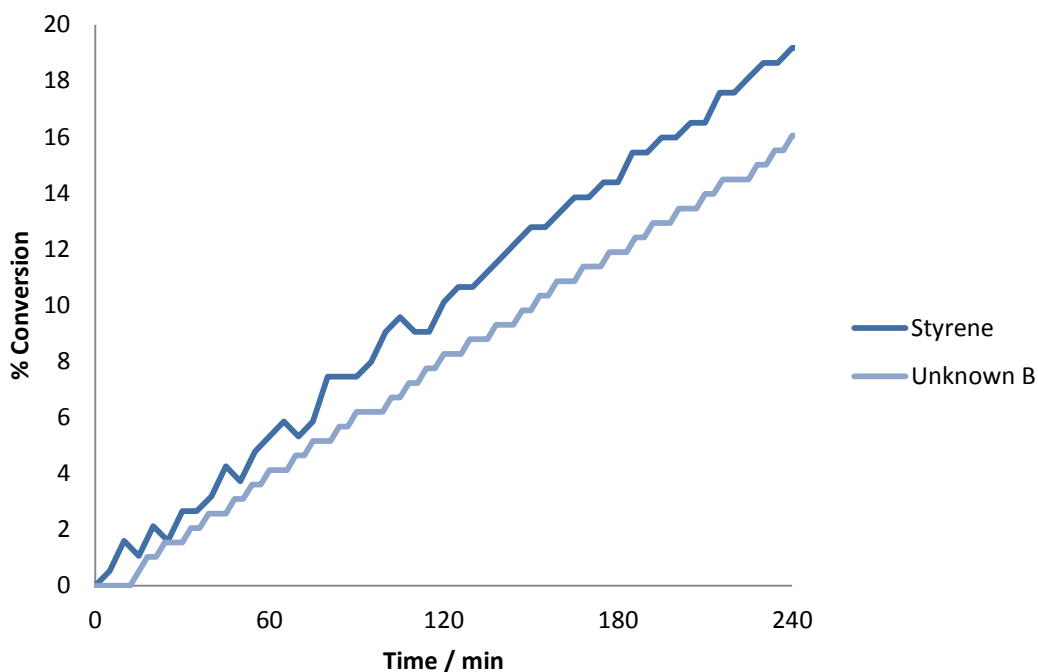


Figure 70. Dilatometry of styrene inhibited by 0.1 M unknown B at 110°C

4.1.4 2-Nitrosophenol

An intermediate in the inhibition of polymerisation by 2-nitrophenol suggested by Jackson and Waters⁴⁶ is 2-nitrosophenol (Section 1.3.1.3 page 39). This is awkward to use in the dilatometer setup as 2-nitrosobenzene is unstable once all solvent used in the synthesis is removed. Therefore concentrated solutions in pentane were used to aid in the preparation of the inhibited styrene samples. The addition of pentane will not affect the dilatometry results.

2-Nitrosophenol shows good inhibition efficiency in Figure 71, similar to 2-nitrophenol at 0.1 M concentration. This could suggest that as 2-nitrophenol inhibits, the products can also go on to inhibit themselves, increasing the efficiency of the inhibitor. However when comparing 2-nitrophenol and 2-nitrosophenol at 3 mmol in Figure 72, 2-nitrosophenol no longer retards as efficiently as 2-nitrophenol. This suggests that the majority of the inhibition by 2-nitrophenol occurs before 2-nitrosophenol is formed, and any inhibition by 2-nitrosophenol is minimal to the overall observed inhibition.

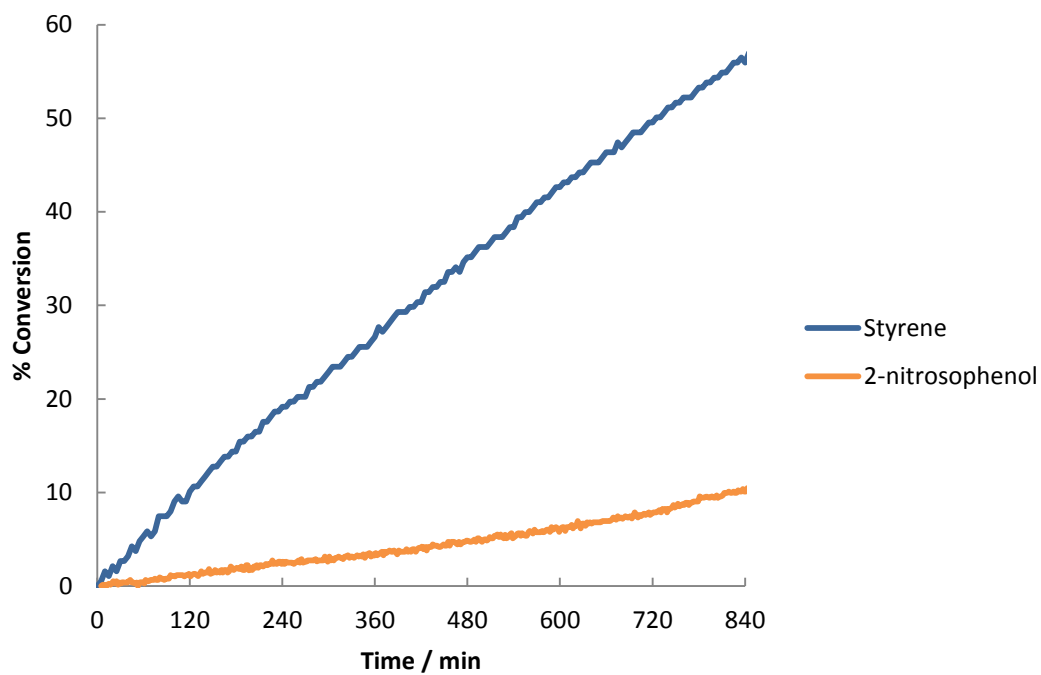


Figure 71. Dilatometry of styrene and styrene inhibited by 0.1 M 2-nitrosophenol at 110°C.

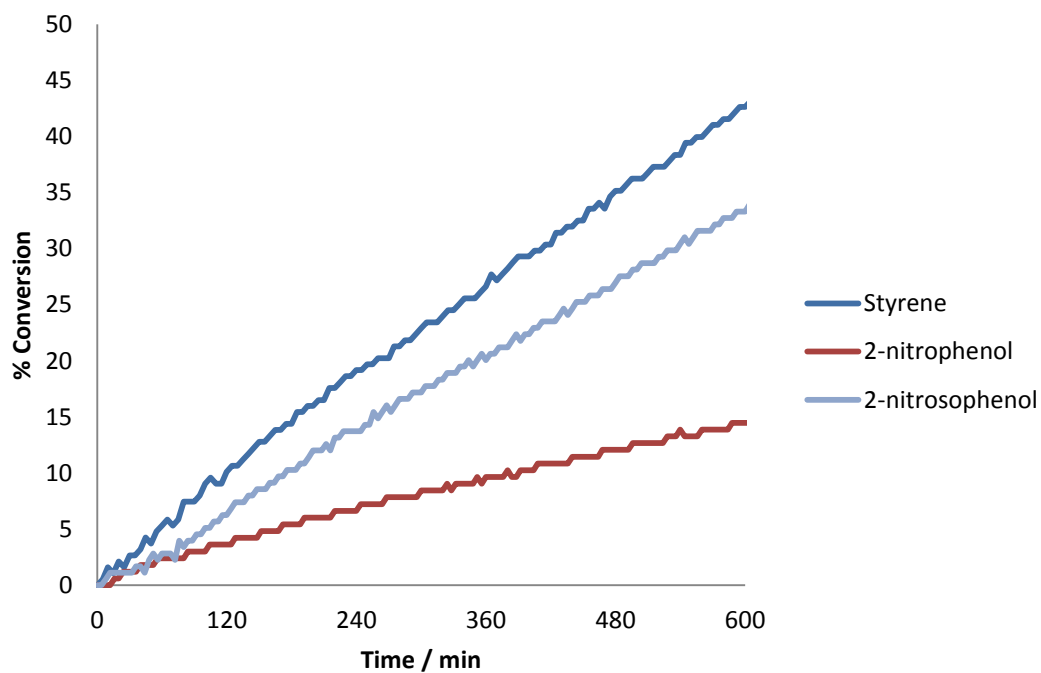


Figure 72. Dilatometry trace styrene inhibited with 3 mmol 2-nitrophenol and 3 mmol 2-nitrosophenol at 110°C.

4.2 Further product analysis

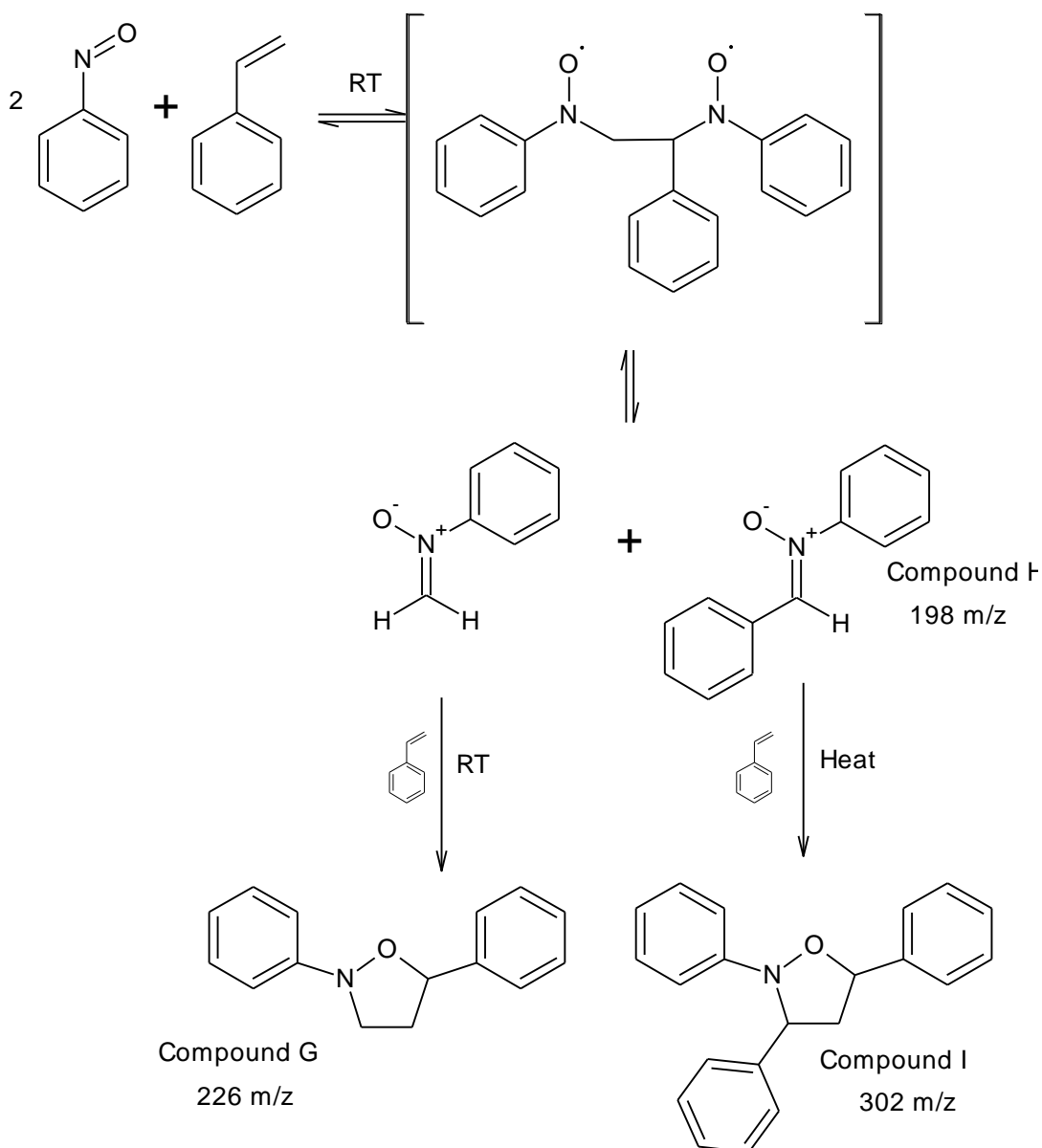
4.2.1 Nitroso intermediates

As discussed previously by Bartlett et al⁹⁴ and Jackson and Waters⁴⁶ (Section 1.3.1.3 page 39), nitroxides form in the nitrophenol inhibition of spontaneous styrene polymerisation, via a nitroso intermediate (See Scheme 28 page 94). Formation of intermediate nitrosophenol is also consistent with the reduction of 2-nitrophenol to 2-aminophenol which was detected in the polymerisation mixture, (See section 3.5 page 96). The 2-nitrosophenol intermediate may have the ability to react with the radical initiator species and remove them from the propagation step. The reactivity of nitroso derivatives in the styrene polymerisation may thus help us further understand the inhibition mechanism. This section describes the investigation into these intermediates and tries to determine if they are a major inhibiting species in a nitrophenol inhibition mechanism.

4.2.1.1 Nitrosobenzene

Nitrosobenzene was investigated first as a baseline for comparison to 2-nitrosophenol. As demonstrated by dilatometry earlier, the position of the nitro and phenol groups affect the inhibition properties of nitrophenol compounds. By looking first at nitrosobenzene, the effect of ortho-hydroxy group on the inhibition properties of this compound can be investigated.

Kang et al¹⁰³ have studied the room temperature reaction between nitrosobenzene and styrene and have identified the products formed. Their mechanism given in Scheme 43 shows the formation of isoxazolidines via a biradical intermediate, and the observed products are labelled in the Scheme as compounds G and I. According to the authors, there are two possible outcomes for the biradical. At room temperature compound H, the nitrene, is observed and only after heating does this nitrene react with another molecule of styrene to form compound I.



Scheme 43. Literature proposed mechanism for reaction of nitrosobenzene and styrene. The m/z values are the $[\text{M}+\text{H}]^+$ ions observed¹⁰³.

An advantage of using nitrosobenzene as a potential inhibitor is that it is readily available, unlike 2-nitrosophenol. When styrene is inhibited by nitrosobenzene, the reactions described by Kang et al¹⁰³ will take place very rapidly at high temperature and any inhibition of polymerisation that is observed will be from the products of the reactions described. Also, the authors have described a low temperature mechanism and a higher temperature mechanism, with different products depending on the route.

Indeed, when making the solutions of nitrosobenzene in styrene for the dilatometer, an observation was made. There was a steady colour change from red to dark brown over

time, consistent with a chemical reaction as described by Kang et al¹⁰³. When samples were run in the dilatometer, there was a difference in the dilatometry trace between freshly prepared samples and samples that were prepared the day before. This is shown in Figure 73. The aged sample was left for 24 hours before being used in the dilatometry experiment. It almost appears to act as an initiator, as shown by the steeper slope than uninhibited styrene.

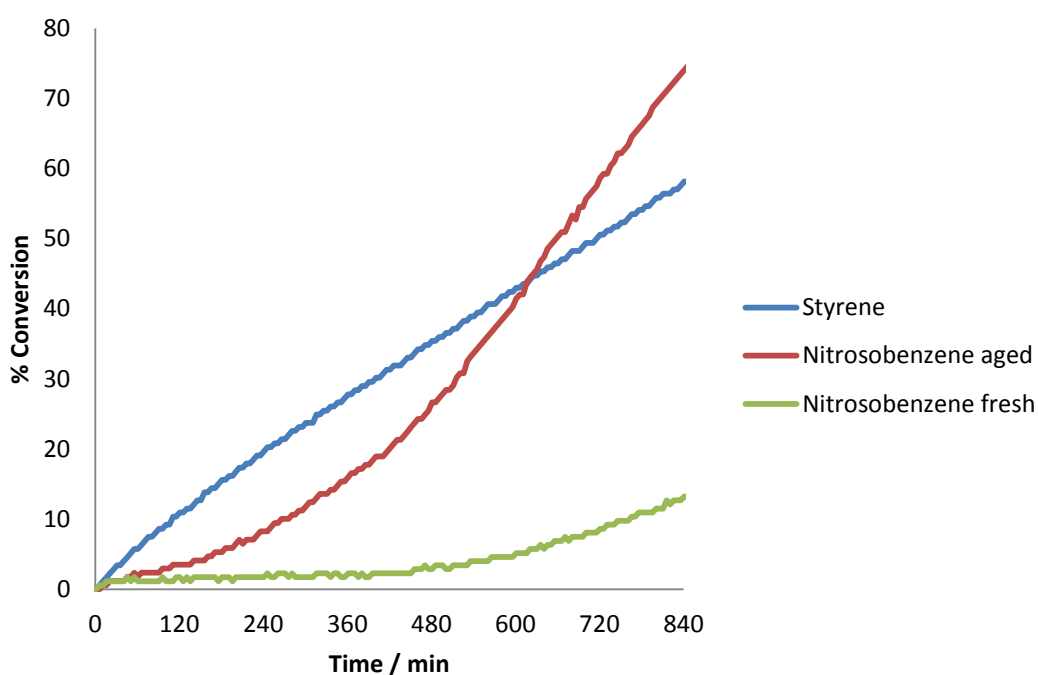


Figure 73. Dilatometry traces of styrene and 0.1 M nitrosobenzene prepared fresh and aged for 24 hours at room temperature. Dilatometry performed at 110°C.

The samples prepared for dilatometry were analysed by MS and by ¹H NMR (after removal of styrene). The samples prepared immediately (Figure 74) showed the same results as Kang et al¹⁰³. However, a sample left for a day at room temperature resulted in compounds H and I being observed, the same as Kang et al¹⁰³ for their heated sample. The ¹H NMR spectrum obtained in Figure 76 was from this second “aged” sample, and gave the same results as reported by Kang et al¹⁰³, for their heated sample (Compounds H and I). The figure is labelled with the structures determined from the literature results. The aromatic peaks all overlap, so no distinction could be made between those peaks.

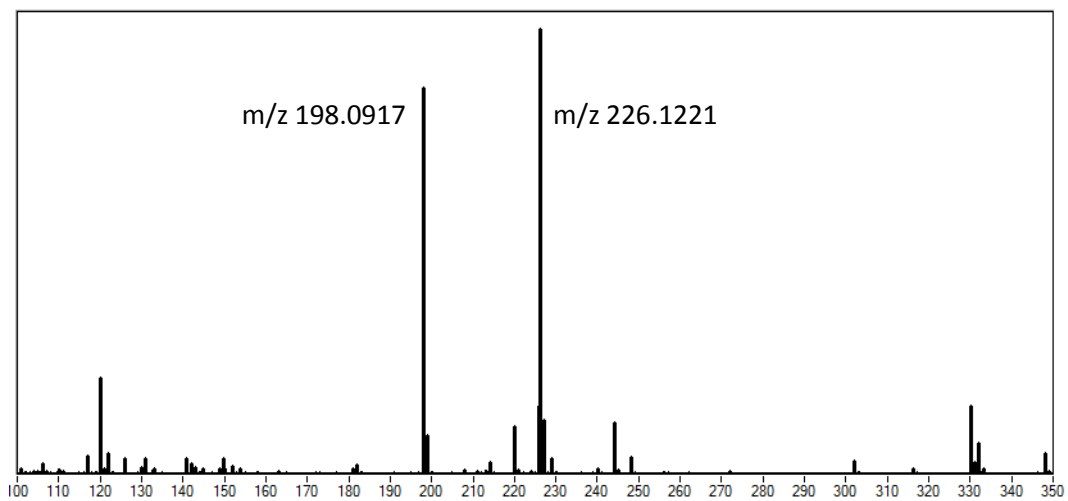


Figure 74. MS of sample of nitrosobenzene in styrene, analysed immediately

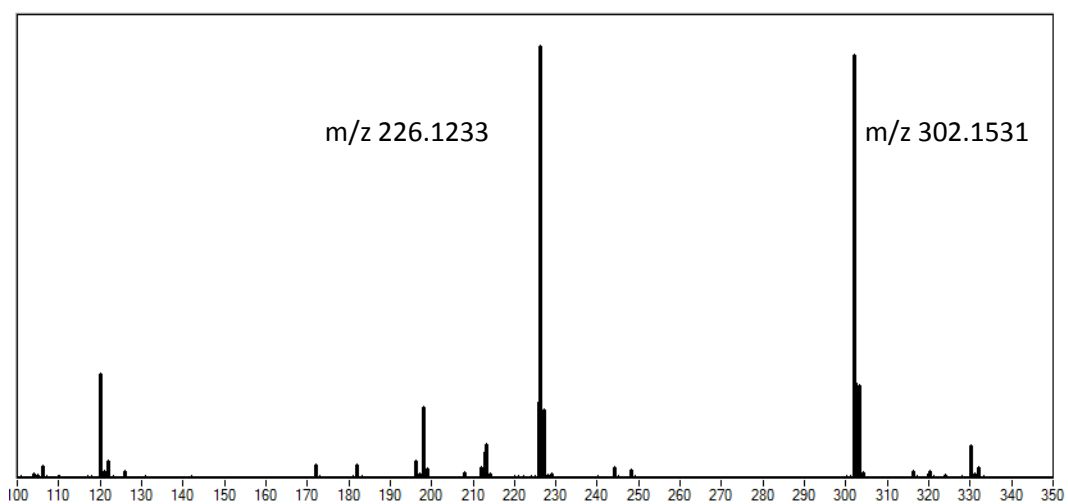


Figure 75. MS of sample of nitrosobenzene in styrene, analysed after 24 hours at room temperature

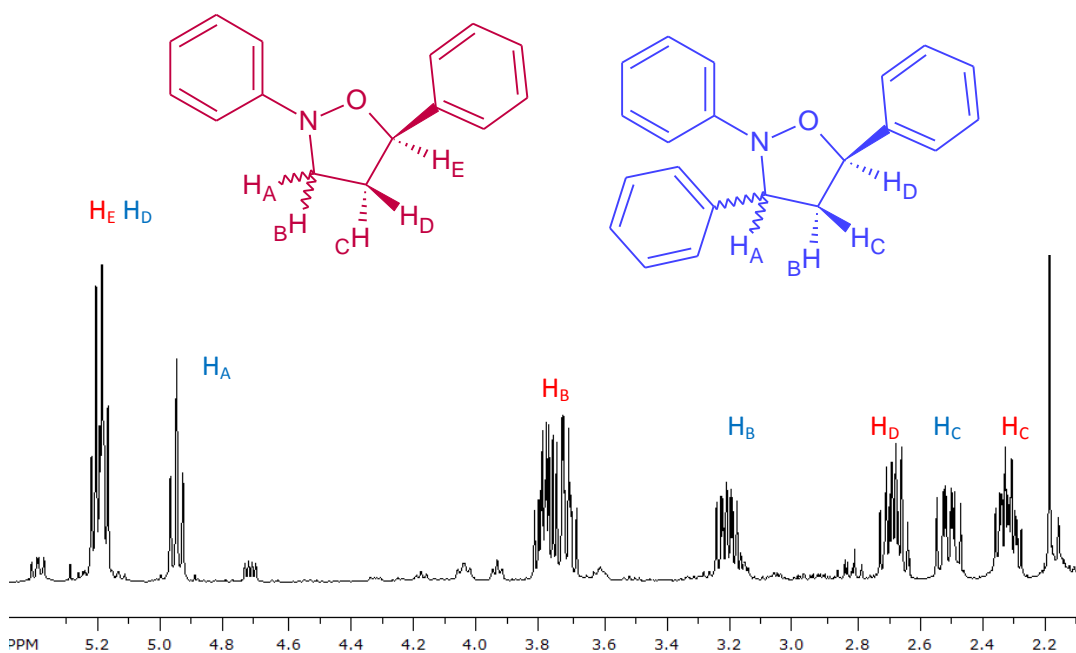


Figure 76. ^1H NMR of the reaction mixture between nitrosobenzene and styrene after solvent removal. (400 MHz, CDCl_3)

The dilatometry traces in Figure 73 can thus be linked to the presence of compounds G and H in the nitrosobenzene-styrene reaction mixtures. The samples that show polymerisation inhibition possibly contain nitron H, whereas the sample that shows limited inhibition followed by increased rate of polymerisation contains only isoxazolidines. This suggests that the nitron formed, compound H, is potentially a weakly inhibiting species, and the isoxazolidines probably break down into initiating species.

This chemistry is directly relevant to nitroso benzene. The effect an ortho hydroxy group has on a nitroso group is the factor to be investigated.

4.2.1.2 2-Nitrosophenol

Applying what has been learnt from nitrosobenzene, samples of 2-nitrosophenol in styrene were analysed. The synthesis is based on procedure by Maruyama et al¹⁰⁴ with full details given in the Experimental, Section 7.9.2 page 210. The dilatometry (Figure 73) showed no difference between samples analysed immediately and those left to age for 24 hours in solution before analysis.

The ESI-MS results (Figure 77) show that 2-nitrosophenol also reacts with styrene immediately to form new products. Figure 77 shows possible structures for the two main peaks observed. The formation of products appears to follow the same route as nitrosobenzene, via a biradical intermediate, to form similar nitrones. These nitrones then form the products observed.

The product observed at m/z 212, compound K, is possibly the product of the nitrone cyclising with the phenol group from the 2-nitrosophenol aromatic ring. The other product observed at 244 m/z , compound J, probably comes from the reaction of the second nitrone with styrene, however the complete mechanism has not been determined and these structures are based solely on the MS data presented. An overview of the possible routes of formation is given in Scheme 44.

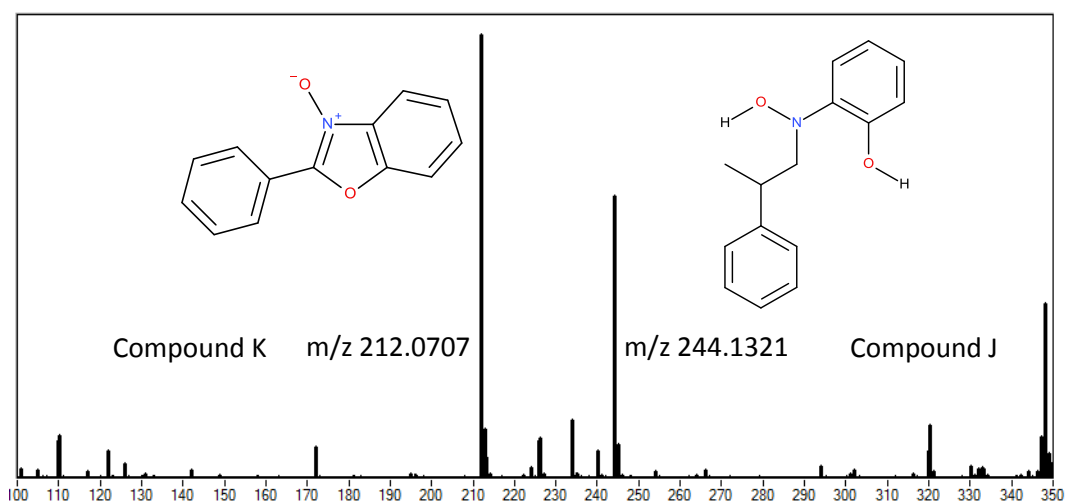
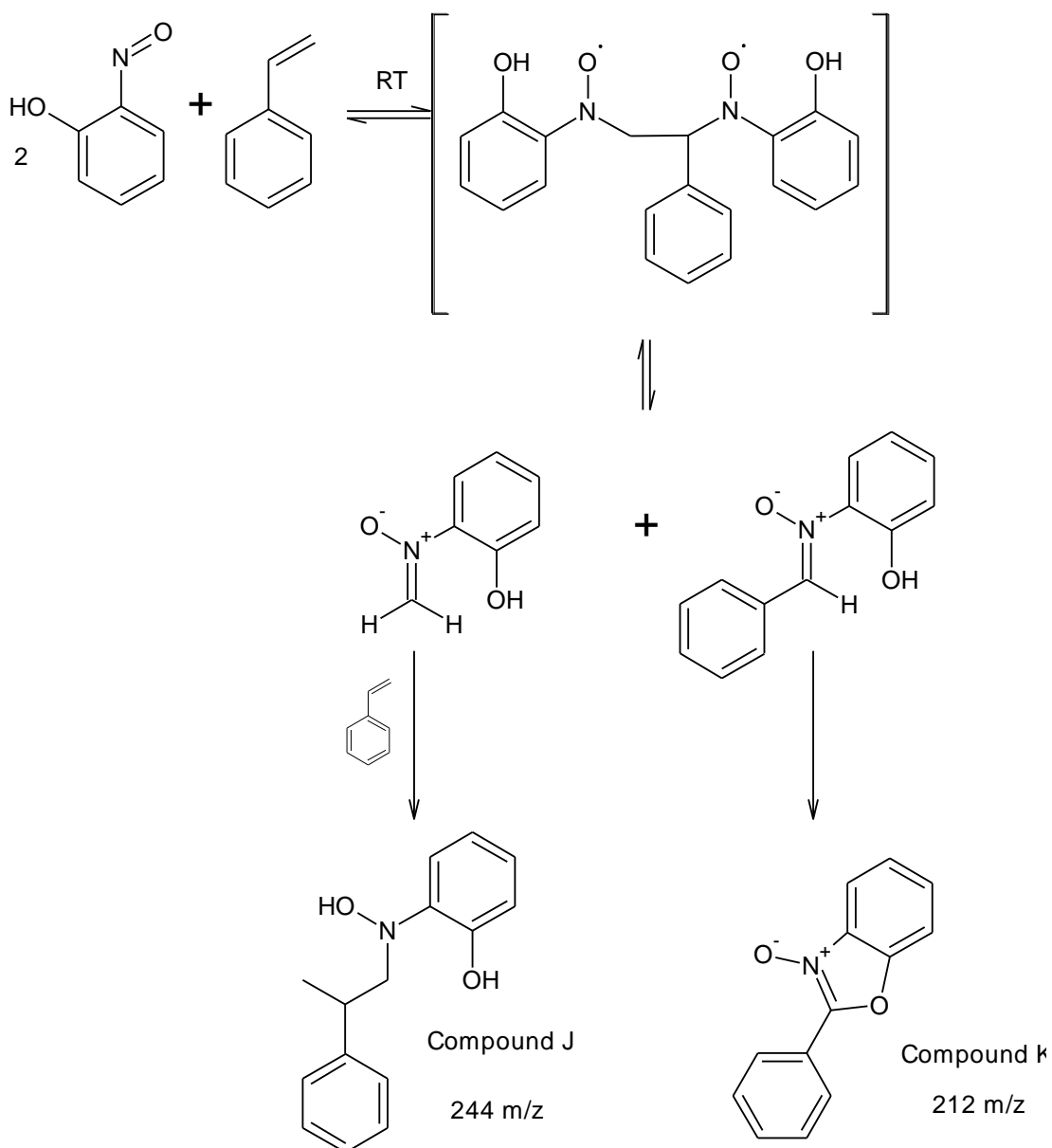


Figure 77. MS of 0.1M 2-nitrosophenol in styrene after 24 hours

However these products are formed, it is unknown if they are the inhibiting species or if they break down into a species that inhibits the polymerisation.



Scheme 44. Possible route for the formation of products observed from the reaction between 2-nitrosophenol and styrene

These samples were heated with styrene to observe the inhibiting effect of the reaction products on the spontaneous polymerisation. MS analysis of the new products formed reveal that the only additional product observed by MS is 2-aminophenol, as shown in Figure 78 as a peak at 110 m/z. 2-aminophenol is also a product observed after the inhibition of polymerisation by 2-nitrophenol. This confirms that 2-nitrophenol is reduced to 2-aminophenol during inhibition via a nitroso intermediate

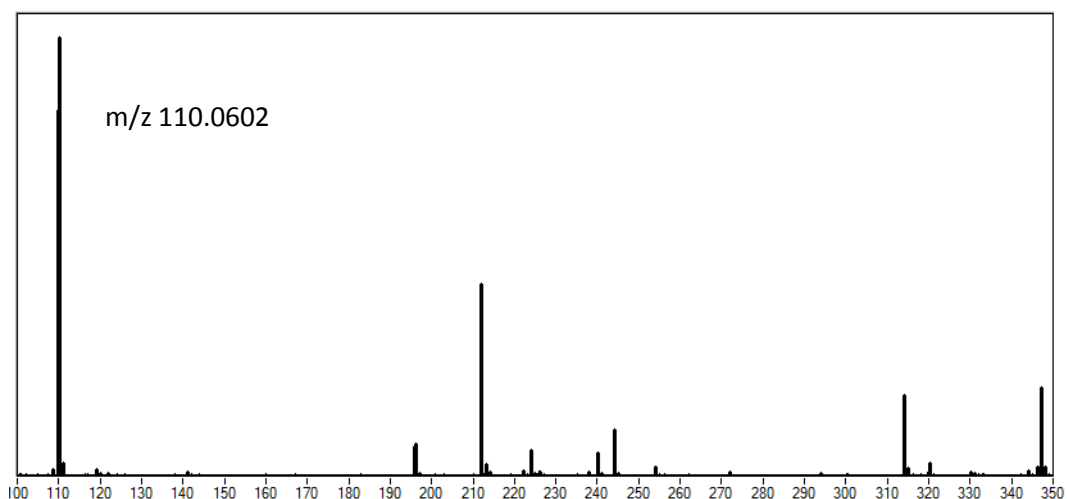
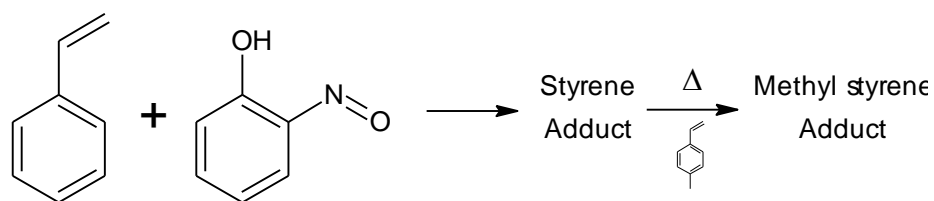


Figure 78. MS of the products of styrene spontaneous polymerisation inhibited by 0.1 M 2-nitrosophenol.

The formation of these products, which are themselves polymerisation inhibitors, could be a property of nitrophenols that make them efficient inhibitors. If a molecule forms other inhibitors during the inhibition of polymerisation, this is going to make them more efficient.

As polymerisation inhibition by both 2-nitrophenol and 2-nitrosophenol produce 2-aminophenol, they may share a common mechanism. However, the evidence so far is that 2-nitrosophenol rapidly reacts with styrene leaving only the products presented above, not 2-aminophenol. One possibility is that the initial products formed between 2-nitrosophenol and styrene (e.g., compounds J and K) “release” 2-nitrosophenol upon heating. Once released it may be reduced to 2-aminophenol. To investigate this, an exchange between styrene and 4-methyl styrene can be used to observe if any “release” of 2-nitrosophenol is occurring.

Samples of 2-nitrosophenol in styrene and methyl styrene will give two different products with MS spectra separated by 14 m/z for the styrene / methyl styrene containing products. By removing excess styrene/methyl styrene from these samples and dissolving the residue in the methyl styrene/styrene, one can monitor the possible exchange, as demonstrated in Scheme 45. If any 2-nitrosophenol is released, it may be “captured” again by the new solvent and will appear in the MS as the peak at ± 14 m/z, depending on which solvents are used.



Scheme 45. Demonstration of the exchange experiment

Figure 79 shows the new peak at 225 m/z for the methyl derivative of compound H, but there is no additional formation of a peak 212 m/z during the heating at various temperatures. The only new peak formed is at 110 m/z, for the formation 2-aminophenol as discussed previously. This is true for both variations of the experiment.

In conclusion, it appears that 2-aminophenol is not formed directly from 2-nitrosophenol, but from the cyclised products presented above. The actual mechanism is still not clear and is likely to be a series of reactions resulting in 2-aminophenol being produced from the breakdown of the cyclised products.

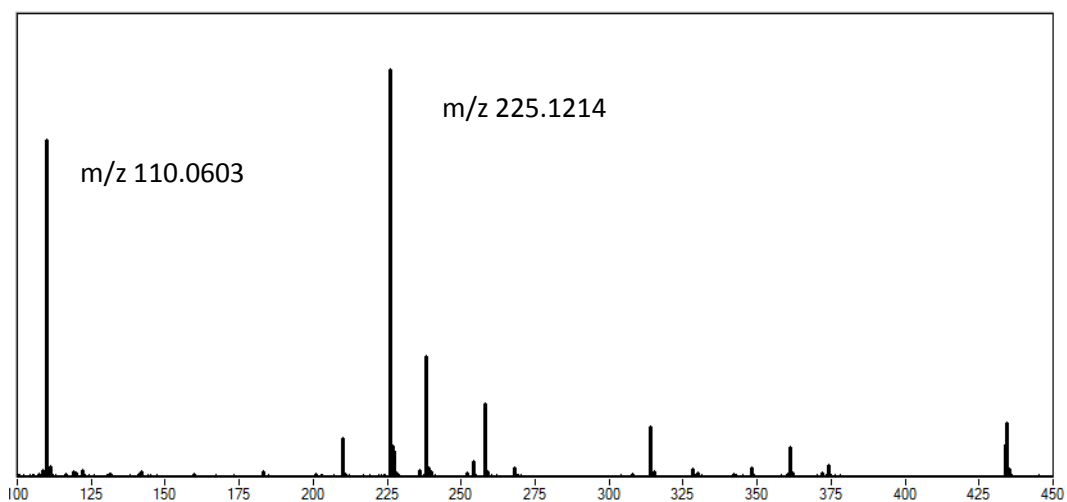


Figure 79. MS of product mixture of 0.1M 2-nitrosophenol in methyl styrene, heated at 110°C for 5 hours

4.2.2 EPR of 2-nitrosophenol in styrene

In order to test if the reaction of 2-nitrosophenol with styrene involves free radical intermediates, a solution of 0.1M 2-nitrosophenol in styrene was submitted for EPR analysis. The black line in Figure 80 shows the spectrum obtained from the reaction mixture prepared immediately before the sample was analysed. The concentration of radical observed was ca. 0.1 mM at its maximum. This is 0.1% of the nitrosophenol used and may not be an important intermediate of the reaction between styrene and 2-nitrosophenol, but merely a by-product.

By simulating the spectrum, the structure of the radical can be obtained. The simulation is given in Figure 80 as the red spectrum. There are two distinct hyperfine splitting, one from the nitrogen of the nitroxide and another from two equivalent hydrogens. The simulation gives the hyperfine values as a_N as 10.17 G and a_H as 3.46 G. These values are typical for nitroxides with two α -hydrogens (Scheme 43), similar to results of Motyakin et al,⁴⁹ who proposed a radical intermediate for the inhibition of styrene polymerisation inhibited by 2,4- dinitrophenol.

Interpretation of the spectra obtained show that there are at least two radical species in the sample. There is the dominant species, which has been simulated, and a minor one, too weak to properly identify. As shown previously, Section 3.4 page 94) the system is complex, and again, complete identification of all species is not possible without separation. This separation may not even be possible depending on the stability of the radicals.

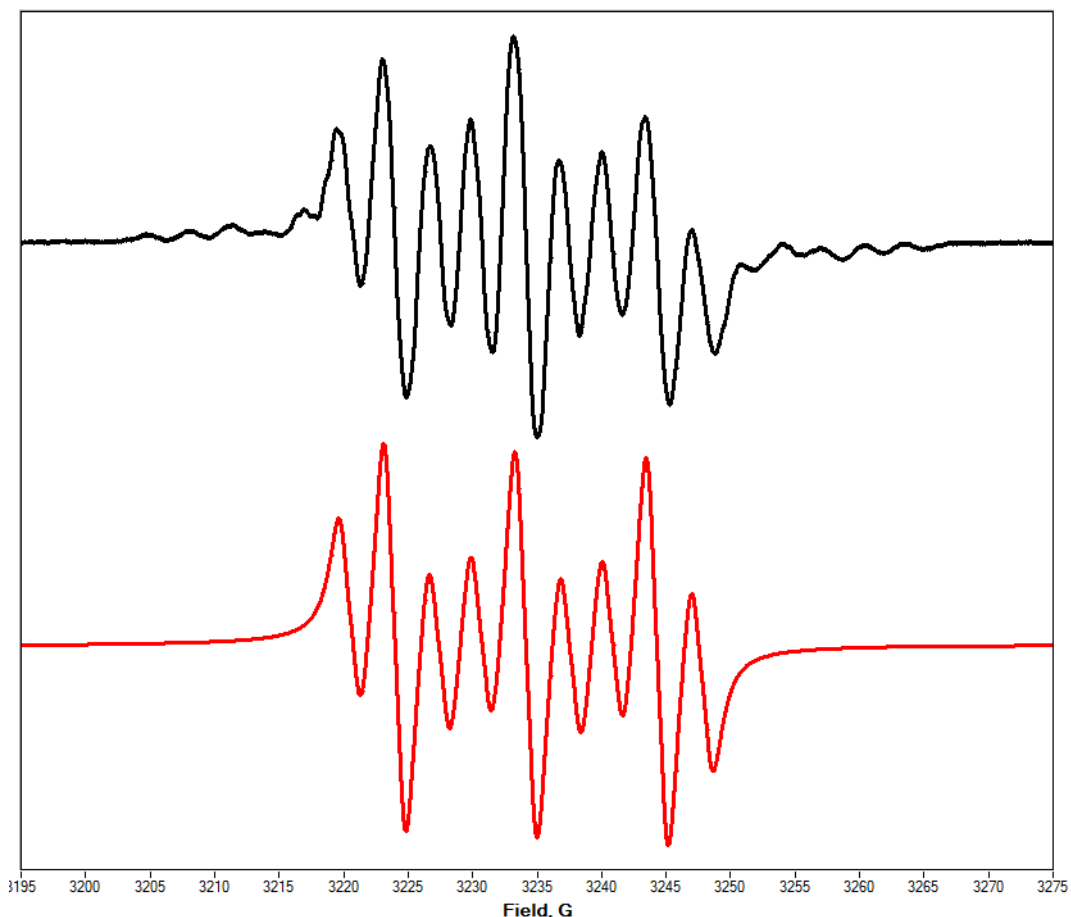
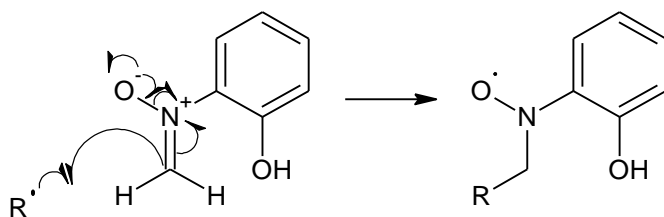


Figure 80. EPR of 2-nitrosophenol in styrene, average of spectra taken 35-55 minutes after addition (Black line) and a simulation of the proposed radical formed (Red line).

A possible route for the formation of this radical could be the reaction between a nitron formed from initial reaction between 2-nitrosophenol and styrene and an initiator species, shown in Scheme 46. If the radical that reacts with nitron is formed from styrene abstracting a hydrogen from another molecule, such as the species observed by Mayo,¹⁹ then this would lead to a similar structure to what has been proposed for the peak at m/z 244 in Figure 77. However, the nitron is never observed in any MS analysis performed on product mixtures.

The other route is that the hydroxyl amine (Compound J in Scheme 44) loses a hydrogen to an initiator species and forms the nitroxide. The nitroxide then inhibits further. This is more likely as only the hydroxyl amine is observed by MS (Figure 77) with small concentration of nitroxide observed in the preheated solution.



Scheme 46. Formation of nitroxide from nitron intermediate postulated based on work by Kang et al¹⁰³

A number of possible species have thus been observed or proposed in the inhibition of styrene spontaneous polymerisation and their inhibition properties have been assessed. In conclusion, the intermediates studied show little inhibition properties are realistic concentrations.

4.3 Conclusions from the additional dilatometry and product analysis

The products identified in the previous chapter were used as potential inhibitors for the spontaneous polymerisation of styrene. At the standard dilatometry concentration (0.1 M) 2-aminophenol (unknown A) showed a good rate of inhibition, reducing the rate of polymerisation to a similar degree as 2-nitrophenol. Unknown B did not show any inhibition at such a high concentration. Unknown B is unstable and is not the end of the reaction pathway. However, as it displayed no inhibition, it is unlikely that its decomposition products are involved in the inhibition mechanism.

A dilatometry trace of styrene polymerisation inhibited by 2-aminophenol at a realistic concentration of 3 mM shows little retardation. This means 2-aminophenol is not the main inhibiting species in the inhibition mechanism by 2-nitrophenol, but once formed, it can continue to retard the rate of polymerisation further. This appears to be an advantage of nitrophenol inhibitors.

In a similar fashion, the imine used to synthesise compound B was studied in the dilatometer. At 0.1M concentration it showed inhibition properties, but again at 3 mM

there was no inhibition. This was also true for another imine synthesised, not related to the inhibition mechanism, but for a comparison only.

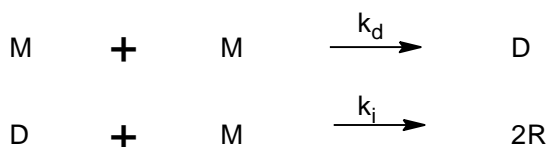
2-Nitrosophenol was synthesised, but was shown to immediately react with styrene at room temperature. In the inhibition mechanism by 2-nitrophenol, this would also occur, rendering 2-nitrosophenol unable to inhibit. Upon heating these cyclised adducts release 2-aminophenol. This is a possible source of aminophenol for the formation of compound B.

4.4 The Mechanism of Inhibition

4.4.1 Is inhibition stoichiometric or catalytic?

If an inhibitor works via a cyclic, catalytic mechanism is going to be more efficient than a stoichiometric mechanism. The inhibition by 2-nitrophenol is unknown as to whether it is either of these scenarios. In order to determine this, the rate of radical production in spontaneous self-polymerisation needs to be estimated and compare it to the rate at which the inhibitor is lost. If the rates are similar, the mechanism is likely to be stoichiometric. If the rate of inhibitor loss is much smaller than the rate of initiator production, the mechanism is likely to be catalytic. The estimations presented below are just that, estimates. Therefore an exact stoichiometric coefficient cannot be determined.

The mechanism of spontaneous polymerisation of styrene is covered in the Introduction, Section 1.2.1 page 30. The initiator radicals form from the reaction between the styrene dimer and another styrene monomer. Scheme 47 shows the simplified steps for the formation of the initiator radicals. There are two steps, the formation of the dimer, D, from the reaction of the monomer, M, and then the formation of the radicals, R.



Scheme 47. The simplified reactions describing the formation of radical initiators, where M is monomer, D is dimer and R the radical initiator.

From Scheme 47, the rate of radical formation can be determined. Equation 4 and Equation 5 show the rates of reaction for the formation of the dimer and the formation of the radicals. Equation 5 takes into account the loss of dimer as it forms the radicals.

$$\frac{d[R]}{dt} = 2k_i[D][M]$$

Equation 4. Rate of formation of initiator radicals, from the reaction between monomer and dimer.

$$\frac{d[D]}{dt} = k_i[M]^2 - k_d[D][M]$$

Equation 5. Rate of formation of the styrene dimer.

The rate constants k_i and k_d have been estimated in literature.^{42, 105-107} At 110 °C, $k_i = 1.7 \times 10^{-8} \text{ L mol}^{-1} \text{ s}^{-1}$, and $k_d = 1.0 \times 10^{-8} \text{ L mol}^{-1} \text{ s}^{-1}$. By combining Equation 4 and Equation 5 and approximately integrating the result for a short time period (t_1-t_0) and a concentration profile for the amount of radical formed can be determined. Note this is the concentration of radical formed without taking into account termination of radicals in the system. The profile is shown in Figure 81. This uses 8.7 M as the concentration of styrene, and makes the assumption that as styrene is the solvent as well it remains constant.

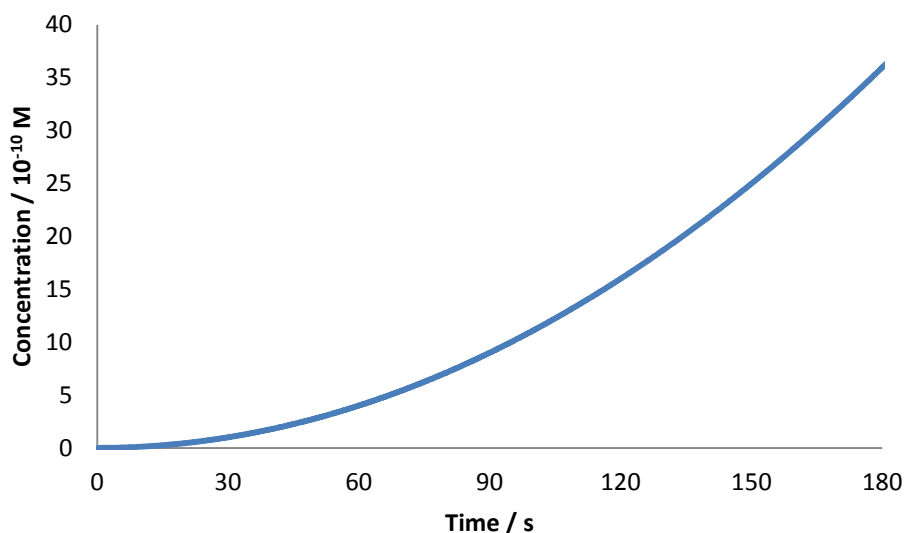


Figure 81. The amount of radical formed during spontaneous initiation of styrene at 110 °C.

To validate this result, the cumulative amount of radicals formed over a period of time can be compared to the inhibition period of 200 ppm TEMPO. The inhibition period is over after 9000 seconds. This suggests that TEMPO is completely consumed after this period. The concentration of radical produced by that point, calculated above, is $9 \times 10^{-6} \text{ mol L}^{-1}$. Compared to the concentration of TEMPO ($1.2 \times 10^{-6} \text{ mol L}^{-1}$) this is 7.5 times lower. The reason for this is due to the comparison above not taking into account the natural termination present in the system. As an estimate however, the model appears to agree with observed results.

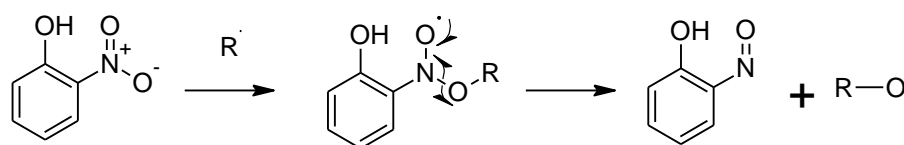
2-nitrophenol is a retarder rather than a true inhibitor. Therefore taking the time at which the slope of the dilatometry trace changes should be an estimation of the time for complete inhibitor consumption. This gives a time of 1500 minutes for inhibitor concentration of 0.1 M. The calculation gives a concentration of radicals roughly 100 times lower than the concentration of inhibitor. This suggests that the reaction is possibly stoichiometric, and that the reaction mechanism is not cyclic.

4.4.2 Reactions with the initiator radical

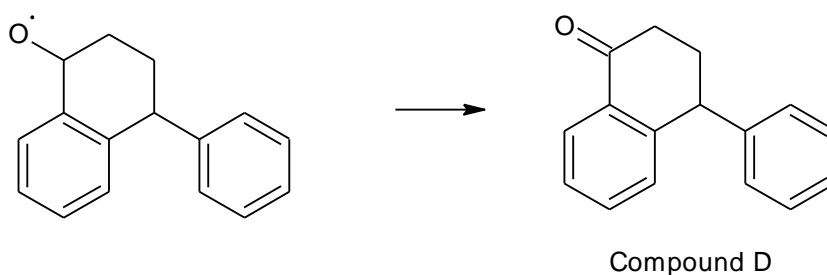
Inhibition occurs when an initiator or propagating radical reacts with an inhibitor before it can activate another monomer, which then continues to propagate the polymerisation. A

number of mechanisms have been used to describe the transformations of 2-nitrophenol during inhibited styrene polymerisation. A summary scheme for these mechanisms is given below.

The initial reaction between an initiator radical and 2-nitrophenol forms first an alkoxy nitroxide which then forms 2-nitrosophenol. This has been determined to be the main inhibition mechanism pathway, as the products from this reaction, such as 2-nitrosophenol, are less effective at inhibiting than 2-nitrophenol. The phenolic group activates the nitro group towards reaction with radicals by H-bond formation. The stoichiometric relationship between 2-nitrophenol and the radical initiator is 1:1.



If initiator is the Diels Alder dimer initiator:

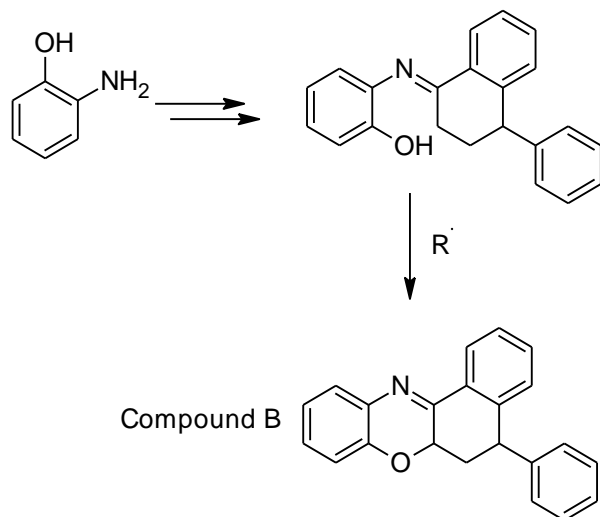


Scheme 48. The initial reaction between 2-nitrophenol and an initiator radical.

As shown previously in the chapter, 2-nitrosophenol will immediately react with styrene to form cyclised adducts. In the heated environment, these cyclised adducts break down releasing aminophenol into the mixture. It is not known exactly how these decompose in the system.

The final reaction pathway that has been suggested is the formation of unknown B. If it proceeds via an imine intermediate, then it would require the formation of a styrene Diels-Alder dimer ketone to form. After the imine is formed, it may require an initiator radical to abstract a hydrogen, removing an initiator from the propagation step. Compound B is

found in low concentrations, so this mechanism may not affect the overall inhibition efficiency of 2-nitrophenol, but may contribute to its effectiveness.



Scheme 49. The formation of Compound B .

4.5 Conclusion

Investigating the reactivity of a number of intermediates in the 2-nitrophenol inhibited spontaneous polymerisation of styrene, an inhibition pathway has been proposed. The inhibition can be described as stoichiometric rather than a cyclic continuous mechanism, although a stoichiometric coefficient cannot be accurately determined.

The start of the pathway begins with the hydrogen abstraction from nitrophenol, which is facilitated by the intramolecular hydrogen bonding between the phenol and nitro groups.

Next is the formation of 2-nitrosophenol. This does not further inhibit, but immediately reacts with styrene to form cycloadducts. These cycloadducts have been shown to decompose at high temperature into aminophenol. This was identified in product mixtures of styrene inhibited by 2-nitrophenol, and 2-nitrosophenol.

The final step of the reaction pathway is the formation of compound B, from 2-aminophenol and a ketone derived from the Diels-Alder initiator molecule. It has been demonstrated that the intermediates from this product formation, and the other intermediate identified, show little to no inhibited properties. This strengthens the conclusion that the initial step is where the inhibition occurs.

5. Chloranil Radical Anion

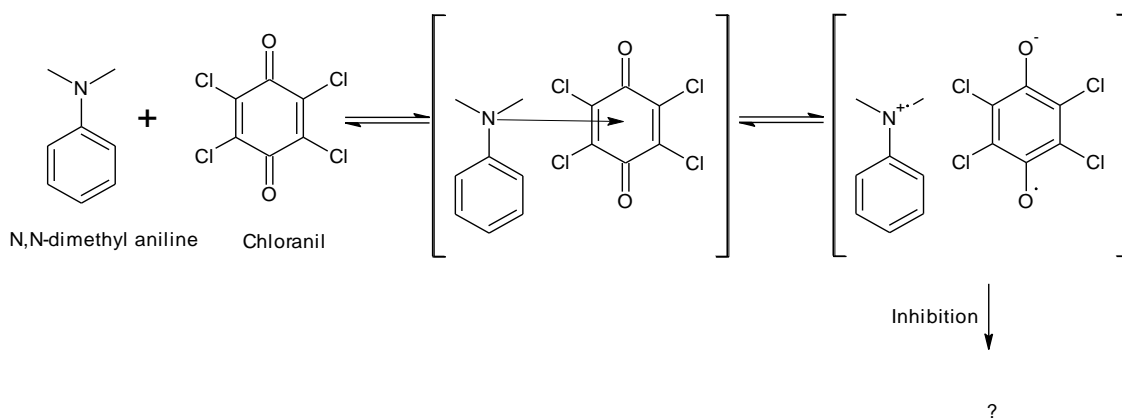
5.1 Introduction

Due to new EU legislation¹⁰⁸, all chemicals produced above a certain amount need to be valuated as to their toxic and environmental properties. This initiative is called the Registration, Evaluation, Authorisation and Restriction of Chemicals, a.k.a. REACH. This will eventually affect inhibitors such as DNBP. Nitro phenols are not without hazards, and will need to be reassessed, with the possibility that they will no longer be allowed to be used. Therefore the search for a new, green and non-toxic inhibitor has begun. This chapter aims to continue the work of Yassin and Rizk⁶¹ into a charge transfer complex which acts as an inhibitor.

5.1.1 A new inhibitor

As discussed in the introduction, quinones and hydroquinones have been used as polymerisation inhibitors (Section 1.3.1.4 page 41). A paper by Yassin and Rizk⁶¹ proposed that a charge transfer complex of 2,3,5,6-tetrachlorocyclohexa-2,5-diene-1,4-dione (Chloranil) to N, N-dimethyl aniline (DMA), acts as a polymerisation inhibitor. The degradation of the charge transfer complex leads to the chloranil radical anion, also known as a semiquinone, which is believed to be the inhibiting species.

Scheme 50 shows the structure of the charge transfer complex which Yassin and Rizk investigated. The first equilibrium shows the formation of the charge transfer complex of DMA and chloranil. The second equilibrium may possibly not be established under reaction conditions, as further reactions of radicals formed will compete with their recombination.

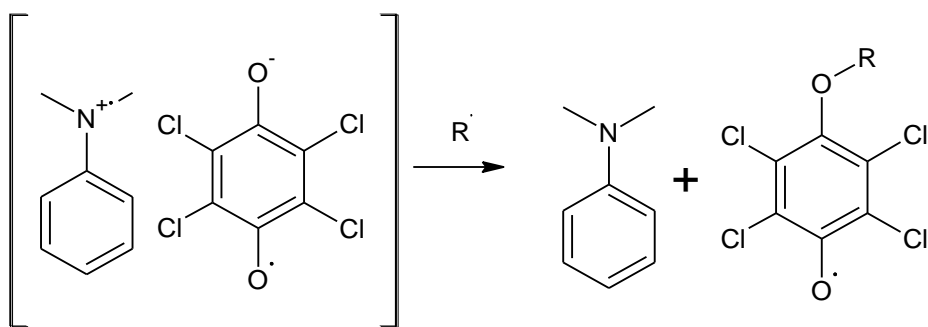


Scheme 50. Formation and degradation of charge transfer complex proposed by Yassin and Rizk.

Yassin and Rizk studied the rates of spontaneous polymerisation of styrene in the presence of chloranil and DMA separately, and observed the rate of polymerisation retarded slightly. When inhibiting styrene with a mixture of the two, they observed an inhibition period, followed by a retarded rate of polymerisation. Another observation is that when they increased the amount of the amine relative to chloranil, the inhibition period increased.

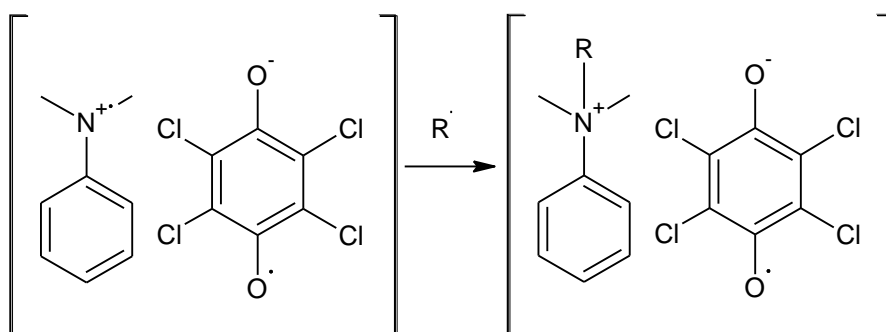
After the authors isolated the polymer from their reactions, they found no trace of nitrogen incorporated within the polymer chains. Their conclusion was that if the amine half of the charge transfer complex was the main inhibiting species in the inhibition, then nitrogen should be incorporated into the polymer. This would occur by the most common form of inhibition; recombination of radicals. However, if the amine inhibited polymerisation by a route that did not involve recombination, for example electron transfer, then nitrogen would not be incorporated in the oligomers. The authors did not discuss this in their report.

The authors have proposed the following mechanisms. First, at low amine concentrations, the radical anion reacts with the growing polymer chain as described in Scheme 51. This prevents the initiator radical from reacting further, causing the inhibition.

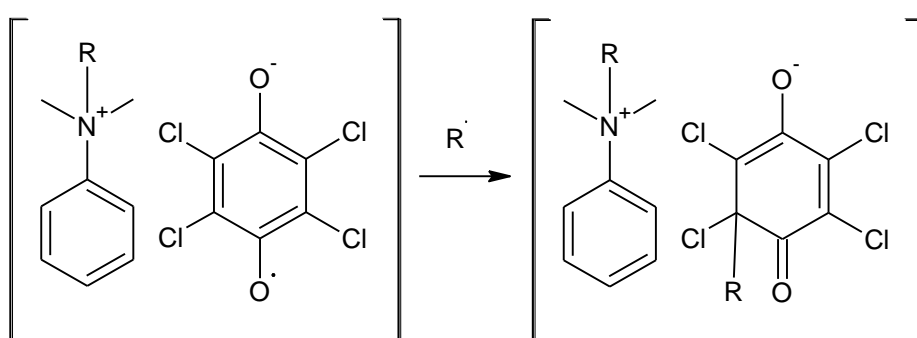


Scheme 51. The proposed mechanism for the inhibition of polymerisation, at low amine concentrations.

At higher amine concentrations, the radical reacts first with the amine, as shown in Scheme 52. The next step effectively removes a second polymerisation radical, as shown in Scheme 53.



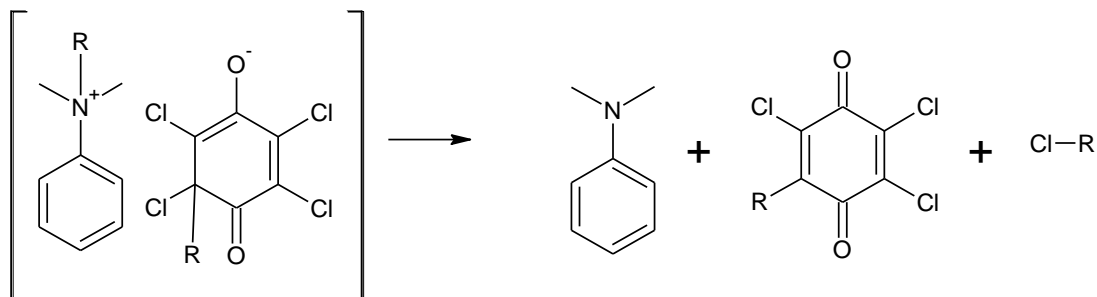
Scheme 52. The initial step in the inhibition of polymerisation at high amine concentrations.



Scheme 53. The second step of the inhibition mechanism.

The final step, shown in Scheme 54, shows the chain transfer from the ammonium ion to the anion of the complex. This demonstrates why increasing the amine concentration

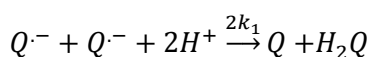
improves the inhibition properties of the complex, as well as why nitrogen is not incorporated into the short chain polymers.



Scheme 54 Chain transfer from ammonium ion to anion of the complex.

The authors do not state if they can observe chlorine incorporation in the isolated short chain polymers, which would help prove this as the mechanism. Understanding the stability of the semiquinone half of the charge transfer complex may help the understanding of the inhibition mechanism.

Generally in literature, the reported reaction of semiquinone under study is their decay, or disproportionation, into the parent quinone and hydroquinone, as described in Equation 6^{109, 110}.



Equation 6. The disproportionation of semiquinone radical to quinone and hydroquinone

Semiquinones readily react with oxygen¹¹¹, which often make them difficult to monitor outside of a biological system, where they can be shielded. There is literature available on semiquinones in aqueous and biological systems^{112, 113}, but very little in organic media.

5.1.2 Aims

The semiquinone has been suggested as the inhibiting species of the quinone-amine charge transfer complex. The overall aim of this chapter is to determine if the semiquinone can

realistically be the inhibiting species. The information about its stability and reactivity may lead to an optimised structure for a new and improved polymerisation inhibitor. Also, if a stable form of the semiquinone can be obtained, the possibility of using it directly as an inhibitor may also be investigated.

In order to determine the radical anion role in the inhibition mechanism, its stability will be assessed. The starting point for this is to observe the radical anion without the amine counter ion. This will require the synthesis of a stable sample of radical anion.

The semiquinone will participate in a comproportionation / disproportionation equilibrium. The thermodynamic parameters of this equilibrium will affect the concentration of semiquinone in solution¹¹⁴, so will need to be determined in order to understand the inhibiting species in Yassin and Rizk's charge transfer complex. Any other side reactions of the semiquinone will also need to be determined, with the view of placing these reactions in the context of polymerisation inhibition, if they take part or not, or if they hinder the inhibition by the semiquinone.

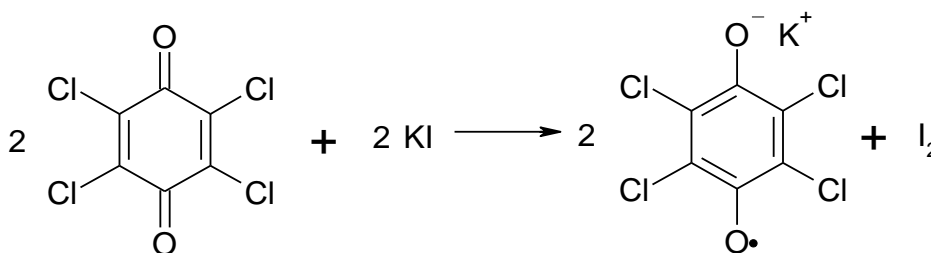
5.2 Chloranil Radical Anion Stability in aqueous solution

In order to study just the proposed chloranil radical anion component of the charge transfer complex proposed by Yassin and Rizk⁶¹, first a way of obtaining the radical without the use of an amine needs to be developed.

A common method of producing the semiquinone radical anions outside of a biological system is through pulse radiolysis¹⁰⁹. Again this comes with its own practical issues. When using the parent quinone to produce the semiquinone, the method is often limited by its solubility in aqueous media. Likewise, if using the parent hydroquinone, the limit is often with organic media. To overcome these issues, aqueous / organic mixtures are used to study semiquinone which will affect its observed stability when produced^{109, 110}.

However, in 1912, Torry and Hunter proposed a procedure to synthesise the potassium salt of the radical anion¹¹⁵ by reduction of the quinone with iodide which was successfully

reproduced for this study Purity and characterisation is in the Experimental (Page 209), and Scheme 55 depicts the reaction¹¹⁶⁻¹¹⁸. In the solid state, the radical anion salt appeared to be stable. i.e. the properties of chloranil radical anion salt appeared unchanged after storage for several months. However this could not be confirmed unambiguously due to reasons given below.



Scheme 55. Synthesis of chloranil radical anion potassium salt

The potassium salt of chloranil radical anion is not soluble in organic media. Therefore, its stability in water was studied first. Figure 82 shows that the EPR signal of the radical anion decays over time. This suggests that it is highly reactive or unstable. In order to establish the main decomposition pathways, the products of chloranil radical anion decay in water were analysed.

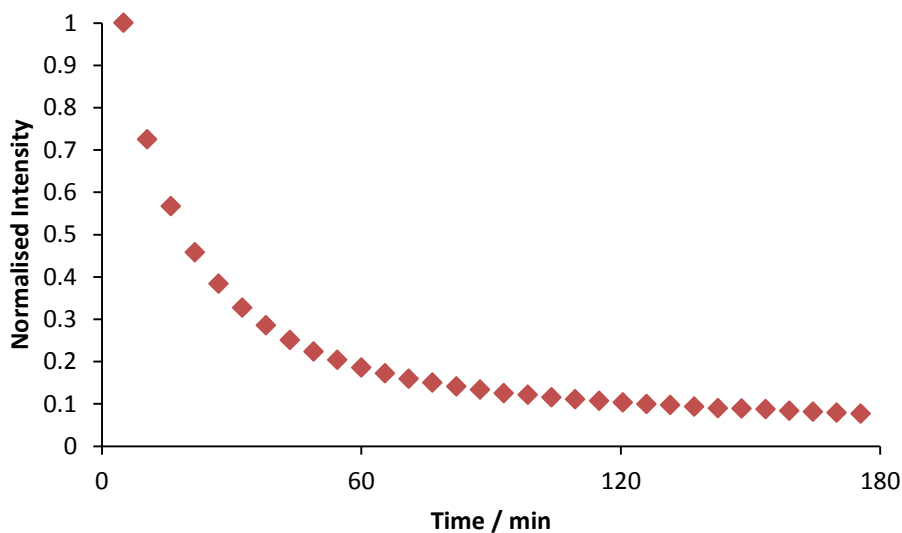


Figure 82. Rate of decomposition of chloranil radical anion potassium salt, as observed from the EPR intensity. The first spectrum was not taken at $t = 0$ minutes, as the equipment can only be tuned once the sample is prepared and in the equipment

5.2.1 Products from the decomposition of chloranil radical anion potassium salt.

A 100 ppm solution of chloranil radical anion potassium salt in water was left until no EPR signal was observable and was then subjected to negative ion ESI MS. A number of species were observed that gave distinct isotope patterns. These patterns could be assigned to chlorine containing compounds, and specifically the number of chlorine atoms in the compounds could be determined.

Figure 83 shows the ESI MS spectrum obtained, labelled with proposed structures given in Table 8. These structures are based on molecular formulas obtained by fitting the experimental isotope patterns to the calculated ones and are the likely products formed. As an example, the isotope pattern for the product at m/z 224 (peak A) is shown in Figure 84 in blue, with a calculated isotope pattern for comparison in red.

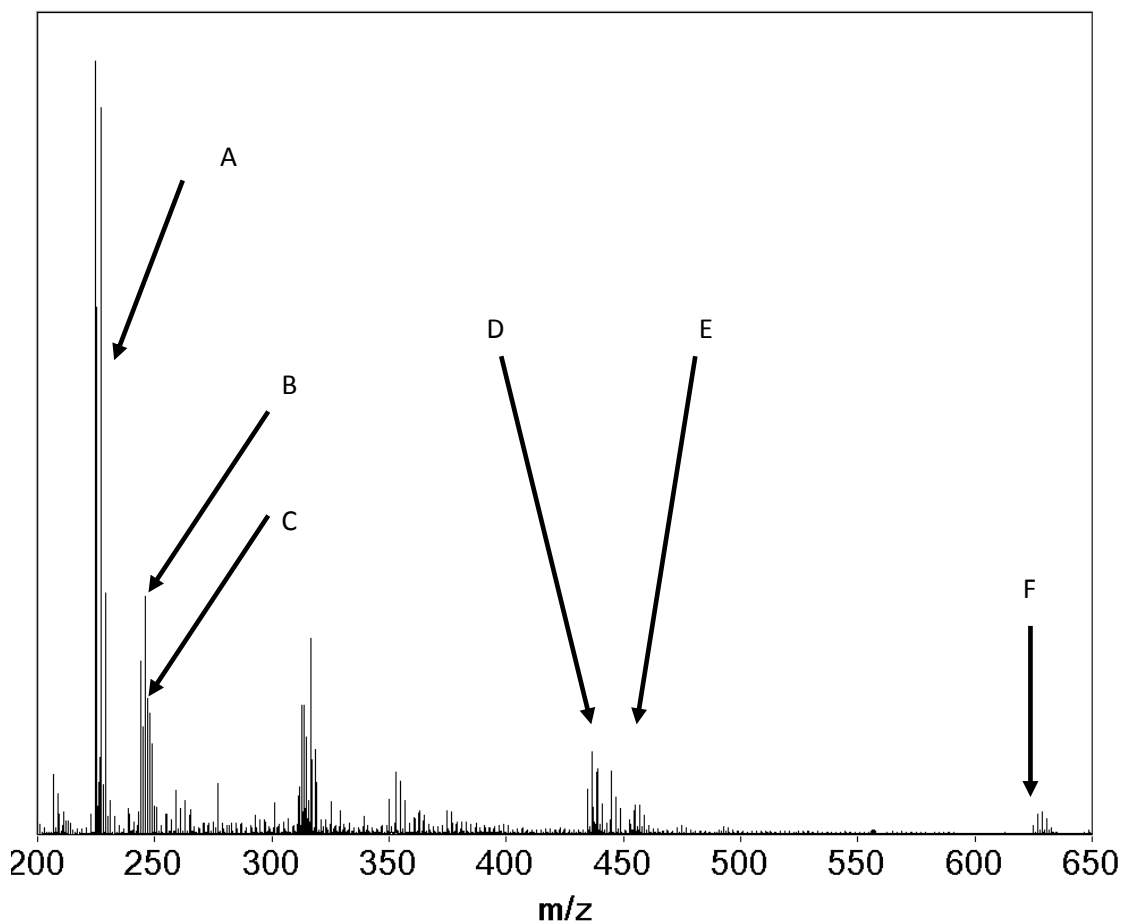


Figure 83 Negative ion ESI mass spectra of the decay products for chloranil radical anion in water, open to air at room temperature.

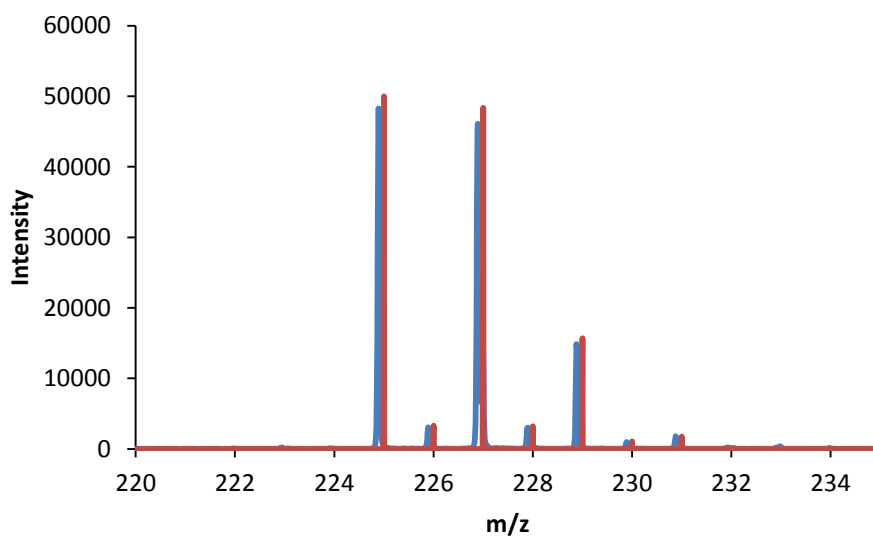
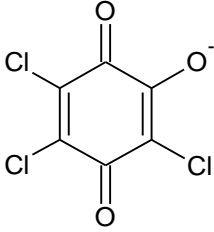
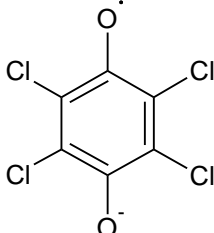
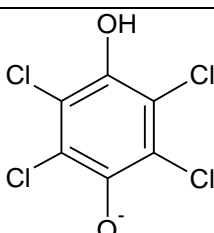
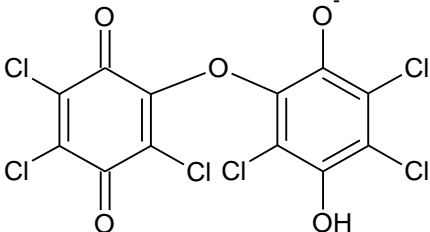
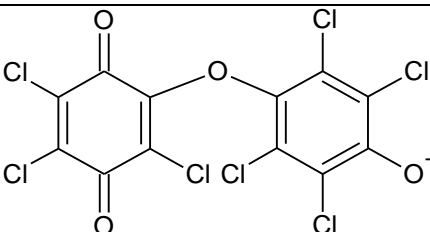
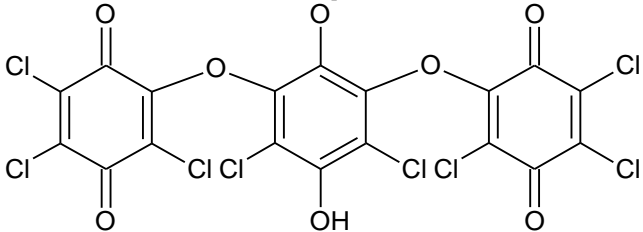
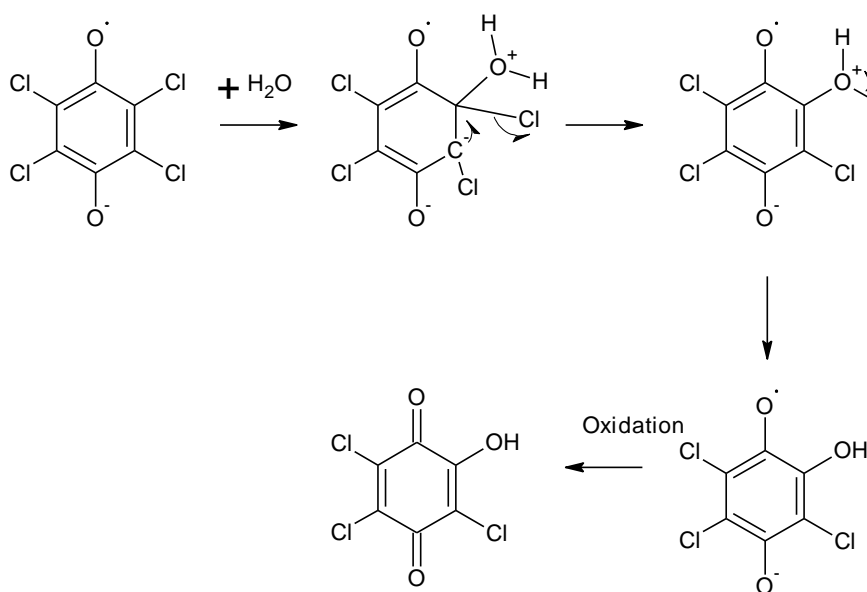


Figure 84. Magnification of isotope pattern for peak A in blue, with the calculated isotope pattern in red.

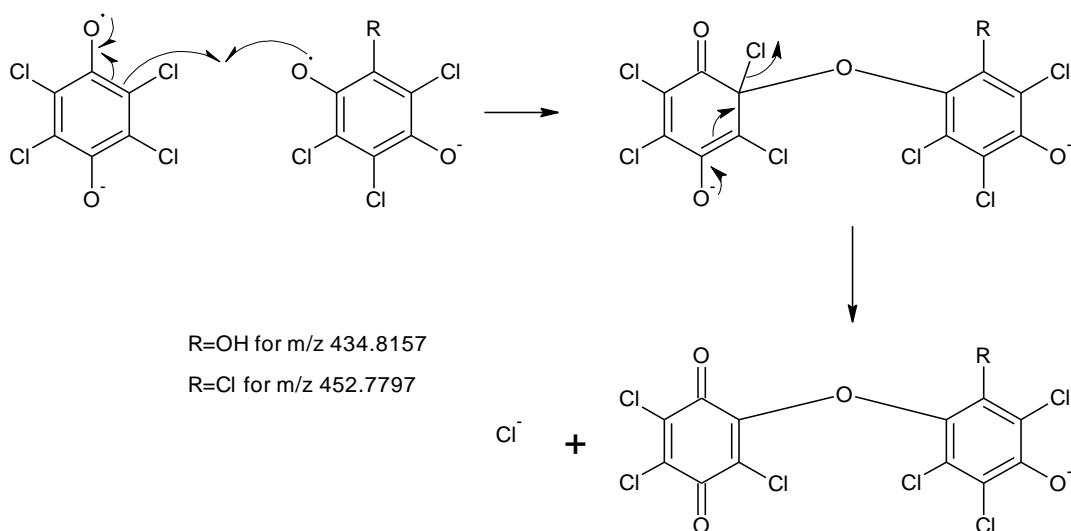
Table 8. Possible structures of products from the decomposition of chloranil radical anion potassium salt in water. The MS peaks correspond to $[M+H]^+$ ions of the proposed structures.

Label	m/z	Structure
A	224.89	
B	243.86	
C	244.87	
D	434.82	
E	452.78	
F	624.76	

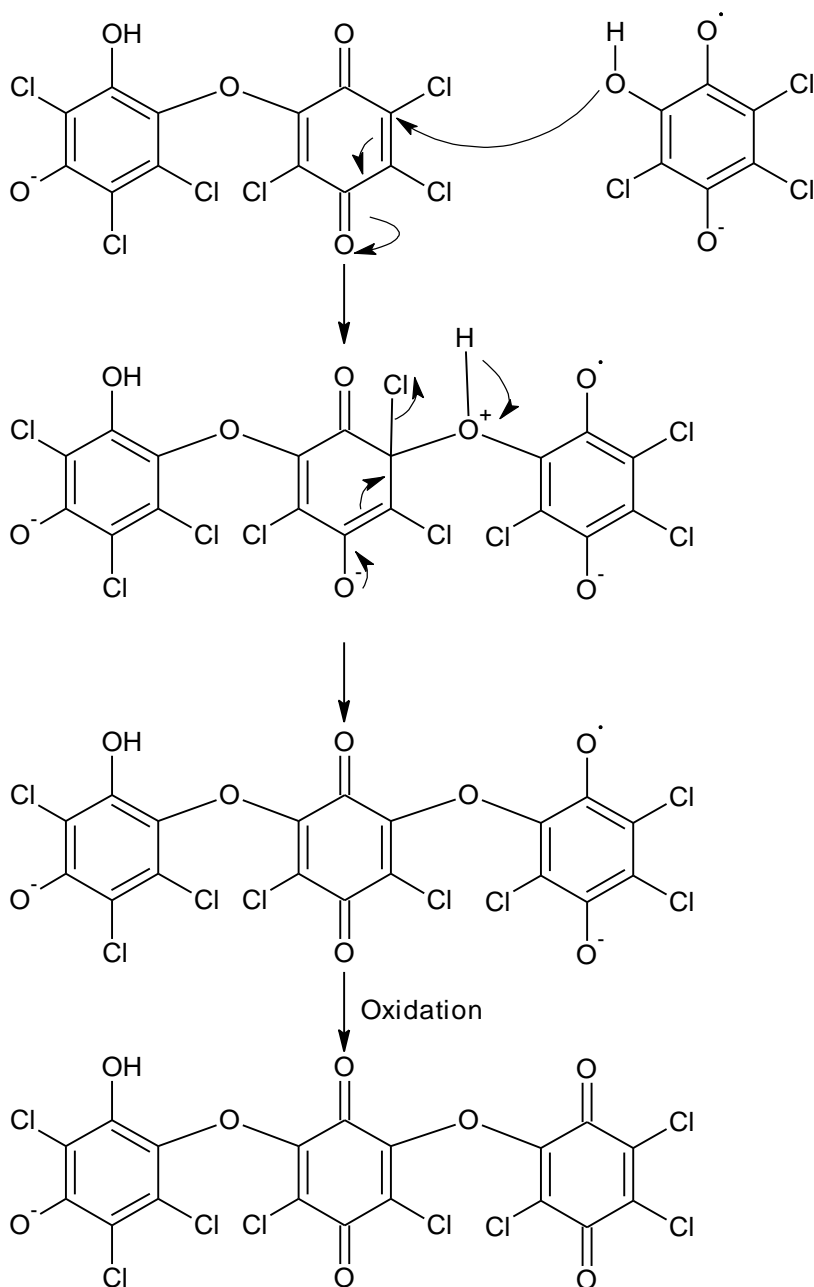
The products appear to be from the nucleophilic substitution of chlorine, or the formation of dimers and trimers of radical anions. Even at this low concentration the radical anion is unstable, reacting with the solvent or another radical anion molecule. Increasing the concentration would likely lead to higher concentrations of dimers and trimers forming. The mechanisms presented below are a selection of possible routes that the radical anion would go through to reach the products observed.



Scheme 56. Formation of mono-hydroxy substituted chloranil



Scheme 57. Formation of radical anion dimers at peaks m/z 434.82 and m/z 452.78



Scheme 58. Formation of a radical anion trimer at peak m/z 624.76

Most observed products are diamagnetic. The above mechanisms show the possible routes for their formation from paramagnetic species. Scheme 56 demonstrates nucleophilic attack forming a mono-substituted semiquinone. However, the observed product is diamagnetic, not the semiquinone. The conversion to a diamagnetic species could occur through oxidation by oxygen or through chemical exchange with another radical. This part of the mechanism appears important as it is needed to explain the observed products in Scheme 58 as well.

Scheme 57 displays the recombination of two radical species. This will be more prevalent at higher concentrations, as this will increase the probability of two radicals reacting. This route removes two radicals per reaction.

Again, in Scheme 58 a radical is produced from the nucleophilic attack, as in Scheme 56, and requires an additional oxidation step to explain the observed product. Oxidation by oxygen can be controlled, but electron transfer or disproportionation is far more difficult to restrict¹¹⁴. Therefore removing oxygen is the best next step to understand the formation of diamagnetic products.

5.2.2 Chloranil radical anion potassium salt under nitrogen

As shown by the postulated mechanisms, oxygen may be required to obtain the observed products in the mass spectrum. Therefore by removing oxygen and maintaining a nitrogen atmosphere, the rate of decay may be reduced, or a different set of products may form.

By working under inert atmosphere and purging all solutions before use, the effect of oxygen was investigated. The result is given in Figure 85.

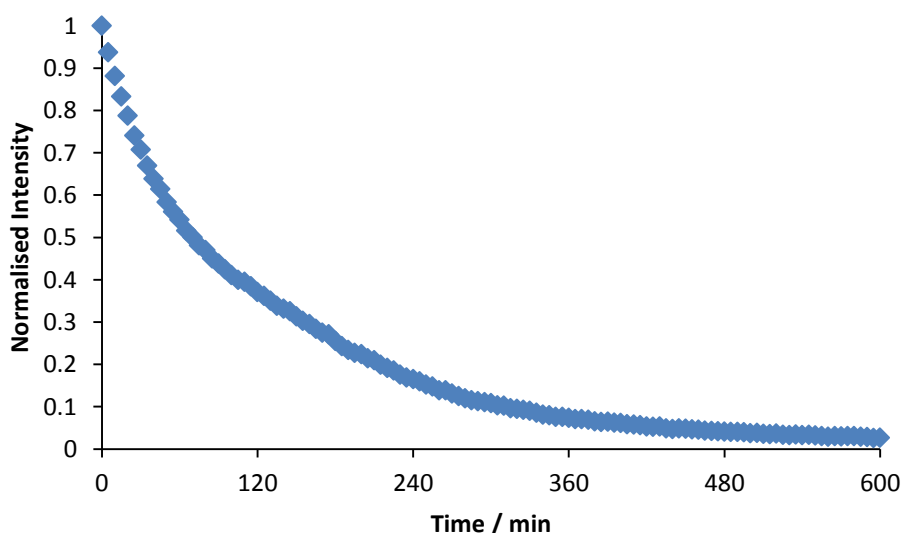


Figure 85 Decay of chloranil radical anion in water under nitrogen environment, as observed from the EPR intensity

The comparison between experiments with and without oxygen in Figure 86 shows that the rate of decay is slower without oxygen. This adds support to the mechanisms suggested in section 5.2.1 (Page 169). However, the radical anion decayed even in the absence of oxygen. This suggests that the radical anion is not only reacting with itself through nucleophilic substitution, but is also involved in intermolecular electron transfer and/or recombination reactions. This means it is very unstable, and unlikely to survive long in any solvent, polar or non-polar, even under inert conditions.

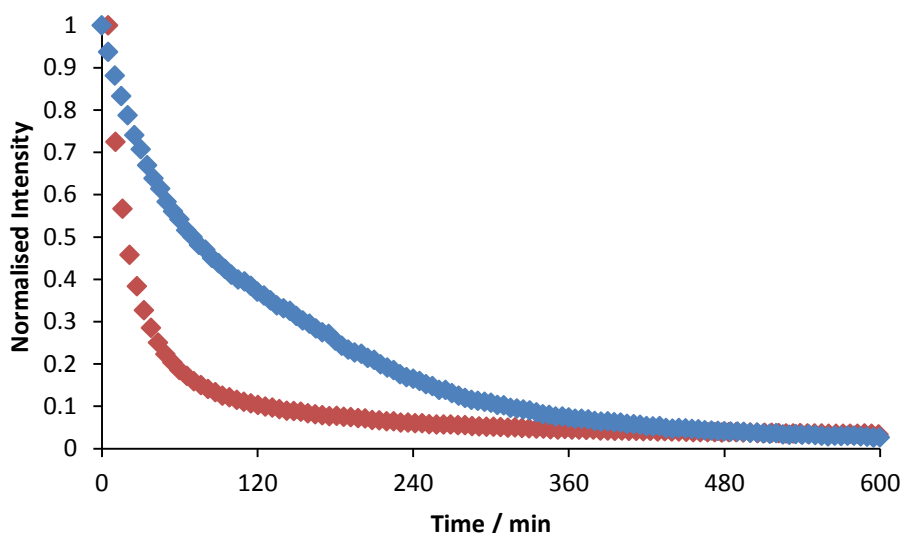


Figure 86. Comparison of the rates of decay under nitrogen (Blue) and open to air (Red).

The decay of the chloranil radical anion potassium salt has also demonstrated the lack of stability in aqueous media through another observation; variability in the rate of decay. This irreproducibility has been a problem that prevented the above results from supplying accurate numbers to the rates of decay.

5.2.3 Lack of reproducibility

All above experiments showed variable rates of decay of the chloranil radical anion salt. Figure 87 shows that the initial EPR signal observed was inconsistent for samples prepared at the same concentration. After normalising the data in Figure 88, the rate of decay also has some variability. It was originally believed to be due to a large error in measuring absolute radical concentrations by EPR.

EPR measurements of aqueous samples can only be done using small sample volumes in small capillaries or flat cells. The samples were thus prepared in narrow tubes, and maintaining the position of the tube inside the EPR cavity would be critical for obtaining accurate and consistent results. The use of a PTFE grooved pedestal to rest the end of the tube ensured the tube was in the same position every time. Control experiments showed that intensity of EPR spectra using a PTFE pedestal is within 20 % of each other. The results in Figure 87 and Figure 88 contain these results. The use of the pedestal resulted in the same amount of scatter thus ruling out the position of the sample in the cavity as the cause of the irreproducibility.

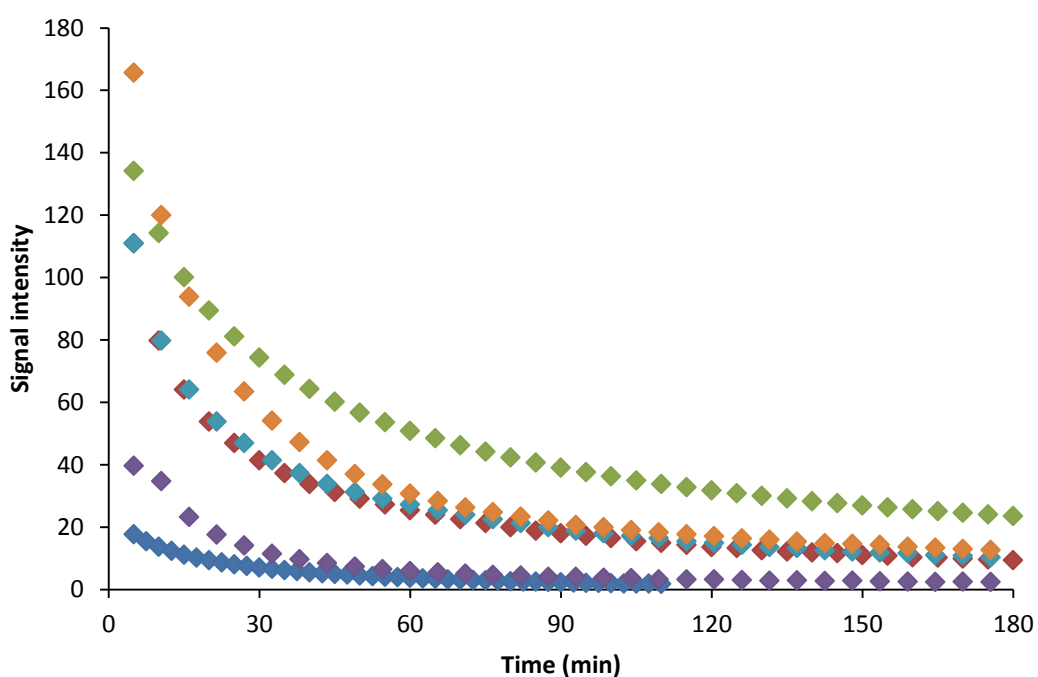


Figure 87. EPR signal decay for chloranil radical anion in deionised water.

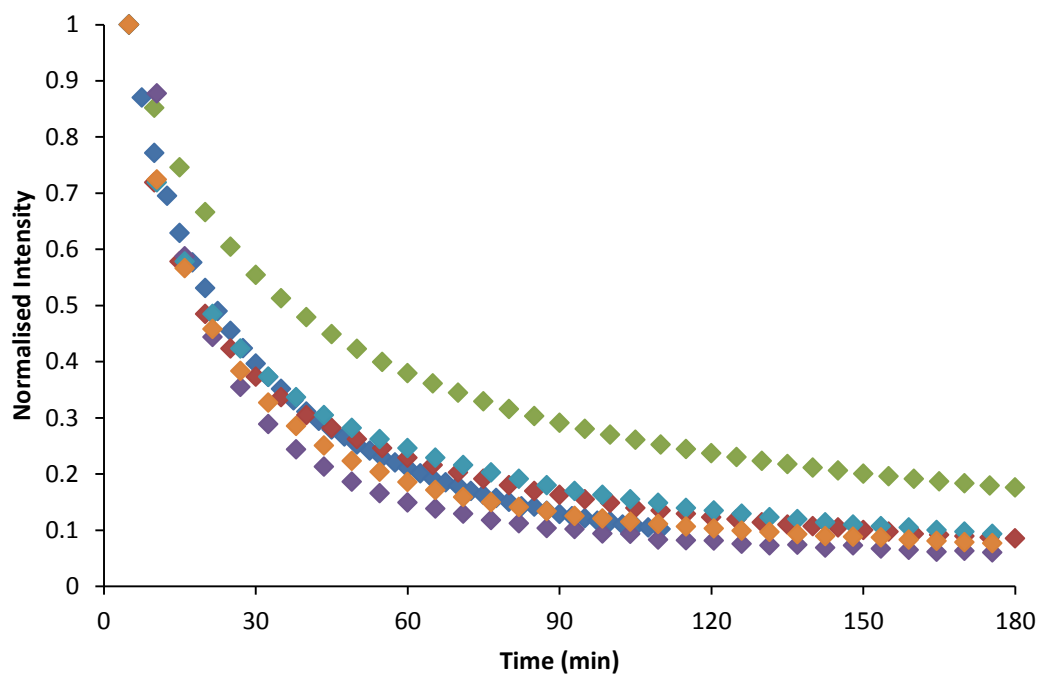


Figure 88. Normalised EPR signal intensities for samples of batch 3 radical anion (100ppm) in water

Another reason for the variable rate of decomposition was the possibility of a variable concentration of oxygen in the water. Different concentrations of dissolved oxygen may lead to differing rates of decay. However the results from deoxygenated samples shown in Figure 89, and again normalised in Figure 90, demonstrated a similar scatter of starting concentrations and rates of decay.

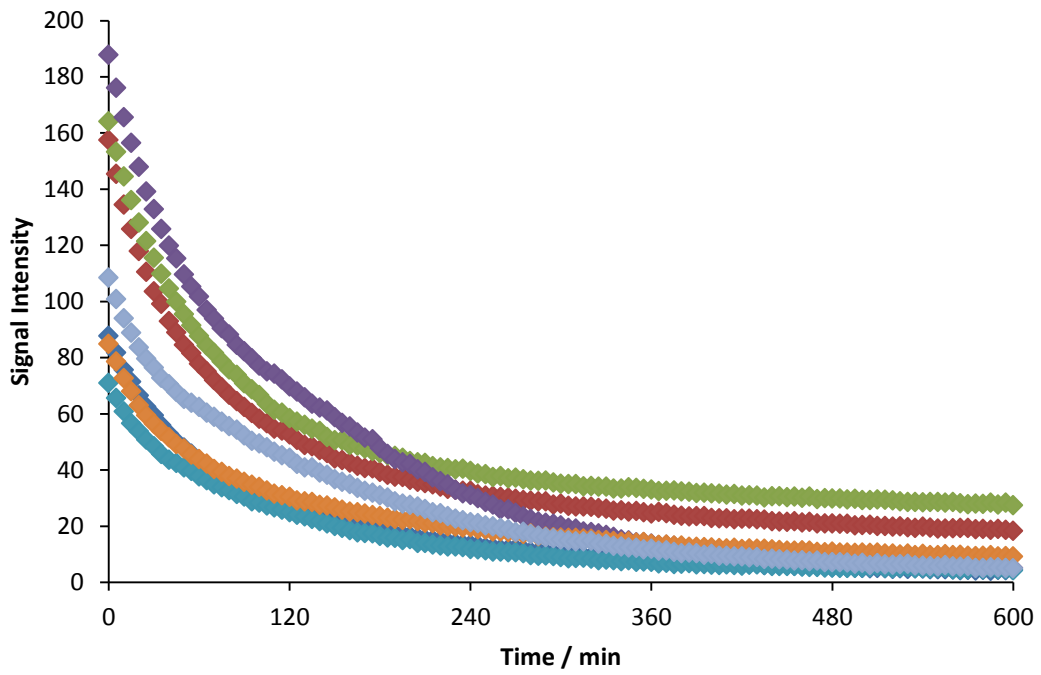


Figure 89. Decay of chloranil radical anion in water under nitrogen environment

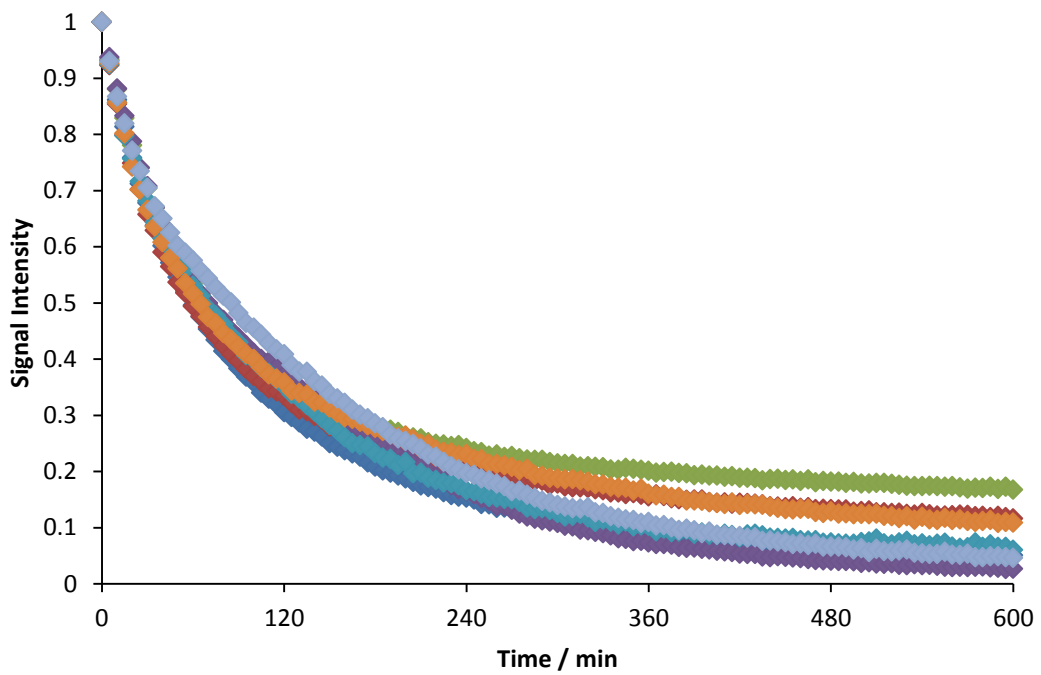


Figure 90. Normalised EPR signal intensities for samples of batch 3 radical anion (100 ppm) in water

Earlier in the chapter, (Section 5.2.2, Page 174) the rates of decay open to air and under nitrogen were discussed, but from these results, an accurate rate of decay cannot be determined due to poor reproducibility. However by comparing the normalised rate from several sets of both these experiments in Figure 91, a relative difference can be observed, showing the radical anion decays slower when oxygen is excluded as concluded in Section 1.2.2.

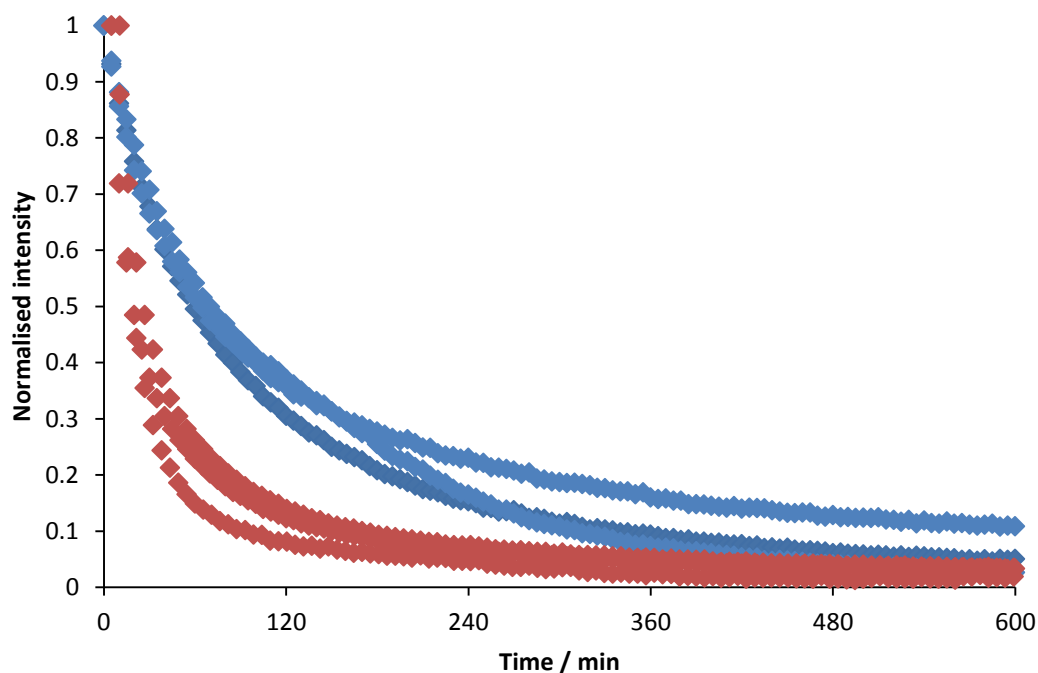


Figure 91. Comparison of the rates of decay under nitrogen (Blue) and open to air (Red).

The poor reproducibility of the decay curves for the same batch of chloranil radical anion thus cannot be explained by EPR errors or differences in oxygen concentrations. One possible explanation is related to the sample preparation. As the solid chloranil radical anion potassium salt dissolves during sample preparation, it is likely to produce localised high concentrations of dissolved chloranil radical anion. As many proposed reactions of chloranil radical anion are 2nd order processes, these high concentrations will result in very fast rates of decay within the pools with localised high concentration. As the solid chloranil radical anion potassium salt produced varied in particle size, this would account for the different initial EPR signals. Large particles would produce less of these high concentration areas, whereas lots of small particles could produce either many high concentration areas, or produce localised areas of every high concentration in comparison.

This theory was not investigated further, as maintaining a consistent rate of dissolution is a challenging task which goes beyond the scope of this thesis.

5.2.4 Conclusions

It is difficult to make solid conclusions from the above work due to the lack of reproducibility in results. The fact that rates of chloranil radical anion decay are not reproducible suggests that it is unstable in water. Its stability is unknown in organic media due to the lack of solubility of the salt in those solvents. The lack of reproducibility could be due to high localised concentrations of the radical anion temporarily formed during its dissolution in water. The poor stability of the radical anion leads to a mixture of nucleophilic substitutions, oxidations and disproportionations.

In terms of polymerisation inhibition, lack of solubility in organic solvents limits which monomers it can protect. However, it is unlikely to be used in its potassium salt form.

It has been shown that the rate of decay in water is slower without oxygen but still significant. From this observation and the products observed, it can be suggested that the main route of decay is from the radical anion reacting with itself. This does not bode well for the radical anion being used as a polymerisation inhibitor. Compounds used as storage inhibitors need to survive for a long time to be of any use at protecting the monomer from polymerising

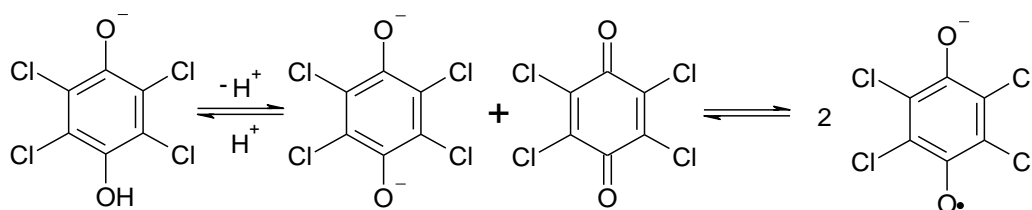
The initial EPR signal obtained from the chloranil radical anion potassium salt dissolved in water never depicted the expected concentration of radicals in solution. The maximum concentration of radical observed was 70% of the salt dissolved, with the average around 50%. This suggests that the radical anion immediately decays or reacts into non radical components. One possibility is that the radical anion disproportionates to give chloranil and tetrachloro hydroquinone dianion. This in turn would establish a comproportionation / disproportionation equilibrium, and understanding the position the equilibrium lies may offer some explanation for the observed discrepancy.

5.3 Comproportionation / disproportionation equilibrium

It has been observed that the chloranil radical anion is unstable. Semiquinones are an important molecule in biology^{112, 113, 119, 120}, and there have been numerous studies on their activity and stability. However, these focused on their stability in aqueous buffered solutions, to simulate a biological environment. The main conclusion that can be drawn though is that they disproportionate quickly. Wong et al¹²¹, plus others^{109, 110, 121} efficiently demonstrate that the products from the decay of the semiquinone is the related hydroquinone and quinone. This could be the route the decay observed above actually follows; at high concentrations of chloranil radical anion it disproportionates.

Roginsky et al¹¹⁰ took advantage of the comproportionation to form semiquinones from their related benzoquinone and hydroquinone, and effectively determined both the directions of the comproportionation / disproportionation equilibrium. By using this method we may also be able to observe the comproportionation / disproportionation equilibrium in organic media to establish the stability of the chloranil radical anion in these environments. Understanding this equilibrium in organic media is essential for predicting if the chloranil radical anion can actually exist in the inhibition system proposed by Yassin and Rizk⁶¹.

Preparing mixtures of chloranil and tetrachloro hydroquinone in different solvents will allow the study of the radical anion in different environments, including organic media. The system prepared is given in Scheme 59^{110, 122}.



Scheme 59. Comproportionation / disproportionation between chloranil and tetrachloro hydroquinone.

However, upon observing the different solutions by EPR, this method appears far more complicated than previously thought. In Figure 92, solutions of 100ppm of tetrachloro

hydroquinone in ethanol under nitrogen still display the formation of a radical. About 1% of the hydroquinone is oxidised, presumably by the residual oxygen. By forming the dianion by adding sodium hydroxide, the concentration observed increases to 10% of the hydroquinone oxidised. It appears that these solutions are extremely sensitive to oxidation which leads to the formation of the radical.

The solutions remained stable once prepared, but obtaining a sample of tetrachloro hydroquinone which did not show an EPR signal was not possible. A number of methods of removing oxygen were used, such as freeze/pump/thaw techniques as well as simple purging of containers. It is clear that tetrachloro hydroquinone is reactive under these conditions, even more so in alkaline media. It was deemed inconsequential to improve on technique, if that is possible, and the decision was made to try a less sensitive quinone / hydroquinone mixture.

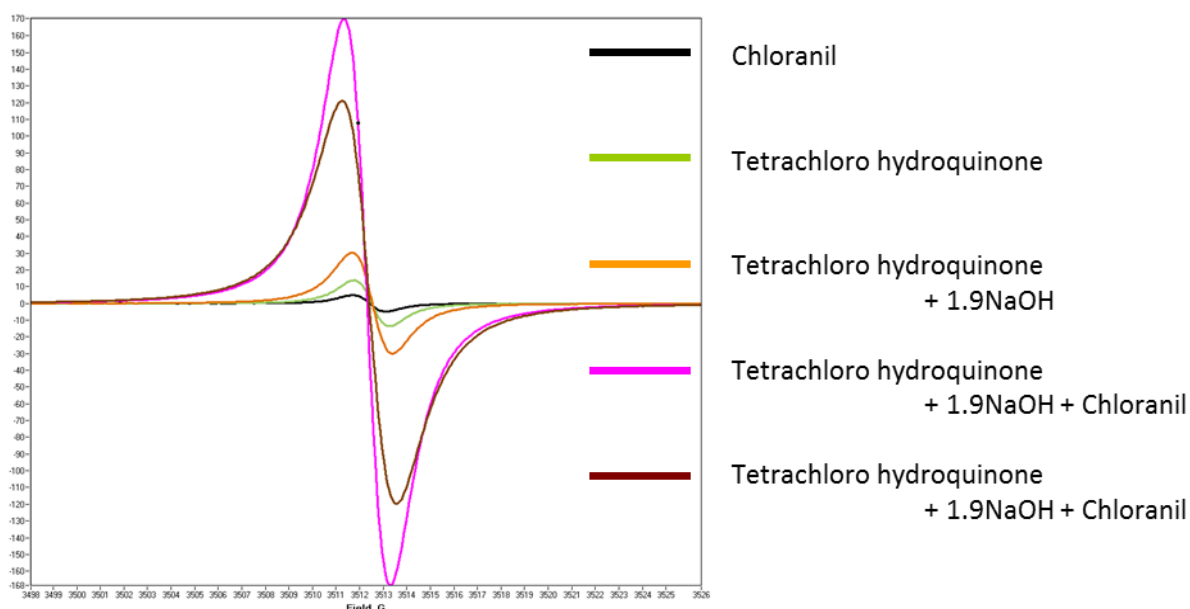


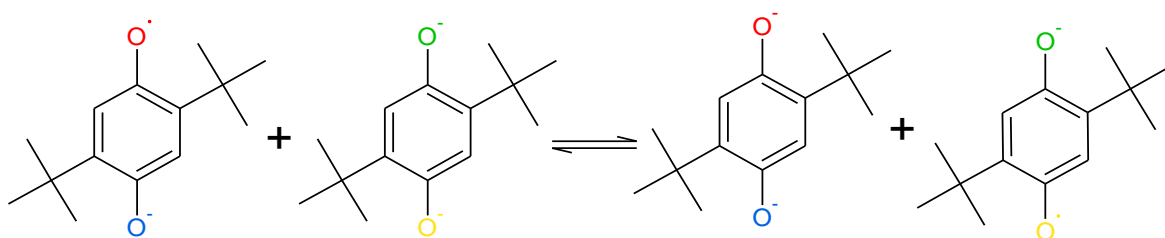
Figure 92. EPR spectra for the formation of the chloranil radical anion from tetrachloro hydroquinone, sodium hydroxide and chloranil, and combinations thereof

The use of a different quinone/hydroquinone mixture may yield information on radical anions in general. Therefore 2,5 – di-tert-butyl hydroquinone and 2,5 – di-tert-butylquinone were selected as alternatives. Chloranil and its radical anion have been seen to be susceptible to nucleophilic substitutions, and so the new hydroquinone and quinone were chosen to try to block and avoid this scenario.

5.3.1 Chemical exchange of 2,5 – di-tert-butyl semiquinone in concentrated solutions of 2,5 – di-tert-butyl hydroquinone

Before comproportionation/disproportionation equilibrium of di-tert-butyl semiquinone can be studied by EPR, the extent of the line broadening from chemical exchange needs to be observed so that any further measurements of an unknown concentration can be relied upon to be accurate and not obscured in anyway due to other, unrelated effects. Chemical exchange is a phenomenon that will affect the broadening of an EPR signal. The exchange occurs when a semiquinone collides with a quinone dianion. An electron can hop from one to the other, as depicted in Scheme 60, increasing the rate of relaxation of the electron spin in the magnetic field. This increase in the relaxation appears as line broadening.

If the broadening is too extreme, signals may disappear altogether. This effect is more prevalent at higher concentrations, due to the increase in intermolecular interactions. To try to observe the possibility of chemical exchange, high concentrations of hydroquinone were prepared and the radical anion resulting from the unavoidable oxidation was observed. Figure 93 shows EPR spectra resulting from these high concentration solutions, with the signal intensity normalised. There is slight broadening of the line width, due to the interactions between the radical anion and the hydroquinone, but not enough to determine the rate of electron transfer.



Scheme 60. Chemical exchange of 2,5 – di-tert-butyl semiquinone with 2,5 – di-tert-butyl hydroquinone dianion.

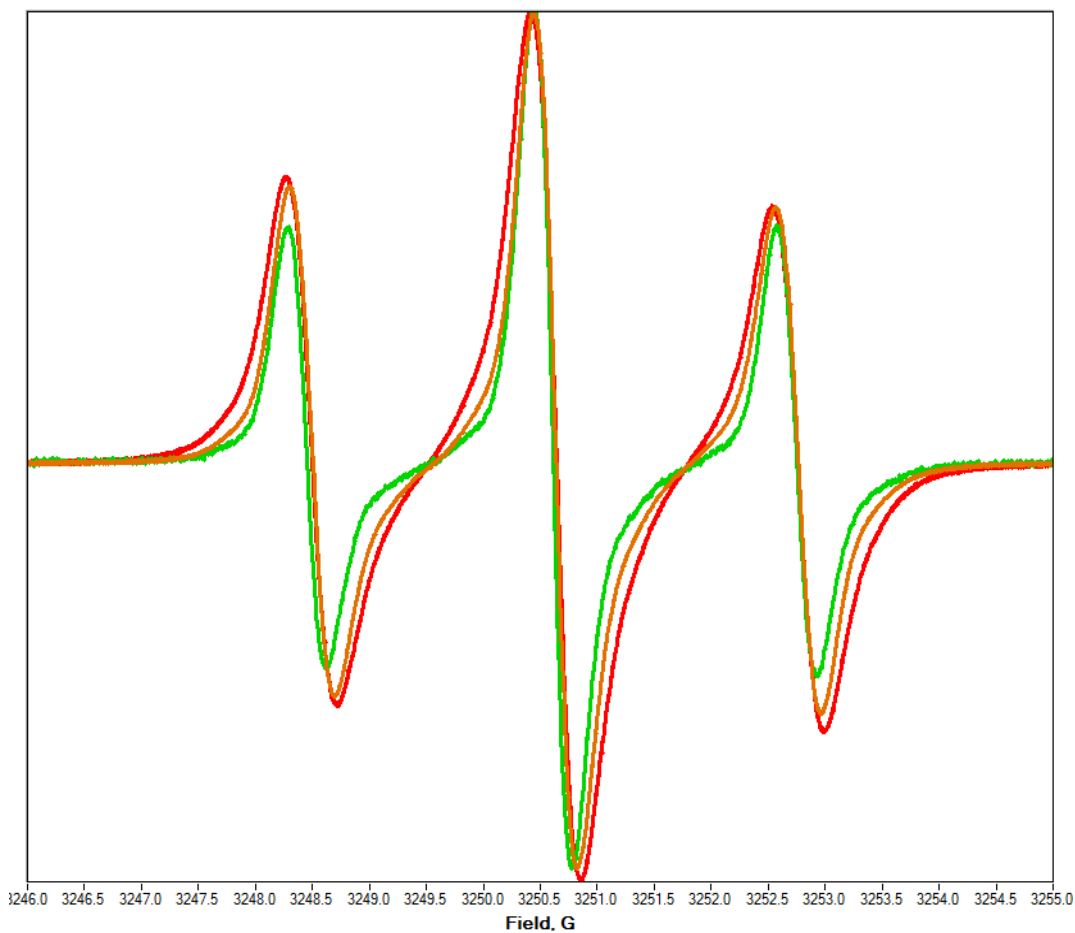


Figure 93. EPR spectra of di-tert-butyl hydroquinone in ethanol at different concentrations, spectra normalised (1mM - Green, 10mM – Blue and 1M - Red)

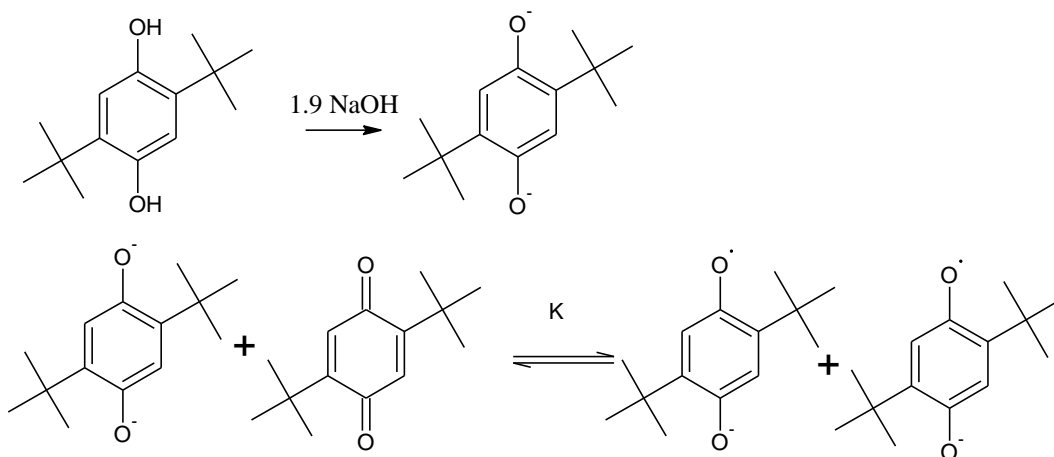
As the concentration has to be taken to extremes to observe chemical exchange in action, i.e. saturated solutions of hydroquinone in ethanol were used, then the effect of chemical exchange at lower concentrations of hydroquinone will not be observable, and the measurements of the semiquinone concentration by EPR will be accurate. Also, as the difference between concentrations of the semiquinone and dianion will be relatively small compared to the differences in the samples in Figure 93, the effect of chemical exchange will be negligible.

5.3.2 Equilibrium constants of the comproportionation / disproportionation equilibrium of 2,5 – di-tert-butyl hydroquinone and 2,5 – di-tert-butylquinone in polar media

To determine the equilibrium constant of the comproportionation / disproportionation equilibrium of 2,5 – di-tert-butyl hydroquinone and 2,5 – di-tert-butylquinone, the concentration of semiquinone can be measured by EPR for different concentrations of quinone and hydroquinone. Due to the method used, it is not possible to perform the experiment in non-polar solvents relevant to polymerisation inhibition, such as styrene or toluene, as the dianion formed after deprotonation of the hydroquinone would not be soluble. Therefore, initially the equilibrium was studied in ethanol.

Scheme 61 below demonstrates the process. First the hydroquinone is deprotonated with 1.9 equivalents sodium hydroxide dissolved in ethanol. The first and second pKa's of 2,5 – di-tert-butyl hydroquinone are 10.5 and 12.2 respectively. 2 equivalents of sodium hydroxide should therefore completely deprotonate the hydroquinone. However, it is unknown if using excess sodium hydroxide will result in side reactions. Therefore, to avoid unwanted reactions, 1.9 equivalents were used.

After the solution of deprotonated hydroquinone is prepared, it is mixed with different equivalents of quinone. This will shift the equilibrium, giving different concentrations of the semiquinone radical. This can then be entered into the equation for the equilibrium to give the equilibrium constant.



Scheme 61. The comproportionation / disproportionation equilibrium of 2,5 – di-tert-butyl hydroquinone and 2,5 – di-tert-butylquinone

Equation 7, gives the equilibrium equation. The concentrations of the quinone and hydroquinone after the equilibrium is established cannot be determined. Therefore by using the relationship between the starting concentrations and the radical anion shown in Equation 8, the bottom of Equation 7 can be substituted for values that can be obtained.

$$K = \frac{[SQ]^2}{[Q][HQ]}$$

Equation 7. The rate equation for the equilibrium ([SQ], [Q] and [HQ] are concentrations of semiquinone, quinone and hydroquinone.)

$$[Q]_0 + [HQ]_0 = [Q] + [HQ] + [SQ]$$

$$[Q] = [Q]_0 - \frac{1}{2}[SQ]$$

$$[HQ] = [HQ]_0 - \frac{1}{2}[SQ]$$

Equation 8. The relationship between initial starting concentrations and the concentration of components once equilibrium is established.

Combining Equation 7 and Equation 8 now gives an equilibrium equation where all values but K are known at different amounts. By taking Equation 9, expanding it and simplifying it a quadratic equation can be obtained and solved. Equation 10 demonstrates how the values for a, b and c were obtained from.

$$K = \frac{[SQ]^2}{([Q]_0 - \frac{1}{2}[SQ])([HQ]_0 - \frac{1}{2}[SQ])}$$

Equation 9. Combination of Equation 7 and Equation 8

$$[SQ]^2 - \frac{K}{4}[SQ]^2 + \frac{1}{2}K[SQ][Q]_0 + \frac{1}{2}K[SQ][HQ]_0 - K[Q]_0[HQ]_0 = 0$$

$$\left(1 - \frac{K}{4}\right)[SQ]^2 + \left(\frac{1}{2}K[Q]_0 + \frac{1}{2}K[HQ]_0\right)[SQ] - K[Q]_0[HQ]_0 = 0$$

$$a = 1 - \frac{K}{4} \quad b = \frac{1}{2}K[Q]_0 + \frac{1}{2}K[HQ]_0 \quad c = -K[Q]_0[HQ]_0$$

Equation 10. The rate equation for the equilibrium expanded, then arranged in way that can be solved, and the coefficients a, b and c used to solve the quadratic equation

To determine K, the values obtained from the experimental are added to the quadratic equation and using a spread sheet program, the theoretical values for semiquinone radical concentration can be obtained. By comparing the differences between experimental and theoretical values, a value for K giving the smallest difference can be determined by minimising the sum of squares of the differences with the Solver plugin in Excel.

The radical concentration was measured at four temperatures at a number of different quinone / hydroquinone ratios. The following charts give the data of the best three runs completed. The data points represent the measured radical concentration whereas the line displays the calculated radical concentrations from the calculations above. The matches between observed and calculated are not perfect, but observing the radicals accurately was difficult. The radicals are extremely sensitive to oxygen.

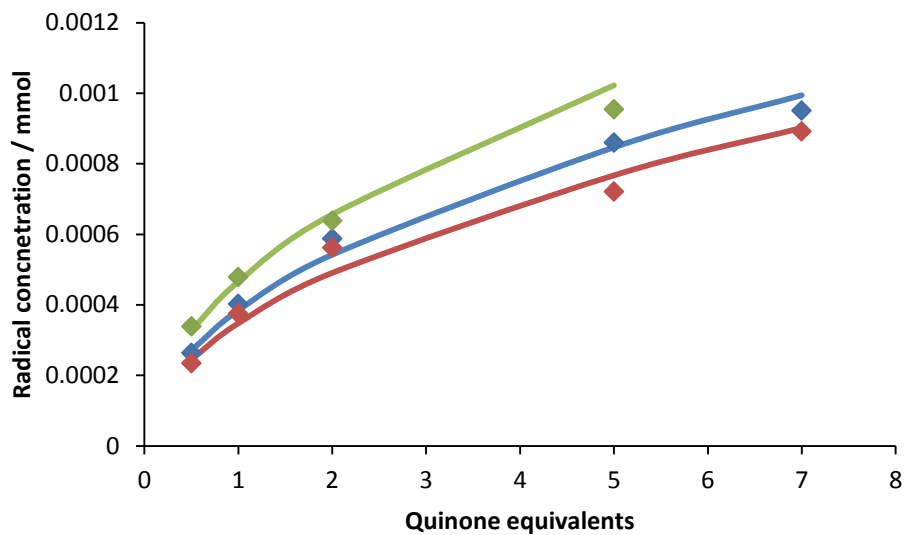


Figure 94. The results of three runs for the comproportionation / disproportionation equilibrium at varying molar equivalents of quinone at -30°C

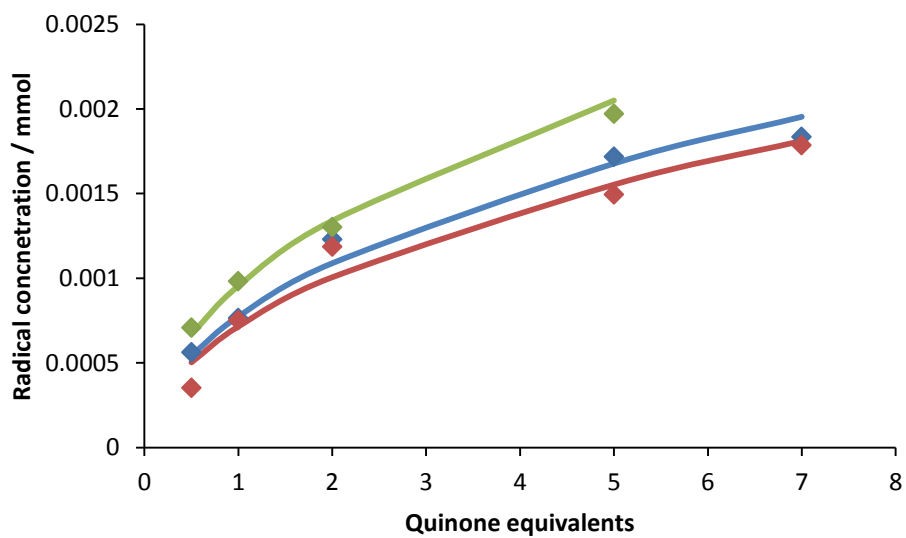


Figure 95. The results of three runs for the comproportionation / disproportionation equilibrium at varying molar equivalents of quinone at 0°C

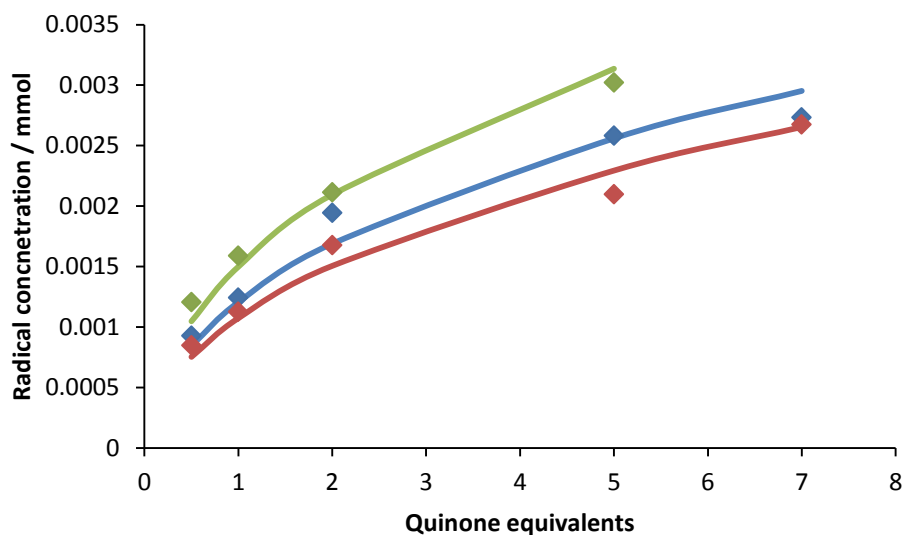


Figure 96. The results of three runs for the comproportionation / disproportionation equilibrium at varying molar equivalents of quinone at 30°C

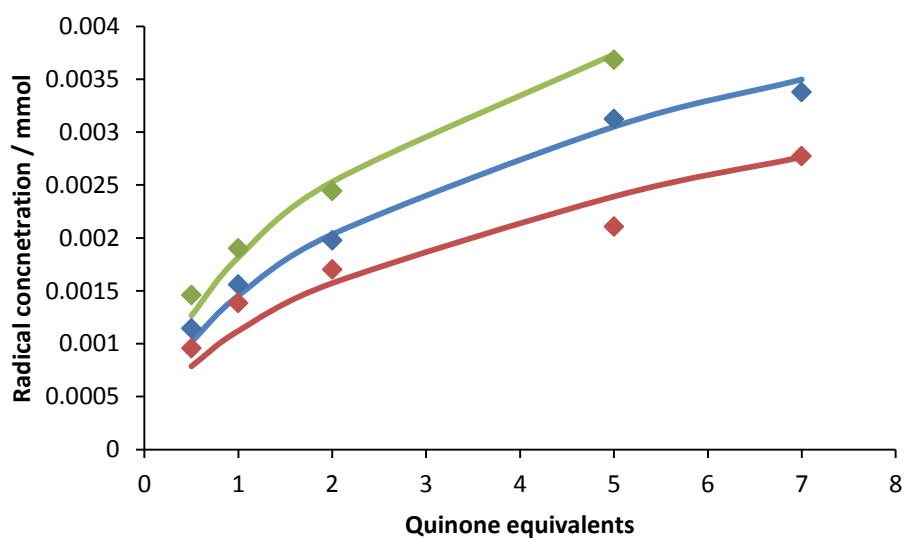


Figure 97. The results of three runs for the comproportionation / disproportionation equilibrium at varying molar equivalents of quinone at 60°C

The equilibrium constants obtained at different temperatures are given in table 2. By using the Arrhenius equation shown in Equation 11, the enthalpy and entropy of reaction can be determined by plotting $\ln K$ against $1/T$. The results are given in Table 9.

$$\ln K = -\frac{\Delta H}{RT} + \frac{\Delta S}{R}$$

Equation 11. The Eyring equation

Temperature (K)	243	273	303	333	ΔH^0 (J mol ⁻¹)	ΔS (J K ⁻¹ mol ⁻¹)
K	7.56E-03	3.16E-02	9.98E-02	1.48E-01	332	0.78

Table 9. Equilibrium constants, enthalpy and entropy for the comproportionation / disproportionation equilibrium in ethanol

The small positive entropy obtained is consistent with the comproportionation / disproportionation equilibrium, as both sides have two species, leading to low change in disorder. The equilibrium constants show that at low temperatures, the radical components are extremely unfavourable, e.g., the equilibrium concentration of radical anion is low. Increasing the temperature shifts the equilibrium to the radicals but would still result in the majority of any radical anion formed disproportionating.

Therefore the comproportionation/disproportionation equilibrium of the radical anion is not susceptible to temperature and its decomposition is more dependent on other factors such as nucleophilic attack from itself or from the solvent.

Roginsky et al¹¹⁰ studied a similar system to the above. They however used 2-terbutyl hydroquinone without deprotonating it first, so their results incorporate the deprotonation of the hydroquinone as well as the comproportionation/disproportionation equilibrium. They also studied the system in a buffer maintained at pH 7.4. In order to compare their results to the above, the amount of deprotonated hydroquinone in Roginsky's work needs to be calculated. This in turn requires more information.

The pK_a of 2,5-ditertbutyl hydroquinone is 10.5. Rearranging Equation 12 and using this value gives the dissociation constant to be 3 x 10⁻¹¹. The dissociation relationship is given in Equation 13. For clarity, HA represents the hydroquinone (i.e. the acid in question) and A⁻ the anion after deprotonation.

$$pK_a = -\log_{10} K_a$$

Equation 12. Relationship between pK_a and K_a

$$K_a = \frac{[A^-][H^+]}{[HA]}$$

Equation 13. Determination of the acid dissociation constant, K_a .

The concentration of the hydroquinone in solution cannot be easily determined, so by using the known amount of hydroquinone ($[HA]_0$) and the amount of deprotonated hydroquinone (the unknown we wish to calculate) this variable can be removed by using Equation 14 in Equation 13, resulting in Equation 15.

$$[HA] = [HA]_0 - [A^-]$$

Equation 14. Relationship between starting concentration of the acid ($[HA]_0$) and the concentration of the acid and the conjugate base in the system.

$$K_a = \frac{[A^-][H^+]}{[HA]_0 - [A^-]}$$

Equation 15. Combining Equation 13 and Equation 14

The final unknown is the concentration of protons in solution. Using Equation 16 with the fact the pH is controlled by a buffer at pH 7.4, the concentration of protons can be determined as 4×10^{-8} M.

$$pH = -\log_{10}[H^+]$$

Equation 16. Determination of pH

Combining these numbers into Equation 15, the relationship between $[HA]_0$ and $[A^-]$ can be determined. At pH 7.4, only 0.075 % of the hydroquinone is deprotonated. By taking the two dissociation equations and following Equation 17 parts A through C, the differences between the literature equilibrium constants and ones obtained can be determined as a factor 1333. This converts the literature equilibrium constant to 1.1×10^{-4} , compared to the observed equilibrium constant of 3.16×10^{-3} . This still favours the non-radical components of the equilibrium.

$$K_{lit} = \frac{[Q^-]^2}{[QH_2][Q]} \quad A$$

$$K' = \frac{[Q^-]^2}{[Q^{2-}][Q]} \quad B$$

$$\frac{K'}{K_{lit}} = \frac{[QH_2]}{[Q^{2-}]} \quad C$$

Equation 17. Method of converting the literature data to a form comparable to the work above.

The reason for the difference between the values could be due to the many approximations and assumptions made in the calculations. Small errors in maintaining pH (in the literature context) or in producing the dianion (in the results presented above) would result in huge differences in the equilibrium constant above. Also, the calculation uses rough pKa values, which would again result in large differences between the results.

5.3.3 Sensitivity of disproportionation/comproportionation equilibrium to reaction conditions

In the absence of excess base in our hydroquinone/quinone reaction mixture, the concentration of hydroxide and ethoxide species will be low as the pK_a of 2,5 – di-tert-butyl hydroquinone is significantly lower than that of water or ethanol. However, should excess base be introduced, these species will form and may react.

Figure 98 shows the results of determining the concentration of radical when 2,5 – di-tert-butylquinone and 2,5 – di-tert-butyl hydroquinone are mixed with different amounts of base. The region around 2 equivalents is relatively steep and small changes in the base concentration will produce different concentrations of radical.

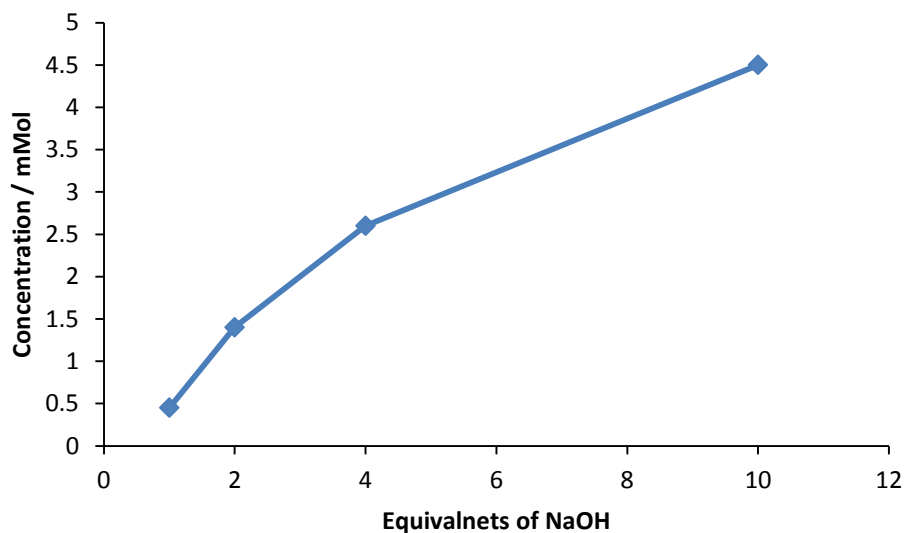


Figure 98. The effect of excess base on a 1:1 hydroquinone: quinone mixture in ethanol. The concentration on the y-axis is the radical observed.

To further understand why this effect is observed, and what consequences this may have, the products of reaction of 2,5-di-tert-butylquinone with 10 equivalents of sodium hydroxide were analysed by ESI-MS. The quinone was chosen, as the hydroquinone equivalent would first deprotonate with the first two equivalents of sodium hydroxide. The possible structures of products are given in Table 10. A possible mechanism is given in Scheme 62.

The main products are from nucleophilic substitution. The resulting products can also take part in the comproportionation / disproportionation equilibrium, as shown in Scheme 63.

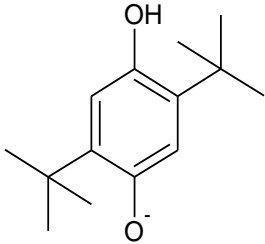
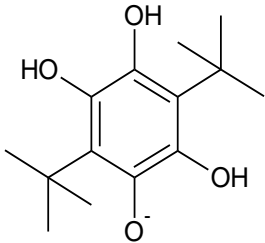
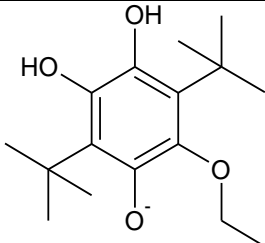
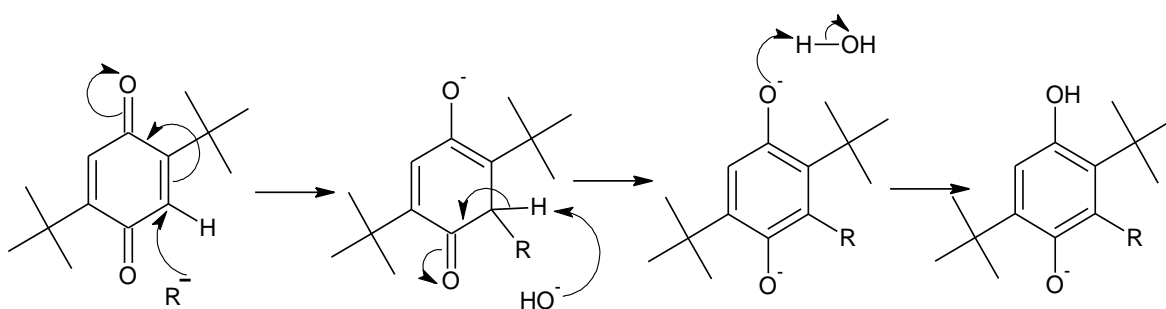
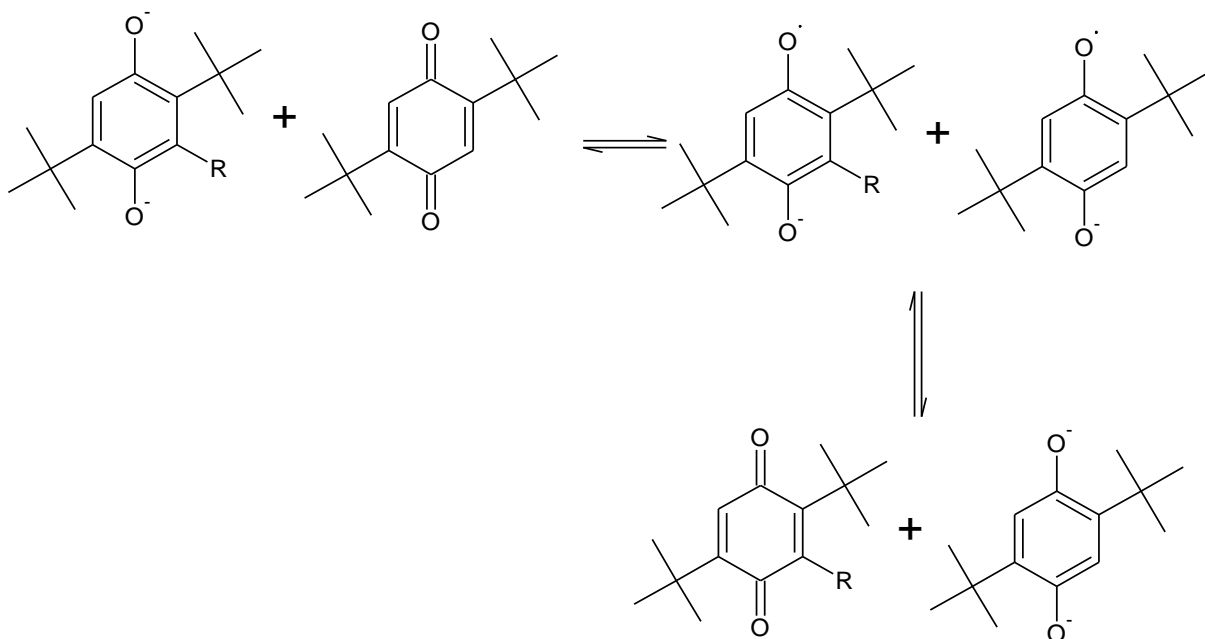
Observed mass	Possible structure	Formula	Calculated mass
237.15		$C_{14}H_{21}O_3$	237.149
253.14		$C_{14}H_{21}O_4$	253.146
281.16		$C_{16}H_{25}O_4$	281.175

Table 10. Structures for possible products for the decomposition of quinone in base



Scheme 62. A possible mechanism for the formation of mono substituted product observed in the reaction between the quinone and excess base.



Scheme 63. The new comproportionation / disproportionation equilibrium set up in a system of quinone and base

These experiments demonstrate a possible source of error and variability in the results obtained. Although the amount of base was controlled as well as possible, any variation in the amount used would result in a different radical concentration observed. As long as the number of equivalents of base was kept below two, then the concentration of free hydroxide and ethoxide would be kept low and not affect the results.

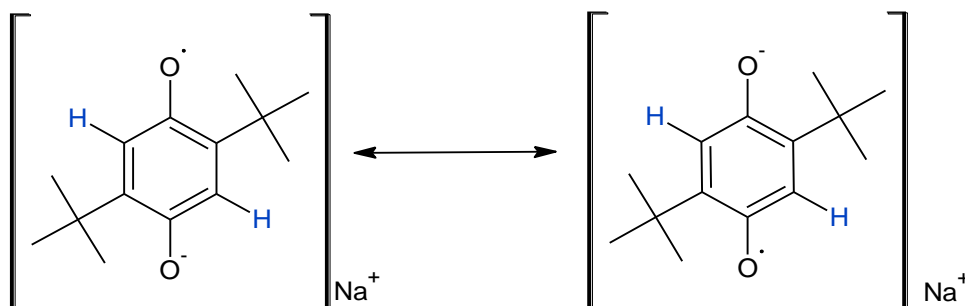
5.3.4 The comproportionation / disproportionation equilibrium in apolar media

In order to analyse the equilibrium in a nonpolar medium, in a way that is directly comparable to the results in ethanol, a compromise must be made. It is not possible to deprotonate the 2,5 – di-tert-butyl hydroquinone with sodium hydroxide in non-polar solvents. Sodium hydroxide is not soluble in non-polar solvents such as toluene. To test the solubility of dianion of hydroquinone, the disodium hydroquinone salt was made in ethanol, solvent removed, and toluene added. This confirmed the salt is also insoluble. However, by using a solvent mixture of 2% ethanol in toluene, the same method as before

can be used without issues. Also, the counter ion to the dianion remains the same as used in the reaction in ethanol, avoiding potential comparison issues.

The 2,5 – di-tert-butyl hydroquinone dianion was prepared in ethanol and then cannula transferred to the solution of 2,5 – di-tert-butylquinone in toluene. The experimental procedure is very similar to the one used in ethanol-only experiments in section 5.3.2 page 185. The method to determine the equilibrium constant in ethanol can thus be directly applied to the 2% ethanol / toluene results. Equation 10 can still be used to determine theoretical values of the equilibrium constant by least square fitting.

Using these conditions, an interesting observation can be made, that does not affect the interpretation of the results. In ethanol the EPR spectra of the semiquinone radical anion appeared as in Figure 98, because the sodium counter ion to the radical anion is solvated by ethanol, and disassociated from the radical. The radical is thus symmetrical and the two aromatic hydrogens are equivalent. This is demonstrated in Scheme 64. The EPR spectrum shows three lines with a 1:2:1 intensity ratio due to hyperfine coupling to the two equivalent hydrogens.



Scheme 64 Resonance structures for the radical anion showing the dissociation of the sodium ion and equivalence of the aromatic hydrogens.

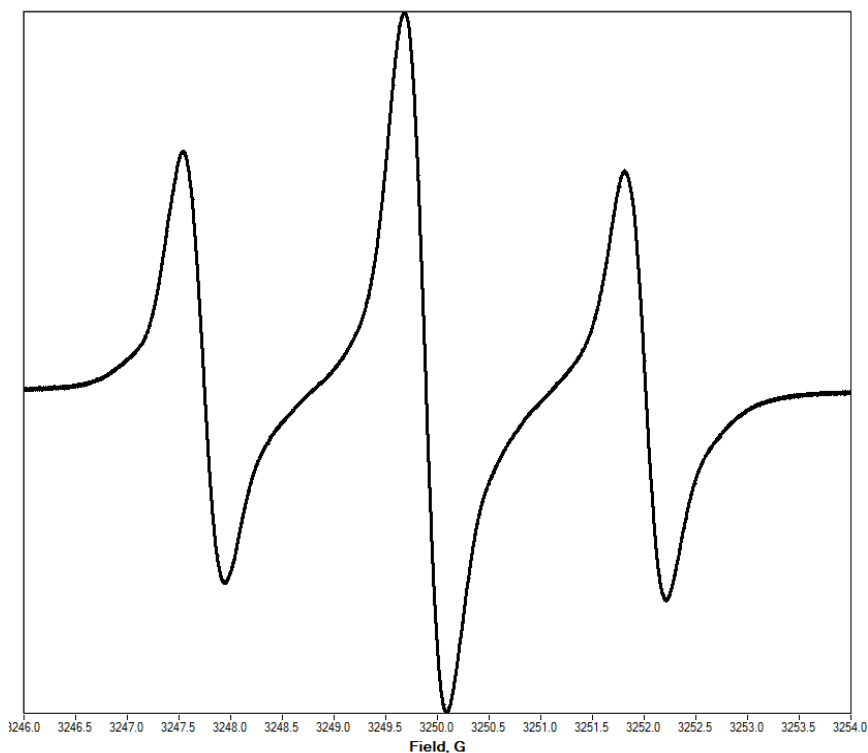
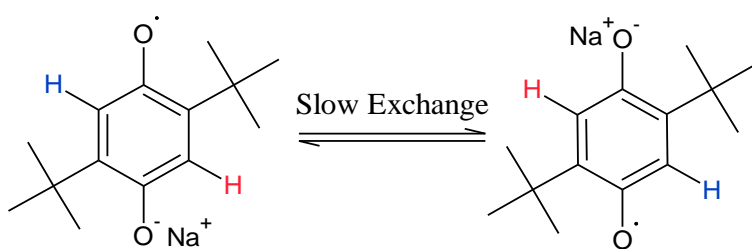


Figure 99. EPR signal of 2,5-diterbutyl semiquinone radical anion in ethanol at room temperature.

However, in a non-polar media, the semiquinone radical anion and the sodium cation form an ion pair, and are much more closely associated. This results in the inequivalent hydrogens depicted in red and blue in Scheme 65. This results in the spectra given in Figure 100. This spectrum was obtained in THF, as a demonstration of what is expected from literature^{123, 124}.



Scheme 65 The slow ion exchange of the sodium ion, demonstrating the two different proton environments

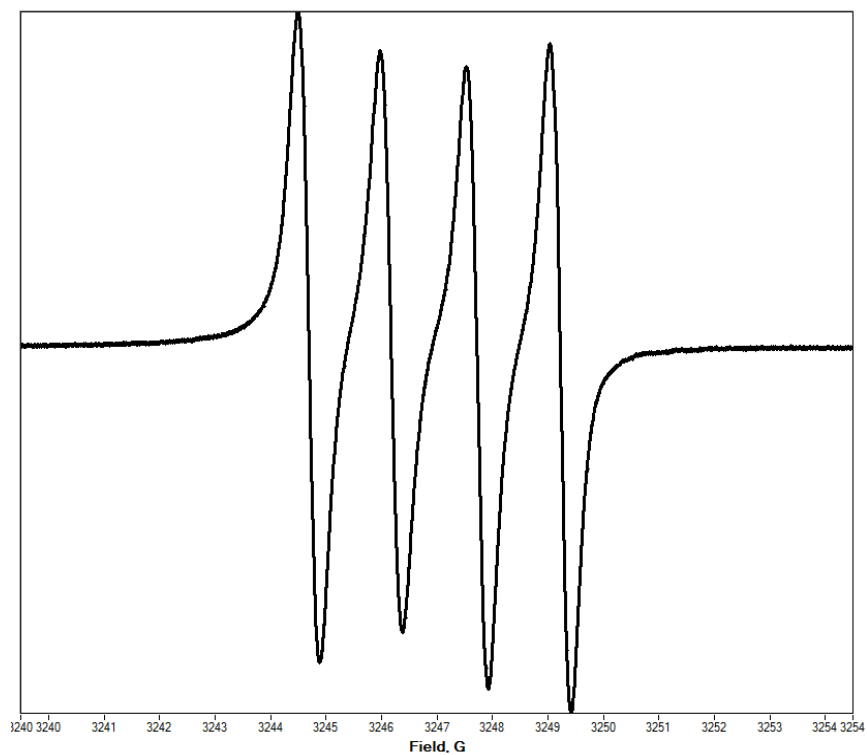


Figure 100. EPR signal of 2,5-diterbutyl semiquinone radical anion in THF at room temperature

In the equilibrium constant experiment performed in 2 % ethanol / toluene, the spectra in Figure 101 was observed.

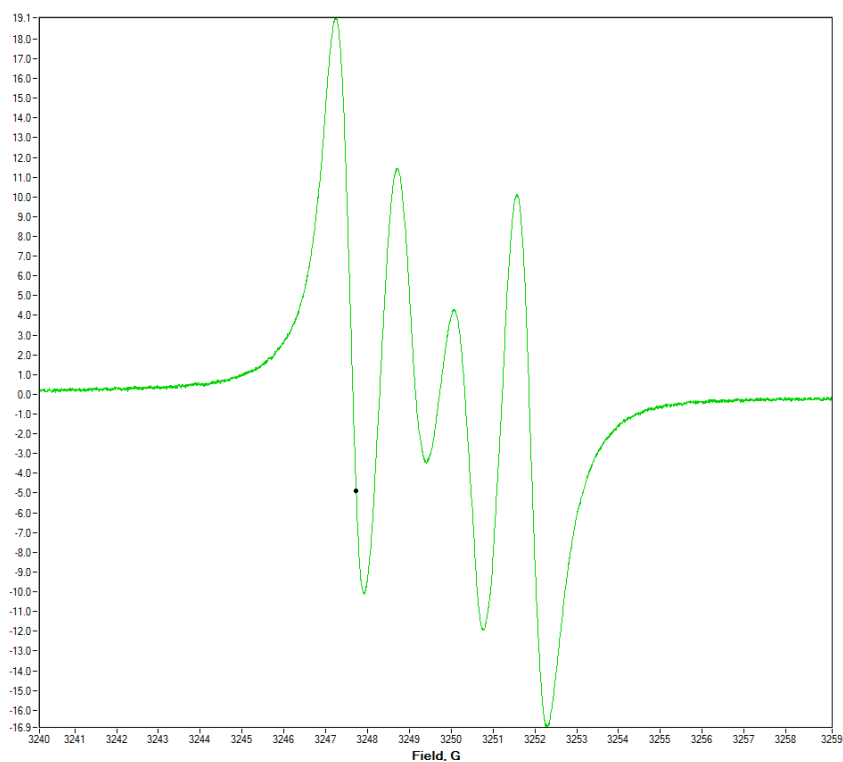


Figure 101. EPR signal of the 2,5-diterbutyl semiquinone radical anion in 2% ethanol / toluene at -60°C

As interesting as these results are, they mainly demonstrate what environment the radical resides in. Also, it is worth noting, that the results obtained from the different observed spectra are the same regardless of environment. Therefore the results obtained are not affected by this phenomenon.

The concentrations determined from these spectra are not affected by the line shape, as the line broadening effects are relatively small. Therefore, the results obtained from this solvent system should be accurate.

Table 11 shows the equilibrium constants, enthalpy and entropy for the reaction in 2% ethanol / toluene, determined by the same method used for Table 9 on page 190.

Temperature (K)	213	243	273	303	ΔH^0 (J mol ⁻¹)	ΔS (J K ⁻¹ mol ⁻¹)
K	2.00E-05	2.57E-05	2.71E-04	4.06E-04	290.3	0.0199

Table 11. Equilibrium constants, enthalpy and entropy for the comproportionation / disproportionation equilibrium of 2,5 – di-tert-butyl hydroquinone and 2,5 – di-tert-butylquinone in 2% ethanol / toluene

The equilibrium constants in the 2% ethanol/toluene mixture are much lower than in ethanol, meaning the equilibrium is shifted much more significantly to the non-radical components, suggesting that the radical anion is very poorly stabilised by solvation in a non-polar media. This means that in an organic monomer, there will be very little radical present to inhibit. The similar values of the enthalpy change in both solvents indicate a similar sensitivity of the position of equilibrium to changes in temperature.

Using the equilibrium constant obtained at 60 °C for 2% ethanol / toluene as a solvent, a hypothetical situation can be investigated. Assuming the concentration of semiquinone is 3 mM, which is a common concentration used of industrial inhibitors, we can estimate how much of the radical will remain after the comproportionation / disproportionation equilibrium has been established. This assumes that a stable sample of just the radical anion can be obtained, and there are no other routes of decay.

Equation 19 shows the relationship between the equilibrium constant, the concentration of semiquinone added ($[SQ]_0$) and the semiquinone remaining in solution ($[SQ]$).

$$[SQ]_0 = [SQ] + \frac{1}{2}[Q] + \frac{1}{2}[Q^{2-}]$$

$$\text{Also as: } [Q] = [Q^{2-}]$$

$$\text{Then the following is also true: } [SQ]_0 = [SQ] + [Q]$$

Equation 18. The relationship between the concentrations of semiquinone, quinone and hydroquinone

$$K = \frac{[SQ]^2}{([SQ]_0 - [SQ])^2}$$

Equation 19. The equilibrium equation simplified to include concentrations of observable species

Equation 19 now contains values that can be determined. When simplified, the result is Equation 20, which can now be solved.

$$0 = (1 - K)[SQ]^2 + K[SQ]_0[SQ] - K[SQ]_0^2$$

Equation 20. The quadratic equation that can be solved, to determine the remaining semiquinone concentration.

The concentration of initial semiquinone radical ($[SQ]_0$) used is 3 mM, and the equilibrium constant used from

Table 11, page 200, at 60°C was 0.000406. This gives a remaining concentration of semiquinone as 6×10^{-2} mM. This is only 2 % of the semiquinone added. Extrapolating the equilibrium measurement results to 110°C gives an equilibrium constant of 0.00216, which leads to a concentration of 0.14 mM (4.6 % of the input semiquinone).

Even though this concentration of accessible radical is low, it may still act as an inhibitor. It depends on the rate of reaction between the radical initiator and the semiquinone being quicker than the rate which the radical initiator can react with a styrene monomer. The rate constant of styrene propagation is $2.2 \times 10^3 \text{ M}^{-1} \text{ s}^{-1}$, which gives a rate of propagating radical adding to styrene $2 \times 10^5 \text{ M s}^{-1}$. If for example the reaction between semiquinone and a styrene radical initiator is diffusion controlled and barrier less, the rate constant for the reaction could be in the order of $10^{10} \text{ M}^{-1} \text{ s}^{-1}$. Taking into account the concentration of semiquinone, this would lead to a rate of propagating radical reaction with semiquinone $1.4 \times 10^7 \text{ M s}^{-1}$. As this rate is faster than the rate of addition of the same radical to the styrene monomer, inhibition will be observed. However this is quite an extreme situation.

There are few molecules that react with a rate constant around $10^{10} \text{ M}^{-1} \text{ s}^{-1}$, and they are usually small. An example is two hydroxide radicals reacting to form hydrogen peroxide¹²⁵. Also to consider is the viscosity of the solvent. A sample of styrene starting to polymerise will be quite viscous, so the rate constant of $10^{10} \text{ M}^{-1} \text{ s}^{-1}$ will not be feasible.

A more realist rate constant for the reaction between semiquinone and initiator is of the magnitude $10^8 \text{ M}^{-1} \text{ s}^{-1}$ based on literature for related reactions¹²⁶. This would lead to a rate of reaction of propagation radical with semiquinone around $1.4 \times 10^4 \text{ s}^{-1}$. This rate is smaller than the rate of reaction of the propagation radical with the monomer but as the

calculations include significant uncertainty, it is possible that some retardation of polymerisation would be observed. Without knowing the exact rate of reaction between semiquinone and initiator, it is only speculation, but it is doubtful the semiquinone would be an effective inhibitor.

In reality, obtaining a stable quantity of semiquinone and dissolving it in organic media without it decomposing via any other routes is not possible. However this exercise shows that any semiquinone that does form in organic media, through a comproportionation / disproportionation equilibrium or charge transfer catalyst, will be present at a fairly low steady state concentration and hence is unlikely to act as a good inhibitor.

5.4 Conclusions

Chloranil radical anion was proposed as the inhibiting species in a chloranil / tertiary amine charge transfer complex.⁶¹ The potassium salt of the radical anion was therefore investigated as a potential inhibitor. However this salt is not soluble in organic media. This limits its use as a potential inhibitor.

When the chloranil radical anion potassium salt is observed in water, it is unstable and the EPR signal decays. By observing the decomposition products, it can be concluded that the radical is susceptible to nucleophilic substitutions and oxidation, and reactions with another radical. This suggests that the chloranil radical anion formed by the decomposition of the charge transfer complex, is unlikely to survive and act as an inhibitor.

When using an inert atmosphere, the rate of decay decreases. This suggests the radical anion is easily oxidised, but that there is still a route for decay, presumably through self-reactions.

The comproportionation/disproportionation equilibrium in the quinone-hydroquinone mixture was explored in order to estimate the steady state concentration of semiquinone in solution, to understand if realistically the semiquinone formed by the degradation of a charge transfer complex can act as an inhibitor. This could not be done with chloranil and tetrachloro hydroquinone due to the high reactivity of the starting materials. The use of

2,5 – di-tert-butylquinone and the 2,5 – di-tert-butyl hydroquinone was possible and investigated as an alternative.

In ethanol, the comproportionation/disproportionation equilibrium for the 2,5 – di-tert-butylquinone and the 2,5 – di-tert-butyl hydroquinone is shifted to the non-radical components, as determined from the equilibrium constant. At lower temperatures, the equilibrium shifts even further to the non-radical components. In a more non-polar medium (e.g., 2% ethanol / toluene mixture), the equilibrium concentration of semiquinone is even lower.

By taking into account the equilibrium concentration of semiquinone under realistic conditions, and comparing the hypothetical rates of reaction between the semiquinone and styrene initiator radicals, we conclude that the semiquinone is unlikely to react fast enough with the propagating radicals to inhibit the polymerisation. It can be concluded therefore that the inhibition observed by Yassin and Rizk⁶¹ is likely to be caused by the trapping of the propagating radicals by the charge transfer complex itself rather than free semiquinone radical anion formed by the degradation of the charge transfer complex.

6. Final conclusions

The overall mission of this study was to develop a better understanding of the mode of action of inhibitors of spontaneous polymerisation. The initial part of the study was to first determine how the current inhibition methods work on a mechanistic level. It has been determined that the current industry standard inhibitor, DNBP, inhibits through aromatic nitro groups. It is more efficacious than nitrobenzene due to the interaction between the ortho nitro and phenol groups. The hydrogen bonding between them makes the nitro group more susceptible to attack by the radicals formed through spontaneous initiation.

The product analysis of styrene inhibited by 2-nitrophenol, a similar molecule to DNBP, has determined a number of products. The mechanism of formation of the intermediate Unknown B was studied, by purposely synthesising it. Through this it has been hypothesised that an imine intermediate is formed, supporting that nitrophenol inhibitors work through the nitro group.

The side products from this initial reaction were investigated. They do not inhibit polymerisation effectively. Also, by comparing the rate of formation of initiator radicals in spontaneous polymerisation, and the rate of nitrophenol inhibitor consumption, it can be suggested that the inhibition reaction is stoichiometric. This shows that there is no catalytic cycle set up, which would have made nitrophenol inhibitors more effective.

A possible new inhibitor has been investigated. The proposed mechanism of action is the charge transfer complex between chloranil and N,N-dimethyl aniline. The proposed inhibiting species, the chloranil radical anion has been found to be too unstable to be the molecule responsible for inhibition. Investigating 2,5-ditertbutyl quinone as a substitute for chloranil showed that a semiquinone intermediate is unlikely to inhibit.

Using the comproportionation / disproportionation equilibrium as a measure of its stability, showed that the equilibrium strongly favours the non-radical products. Therefore it is unlikely that the semiquinone radical would be available in high enough concentration to inhibit the spontaneously initiated polymerisation.

As the presence of a nitro group is essential for DNBP to work, and nitro compounds are too toxic by according to new legislation, it may not be possible to develop new inhibitors

based on such compounds; hence alternative mechanisms should be targeted. The quinone example shows that there is a lot of promise in synergistic action of mixtures of different inhibitors, even though the mechanisms are quite hard to understand in these cases; you can predict therefore that this is where the future research may be concentrated

7. Experimental

7.1 Chemicals and materials

All chemicals including deuterated solvents were purchased from Sigma-Aldrich, and used, unless stated, without further purification. Solvents were supplied by Fisher, and were used without further purification, unless otherwise stated. DNBP was provided by Nufarm UK Ltd.

7.1.1 Styrene preparation

Stock styrene from Aldrich included a transport inhibitor, 4-tert-butylcatechol, at ~10ppm. Inhibitor was removed by running styrene through alumina column immediately before use.

7.2 NMR

^1H and ^{13}C NMR spectra were recorded in the deuterated solvent as indicated, on JEOL ECX 270 MHz, ECX 400 MHz or ECS 400 MHz spectrometers. Chemical shifts are reported in parts per million using the deuterated solvent as a internal reference. Spin multiplicities are indicated by the following symbols: s (singlet), d (doublet), t (triplet), q (quartet), qu (quintet), sx (sextet), sept (septet), m (multiplet), br (broad).

7.3 EPR

Electron paramagnetic resonance spectra were recorded on a JEOL JES-RE1X X-band spectrometer. A sealed Pasteur pipette was used for samples unless otherwise stated. Typical parameters were; power 5.0 mW, frequency 9.105 GHz, field modulation width 1.0 G, sweep time 90 s.

Where spectra were averaged, scans were recorded individually at a set time interval and manipulated using Spectrum Viewer Plus 2.6.3.

7.4 MS

Mass spectra, both positive and negative mode, were recorded on a Bruker micro-TOF with LCQ ion trap with electron spray ionisation. The samples were dissolved in an appropriate solvent and then diluted in methanol or acetonitrile as needed. The approximate concentration of a sample is 5 mg of sample in 2 ml of solvent, dependent on solubility of the sample, and how much of the sample was available. The solution was then submitted to the mass spectrometer by an Agilent 1200 series Liquid Chromatography system pump. No chromatography was performed by the equipment.

7.5 Dilatometry

Samples were prepared at 0.1M concentration (5 mL scale unless limited inhibitor available). Fine glass pipette was used to insert sample into capillary tube. Compressed air and fine pipette were used to remove excess styrene and inhibitor from headspace. Samples were sealed by Bunsen burner.

Oil bath was pre-heated to 113°C for a 110°C experiment. Temperature was reset to 110°C once rack was inserted into bath. Images of rack were taken immediately after insertion.

7.6 Oximetry (Oxygen diffusion into chlorobenzene)

TEMPO (100ppm) solution in chlorobenzene (5 mL) was prepared in a sample vial open to air. This solution (0.1mL) was added to a sealed Pasteur pipette and oxygen was removed by freeze-pump-thaw method under nitrogen. In the final stage, the headspace was evacuated with the sample frozen, and backfilled with air while keeping the sample frozen. This ensured the absence of oxygen in the solution which is exposed to air. The sample was carefully moved from Schlenk line to EPR machine, and thawed, keeping the sample undisturbed when inserting into EPR spectrometer.

7.7 Column Chromatography / Thin Layer Chromatography

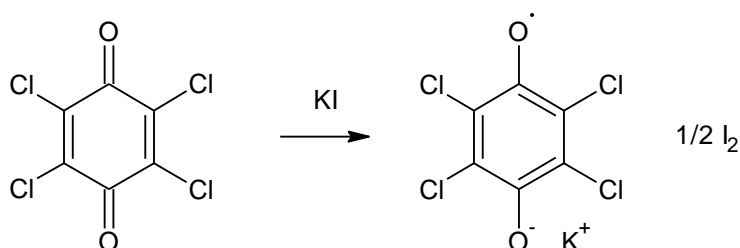
Flash column chromatography was performed with Fluka Analytical Silica Gel 60 (pores size 60 Å, 220-440 mesh particle size, 35-75 µm particle size). TLC was performed using Merck TLC Silica 60 F₂₅₆ on aluminium sheets, cut into smaller tiles before use.

7.8 X-ray crystallography

A sample of Unknown B was dissolved in CDCl₃ and the solvent allowed to evaporate at room temperature in an open vial to produce crystals. A suitable crystal was selected and the experiment was performed on an Oxford Diffraction Supernova diffractometer. The crystal was kept at 109.9(2) K during data collection. Using Olex2¹²⁷, the structure was solved with the Superflip¹²⁸ structure solution program using Charge Flipping and refined with the ShelXL¹²⁹ refinement package using Least Squares minimisation.

7.9 Synthesis

7.9.1 Chloranil radical anion potassium salt synthesis

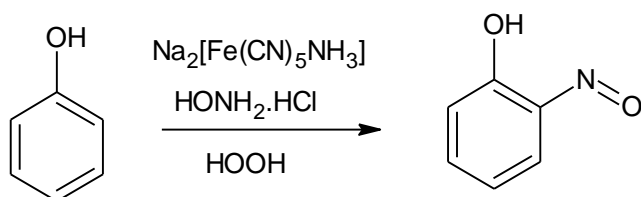


The synthesis is based on procedure by Torrey and Hunter¹¹⁵. A saturated solution of chloranil (1 g, 4.06×10^{-3} mol) in the minimum volume of heated (30°C) acetone (ca. 75ml), was prepared. Potassium iodide (0.68 g, 4.06×10^{-3} mol) was dissolved in a minimum volume of deionised water (ca. 1 mL). The KI solution was added to the chloranil solution, where a dark green precipitate was formed in a dark brown solution. The suspension was separated by centrifugation. The residue was washed with cold acetone ($3 \times 30\text{mL}$). The last wash was filtered by vacuum filtration and washed with cold acetone. Once removed from the filtration, the sample was dried under vacuum in the sample vial on a Schlenk line. The yield was ca. 70%. The average of 3 CHN analyses determined the carbon, hydrogen and nitrogen content consistent with theoretical values, as shown in Table 12.

Element	Determined / %	Theoretical / %
C	25.0	25.5
H	0.1	0
N	0	0
Remaining	74.9	74.5

Table 12. CHN results for chloranil radical anion potassium salt

7.9.2 2-nitrosophenol synthesis



The synthesis is based on procedure by Maruyama et al¹⁰⁴. The reaction mixture contained sodium pentacyanoamine ferrate (II) (2 g), phenol (1 g), hydroxyl amine hydrochloride (4 g), hydrogen peroxide (30% solution, 4 mL) in water (200 mL) and petroleum ether (60 mL), and was stirred at room temperature for 1 hour. Ether layer was separated, and the aqueous layer washed with ether (3 x 50 mL). The ether solutions were combined and washed with water (2 x 50 mL) and then with a dilute copper sulphate solution (5 x 100 mL). The copper complex of 2-nitrosophenol thus formed was stored in the fridge until required.

To obtain 2-nitrophenol for use, an aliquot of the copper dimer was acidified and then washed with pentane (4 x 100 mL). The pentane was removed by rotary evaporation, on a low vacuum, in order to reduce the loss of volatile 2-nitrosophenol. 5 ml of copper dimer solution yielded 2 mg of 2-nitrosophenol.

7.9.3 Unknown B isolation

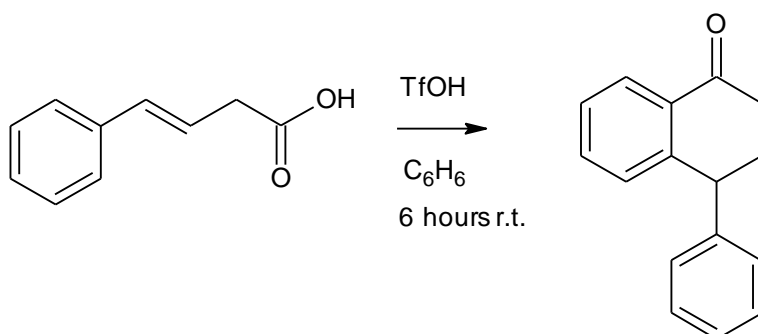
Synthetic procedure was based upon work by Bushby et al⁴⁵. Styrene (50 ml) was inhibited by 2-nitrophenol (0.5M, 1.39g) and the mixture was heated at 150°C for 3 days under reflux.

The crude reaction mixture (5 g) was dissolved in diethyl ether (50 mL), and washed with HCl (5M, 250 mL) and NaOH (5M, 250 mL). Aminophenol (Unknown A) was isolated from the acidic wash by rotary evaporation. MS-ESI –ve mode: 110 m/z. ¹H NMR (400 MHz,

CDCl₃): δ 7.17 (m, 2H), δ 6.88 (dd, 1.22 Hz, 8.54 Hz, 1H), δ 6.83 (td, 1.22 Hz, 7.94 Hz, 1H) 4.67 (s).

The ether solution from the acid / base extraction was slowly added to methanol (100 mL). The methanol was stirred vigorously, to allow greater dispersal of the oil and avoid precipitate agglomeration on the glass. The mixture was cooled in a freezer overnight. Suspension was filtered through celite. Methanol / diethyl ether solvent was removed by rotary evaporator. The residue was separated by column chromatography (diethyl ether, R_f ~0.5). The yield from 5 g of unpurified solution was ca. 1 g. ¹H NMR (400 MHz, CDCl₃): δ 7-8.5 (Broad) ESI-MS –ve mode: 312 m/z.

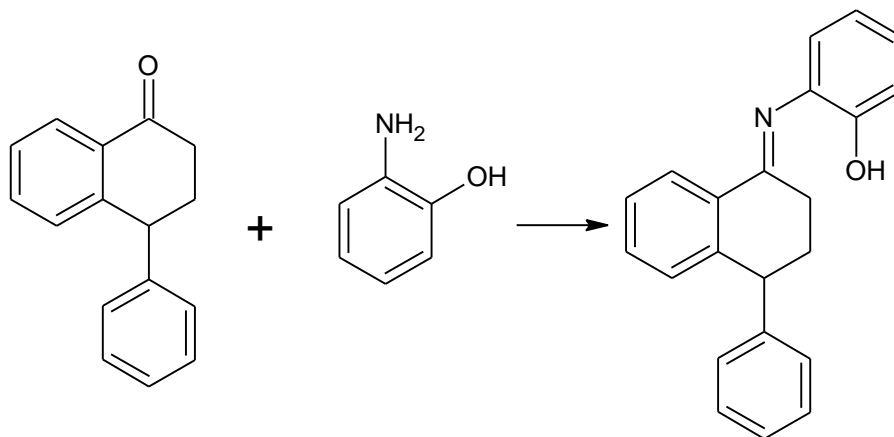
7.9.4 Compound C synthesis – ketone precursor (Compound D)



The synthetic procedure was scaled up from Rendy et al¹⁰⁰. Trans-Styrylacetic acid (1 g, 6 mmol) was dissolved in benzene (5 mL). Triflic acid (20 mL) was added to the solution and stirred for 6 hours. The mixture was poured over ice (50 g), and the product was extracted twice with chloroform (2 x 50 mL). The chloroform extract was then washed with water (3 x 50 mL) and then brine (1 x 50 mL) and dried over magnesium sulphate. The extract was filtered and solvent was removed in vacuo. The crude sample was purified by column chromatography (1:1 ethyl acetate : 40-60 pet ether, R_f 0.3) Yield ca. 64 %. Pure ketone was stored in fridge. The full NMR analysis is given in Section 3.6 page 104. ¹H NMR (400 MHz, CDCl₃): δ 8.06 (dd, 1.83 Hz, 7.93 Hz, 1H), 7.36 (td, 1.53 Hz, 7.63 Hz, 3H), 7.30-7.24 (m, 3H), 7.21-7.17 (m, 1H), 7.06-7.03 (m, 2H), 6.92 (dd, 1.83 Hz, 7.63 Hz, 1H), 4.24 (dd,

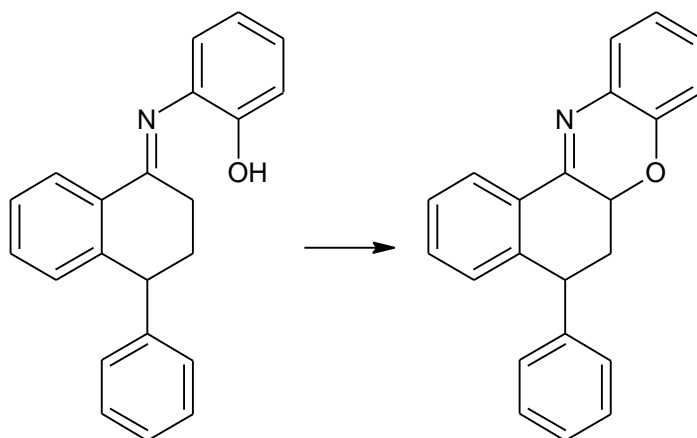
4.58 Hz, 8.24 Hz, 1H), 2.67 (ddd, 4.27 Hz, 17.08 Hz, 28.37 Hz, 1H), 2.55 (ddd, 4.27 Hz, 8.85 Hz, 17.09 Hz, 1H), 2.44-2.36 (m, 1H), 2.28-2.19 (m, 1H). ESI-MS –ve mode: 222 m/z

7.9.5 Synthesis of Compound E



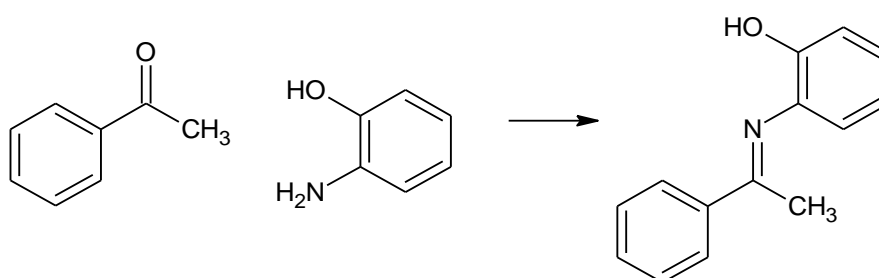
A 1:1 mixture of compound D (200 mg, 9 mmol) and 2-aminophenol (98 mg, 9 mmol) in toluene (ca. 10 ml) and molecular sieves were sealed in a Fisher-Porter bottle under argon. The reaction mixture was heated at 150°C for 16 hours. Solvent was removed by rotary evaporation. The composition of the crude produced was determined as 1:1:1 compound D : aminophenol : compound D by NMR as explained Section 3.9.3 page 128. The mixture cannot be separated without hydrolysis of imine.

7.9.6 Compound E to Compound C reaction



A 0.1 M Compound D / E / 2-aminophenol mixture (from above) in 1:1 styrene : toluene (1 mL) was heated for 4 hours. The product mixture was analysed as described in Section 3.9.4 page 130. ESI-MS: Loss of 314 m/z during reaction. Occurrence of 312 m/z as reaction progressed.

7.9.7 N-(1-Phenylethylene)-o-aminophenol - Compound F



The synthesis followed the procedure by Tauer and Grellmann¹⁰². 2-Aminophenol (0.2 mol) and acetophenone (0.22 mol) were refluxed in toluene (150 mL) in a Dean-Stark apparatus, until 0.2 mol of water were removed. The reaction mixture was concentrated by 50% and solid was separated by vacuum filtration. The yield was 55 %. MS-ESI –ve mode: 210.1 m/z. ¹H NMR (400 MHz, CDCl₃): δ 8.02 (dd, 1.53 Hz, 8.09 Hz, 2H), δ 7.48 (m, 3H), δ 7.09

(td, 1.53 Hz, 7.32 Hz, 1H), δ 7.00 (dd, 1.22 Hz, 8.09 Hz, 1H), δ 6.89 (td, 1.53 Hz, 7.32 Hz, 1H), δ 6.80 (dd, 1.53 Hz, 7.63 Hz, 1H), δ 2.45 (s, 3H)

8. Appendices

The following are the spectra and tables of information referred to in the previous text

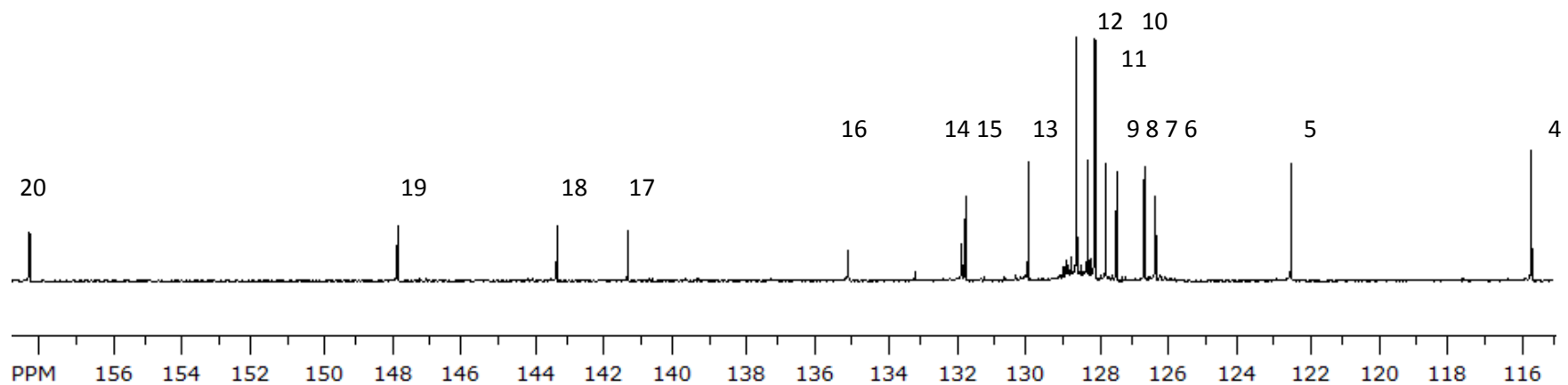


Figure 102. ¹³C NMR 700MHz of 312 fraction, low field, in CDCl₃.

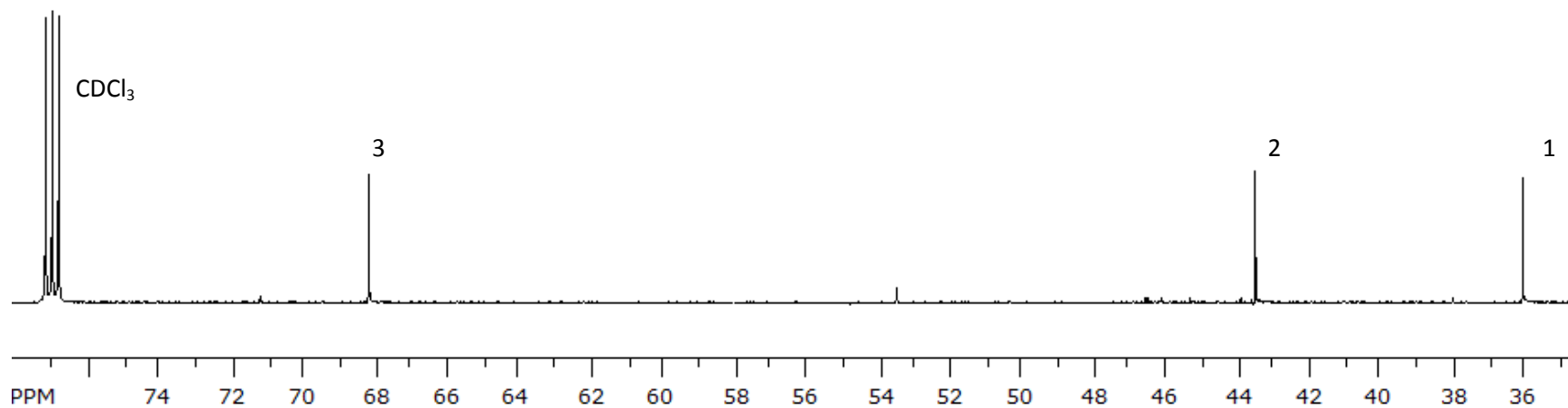


Figure 103. ¹³C NMR 700MHz of 312 fraction, high field, in CDCl₃.

SpinWorks 3: TN_RHC16_312
~35mg in CDCl₃
1H COSY

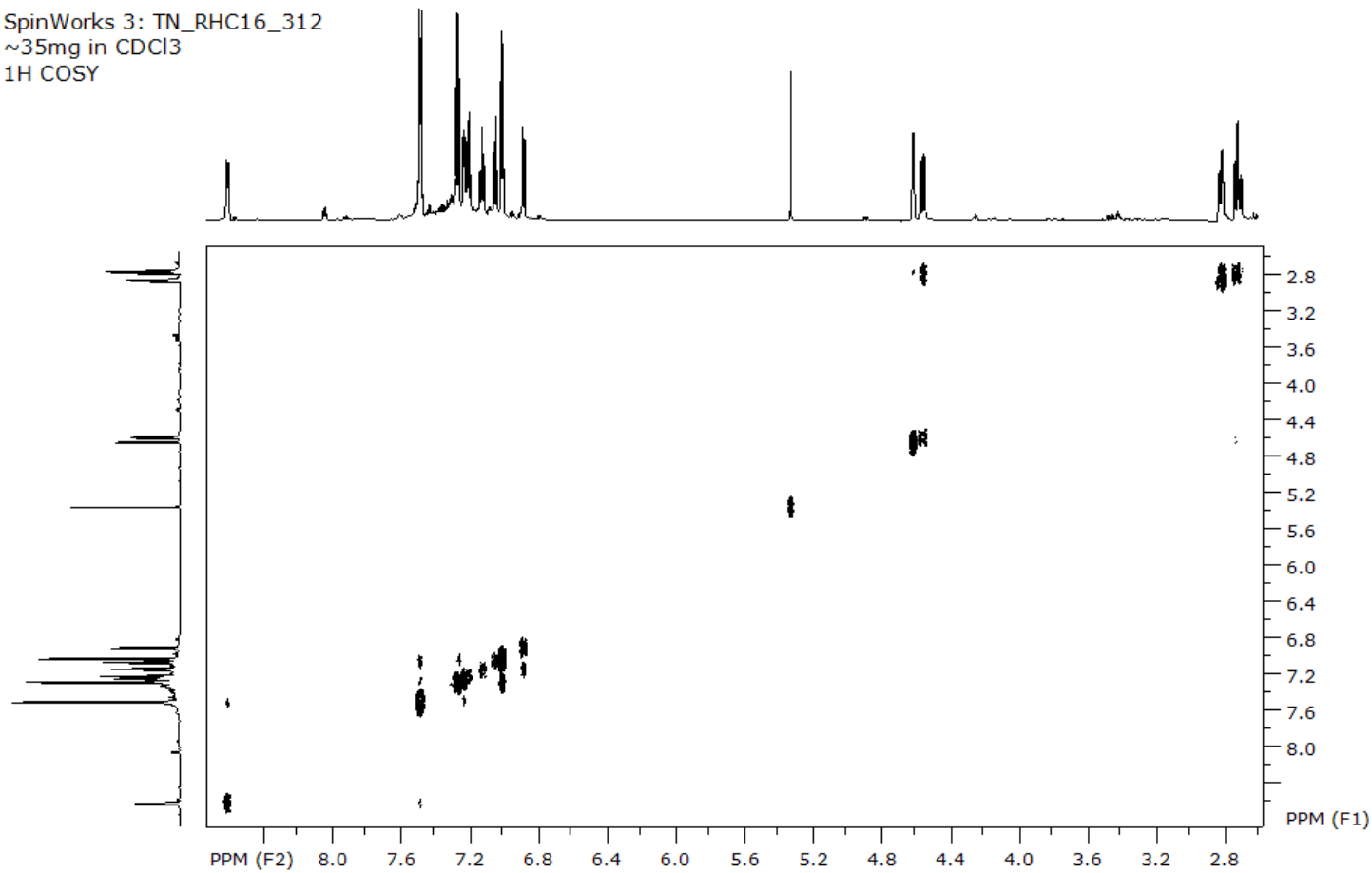


Figure 104. COSY spectra of compound B. (700MHz, CDCl₃)

SpinWorks 3: HSQCETGPSI

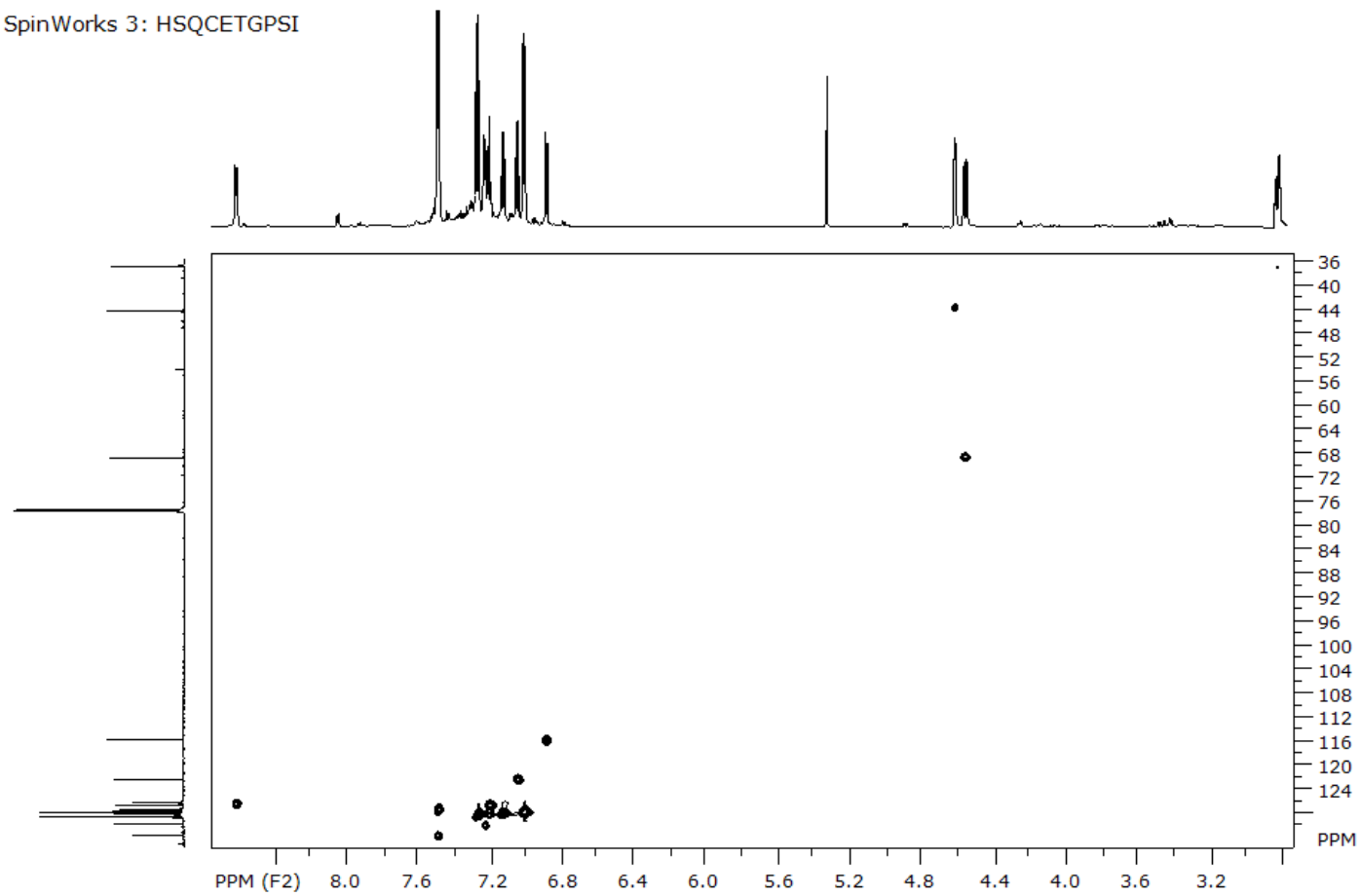


Figure 105. HSQC spectra of compound B. (700MHz, CDCl_3)

SpinWorks 3: HMBCGP

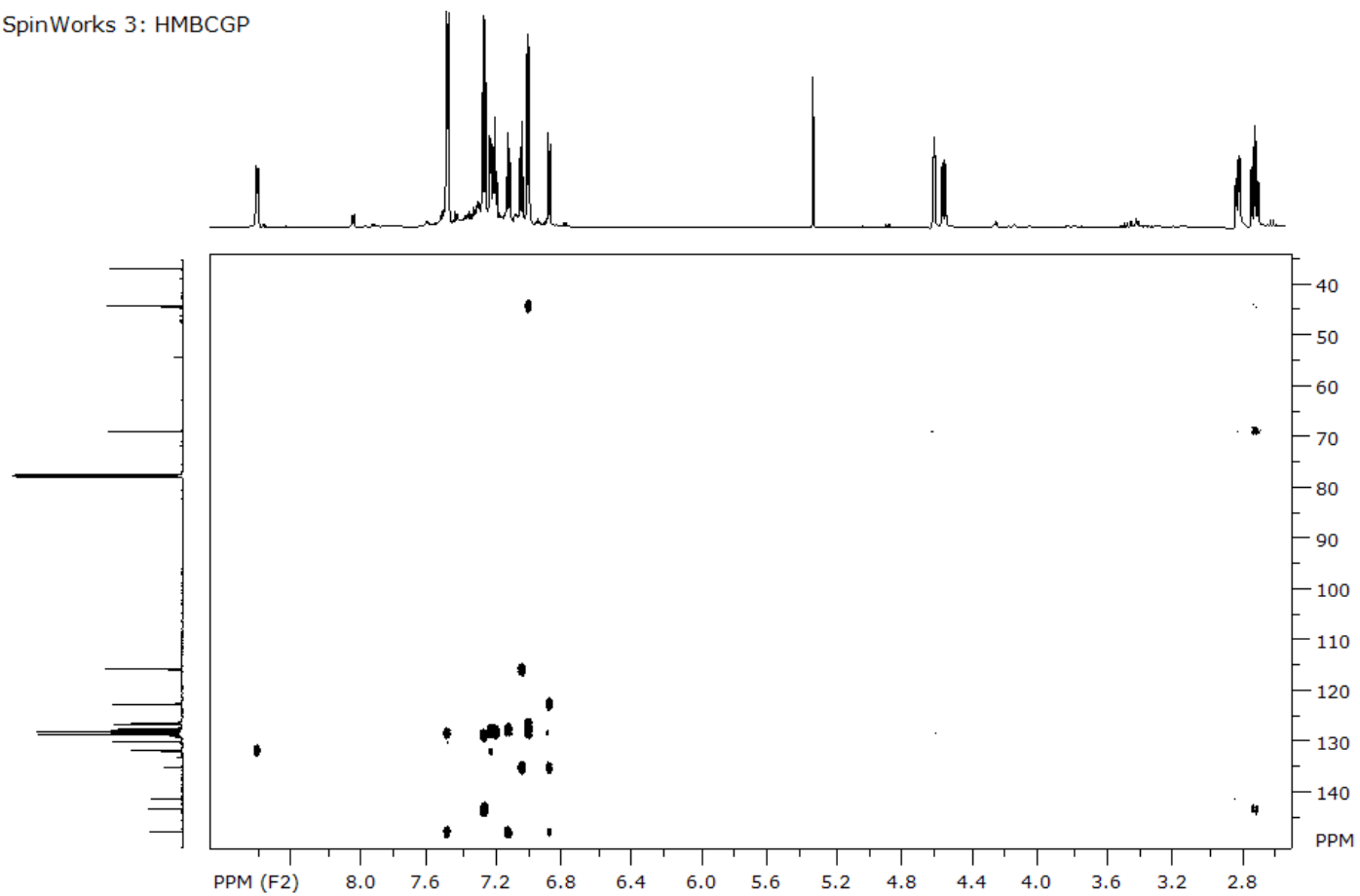


Figure 106. HMBC spectra of compound B. (700MHz, CDCl₃)

Table 13. Summary of carbon signals and their couplings in HSQC and HMBC NMR experiments (700MHz, CDCl₃)

Carbon	δ (ppm)	HSQC	HMBC
1	36.1	L, M	J, K
2	43.5	J	L(w), M, H, D
3	68.3	K	L, M, J(w)
4	115.7	I	F(w), G
5	122.5	G	I
6	126.4	A	B
7	126.7	E	H
8	127.5	B	F, G(w)
9	127.8	B	D
10	128.1	H	C, E, H, J
11	128.3	F	B, J, L, M
12	128.6	C	C, E, H, J
13	130.0	D	A(w), B, J
14	131.8	B	A, B, D, J
15	131.9		
16	135.1		B(w), F(w), G, I, K
17	141.4		A, B(w), D, J, L, M
18	143.4		C, E(w), J, L, M
19	148.0		B, F, G, I, K
20	158.5		A, B(W), D, K, L, M

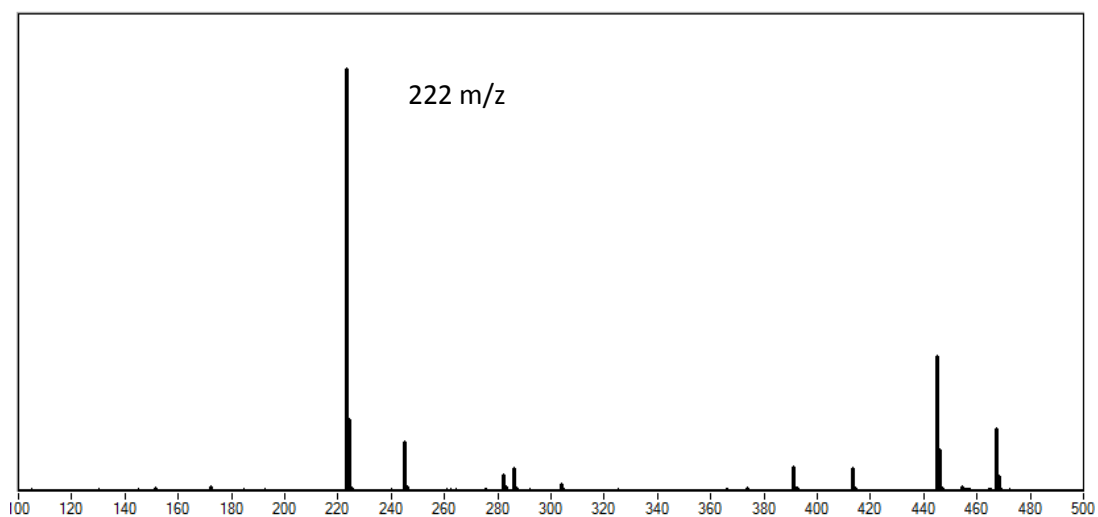


Figure 107. MS of compound D synthesised following the procedure by Rendy et al¹⁰⁰.

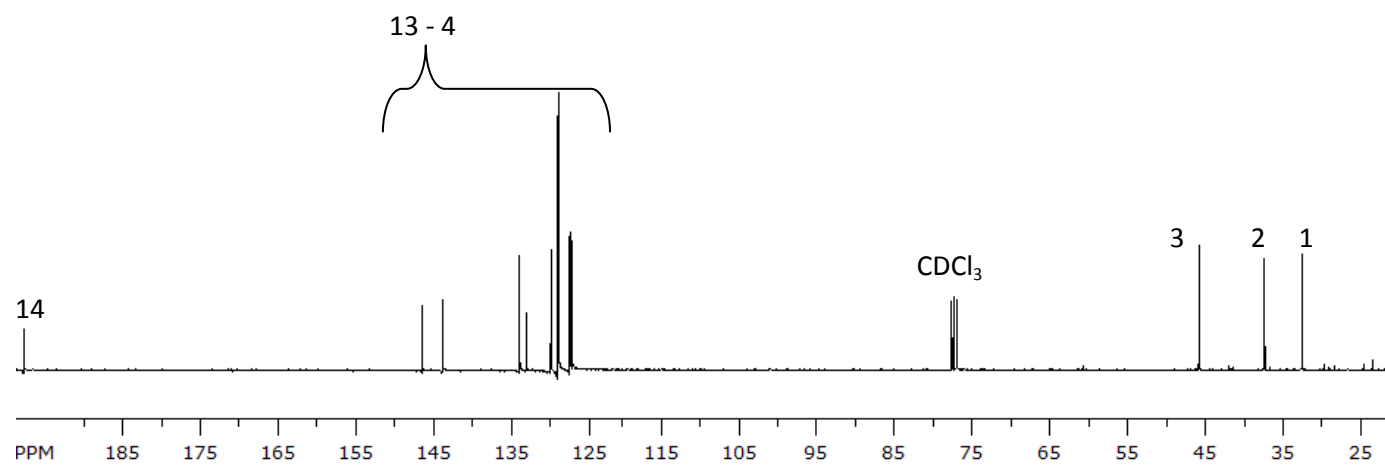


Figure 108. ^{13}C NMR of the compound **D**. (400MHz, CDCl_3)

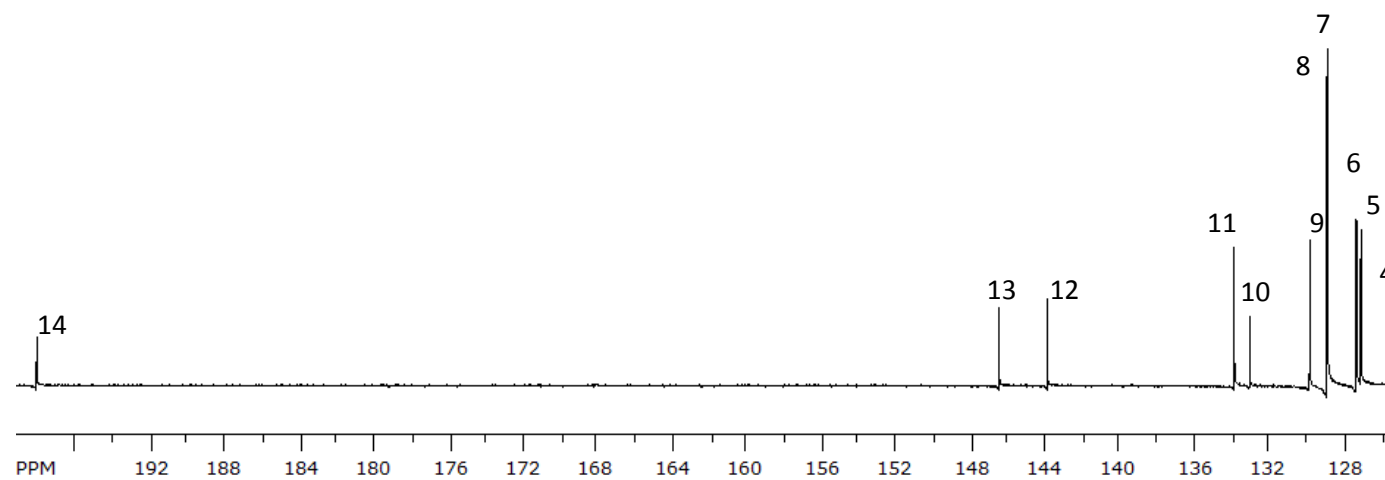


Figure 109. ^{13}C NMR of the compound **D**, low field magnification. (400MHz, CDCl_3)

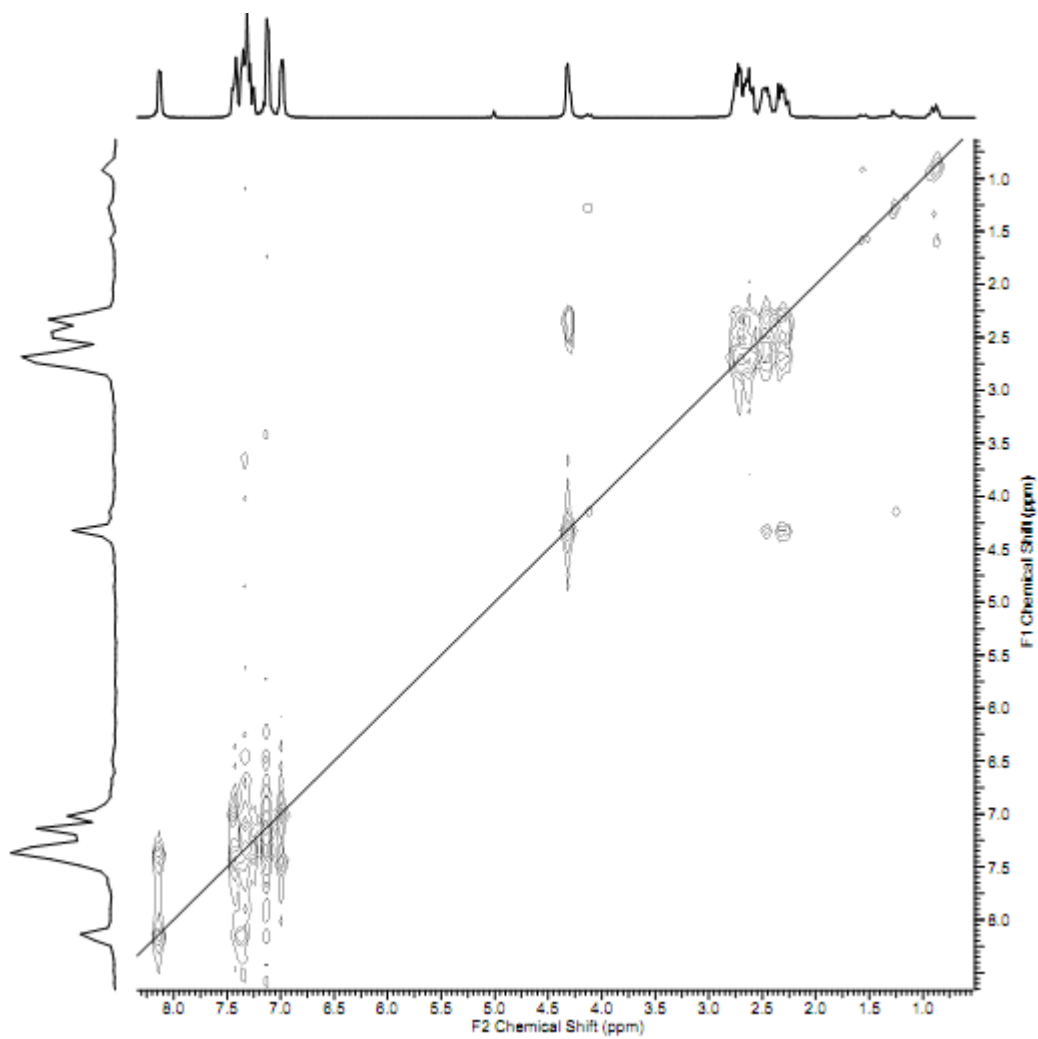


Figure 110. COSY spectra of compound D. (400MHz, CDCl_3)

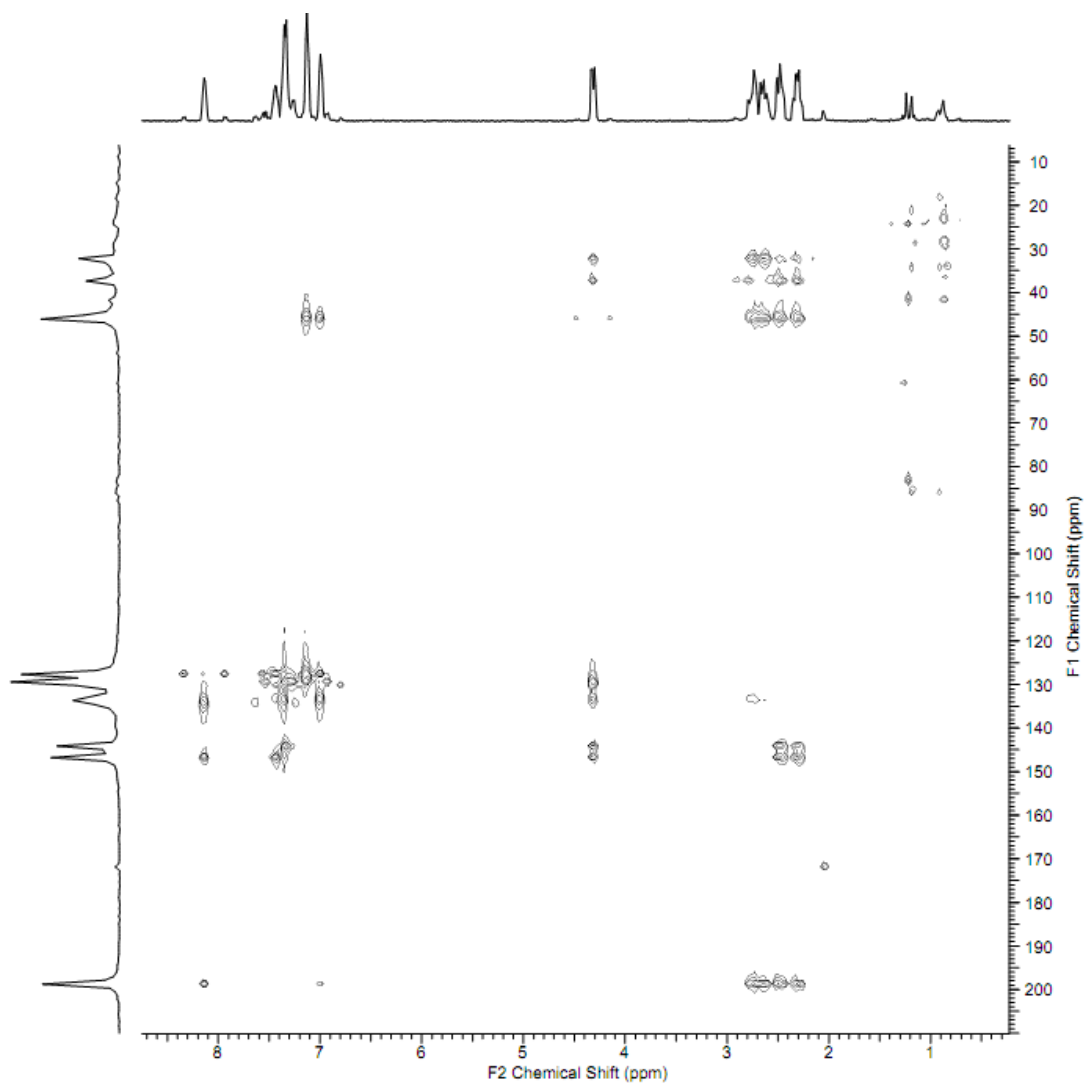


Figure 111. HSQC spectra of compound D. (400MHz, CDCl₃)

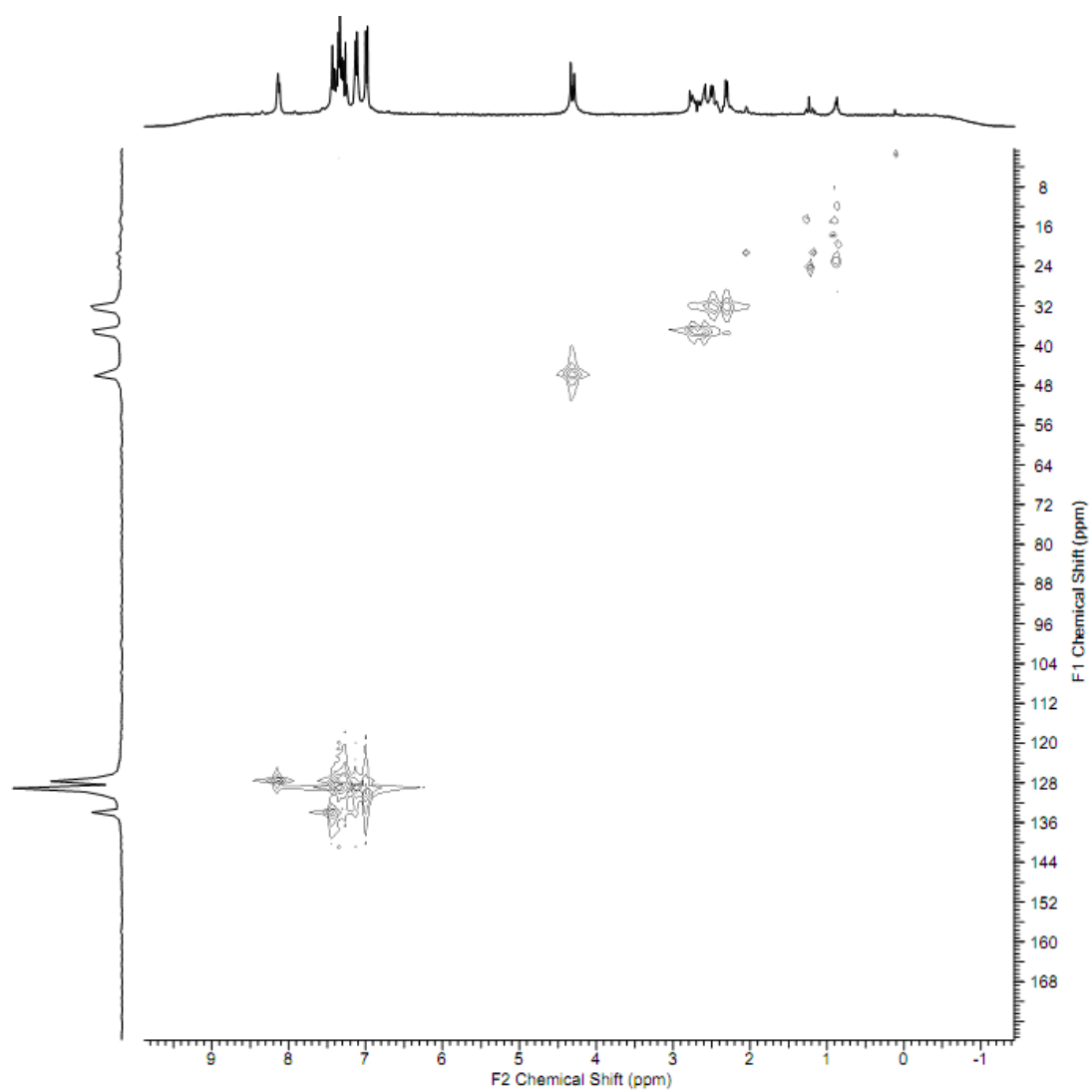


Figure 112. HMBC spectra of compound D. (400MHz, CDCl_3)

Table 14. Summary of carbon signals of compound D and their couplings in COSY, TOCSY, HSQC and HMBC NMR experiments. (400MHz, CDCl₃)

Carbon	Chemical shift (ppm)	HSQC	HMBC
1	31.9	J/K	H, I, G
2	36.8	H/I	J, K, G(w)
3	45.3	G	F, E, H, I, J, K
4	126.9	D	E(w)
5	127.1	A/C	F, E, B
6	127.1		
7	128.7	C/E	G, E, C, D
8	128.7		
9	129.6	F	-
10	132.8	-	C, F
11	133.7	B	A
12	143.7	-	C, G, J, K
13	146.3	-	A, B, G, J, K
14	198.2	-	A, F(w), H, I, J, K

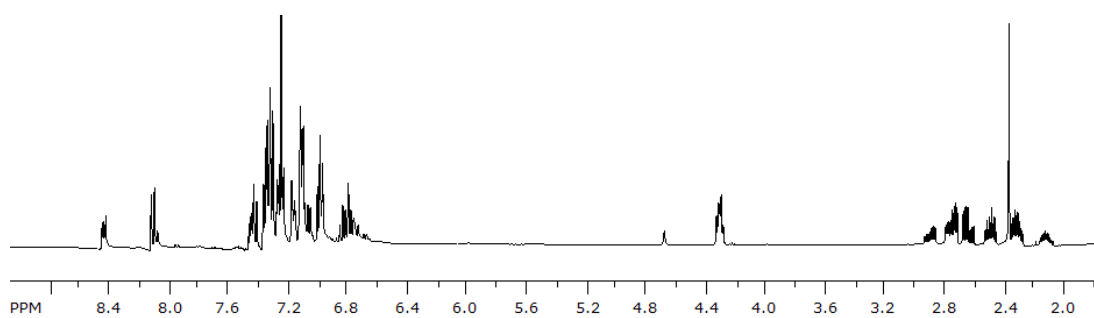


Figure 113. NMR of compound E mixture. (400MHz, CDCl₃)

Table 15. Crystal data and structure refinement for Unknown B

Empirical formula	C ₂₂ H _{14.5} Cl _{0.5} NO
Formula weight	344.80
Temperature/K	109.9(2)
Crystal system	orthorhombic
Space group	Pccn
a/Å	22.2241(12)
b/Å	19.7661(12)
c/Å	6.9639(4)
α/°	90.00
β/°	90.00
γ/°	90.00
Volume/Å ³	3059.1(3)
Z	8
ρ _{calc} /mg/mm ³	1.497
m/mm ⁻¹	0.260
F(000)	1432.0
Crystal size / mm	0.292 × 0.1214 × 0.0264
2 θ range for data collection	5.88 to 50.12°
Index ranges	-22 ≤ h ≤ 26, -23 ≤ k ≤ 10, -7 ≤ l ≤ 8
Reflections collected	6809
Independent reflections	2720[R(int) = 0.0364]
Data / restraints / parameters	2720/0/226
Goodness-of-fit on F ²	1.064
Final R indexes [I >= 2σ (I)]	R ₁ = 0.0884, wR ₂ = 0.2573
Final R indexes [all data]	R ₁ = 0.1153, wR ₂ = 0.2813
Largest diff. peak/hole / e Å ⁻³	0.41/-1.37

Table 16. Fractional Atomic Coordinates ($\times 10^4$) and Equivalent Isotropic Displacement Parameters ($\text{\AA}^2 \times 10^3$) for vc1301. U_{eq} is defined as 1/3 of of the trace of the orthogonalised U_{ij} tensor.

Atom	x	y	z	U(eq)
C1	4172.5(19)	2718(2)	3947(6)	17(1)
C2	4694.2(19)	3087(2)	4271(6)	16.1(10)
C3	5240.1(19)	2782(2)	4631(6)	16.3(9)
C4	5296.8(18)	2092(2)	4617(6)	14.8(9)
C5	4784.2(19)	1685(2)	4237(6)	16.1(10)
C6	4209.9(18)	2002(2)	3926(6)	14.5(9)
C7	3696(2)	1597(2)	3566(7)	20.1(10)
C8	3747(2)	907(2)	3479(7)	21.2(10)
C9	4307.9(19)	593(2)	3706(6)	18.4(10)
C10	4808.8(19)	970(2)	4070(6)	16.6(9)
C11	5904.4(19)	1794(2)	4941(6)	14.9(9)
C12	6397.0(19)	2033(2)	3913(6)	19(1)
C13	6967(2)	1768(2)	4200(7)	24.2(11)
C14	7059(2)	1264(2)	5523(7)	23.7(11)
C15	6578(2)	1029(2)	6601(7)	22.6(10)
C16	6007(2)	1286(2)	6302(6)	17.8(10)
C17	3627(2)	3757(2)	3511(6)	19.5(10)
C18	4156.3(19)	4116(2)	3827(6)	16.3(10)
C19	4164(2)	4811(2)	3703(6)	21.2(10)
C20	3646(2)	5157(2)	3261(7)	25.0(11)
C21	3113(2)	4803(2)	2947(8)	31.2(12)
C22	3102(2)	4107(2)	3087(7)	26.7(11)
N1	3631.3(19)	3051(2)	3631(6)	23.8(10)

Table 17. Anisotropic Displacement Parameters ($\text{\AA}^2 \times 10^3$) for vc1301. The Anisotropic displacement factor exponent takes the form: $-2\pi^2[h^2a^{*2}U_{11}+\dots+2hka \times b \times U_{12}]$

Atom	U_{11}	U_{22}	U_{33}	U_{23}	U_{13}	U_{12}
C1	21(2)	16(2)	14(2)	0.6(17)	3.5(17)	5.2(17)
C2	26(2)	10(2)	12(2)	1.5(16)	3.1(18)	0.5(17)
C3	18(2)	13(2)	17(2)	3.0(17)	-2.2(18)	-1.5(17)
C4	20(2)	13(2)	11.6(19)	0.5(17)	1.2(17)	2.9(17)
C5	21(2)	18(2)	9(2)	-0.3(17)	2.1(17)	3.2(17)
C6	20(2)	12(2)	12(2)	2.5(16)	4.2(17)	5.3(17)
C7	20(2)	16(2)	25(2)	-0.4(18)	-1.1(19)	4.3(18)
C8	21(2)	17(2)	26(2)	0.5(19)	2(2)	-2.7(18)
C9	26(2)	10(2)	20(2)	-0.3(17)	-1.3(19)	0.0(18)
C10	21(2)	12(2)	16(2)	3.2(17)	-0.5(18)	7.5(17)
C11	19(2)	10(2)	16(2)	-5.4(17)	-1.3(17)	0.6(17)
C12	27(2)	12(2)	18(2)	-2.3(17)	-2.1(19)	0.6(18)
C13	23(2)	20(2)	30(3)	-7(2)	4(2)	-5.4(19)
C14	20(2)	15(2)	36(3)	-9(2)	-8(2)	4.8(18)
C15	28(2)	14(2)	26(2)	1.1(19)	-12(2)	1.4(19)
C16	26(2)	10(2)	17(2)	-1.4(17)	0.6(18)	-0.7(17)
C17	23(2)	14(2)	21(2)	1.8(18)	6.8(19)	5.6(18)
C18	22(2)	15(2)	12(2)	1.3(17)	2.7(17)	9.7(17)
C19	30(2)	17(2)	16(2)	1.3(18)	1.0(19)	1.1(19)
C20	34(3)	13(2)	28(3)	3.0(19)	7(2)	9(2)
C21	26(2)	22(3)	46(3)	0(2)	0(2)	15(2)
C22	22(2)	20(2)	39(3)	-1(2)	5(2)	4.1(19)
N1	18(2)	13(2)	41(3)	3.0(18)	1.6(19)	5.8(17)
O1	24.3(17)	8.2(15)	27.9(18)	1.9(13)	-0.7(14)	4.0(12)
Cl1	42.9(12)	49.0(13)	78.6(18)	0	0	0.9(10)

Table 18. Bond lengths for Unknown B as determined by X-ray crystallography

Atom	Atom	Length/Å		Atom	Atom	Length/Å
C1	C2	1.388(6)		C11	C12	1.391(6)
C1	C6	1.420(6)		C11	C16	1.400(6)
C1	N1	1.388(6)		C12	C13	1.384(6)
C2	C3	1.378(6)		C13	C14	1.373(7)
C2	O1	1.396(5)		C14	C15	1.388(7)
C3	C4	1.370(6)		C15	C16	1.383(6)
C4	C5	1.419(6)		C17	C18	1.392(6)
C4	C11	1.490(6)		C17	C22	1.387(6)
C5	C6	1.438(6)		C17	N1	1.398(6)
C5	C10	1.420(6)		C18	C19	1.377(6)
C6	C7	1.417(6)		C18	O1	1.389(5)
C7	C8	1.369(6)		C19	C20	1.374(6)
C8	C9	1.402(6)		C20	C21	1.392(7)
C9	C10	1.363(6)		C21	C22	1.380(7)

Table 19. Bond Angles for Unknown B as determined by X-ray crystallography

Atom	Atom	Atom	Angle/°		Atom	Atom	Atom	Angle/°
C2	C1	C6	118.5(4)		C12	C11	C4	120.1(4)
C2	C1	N1	120.1(4)		C12	C11	C16	117.7(4)
N1	C1	C6	121.5(4)		C16	C11	C4	122.2(4)
C1	C2	O1	121.6(4)		C13	C12	C11	121.1(4)
C3	C2	C1	122.4(4)		C14	C13	C12	120.5(4)
C3	C2	O1	116.0(4)		C13	C14	C15	119.4(4)
C4	C3	C2	121.0(4)		C16	C15	C14	120.2(4)
C3	C4	C5	119.4(4)		C15	C16	C11	121.0(4)
C3	C4	C11	118.4(4)		C18	C17	N1	119.5(4)
C5	C4	C11	122.1(4)		C22	C17	C18	119.4(4)
C4	C5	C6	119.6(4)		C22	C17	N1	121.1(4)
C4	C5	C10	123.3(4)		C19	C18	C17	120.6(4)
C10	C5	C6	117.1(4)		C19	C18	O1	117.5(4)
C1	C6	C5	119.0(4)		O1	C18	C17	121.9(4)
C7	C6	C1	121.2(4)		C20	C19	C18	120.0(4)
C7	C6	C5	119.8(4)		C19	C20	C21	119.9(4)
C8	C7	C6	120.2(4)		C22	C21	C20	120.3(4)
C7	C8	C9	120.6(4)		C21	C22	C17	119.8(5)
C10	C9	C8	120.4(4)		C1	N1	C17	119.3(4)
C9	C10	C5	121.8(4)		C18	O1	C2	117.4(3)

Table 20. Hydrogen Atom Coordinates ($\text{\AA}\times 10^4$) and Isotropic Displacement Parameters ($\text{\AA}^2\times 10^3$) for vc1301.

Atom	x	y	z	U(eq)
H3	5575	3048	4888	20
H7	3323	1800	3388	24
H8	3406	644	3268	25
H9	4339	125	3608	22
H10	5177	752	4213	20
H12	6343	2377	3018	23
H13	7289	1933	3490	29
H14	7441	1082	5695	28
H15	6639	697	7528	27
H16	5686	1119	7016	21
H19	4520	5047	3918	25
H20	3651	5626	3173	30
H21	2763	5038	2641	37
H22	2744	3873	2898	32
H1	3350(30)	2880(30)	3440(100)	50(20)

8.1 Glossary

Abbreviation	Meaning
+ve	positive
-ve	negative
CHN	Carbon, Hydrogen and Nitrogen elemental analysis
COSY	Homonuclear correlation spectroscopy (NMR)
d	doublet
DCM	Dichloromethane
dd	double doublet
ddd	double double doublet
DNBP	2,4-dinitro-6-sec butyl phenol
EPR	Electron Paramagnetic resonance
ESI	Electron Spray Ionisation (Mass Spectrometry)
G	Gauss (Unit)
GC / MS	Gas chromatography–mass spectrometry
HMBC	Heteronuclear single-quantum correlation spectroscopy (NMR)
HSQC	Heteronuclear multiple-bond correlation spectroscopy (NMR)
J	J coupling (NMR)
m	multiplet
MS	Mass spectrometry
NMR	Nuclear Magnetic Resonance
T	Telsa (Unit)
t	triplet
td	triplet of doublets
TfOH	Triflic Acid (Trifluoromethanesulfonic acid)
TOCSY	Total correlation spectroscopy (NMR)

9. References

1. Energy, U. S. D. o., New Process for Producing Styrene Cuts Costs, Saves Energy, and Reduces Greenhouse Gas Emissions. 2010.
2. Williams, M. L.; Landel, R. F.; Ferry, J. D., *Journal of the American Chemical Society* **1955**, 77 (14), 3701-3707.
3. Burnett, G. M.; Tait, P. J. T., *Polymer* **1960**, 1 (2), 151-162.
4. Odian, G. G., *Principles of Polymerization*. 3rd ed.; Wiley-Interscience: 1991; p 768.
5. Chodák, I.; Zimányová, E., *European Polymer Journal* **1984**, 20 (1), 81-84.
6. Vanhook, J. P.; Tobolsky, A. V., *Journal of Polymer Science* **1958**, 33 (126), 429-445.
7. Bengough, W. I.; Park, G. B., *European Polymer Journal* **1976**, 12 (7), 431-433.
8. Gee, G.; Rideal, E. K., *Transactions of the Faraday Society* **1935**, 31 (0), 969-979.
9. Matyjaszewski, K.; Xia, J., *Chemical Reviews* **2001**, 101 (9), 2921-2990.
10. Flory, P. J., *Journal of the American Chemical Society* **1937**, 59, 241-253.
11. Hall, H. K., *Angewandte Chemie International Edition in English* **1983**, 22 (6), 440-455.
12. Hall, H. K.; Padias, A. B., *Accounts of Chemical Research* **1990**, 23 (1), 3-9.
13. Lingnau, J.; Stickler, M.; Meyerhoff, G., *European Polymer Journal* **1980**, 16 (8), 785-791.
14. Husain, A.; Hamielec, A. E., *Journal of Applied Polymer Science* **1978**, 22 (5), 1207-1223.
15. Barr, N. J.; Bengough, W. I.; Beveridge, G.; Park, G. B., *European Polymer Journal* **1978**, 14 (4), 245-250.
16. Corson, B. B.; Dorsky, J.; Nickels, J. E.; Kutz, W. M.; Thayer, H. I., *Journal of Organic Chemistry* **1954**, 19 (1), 17-26.
17. Burnett, G. M.; Mark, H. F., *Mechanism of polymer reactions*. Interscience Publishers: 1954.
18. Mayo, F. R., *Journal of the American Chemical Society* **1953**, 75 (24), 6133-6141.
19. Mayo, F. R., *Journal of the American Chemical Society* **1968**, 90 (5), 1289-1295.
20. Miller, A. A.; Mayo, F. R., *Journal of the American Chemical Society* **1956**, 78 (5), 1017-1023.
21. Foord, S. G., *Journal of the Chemical Society* **1940**, 48-56.
22. Khuong, K. S.; Jones, W. H.; Pryor, W. A.; Houk, K. N., *Journal of the American Chemical Society* **2005**, 127 (4), 1265-1277.
23. Kothe, T.; Fischer, H., *Journal of Polymer Science Part A: Polymer Chemistry* **2001**, 39 (22), 4009-4013.

24. Zhang, C.; Wang, X.; Liu, L.; Wang, Y.; Peng, X., *Journal of Molecular Modeling* **2008**, *14* (11), 1053-1064.
25. Stickler, M.; Meyerhoff, G., *Makromolekulare Chemie-Macromolecular Chemistry and Physics* **1980**, *181* (1), 131-147.
26. Stickler, M.; Meyerhoff, G., *Polymer* **1981**, *22* (7), 928-933.
27. Lehrle, R. S.; Shortland, A., *European Polymer Journal* **1988**, *24* (5), 425-429.
28. Lingnau, J.; Meyerhoff, G., *Macromolecules* **1984**, *17* (4), 941-945.
29. Albisetti, C. J.; England, D. C.; Hogsed, M. J.; Joyce, R. M., *Journal of the American Chemical Society* **1956**, *78* (2), 472-475.
30. Bhanu, V. A.; Kishore, K., *Chemical Reviews* **1991**, *91* (2), 99-117.
31. Graham, W. D.; Green, J. G.; Pryor, W. A., *Journal of Organic Chemistry* **1979**, *44* (6), 907-914.
32. Hilditch, T. P., *Nature* **1950**, *166* (4222), 558-559.
33. Khan, N. A., *Journal of Chemical Physics* **1953**, *21* (5), 952-952.
34. Khan, N. A., *Journal of Chemical Physics* **1954**, *22* (12), 2090-2090.
35. Khan, N. A., *Canadian Journal of Chemistry-Revue Canadienne De Chimie* **1959**, *37* (6), 1029-1034.
36. Tornero-Velez, R.; Waidyanatha, S.; Echeverria, D.; Rappaport, S. M., *Journal of Environmental Monitoring* **2000**, *2* (2), 111-117.
37. Schulze, S.; Vogel, H., *Chemical Engineering & Technology* **1998**, *21* (10), 829-837.
38. Denisov, E. T.; Afanas'ev, I. B., *Oxidation and Antioxidants in Organic Chemistry and Biology*. Taylor & Francis: 2005.
39. Bevington, J. C.; Hunt, B. J., *Journal of Macromolecular Science-Pure and Applied Chemistry* **2005**, *A42* (2), 203-210.
40. Kolyakina, E. V.; Grishin, D. F., *Russian Chemical Reviews* **2009**, *78* (6), 535-568.
41. Lalevée, J.; Gimes, D.; Bertin, D.; Allonas, X.; Fouassier, J. P., *Chemical Physics Letters* **2007**, *449* (1-3), 231-235.
42. Greszta, D.; Matyjaszewski, K., *Macromolecules* **1996**, *29* (24), 7661-7670.
43. Odell, P. G.; Veregin, R. P. N.; Michalak, L. M.; Georges, M. K., *Macromolecules* **1997**, *30* (8), 2232-2237.
44. Webster, O. W., *Science* **1991**, *251* (4996), 887-893.
45. Bushby, R. J.; Lord, N.; McRobbie, I.; Pryce, A., *Polymer* **1998**, *39* (22), 5567-5571.
46. Jackson, R. A.; Waters, W. A., *Journal of the Chemical Society* **1960**, (Apr), 1653-1657.
47. Tudos, F.; Foldesberezsnich, T., *Progress in Polymer Science* **1989**, *14* (6), 717-761.
48. Gingras, B. A.; Waters, W. A., *Journal of the Chemical Society* **1954**, (JUN), 1920-1924.

49. Motyakin, M. V.; Wasserman, A. M.; Stott, P. E.; Zaikov, G. E., *Journal of Applied Polymer Science* **2004**, *91* (3), 1599-1603.
50. Cohen, S. G., *Journal of the American Chemical Society* **1947**, *69* (5), 1057-1064.
51. Cohen, S. G., *Journal of Polymer Science* **1947**, *2* (5), 511-521.
52. Bevington, J. C.; Ghanem, N. A.; Melville, H. W., *Journal of the Chemical Society* **1955**, 2822-2830.
53. Bevington, J. C.; Ghanem, N. A.; Melville, H. W., *Transactions of the Faraday Society* **1955**, *51* (7), 946-953.
54. Eastmond, G. C., Chain Transfer, Inhibition and Retardation. In *Comprehensive Chemical Kinetics*, 1st ed.; Bamford, C. H.; Tipper, C. F. H., Eds. Elsevier Scientific Publishing Company: 1976; Vol. 14A, pp 105-152.
55. Levy, L. B., *Journal of Polymer Science Part a-Polymer Chemistry* **1992**, *30* (4), 569-576.
56. Brand, R. H.; Hartwig, A.; Opitz, B.; Pfeifer, C.; Drochner, A.; Vogel, G. H., *Macromolecular Reaction Engineering* **2011**, *5* (5-6), 212-222.
57. Kolyakina, E. V.; Grishin, D. F., *Russian Chemical Reviews* **2011**, *80* (7), 683-704.
58. Bickel, A. F.; Kooyman, E. C., *Journal of the Chemical Society (Resumed)* **1956**, (0), 2215-2221.
59. Atherton, N. M., *Principles of Electron Spin Resonance*. Ellis Horwood: 1993.
60. Gerson, F.; Huber, W., Part Introduction. In *Electron Spin Resonance Spectroscopy of Organic Radicals*, Wiley-VCH Verlag GmbH & Co. KGaA: 2004; pp 1-1.
61. Yassin, A. A.; Rizk, N. A., *British Polymer Journal* **1977**, *9* (4), 322-325.
62. Yun, M., Anitoxidant activity in styrene, Unpublished work. 2008.
63. Noel, L. F. J.; Brouwer, E. C. P.; Vanherk, A. M.; German, A. L., *Journal of Applied Polymer Science* **1995**, *57* (3), 245-254.
64. Hoogenboom, R.; Fijten, M. W. M.; Abeln, C. H.; Schubert, U. S., *Macromolecular Rapid Communications* **2004**, *25* (1), 237-242.
65. Jallapuram, R.; Naydenova, I.; Byrne, H. J.; Martin, S.; Howard, R.; Toal, V., *Appl. Opt.* **2008**, *47* (2), 206-212.
66. McGill, C. A.; Ferguson, R. H.; Donoghue, K.; Nordon, A.; Littlejohn, D., *Analyst* **2003**, *128* (12), 1467-1470.
67. Jovanovic, R.; Dube, M. A., *Polymer Reaction Engineering* **2003**, *11* (3), 233-257.
68. Udagawa, A.; Sakurai, F.; Takahashi, T., *Journal of Applied Polymer Science* **1991**, *42* (7), 1861-1867.
69. Aldridge, P. K.; Kelly, J. J.; Callis, J. B.; Burns, D. H., *Analytical Chemistry* **1993**, *65* (24), 3581-3585.

70. Gulari, E.; McKeigue, K.; Ng, K. Y. S., *Macromolecules* **1984**, *17* (9), 1822-1825.
71. Starkweather, H. W.; Taylor, G. B., *Journal of the American Chemical Society* **1930**, *52* (12), 4708-4714.
72. Goldfinger, G.; Lauterbach, K. E., *Journal of Polymer Science* **1948**, *3* (2), 145-156.
73. Schulz, G. V.; Harborth, G., *Angewandte Chemie* **1947**, *59* (3), 90-92.
74. Patnode, W.; Scheiber, W. J., *Journal of the American Chemical Society* **1939**, *61* (12), 3449-3451.
75. Nichols, F. S.; Flowers, R. G., *Industrial & Engineering Chemistry* **1950**, *42* (2), 292-295.
76. Bernatchez, P.; Goutier, D., *Review of Scientific Instruments* **1973**, *44* (12), 1790-1791.
77. Frey, S.; Richert, R., *Review of Scientific Instruments* **2010**, *81* (3), 034702.
78. Karcz, J.; Streck, F., *Chemical Engineering Journal and the Biochemical Engineering Journal* **1995**, *58* (2), 135-143.
79. Eckert, E. r. g.; Goldstein, R. J.; Ibele, W. e.; Patankar, S. V.; Simon, T. W.; Strykowski, P. J.; Tamma, K. K.; Kuehn, T. H.; Bar-Cohen, A.; Heberlein, J. V. R.; Davidson, J. H.; Bischof, J.; Kulacki, F.; Kortshagen, U., *International Journal of Heat and Mass Transfer* **1999**, *42* (15), 2717-2797.
80. Conte, M.; Ma, Y.; Loyns, C.; Price, P.; Rippon, D.; Chechik, V., *Organic & Biomolecular Chemistry* **2009**, *7* (13), 2685-2687.
81. Smirnov, A. I.; Clarkson, R. B.; Belford, R. L., *Journal of Magnetic Resonance, Series B* **1996**, *111* (2), 149-157.
82. Smirnova, T. I.; Smirnov, A. I., High-field ESR spectroscopy in membrane and protein biophysics. In *ESR Spectroscopy in Membrane Biophysics*, Hemminga, M. A.; Berliner, L. J., Eds. Kluwer Academic/Plenum Publ: New York, 2007; Vol. 27, pp 165-251.
83. Pedulli, G.; Lucarini, M.; Pedrielli, P.; Sagrini, M.; Cipollone, M., *Research on Chemical Intermediates* **1996**, *22* (1), 1-14.
84. East, G. C.; Margerison, D.; Pulat, E., *Transactions of the Faraday Society* **1966**, *62* (0), 1301-1307.
85. Levy, L. B., *Journal of Polymer Science: Polymer Chemistry Edition* **1985**, *23* (5), 1505-1515.
86. Kurland, J. J., *Journal of Polymer Science: Polymer Chemistry Edition* **1980**, *18* (3), 1139-1145.
87. Bakalbassis, E. G.; Lithoxidou, A. T.; Vafiadis, A. P., *The Journal of Physical Chemistry A* **2006**, *110* (38), 11151-11159.
88. Himo, F.; Eriksson, L. A.; Blomberg, M. R. A.; Siegbahn, P. E. M., *International Journal of Quantum Chemistry* **2000**, *76* (6), 714-723.
89. Hepworth, J. D.; Waring, D. R.; Waring, M. J.; Chemistry, R. S. o., *Aromatic Chemistry*. Royal Society of Chemistry: 2002.

90. Lithoxidou, A. T.; Bakalbassis, E. G., *The Journal of Physical Chemistry A* **2004**, *109* (2), 366-377.
91. Korth, H.-G.; de Heer, M. I.; Mulder, P., *The Journal of Physical Chemistry A* **2002**, *106* (37), 8779-8789.
92. Borges dos Santos, R. M.; Martinho Simões, J. A., *J. Phys. Chem. Ref. Data* **1998**, *27* (3), 707-739.
93. Suryan, M. M.; Kafafi, S. A.; Stein, S. E., *Journal of the American Chemical Society* **1989**, *111* (13), 4594-4600.
94. Bartlett, P. D.; Kwart, H., *Journal of the American Chemical Society* **1952**, *74* (16), 3969-3973.
95. Bevington, J. C.; Hunt, B. J., *Journal of Polymer Materials* **2005**, *22* (4), 445-448.
96. Still, W. C.; Kahn, M.; Mitra, A., *The Journal of Organic Chemistry* **1978**, *43* (14), 2923-2925.
97. Clover, A. M., *Journal of the American Chemical Society* **1923**, *45* (12), 3133-3138.
98. Gäb, S.; Turner, W. V., *Angewandte Chemie International Edition in English* **1985**, *24* (1), 50-50.
99. Yu, W. H. S.; Wijnen, M. H. J., *The Journal of Chemical Physics* **1970**, *52* (5), 2736-2739.
100. Rendy, R.; Zhang, Y.; McElrea, A.; Gomez, A.; Klumpp, D. A., *Journal of Organic Chemistry* **2004**, *69* (7), 2340-2347.
101. Haworth, R. D., *Journal of the Chemical Society (Resumed)* **1932**, (0), 1125-1133.
102. Tauer, E.; Grellmann, K. H., *The Journal of Organic Chemistry* **1981**, *46* (21), 4252-4258.
103. Kang, J. Y.; Bugarin, A.; Connell, B. T., *Chemical Communications* **2008**, (30), 3522-3524.
104. Maruyama, K.; Tanimoto, I.; Goto, R., *The Journal of Organic Chemistry* **1967**, *32* (8), 2516-2520.
105. Hui, A. W.; Hamielec, A. E., *Journal of Applied Polymer Science* **1972**, *16* (3), 749-769.
106. Moad, G.; Rizzardo, E.; Solomon, D., *Polymer Bulletin* **1982**, *6* (11-12), 589-593.
107. Russell, K. E.; Tobolsky, A. V., *Journal of the American Chemical Society* **1953**, *75* (20), 5052-5054.
108. *Official Journal of the European Union* **2007**.
109. Roginsky, V. A.; Pisarenko, L. M.; Bors, W.; Michel, C.; Saran, M., *Journal of the Chemical Society-Faraday Transactions* **1998**, *94* (13), 1835-1840.
110. Roginsky, V. A.; Pisarenko, L. M.; Bors, W.; Michel, C., *Journal of the Chemical Society-Perkin Transactions 2* **1999**, (4), 871-876.
111. Wardman, P., *J. Phys. Chem. Ref. Data* **1989**, *18* (4), 1637-1755.
112. Maliszka, K. L.; Hasinoff, B. B., *Free Radical Biology and Medicine* **1996**, *20* (7), 905-914.

113. Brunmark, A.; Cadenas, E., *Free Radical Biology and Medicine* **1989**, 7 (4), 435-477.
114. Alegria, A. E.; Lopez, M.; Guevara, N., *Journal of the Chemical Society-Faraday Transactions* **1996**, 92 (24), 4965-4968.
115. Torrey, H. A.; Hunter, W. H., *Journal of the American Chemical Society* **1912**, 34, 702-716.
116. Konno, M.; Kobayash.H; Marumo, F.; Saito, Y., *Bulletin of the Chemical Society of Japan* **1973**, 46 (7), 1987-1990.
117. Kainer, H.; Bijl, D.; Roseinnes, A. C., *Nature* **1956**, 178 (4548), 1463-1463.
118. Andre, J. J.; Weill, G., *Chemical Physics Letters* **1971**, 9 (1), 27-&.
119. Folkers, K., *Journal of the American Chemical Society* **1966**, 88 (22), 5370-5370.
120. Morton, R. A., *Biochemistry of quinones*. Academic Press: 1965.
121. Wong, S. K.; Sytnyk, W.; Wan, J. K. S., *Canadian Journal of Chemistry* **1972**, 50 (18), 3052-3057.
122. Roginsky, V.; Barsukova, T.; Loshadkin, D.; Pliss, E., *Chemistry and Physics of Lipids* **2003**, 125 (1), 49-58.
123. Hudson, A.; Luckhurst, G. R., *Chemical Reviews* **1969**, 69 (2), 191-225.
124. Adam, F. C.; Weissman, S. I., *Journal of the American Chemical Society* **1958**, 80 (6), 1518-1519.
125. Elliot, A. J.; McCracken, D. R.; Buxton, G. V.; Wood, N. D., *Journal of the Chemical Society, Faraday Transactions* **1990**, 86 (9), 1539-1547.
126. Neta, P.; Grodkowski, J., *J. Phys. Chem. Ref. Data* **2005**, 34 (1), 109-199.
127. Dolomanov, O. V.; Bourhis, L. J.; Gildea, R. J.; Howard, J. A. K.; Puschmann, H., *J. Appl. Crystallogr.* **2009**, 42, 339-341.
128. Palatinus, L.; Chapuis, G., *J. Appl. Crystallogr.* **2007**, 40, 786-790.
129. Sheldrick, G. M., *Acta Crystallographica Section A* **2008**, 64 (1), 112-122.